OIL WHIRL OF FLEXIBLE ROTORS

ALEXANDER NEIL PATERSON

A THESIS

submitted to the

UNIVERSITY of GLASGOW

for the DEGREE

of

DOCTOR of PHILOSOPHY

JUNE 1966

ACKNOWLEDGEMENTS

In the preparation of the work of this thesis the writer wishes to acknowledge the assistance he has received from three sources in particular - his supervisors, the University of Glasgow and financial sponsors of the experimental rigs.

Dr. D. Morrison, at present employed by A.E.I. Ltd., Manchester, conceived the need for the writer's work and supervised it from June 1962 until December 1964. During this time his ready, experienced advice was of great assistance and encouragement to the writer.

Professor G.D.S. MacLellan, at present head of the Department of Engineering at Leicester University, indirectly supervised the writer from the beginning of his work and directly supervised him from January 1965 until September 1965. Throughout, he provided the writer with firm support and valuable advice.

Since October 1965, the writer has benefitted from the generous supervision of Professor J.D. Robson, at present Rankine Professor of Mechanics and Mechanism at the University of Glasgow.

The University of Glasgow has provided excellent facilities for the writer's work. The foreman of the engineering workshop, Mr. Archie Macneil, was of great assistance during the construction of the experimental rigs.

The rig for the unstable oil whirl experiments was largely financed by a grant from the National Engineering Laboratory, East Kilbride. Further grants from the Science Research Council and the English Electric Co. Ltd., Rugby, allowed modification of the rig to a form suitable for the synchronous oil whirl experiments.

The writer is most grateful for the assistance of these sources.

C O N T E N T S

PAGE

NOTATION

D	differential operator
F	force
$G = \frac{D}{\omega_s}$	
L	rotor mass eccentricity
M	rotor end moment
$N_L = \frac{2\pi}{\omega_s \eta}\left(\frac{W}{ld}\right)\left(\frac{2c}{d}\right)^2\left(\frac{d}{l}\right)^2$	(Ockvirk load Number)
P	rotor general receptance coefficient; also unstable oil whirl bearing paramet
Q	unstable oil whirl bearing parameter.
R	radius of bearing bore.
$S = \frac{2\pi}{\omega_s \eta}\left(\frac{W}{ld}\right)\left(\frac{2c}{d}\right)^2$	(Sommerfelt load number)
$S = \sqrt{mr}$	
W	load on bearing
V	$\frac{\partial h}{\partial t}$
a	oil displacement force coefficient
b	oil velocity force coefficient
c	radial clearance of bearing
d	diameter of bearing bore
e	journal centre eccentricity from bearing centre
g	gravitational constant
h	clearance between journal and bearing at angle Θ
k	shaft stiffness
l	bearing length, also rotor span

m	rotor mass
n	oil force coefficient for synchronous whirl
p	oil pressure, also rotor receptance coefficient
q	oil flow per unit bearing length
r	rotor displacement due to bending, also journal displacement along line of centres
s	journal displacement perpendicular to line of centres
t	time
$u = \sqrt{m}y,$	also oil velocity in circumferential direct
x	journal displacement perpendicular to the direction of journal static load
y	journal displacement in the opposite direct to direction of journal static load, also rotor displacement directly due to journal displacement, also oil film radial coordina
z	oil film axial coordinate
α	Non-dimensional oil displacement force coefficient
β	non-dimensional oil velocity force coeffici
γ	non-dimensional distance of rotor mass fron journals, also compound oil coefficient
$\epsilon = \frac{e}{c}$	journal eccentricity ratio
ρ	non-dimensional oil film stiffness at stability boundary
$\tau = -\frac{l}{D}_2$	
$\tau_{jk} = \sqrt{m_j}\sqrt{m_k}\,\eta_{jk}$	

ϕ	journal attitude angle
ω	angular velocities, phase velocities
η	absolute viscosity, also rotor flexibility coefficient
θ	circumferential reference angle within oil film, also journal force and displacement lag angles
$\lambda = \frac{\omega_b}{\omega_r}$	ratio of rotor whirl frequency to running frequency
ψ	phase reference angle of rotor out-of-balance masses

INTRODUCTION

Object of the work

The work of this thesis is intended as a contribution to the understanding of the influence of hydrodynamic journal bearings on the whirling motion of the rotors of turbo-alternator sets.

Since about the beginning of this century this type of machine has provided almost all the electrical power consumed in the world. It will continue to be used to meet the rapidly expanding demand for electrical power in the foreseeable future because of the lack of success of more direct methods of energy conversion.

Due to their long history, present turbo-alternator designs are based on proven practices and tried empirical methods. Hence this thesis can be fairly described as yet another instance of science following well behind engineering practice.

It is probably true that in answer to his question "Why do you think this design will work?" an engineer is often more reassured to hear the reply "It has worked on n previous occasions" than to be given a justification of the design on the basis of a scientific analysis. In the case of the whirling problems associated with turbo-

alternator rotors, the turbine engineer has had no choice but to rely on experience since there has been practically no guidance from science on the dynamic characteristics of hydrodynamic journal bearings which often dominate the dynamic problem. That the engineer has succeeded so admirably is due partly to his ingenuity but also to the remarkably favourable dynamic characteristics of oil bearings which he has appreciated and used but not fully understood.

The need for a scientific approach has become more urgent as, in the interests of efficiency, the size of turbo-alternator sets has continued to increase. For since the diameter of the rotor discs in the final stages of large sets are limited by centrifugal stress considerations, the trend has been to increase the length of the sets. To some extent this has been achieved by increasing the length of the individual rotor spans which makes them correspondingly more flexible and thus more prone to whirling problems.

If whirling problems are going to appear they will do so at a late stage in the commissioning of a set when at best delays are expensive and at worst the machine may not be able to operate safely. Turbo-alternator rotors have a large capacity for rotational kinetic

energy and any conditions, such as whirling, which encourage conversion of rotational energy to flexural or translational motion of the rotor are thus potentially serious. Less drastically, a rough running rotor could result in rapid wear and the harmful effect on other components of the associated vibration of the whole set could mean a reduction in the useful life of the set.

Considerations such as these have inspired much study of the influence of the dynamic characteristics of journal bearings on rotor whirl, the results of which have only fairly recently begun to provide useful quantitative data. This thesis will show that the theory is now at a stage where it can predict the significant features of the oil whirl of simple rotor systems and will suggest that, together with the numerical facilities of modern high speed digital computers, a prediction of the whirl behaviour of the largest turbo-alternator sets is now also attainable.

DESCRIPTION of the SYSTEM

For the purposes of vibration analysis, a turbo-alternator set can be considered as an assembly of three sub-systems:

i bearing housings and set foundation

ii oil films

iii rotor

In the present analyses, the bearing housings and set foundations are assumed immovable. It is realised that on account of the fabrication methods used, the relative stiffness and mass of this subsystem probably decreases in proportion to the size of the set so as to be sufficiently low to effect the whirling motion of the largest assemblies particularly. However, here the approach has been to emphasise the influence of the dynamic force characteristics of oil bearings about which the lack of information seems to have been the main stumbling block for a realistic dynamic analysis.

In Part 1 theories for the dynamic force characteristics of hydrodynamic journal bearings and of rotors are discussed.

The dynamic characteristics of the bearings are considered in Chapter 1 where, as throughout the work, attention is restricted to the case of plain, cylindrical, laminar and incompressible flow, hydrodynamic journal bearings, hereafter called journal bearings.

The receptance method for the analysis of rotor whirl is described and developed in Chapter 2. The most

usual type of turbo-alternator rotor is considered, constructed from discs which are either shrunk on to or integral with a stepped shaft, the rotor assembly being practically rotationally symmetric. The gyroscopic effects of the rotor discs should be examined in a more complete analysis but are usually small for rotors which do not overhang and are neglected throughout the present work.

In all cases the rotor is considered to be mounted horizontally which implies that the static bearing load required for the calculation of the bearing running conditions is due to gravitational attraction on the rotor.

DESCRIPTION of the SYSTEM'S DYNAMIC PHENOMENA

It will be found in Chapter 2 that the condition in which a rotor does not rotate but lies at the bottom of its journals is not a trivial one for the purposes of the present work if the journals are then assumed to provide a support which prevents transverse translation but offers no restraint to transverse rotation - hereafter called a simple support. The system has theoretical rather than practical importance since the dynamic analysis of it provides results which are useful

for fuller analyses which take account of support flexibility.

In the present work attention will be confined to cases in which the rotor is rotating and rotating fast enough to form hydrodynamic oil films under its journals. If the rotor could be perfectly balanced and was stable on the oil films supporting it, the axis of rotation of the rotor including the centres of the rotor's journals would take up a unique position of equilibrium within its journal bearings which will be referred to as the position of static equilibrium. Thus if it is remembered that in the present context the terms 'static' and 'dynamic' will always be used with reference to the rotor rotational axis, there should be no ambiguity between them and the terms 'not rotating' and 'rotating.'

The whirl of a rotating rotor is defined as any orbital motion of points on the rotor rotational axis in planes normal to the bearing axis.

For a flexible rotor supported in oil film bearings, whirl normally consists of the combined effect of the flexing of the rotor and whirl of the rotor journals relative to the bearings and is then defined as oil whirl. There are at least two different types of oil whirl and these are considered separately in Part 2 and Part 3 respectively.

The theoretical and experimental investigation described in Part 2 is concerned with the response of a rotor supported on oil film bearings to the forcing effect of its inherent out-of-balance. The response is normally an oil whirl with a frequency equal to that of the rotor running frequency and is therefore known as synchronous whirl. For a running frequency in the vicinity of a natural frequency of the rotor on simple supports, synchronous whirl is observed to exhibit a resonance which, however, is normally mild for a well balanced rotor.

Part 3 describes a theoretical and experimental investigation of a second type of oil whirl attributable to instability caused by the oil films. The instability can be sudden and can lead to rotor displacement amplitudes at the journals of the order of the bearing clearance. The whirl usually has a frequency just below half the rotor running frequency when it is called half speed whirl, oil whip or unstable oil whirl. The last term shall be used throughout this work.

A third type of oil whirl has been observed with a frequency locked onto an exact fraction e.g. $\frac{1}{2}$, $\frac{1}{3}$, $\frac{1}{4}$.. of the rotor running frequency. This whirl is probably a consequence of non-linear force characteristics of the oil film. Since the analytical approach

used in the present work assumes that the oil film forces are linear with respect to journal displacement and velocity, this type of whirl could not be predicted. The whirl was observed experimentally but only on rare occasions.

PART 1

Dynamic force characteristics of hydrodynamic journal bearings and of flexible rotors

CHAPTER 1

Hydrodynamic oil pressure force on statically loaded and dynamically loaded rotating journals

The purpose of this chapter is to concisely review those parts of hydrodynamic journal bearing theory which describe the unique ability of these bearings to support static and dynamic transverse loads.

A brief description of journal bearing operation and of the theory of the oil pressure forces on a statically loaded rotating journal are preludes to the dynamic case which is more fully discussed and to the theory of which a contribution is made.

1.1. Hydrodynamic lubrication of plain cylindrical journal bearings

1.1 - 1 Nature of hydrodynamic journal bearing lubrication.

It usually surprises the uninitiated to learn that a transversely loaded journal which is rapidly rotating in a cylindrical bearing, to the clearance of which is supplied an appropriately viscous fluid, drags the fluid around and underneath it in such a way that the journal literally floats upon a film of fluid as shown diagrammatically in Fig. 1.1.

The surprise is natural. In fact the primary purpose of the fluid isusually to reduce the friction between journal and bearing caused by their relative motion under heavy transverse loading. The designers of early journal bearings realised that this end was achieved basically by making the mating surfaces slippery For low speed, high load, poorly machined bearings the reasoning is sound, for oils and greases are much more efficient for that purpose than other non-slippery substances. These greasy lubricants are characterised by long chain molecular structures and operate chiefly by slightly separating the surfaces in relative motion so that the lubricant molecules are sheared thereby reducing the mutual shearing of surface protrusions which appears to be the mechanism of dry friction. The improvement is known as boundary lubrication.

When shafts with well machined, lightly loaded journals began operating at high speeds it became evident that new factors were coming into play and experimental investigation of the system by Towers in 1883 (ref. 1) and 1886 (ref. 2) revealed the situation described at the beginning of this section. In a paper in 1886 (ref. 3) Reynolds explained the mechanism by which pressure was generated in a viscous fluid if

it was sheared into a converging wedge between two surfaces in relative motion. In the case of a journal bearing the converging wedge is formed in the clearance between the journal and bearing from $\theta = 0$ to $\theta = \pi$. and the relative motion is caused by the journal's rotation.

Due to the formation of this self-generated pressure film, journal bearings offer at least three major advantages to the designers of bearings for heavy, high speed rotors:

1. Low friction (mainly because of the relatively large separation of the moving surfaces).

2. Low peak load stress (since the journal load is carried over the whole of the projected bearing area).

3. Favourable dynamic properties (with the exception of problems of stability).

The present work is restricted to the nature of this third advantage for the appreciation of which Reynold's equation is an almost inevitable starting point.

1.1 - 2 Reynold's equation.

Reynold's equation may be derived from first principles or from the Navier-Stokes equations (ref 4).

For the case of a laminar, incompressible lubricant and the journal bearing configuration of Fig 1.1, a general practical form of the equation is:

$$\frac{1}{R^2}\frac{\partial}{\partial\theta}\left(\frac{h^3}{\eta}\cdot\frac{\partial p}{\partial\theta}\right) + \frac{\partial}{\partial z}\left(\frac{h^3}{\eta}\frac{\partial p}{\partial z}\right) = 6\omega_s\frac{\partial h}{\partial\theta} + 12\,V \qquad (1.1)$$

To arrive at this equation several assumptions are necessary and most of these are well justified by the fact that usually $\frac{2c}{d} < \frac{1}{1000}$.

The significance of the equation for bearing load carrying analysis is that it implicitly relates the pressure generated at any point in the oil film to the major bearing variables. If this relation could be made explicit, the total oil pressure force on the journal could be obtained by integrating the pressure profile circumferentially around and axially across the oil film.

The oil frictional forces are negligible compared with the oil pressure forces since they are usually of the order of $\frac{2c}{d}$ smaller than them (ref. 5).

A serious restriction of the theory from the point of view of the design of bearings for the largest

turbo-alternators, most of which operate with turbulent oil films, is that the analysis of the turbulent equations corresponding to equation 1.1 is at an early stage of development.

Since it will become apparent that a satisfactory analysis of the dynamic behaviour of journals in hydrodynamic bearings depends on a correct static analysis, a short review of the state of the theory on static operation follows. The reader is also referred to a recent general review by Barwell (ref.39).

1.2. Hydrodynamic oil pressure force on a statically loaded rotating journal

In this case V = o in equation 1.1 which becomes

$$\frac{1}{R^2}\frac{\partial}{\partial\theta}\left(\frac{h^3}{\eta}\frac{\partial p}{\partial\theta}\right) + \frac{\partial}{\partial z}\left(\frac{h^3}{\eta}\frac{\partial p}{\partial z}\right) = 6\omega_s\frac{\partial h}{\partial\theta} \qquad (1.2)$$

There is no closed form solution of equation 1.2. The approach has therefore been either to solve simple special cases of equation 1.2 analytically or to use numerical methods to solve the full equation.

1.2 - 1 Analytical solution of simple special cases of Reynold's equation.

Much analytical work has been confined to two special cases of equation 1.2 which are associated with the names of Sommerfelt (ref. 6) and Ockvirk (ref. 7) respectively.

If a bearing is assumed to be so long that the pressure gradient in the axial direction is negligible i.e. $\frac{dp}{dz} \doteq 0$, equation 1.2 becomes:

$$\frac{1}{R^2} \frac{d}{d\theta} \left(\frac{h^3}{\eta} \frac{dp}{d\theta} \right) = 6\omega \frac{dh}{d\theta} \qquad (1.3)$$

Alternatively, if the bearing is assumed to be so short that the flow due to the pressure gradients in the circumferential direction is negligible when compared with circumferential shear flow and axial pressure flow, i.e. $\frac{1}{R^2} \frac{\partial}{\partial \theta} \left(\frac{h^3}{\eta} \frac{\partial p}{\partial \theta} \right) = 0$, equation 1.2 becomes:

$$\frac{\partial}{\partial z} \left(\frac{h^3}{\eta} \frac{\partial p}{\partial z} \right) = 6\omega \frac{dh}{d\theta} \qquad (1.4)$$

Both equation 1.3 and equation 1.4 are readily integrated and have been most useful in providing a simple approximate description of journal bearing operation. The integrations yield dimensionless load numbers which are functions of the variables influencing the bearing running condition and relate the steady load on a journal to the equilibrium running position of the journal centre. For the long bearing case:

Sommerfelt number, $S = \frac{W}{ld} \cdot \frac{2\pi}{\eta\omega_r}\left(\frac{2c}{d}\right)^2$ ——— (1.5)

while for the short bearing case:

Ockvirk load number, $N_L = \frac{W}{ld} \cdot \frac{2\pi}{\eta\omega_r}\left(\frac{2c}{d}\right)^2 \left(\frac{d}{l}\right)^2$ — (1.6)

$\left(\frac{l}{d} \leq 1\right)$

Some solutions are based on interpolations between these two limiting cases. For example using a procedure due to Galerkin and making a simplifying assumption about the axial pressure profile, Korovschinski (ref. 8) has obtained such a solution.

1.2 - 2 Numerical solutions of Reynold's equation.

Solutions of equation 1.2 by reiterative or relaxation methods have been given by Cameron & Wood (ref.40), Sassenfeld & Walther (ref.41) and Pinkus & Sternlicht (ref. 4). The results of these methods are as accurate as any available at present.

Potentially an even more accurate method is that of Motosh (ref. 9). Although a large amount of numerical work is involved, by taking acount of the circumferential variation of lubricant viscosity this method overcomes a basic defect of all the other methods.

1.2 - 3 Uncertainty of circumferential extent of oil film pressure.

No matter what method has been used for the solution of the oil pressure profile in bearings of finite width the circumferential extent of the oil film pressure, that is the location of θ_1 and θ_2, has been a matter for considerable conjecture. For if it is assumed that a laminar flow of lubricant fills the clearance, equation 1.2 normally requires the lubricant to supply a negative (with respect to atmosphere) pressure over part of the diverging clearance space. While there is some experimental evidence to suggest that small negative pressures can occur, for example recently in (ref. 10), the measured pressure distribution usually resembles that shown in Fig. 1.1.

That the literature contains solutions with a wide variety of assumptions about the film extent is shown by the selection given in Table 1, Fig. 1.7. The eccentricity/attitude and load/eccentricity relations corresponding to some of these assumptions are compared in Fig. 1.2 and Fig. 1.3 respectively.

1.3. Hydrodynamic pressure force on a dynamically loaded rotating journal

1.3 - 1 Nature of the problem.

The work on oil pressure forces on transversely moving journals may be divided into those studies in which the journal amplitude is of the same order as the bearing clearance and into those in which the amplitude is much smaller than the bearing clearance.

The former case is particularly of application to the design of big end bearings for reciprocating engines and is characterised by the fact that the whole oil regime usually rotates with the journal. Since this problem is of considerable mathematical complexity because of the highly non-linear form of the oil forces, early approaches were directed at calculating the transverse displacement of a journal under a given external loading cycle or at calculating the oil force on a journal for a given cycle of journal transverse displacement. This approach avoids taking account of the journal inertia force.

In the next chapter it will be shown that the inertia loadings at the journals of a turbo-alternator rotor are fairly complicated functions of the journal displacements. On the credit side, however, in this problem the chief interest lies in that range of journal

displacements which are small relative to the bearing clearance. For, with the case of out-of-balance excitation, journal amplitudes greater than .001 in are usually considered serious and this compares with bearing radial clearances of up to .010 in. For the purposes of stability analyses, although it would be useful to understand the nature of the fully developed instability, the primary concern of a turbine designer must be to avoid the initiation of any instability - a small amplitude problem. Based on these considerations, linearisation of the oil forces has been taken as the first step towards a satisfactory solution and the theoretical and experimental investigations of this thesis show that the potential of these linearised forces to predict the whirling behaviour of turbo-alternator rotors is great. The reliability of predictions based on the linear oil force approximation must be questionable until the accuracy of the linearisation itself has been justified. The experimental work of this thesis goes some way towards providing evidence for such a justification.

A possibility which the linear oil force analyses cannot reveal is that of non-linear modes of instability. This feature has recently attracted attention in analyses

which take account of simple rotor inertias and include non-linear oil force components. Further reference will be made to these analyses after a review of the work on the linear oil force approach.

1.3 - 2 Linear approximations to the hydrodynamic oil pressure force on a dynamically loaded journal.

In 1926 Hummel (ref.11) suggested a theory for the vibration of rotating journal on an oil film in which, referring to the frames of reference shown in Fig.1.6, the incremental forces F_r, F_s exerted on a journal by an oil film in response to small displacements r, s of the journal from its position of static equilibrium were of the form:

$$\begin{bmatrix} F_r \\ F_s \end{bmatrix} = \begin{bmatrix} a_{rr} & a_{rs} \\ a_{sr} & a_{ss} \end{bmatrix} \begin{bmatrix} r \\ s \end{bmatrix} \qquad (1.7)$$

The a_s, which are calculable from hydrodynamic theory, will be referred to as displacement force coefficients.

Successive improvements of the theory has led to the form:

$$\begin{bmatrix} F_r \\ F_s \end{bmatrix} = \begin{bmatrix} a_{rr} + b_{rr}D & a_{rs} + b_{rs}D \\ a_{sr} + b_{sr}D & a_{ss} + b_{ss}D \end{bmatrix} \begin{bmatrix} r \\ s \end{bmatrix} \qquad (1.8)$$

where the as correspond to those in equation 1.7. The bs, which are also calculable from hydrodynamic theory, will be referred to as velocity force coefficients. The equation is more convenient when expressed in non-dimensional form

$$\frac{c}{W}\begin{bmatrix} F_r \\ F_s \end{bmatrix} = \begin{bmatrix} (\alpha_{rr} + \beta_{rr}\frac{D}{\omega_r}) & (\alpha_{rs} + \beta_{rs}\frac{D}{\omega_r}) \\ (\alpha_{sr} + \beta_{sr}\frac{D}{\omega_r}) & (\alpha_{ss} + \beta_{ss}\frac{D}{\omega_r}) \end{bmatrix}\begin{bmatrix} r \\ s \end{bmatrix} \qquad (1.9)$$

where $\alpha = \frac{c}{W}\, a$

$\beta = \frac{c}{W}\, b.$

In the West an important intermediate step between the two forms was provided by the work of Hagg (ref.12) and Poritsky (ref. 13). The final form has been the basis of the work of several writers: Hori (ref.14), Holmes (refs.15,16), Pinkus & Sternlicht (ref. 4), Lund & Sternlicht (ref.17), Morrison (ref.18) and Morrison & Paterson (ref.19).

In the U.S.S.R. the development of the form is described by Korovschinskii (ref. 8).

Almost all of the above papers were concerned with the problem of unstable oil whirl and it appears that the form equation 1.9 does predict many of the features of the instability that have been observed. However, as shown by the selection of results given in Fig. 1.4

large differences exist between the numerical values suggested for the force coefficients presumably because of the variety of assumptions made when defining the steady running conditions of the bearings.

In this respect, Morrison's contribution (ref.18) is useful since it gives a general form for the displacement force coefficients in terms of steady running bearing data which can be obtained theoretically or experimentally. It also shows that for the short bearing case, simple relations should exist between the velocity force coefficients and the displacement force coefficients, independently of film extent. Direct experimental determination of all eight coefficients had seemed improbable. However, Morrison's work is contributing to the experimental determination of displacement force coefficients being made by Holmes in Loughborough and to the experimental determination of the velocity force coefficients being made by L. Paterson in Glasgow.

It was in the above context that the writer set out to consider the nature of the velocity force coefficients for a long bearing and in particular to try to determine whether in this case, as for the short bearing case, simple relations existed between the velocity and displacement force coefficients. The result of this

work is given in Appendix 1. Briefly, it was found that definition of the oil film extent has a vital effect on two of the sought relations. The most general end conditions used were independent of film extent and suggested that three of the four velocity force coefficients were related to the displacement force coefficients in the same simple way as for the short bearing case. Despite several attempts, no simple relation could be found for the fourth velocity force coefficient.

The above result has already been assumed by Smith (ref.20). The coefficients which he has plotted are probably as good as any available at present and will be used later in this work. The limiting cases of the short and long bearing coefficients are plotted in Fig. 1.5 in terms of axes aligned with the direction of the steady journal transverse load. In this form the coefficients are more useful for general rotor/bearing analyses than those expressed in terms of axes aligned with the line of centres, the attitude of which changes for different bearing operating conditions. The transfor tion is given in Fig. 1.6.

1.3 - 3 Non-linear approximations to the hydrodynamic oil pressure force on a statically loaded journal.

In the U.S.S.R., Korovschinskii (ref. 8) was probably among the first to seriously question the validity of stability analyses based on the assumption of linear oil force characteristics.

Among early work in the West is the digital investigations of Reddi & Trumpler (ref. 21) and Milne (ref.22). The former took account of the non-linear oil force components of a 360° film in an analysis of the instability of a journal with mass while Milne used in addition the short bearing oil film equations to examine the behaviour of a massless journal under imposed displacement and load cycles.

Jennings & Ockvirk (ref.23) and Huggins (ref.24) have investigated the possibility of using analogue computer methods for taking account of non-linear oil force components. Simplified oil force forms were used in both cases.

The effect of non-linear oil force components in short and long 360° oil films on the stability of a journal with mass has been investigated by digital,

analogue and experimental methods in Loughborough, reported in (refs. 16,5).

Someya (ref.25) has examined the effect of non-linear oil film forces at the stability boundary of a flexible rotor.

The non-linear oil force analyses referred to above have shown that it is possible to take account of non-linear terms in the oil force equations for the whirl analysis of simple journal systems. The experimental work reported with idealised bearings has shown confirmation of the predictions of these analyses, including limitations of the linear oil force theory.

The extent to which it is possible or desirable to take full account of the non-linear oil force components in analyses of the whirling of turbo-alternator systems will be briefly discussed in sect. 5.1.

CHAPTER 2

Receptances at the journals of whirling, flexible rotors

A variety of approaches exist for the analysis of the dynamic behaviour of flexible rotors. The approach adopted will usually be decided by the extent to which account is to be taken of the various rotor imperfections and asymmetries or of the rotor support flexibilities which are always present to some extent in practice. These effects include:

eccentricity of rotor mass centre axis from the rotational centre axis (mass out-of-balance).

lack of straightness of rotor shaft.

asymmetry of transverse bending stiffness at a rotor section (shaft ovality, slots, keyways etc.)

gravitational sag.

internal damping (hysteresis stress effect of rotor material, cramp fits of shrunk on discs.)

flexibility of rotor supports (oil film, bearing housing and housing foundation flexibilities).

Under appropriate conditions, each of these factors can play a dominant part in rotor dynamic behaviour. It turns out that in the case of large turbo-alternator

sets the first and last factors mentioned are usually of primary importance. There are at least two different approaches to the analysis of this problem which take account of these two factors.

One approach is by the transfer matrix method recently set out by Pestel & Leckie (ref.26) and used by Koenig (ref.27). Briefly, this method involves describing the condition of the dynamic system by state vectors while the system's dynamic characteristics are included in point and field matrices. Sequential multiplication of the characteristic matrices and substitution of the restrained components of the state vectors allows solution of the system's behaviour.

An alternative approach is by a receptance method. Some features of this method have been set out in a group of recent papers (refs. 28 , 29 , 30 , 31) where the analyses were largely confined to the behaviour of rotors supported on ideal (defined as clamped, pinned, free or sliding) supports or on elastic supports with rotational symmetry. The general rotor receptances described in the present chapter, although admittedly in a most inconvenient form for general stability analyses, are intended to represent the effective inertia forces at the journals of rotors

supported in any bearings. If the bearing forces are also known in terms of the journal displacements, as in the present case for oil bearings (Chapter 1), the rotor equation of motion can be set up. Derived from these general rotor receptances are receptances corresponding to harmonic motion of a rotor which are intended for the analysis of harmonic rotor motion in any bearings, provided the system is stable, as for the synchronous whirl analyses of Chapter 3. The receptances corresponding to harmonic motion are also of use in certain specialised stability analyses such as in section 5.6 - 2.

The present use of the receptance method relies on the orthogonal properties of the rotor modal matrix corresponding to the natural frequencies of the rotor on simple supports. These modes and frequencies can be determined in a variety of ways e.g. transfer matrix method (ref.26), rotor receptance method (ref.29), flexibility matrix method (ref.32). Although the input data for the first two methods is more readily obtainable than that for the third this is balanced by the fact that the frequency equation for the third method is usually in a convenient form for solution. In a manner suggested to the writer by Morrison, the orthogonal properties of the rotor modal matrix are used to take account of mass out-of-balance and bearing flexibility for a single-span rotor.

The single span case is of considerable practical interest since the rotors of multi-span sets are balanced individually. Additionally, if the transverse flexibility of the couplings of a flexibly coupled multi-span set was of an order of magnitude higher than the rotor flexibilities, then the rotors would scarcely influence each others whirling behaviour. The whirling characteristics of such a set could therefore be analysed by using the receptances of the individual uncoupled rotors.

The analysis is extended to give a method for the calculation of the receptances of multi-span rotors which are, in accordance with modern practice, rigidly coupled. The effect of couplings of intermediate transverse flexibility is not considered.

The receptance concept is considered first of all with respect to simple rotors, which are useful for preliminary studies of mass-out-of-balance and support flexibility.

2.1 Receptances of simple rotors

2.1 - 1 Rigid rotor

The unsymmetrical (with respect to axial mass distribution) rigid rotor shown in Fig. 2.1 is simultaneously rotating about its geometric centre and whirling about its static equilibrium position, the axis joining the origin of the bearings at L and R.

For the purposes of practical dynamic analysis, the rotor has been approximated by n concentrated masses connected by rigid massless shaft lengths. No matter how carefully a rotor is manufactured, in practice it is never possible to ensure that the rotor's mass axis coincides exactly with its geometric axis. In fact the mass axis will normally be fairly randomly displaced by a slight amount relative to the geometric axis and some account of this has been taken by allocating an eccentricity L_i and phase angle ψ_i to each of the concentrated masses of the approximating rotor.

If it is initially assumed that the rotor is free from imperfections including the mass eccentricities, the fact that the rotor is rotating will not effect the inertia loads at its journals due to the whirling. In the vertical plane the inertia load corresponding to mass m_i is:

$$F_{yi} = -D^2 m_i y_i$$

$$= -D^2 m_i \left[\gamma_i y_L + (1 - \gamma_i) y_R\right]$$

where D is the differential operator with respect to time. Thus the total inertia loadings at the journals are:

$$\begin{bmatrix} F_{yL} \\ F_{yR} \end{bmatrix} = -D^2 \begin{bmatrix} \sum_{i=1}^{n} \gamma_i^2 m_i & \sum_{i=1}^{n} \gamma_i (1-\gamma_i) m_i \\ \sum_{i=1}^{n} \gamma_i (1-\gamma_i) m_i & \sum_{i=1}^{n} (1-\gamma_i)^2 m_i \end{bmatrix} \begin{bmatrix} y_L \\ y_R \end{bmatrix} \qquad (2)$$

When the form of the bearing reaction is known the stability of the rotor motion can be investigated.

Let the rotor mass eccentricity now be considered so that at any time the projection of a typical eccentricity in the vertical plane is $L_i \sin(\omega_+ t + \psi_i)$, where ω_+ is the rotational phase velocity of the rotor. Then rotation results in harmonic excitation of the rotor so that, if the system is stable and if the bearing force can be expressed by a function, both of D (or powers of D) and the bearing characteristics, which operates only on the journal displacement vector (a linear force response), the motion will be describable by a linear differential equation, $D = i\omega_+$, and the effective rotor inertia forces in the vertical plane at the rotor journals are:

$$\begin{bmatrix} F_{YL} \\ F_{YR} \end{bmatrix} = \omega_+^2 \begin{bmatrix} \sum \gamma_i^2 M_i & \sum \gamma_i(1-\gamma_i) M_i \\ \sum \gamma_i(1-\gamma_i) M_i & \sum (1-\gamma_i)^2 M_i \end{bmatrix} \begin{bmatrix} Y_L \\ Y_R \end{bmatrix} + \omega_+^2 \begin{bmatrix} \sum_{i=1}^{n} \gamma_i M_i L_i (\sin \omega_+ t + \psi_i) \\ \sum_{i=1}^{n} (1-\gamma_i) M_i L_i (\sin \omega_+ t + \psi_i) \end{bmatrix} \quad \text{——2.2}$$

The matrix operators expressed in terms of D as for equation 2.1 will be referred to as general receptance matrices while those with $D = i\omega_+$ or $D = i\lambda\omega_+$, where λ is real, will be referred to simply as receptance matrices.

Although the full inertia forces at the journals include horizontal components these are clearly similar to vertical components to which attention will be restricted for the sake of brevity.

2.1 - 2 Single mass flexible rotor

In Fig. 2.2 is shown the idealised case of a concentrated mass whirling on a massless flexible shaft about a static equilibrium position which, as for all flexible rotors, is the vertically downwards deflection of the shaft due to gravity. For the present purposes, in dealing with ideal rotors it will be convenient to refer to this datum as a straight line and this will introduce negligible errors. Because the shaft's flexibility allows t rotor to bow when whirling, to evaluate the effective

rotor inertia load at the journals in terms of the journal displacements it is necessary to express the rotor elastic deflection r in terms of the journal displacements. If initially the mass eccentricity is neglected:

$$\begin{bmatrix} F_{YL} \\ F_{YR} \end{bmatrix} = -M D^2(y+r) \begin{bmatrix} \gamma \\ (1-\gamma) \end{bmatrix} = (k_L+k_R) r \begin{bmatrix} \gamma \\ (1-\gamma) \end{bmatrix} \qquad 2.3$$

where (k_L+k_R) is the total stiffness of the shaft at the mass. Thus

$$r = \frac{-mD^2}{(k_L+k_R) + M D^2} y = \frac{-D^2}{\omega_1^2 + D^2} y \qquad 2.4$$

where $\omega_1^2 = \frac{k_L+k_R}{M}$. Hence, eliminating r in equation 2.3

$$\begin{bmatrix} F_{YL} \\ F_{yR} \end{bmatrix} = \frac{-(k_L+k_R) D^2}{\omega_1^2 + D^2} \begin{bmatrix} \gamma^2 & \gamma(1-\gamma) \\ \gamma(1-\gamma) & (1-\gamma)^2 \end{bmatrix} \begin{bmatrix} Y_L \\ Y_R \end{bmatrix} \qquad 2.5$$

If account is taken of the mass eccentricity, then the journal forces in the vertical plane corresponding to a stable harmonic whirl can be expressed as follows, when the bearing response is of the type described in sect. 2.1 - 1:

$$\begin{bmatrix} F_{YL} \\ F_{YR} \end{bmatrix} = \frac{(k_L+k_R)\omega_+^2}{\omega_1^2-\omega_+^2} \begin{bmatrix} \gamma^2 & \gamma(1-\gamma) \\ \gamma(1-\gamma) & (1-\gamma)^2 \end{bmatrix} \begin{bmatrix} Y_L \\ Y_R \end{bmatrix} + \frac{(k_L+k_R)\omega_+^2}{\omega_1^2-\omega_+^2} L \sin\omega_+ t \begin{bmatrix} \gamma \\ 1-\gamma \end{bmatrix} \qquad 2.6$$

where the phase of the mass eccentricity is referred to the x axis.

For the symmetrical case $\gamma = (1-\gamma) = \frac{1}{2}$

$$Y_L = Y_R = Y$$

$$k_L = k_R = k$$

$$\omega_1^2 = \frac{2k}{M}$$

and the equations corresponding to equation 2.5 and equation 2.6 are:

$$F_y = \frac{-k D^2}{\omega_1^2 + D^2} y \qquad 2.7$$

and $$F_y = \frac{k\omega_+^2}{\omega_1^2 - \omega_+^2} (y + L \sin \omega_+ t) \qquad 2.8$$

The phase velocity ω_+ is the one at which the rotor freely vibrates when supported on simple supports and is known as the rotor natural frequency. If the rotor is placed in simple supports ($Y_L = Y_R = 0$) and rotated at its natural frequency ($\omega_+ = \omega_1$) equation 2.6 predicts tha the journal forces will tend to become infinitely large and from this result equation 2.3 predicts that the mass deflection r will also tend to become infinitely large.

When the rotor is mounted in flexible supports ($Y_L \neq 0$, $Y_R \neq 0$) it would appear from equation 2.6 that the same form of result holds. In fact where the support is equivalent to a simple radial spring, the rotor mass will

be supported by the radial spring stiffness in series with the rotor shaft stiffness and this will simply have the effect of lowering the running frequency at which infinitely large amplitudes are predicted.

It is only when account is taken of other of the system's dynamic characteristics such as unusual bearing reactions, equation 1.8, that the theory can explain why it is quite possible for well balanced flexible rotors to run relatively smoothly through the natural frequency range.

2.2 Receptances of single-span flexible rotors

2.2 - 1 Balanced flexible rotor on simple supports.

As a preliminary step towards the analysis of the motion of an unbalanced flexible rotor on flexible supports consider the balanced flexible rotor on simple supports shown in Fig. 2.3. As for the rigid rotor case of section 2.1 - 1, the actual rotor has been approximated by concentrated masses but on this occasion the intervening shaft elements are flexible (a Myklestad rotor ref. 33). For simplicity the analysis is expressed in terms of three masses and of the projection of the system in the vertical plane.

The journal forces are readily obtained in terms of the interspan inertia forces:

$$\begin{bmatrix} F_{YL} \\ F_{YR} \end{bmatrix} = \begin{bmatrix} \gamma_1 & \gamma_2 & \gamma_3 \\ (1-\gamma_1) & (1-\gamma_2) & (1-\gamma_3) \end{bmatrix} \begin{bmatrix} F_{Y1} \\ F_{Y2} \\ F_{Y3} \end{bmatrix} \qquad 2.9$$

The interspan inertia forces are expressible as:

$$\begin{bmatrix} F_{Y1} \\ F_{Y2} \\ F_{Y3} \end{bmatrix} = -D^2 \begin{bmatrix} M_1 r_1 \\ M_2 r_2 \\ M_3 r_3 \end{bmatrix} = \begin{bmatrix} \eta_{11} & \eta_{12} & \eta_{13} \\ \eta_{12} & \eta_{22} & \eta_{23} \\ \eta_{13} & \eta_{23} & \eta_{33} \end{bmatrix}^{-1} \begin{bmatrix} r_1 \\ r_2 \\ r_3 \end{bmatrix} \qquad 2.10$$

where $[\eta]$, the flexibility matrix, can be calculated from the theory of structures and is always symmetrical, by the Reciprocal Theorem. It is easier to work with here than its inverse, the rotor stiffness matrix. From equation 2.10:

$$-\frac{1}{D}2\begin{bmatrix} r_1 \\ r_2 \\ r_3 \end{bmatrix} = \begin{bmatrix} \eta_{11} & \eta_{12} & \eta_{13} \\ \eta_{12} & \eta_{22} & \eta_{23} \\ \eta_{13} & \eta_{23} & \eta_{33} \end{bmatrix}\begin{bmatrix} M_1 r_1 \\ M_2 r_2 \\ M_3 r_3 \end{bmatrix} \qquad \text{2.11}$$

Simplify this equation by

i Putting $-\frac{1}{D}2 = \tau$

ii Following a method described by Morris (ref.32), premultiply both sides by

$$\begin{bmatrix} \sqrt{M}_1 & 0 & 0 \\ 0 & \sqrt{M}_2 & 0 \\ 0 & 0 & \sqrt{M}_3 \end{bmatrix} \qquad \text{2.12}$$

and let $\sqrt{M}_1 \; r_1 = S_1$, $\sqrt{M}_1 \sqrt{M}_2 \; \eta_{12} = \tau_{12}$, $M_1 \eta_{11} = \tau_{11}$ etc. Then equation 2.11 becomes

$$\begin{bmatrix} \tau_{11}-\tau & \tau_{12} & \tau_{13} \\ \tau_{12} & \tau_{22}-\tau & \tau_{23} \\ \tau_{13} & \tau_{23} & \tau_{33}-\tau \end{bmatrix}\begin{bmatrix} S_1 \\ S_2 \\ S_3 \end{bmatrix} = 0 \qquad \text{2.13}$$

The frequency determinant corresponding to equation 2.13 has been called a characteristic value equation and since it frequently occurs in vibration analysis its solution has attracted much attention. Considerable effort used to be required for the solution of such equations but the advent of fast electronic computers has considerably improved the situation. An account of recent methods has been given by Michaelson (ref. 34).

The orthogonal properties of the modes of rotor deflection corresponding to the roots of the characteristic equation are well known and are derived in Appendix 2 for the present context. Because of the symmetry of equation 2.13, the normalised modal matrix is also symmetrical.

Using the orthogonal properties,

$$\begin{bmatrix} \tau & 0 & 0 \\ 0 & \tau & 0 \\ 0 & 0 & \tau \end{bmatrix} = \begin{bmatrix} S_{11} & S_{12} & S_{13} \\ S_{12} & S_{22} & S_{23} \\ S_{13} & S_{23} & S_{33} \end{bmatrix} \begin{bmatrix} \tau & 0 & 0 \\ 0 & \tau & 0 \\ 0 & 0 & \tau \end{bmatrix} \begin{bmatrix} S_{11} & S_{12} & S_{13} \\ S_{12} & S_{22} & S_{23} \\ S_{13} & S_{23} & S_{33} \end{bmatrix} \quad \text{2.14}$$

Substituting equations A.26 and 2.14 into equation 2.13:

$$\begin{bmatrix} \tau_{11}-\tau & \tau_{12} & \tau_{13} \\ \tau_{12} & \tau_{22}-\tau & \tau_{23} \\ \tau_{13} & \tau_{23} & \tau_{33}-\tau \end{bmatrix} \begin{bmatrix} S_1 \\ S_2 \\ S_3 \end{bmatrix} = \begin{bmatrix} S_{11} & S_{12} & S_{13} \\ S_{12} & S_{22} & S_{23} \\ S_{13} & S_{23} & S_{33} \end{bmatrix} \begin{bmatrix} \tau_1-\tau & 0 & 0 \\ 0 & \tau_2-\tau & 0 \\ 0 & 0 & \tau_3-\tau \end{bmatrix} \begin{bmatrix} S_{11} & S_{12} & S_{13} \\ S_{12} & S_{22} & S_{23} \\ S_{13} & S_{23} & S_{33} \end{bmatrix} \begin{bmatrix} S_1 \\ S_2 \\ S_3 \end{bmatrix} =$$

2 15

The characteristic matrix of equation 2.13 has thus been diagonalised. The rotor elastic deflections and hence the journal forces are simple harmonic functions, the amplitudes of which will depend on the initial conditions of the free vibration.

2.2 - 2 Balanced flexible rotor on flexible supports

The same rotor of Fig. 2.3 is shown in Fig. 2.4 whirling in flexible supports at L and R. Since for a turbo-alternator rotor in oil bearings the journal displacements from the static equilibrium position Y_L, Y_R, X_L, X_R, are usually of the same order as the rotor elastic deflection r, analyses based on the assumption of simple supports could conceivably be quite misleading.

Although equation 2.9 still holds, equation 2.10 must be modified to show the effect on the inertia loading of the journal displacements. If mass eccentricities are neglected, then in the vertical plane:

$$\begin{bmatrix} F_{Y1} \\ F_{Y2} \\ F_{Y3} \end{bmatrix} = -D^2 \begin{bmatrix} M_1(r_1 + y_1) \\ M_2(r_2 + y_2) \\ M_3(r_3 + y_3) \end{bmatrix} \qquad \text{2.16}$$

Y_i is simply expressed in terms of Y_L, Y_R. However, to obtain the journal forces F_{yL}, F_{yR} in terms of the journal displacements, that is to obtain the rotor receptance at the journals, the elastic deflections r_i must also be expressed in terms of Y_L, Y_R. This can be done by using the orthogonal modal properties already discussed.

Corresponding to equation 2.11, in the present case:

$$-\frac{1}{D^2}\begin{bmatrix} r_1 \\ r_2 \\ r_3 \end{bmatrix} = \begin{bmatrix} \eta_{11} & \eta_{12} & \eta_{13} \\ \eta_{12} & \eta_{22} & \eta_{23} \\ \eta_{13} & \eta_{23} & \eta_{33} \end{bmatrix} \begin{bmatrix} M_1(r_1 + y_1) \\ M_2(r_2 + y_2) \\ M_3(r_3 + y_3) \end{bmatrix} \qquad \text{2.17}$$

Simplify this equation in the same way as equation 2.11 with now additionally : $\sqrt{M_1}\, Y_1 = u_1$ etc. to obtain:

$$\begin{bmatrix} \tau_{11}-\tau & \tau_{12} & \tau_{13} \\ \tau_{12} & \tau_{22}-\tau & \tau_{23} \\ \tau_{13} & \tau_{23} & \tau_{33}-\tau \end{bmatrix} \begin{bmatrix} S_1 \\ S_2 \\ S_3 \end{bmatrix} = - \begin{bmatrix} \tau_{11} & \tau_{12} & \tau_{13} \\ \tau_{12} & \tau_{22} & \tau_{23} \\ \tau_{13} & \tau_{23} & \tau_{33} \end{bmatrix} \begin{bmatrix} u_1 \\ u_2 \\ u_3 \end{bmatrix} \qquad \text{2.18}$$

Substitute equation A2.6 in equation2.18 to obtain the equation corresponding to equation 2.15:

$$\begin{bmatrix} s_{11} & s_{12} & s_{13} \\ s_{12} & s_{22} & s_{23} \\ s_{13} & s_{23} & s_{33} \end{bmatrix} \begin{bmatrix} \tau_1-\tau & 0 & 0 \\ 0 & \tau_2-\tau & 0 \\ 0 & 0 & \tau_3-\tau \end{bmatrix} \begin{bmatrix} s_{11} & s_{12} & s_{13} \\ s_{12} & s_{22} & s_{23} \\ s_{13} & s_{23} & s_{33} \end{bmatrix} \begin{bmatrix} s_1 \\ s_2 \\ s_3 \end{bmatrix} =$$

$$-\begin{bmatrix} s_{11} & s_{12} & s_{13} \\ s_{12} & s_{22} & s_{23} \\ s_{13} & s_{23} & s_{33} \end{bmatrix} \begin{bmatrix} \tau_1 & 0 & 0 \\ 0 & \tau_2 & 0 \\ 0 & 0 & \tau_3 \end{bmatrix} \begin{bmatrix} s_{11} & s_{12} & s_{13} \\ s_{12} & s_{22} & s_{23} \\ s_{13} & s_{23} & s_{33} \end{bmatrix} \begin{bmatrix} u_1 \\ u_2 \\ u_3 \end{bmatrix} \qquad 2.1$$

By premultiplications of each side, equation 2.19 reduces to

$$\begin{bmatrix} s_1 \\ s_2 \\ s_3 \end{bmatrix} = \begin{bmatrix} s_{11} & s_{12} & s_{13} \\ s_{12} & s_{22} & s_{23} \\ s_{13} & s_{23} & s_{33} \end{bmatrix} \begin{bmatrix} \frac{\tau_1}{\tau-\tau_1} & 0 & 0 \\ 0 & \frac{\tau_2}{\tau-\tau_2} & 0 \\ 0 & 0 & \frac{\tau_3}{\tau-\tau_3} \end{bmatrix} \begin{bmatrix} s_{11} & s_{12} & s_{13} \\ s_{12} & s_{22} & s_{23} \\ s_{13} & s_{23} & s_{33} \end{bmatrix} \begin{bmatrix} u_1 \\ u_2 \\ u_3 \end{bmatrix}$$

$$\qquad\qquad\qquad\qquad\qquad\qquad\qquad\qquad\qquad\qquad\qquad\qquad\qquad\qquad\qquad\qquad 2.2($$

Using the orthogonal properties of the modal matrices:

$$\begin{bmatrix} u_1 \\ u_2 \\ u_3 \end{bmatrix} = \begin{bmatrix} S_{11}S_{12}S_{13} \\ S_{12}S_{22}S_{23} \\ S_{13}S_{23}S_{33} \end{bmatrix} \begin{bmatrix} 1 & 0 & 0 \\ 0 & 1 & 0 \\ 0 & 0 & 1 \end{bmatrix} \begin{bmatrix} S_{11}S_{12}S_{13} \\ S_{12}S_{22}S_{27} \\ S_{13}S_{23}S_{33} \end{bmatrix} \begin{bmatrix} u_1 \\ u_2 \\ u_3 \end{bmatrix} \qquad 2.21$$

Adding equation 2.20 and equation 2.21:

$$\begin{bmatrix} S_1+u_1 \\ S_2+u_2 \\ S_3+u_3 \end{bmatrix} = \begin{bmatrix} S_{11}S_{12}S_{13} \\ S_{12}S_{22}S_{23} \\ S_{13}S_{23}S_{33} \end{bmatrix} \begin{bmatrix} \frac{\tau}{\tau-\tau_1} & 0 & 0 \\ 0 & \frac{\tau}{\tau-\tau_2} & 0 \\ 0 & 0 & \frac{\tau}{\tau-\tau_3} \end{bmatrix} \begin{bmatrix} S_{11}S_{12}S_{13} \\ S_{12}S_{22}S_{23} \\ S_{13}S_{23}S_{33} \end{bmatrix} \begin{bmatrix} u_1 \\ u_2 \\ u_3 \end{bmatrix} \qquad 2.22$$

Using equation 2.12:

$$\begin{bmatrix} r_1+y_1 \\ r_2+y_2 \\ r_3+y_3 \end{bmatrix} = \begin{bmatrix} \frac{1}{\sqrt{m_1}} & 0 & 0 \\ 0 & \frac{1}{\sqrt{m_2}} & 0 \\ 0 & 0 & \frac{1}{\sqrt{m_3}} \end{bmatrix} \begin{bmatrix} S_{11}S_{12}S_{13} \\ S_{12}S_{22}S_{23} \\ S_{13}S_{23}S_{33} \end{bmatrix} \begin{bmatrix} \frac{\tau}{\tau-\tau_1} & 0 & 0 \\ 0 & \frac{\tau}{\tau-\tau_2} & 0 \\ 0 & 0 & \frac{\tau}{\tau-\tau_3} \end{bmatrix} \begin{bmatrix} S_{11}S_{12}S_{13} \\ S_{12}S_{22}S_{23} \\ S_{13}S_{23}S_{33} \end{bmatrix} \begin{bmatrix} M_1 & 0 & 0 \\ 0 & \sqrt{m_2} & 0 \\ 0 & 0 & \sqrt{m_3} \end{bmatrix} \begin{bmatrix} y_1 \\ y_2 \\ y_3 \end{bmatrix} \qquad 2.23$$

Using equation 2.16:

$$\begin{bmatrix} F_{y1} \\ F_{y2} \\ F_{y3} \end{bmatrix} = \begin{bmatrix} \sqrt{m_1} & 0 & 0 \\ 0 & \sqrt{m_2} & 0 \\ 0 & 0 & \sqrt{m_3} \end{bmatrix} \begin{bmatrix} S_{11}S_{12}S_{13} \\ S_{12}S_{22}S_{23} \\ S_{13}S_{23}S_{33} \end{bmatrix} \begin{bmatrix} \frac{1}{\tau-\tau_1} & 0 & 0 \\ 0 & \frac{1}{\tau-\tau_2} & 0 \\ 0 & 0 & \frac{1}{\tau-\tau_3} \end{bmatrix} \begin{bmatrix} S_{11}S_{12}S_{13} \\ S_{12}S_{22}S_{23} \\ S_{13}S_{23}S_{33} \end{bmatrix} \begin{bmatrix} \sqrt{m_1} & 0 & 0 \\ 0 & \sqrt{m_2} & \\ 0 & 0 & \sqrt{m_3} \end{bmatrix} \begin{bmatrix} y_1 \\ y_2 \\ y_3 \end{bmatrix} \qquad 2.24$$

That is:

$$\begin{bmatrix} F_{Y1} \\ F_{Y2} \\ F_{Y3} \end{bmatrix} = \begin{bmatrix} U_{11} & U_{12} & U_{13} \\ U_{21} & U_{22} & U_{23} \\ U_{31} & U_{32} & U_{33} \end{bmatrix} \begin{bmatrix} Y_1 \\ Y_2 \\ Y_3 \end{bmatrix} \qquad \text{2.25}$$

where

$$U_{jk} = \sqrt{M_j}\ \sqrt{M_k} \sum_{i=1}^{3} \left(\frac{S_{ji}\ S_{ki}}{\tau - \tau_i} \right) \qquad \text{2.26}$$

Substituting for Y_i in equation 2.25 from Fig.24 and then substituting equation 2.25 in equation 2.9:

$$\begin{bmatrix} F_{YL} \\ F_{YR} \end{bmatrix} = \begin{bmatrix} \gamma_1 & \gamma_2 & \gamma_3 \\ (1-\gamma_1) & (1-\gamma_2) & (1-\gamma_3) \end{bmatrix} \begin{bmatrix} U_{11} & U_{12} & U_{13} \\ U_{21} & U_{22} & U_{23} \\ U_{31} & U_{32} & U_{33} \end{bmatrix} \begin{bmatrix} \gamma_1 & (1-\gamma_1) \\ \gamma_2 & (1-\gamma_2) \\ \gamma_3 & (1-\gamma_3) \end{bmatrix} \begin{bmatrix} Y_L \\ Y_R \end{bmatrix}$$

$$= \begin{bmatrix} \left\{ \frac{W_1^2}{\tau-\tau_1} + \frac{W_2^2}{\tau-\tau_2} + \frac{W_3^2}{\tau-\tau_3} \right\} & \left\{ \frac{W_1 V_1}{\tau-\tau_1} + \frac{W_2 V_2}{\tau-\tau_2} + \frac{W_3 V_3}{\tau-\tau_3} \right\} \\ \left\{ \frac{W_1 V_1}{\tau-\tau_1} + \frac{W_2 V_2}{\tau-\tau_2} + \frac{W_3 V_3}{\tau-\tau_3} \right\} & \left\{ \frac{V_1^2}{\tau-\tau_1} + \frac{V_2^2}{\tau-\tau_2} + \frac{V_3^2}{\tau-\tau_3} \right\} \end{bmatrix} \begin{bmatrix} Y_L \\ Y_R \end{bmatrix} \qquad \text{2.27}$$

where $W_i = \sum_{h=1}^{3} S_{hi}\ \gamma_h \sqrt{M_h}$, $V_i = \sum_{h=1}^{3} S_{hi}(1-\gamma_h)\ \sqrt{M_h}$ ——— 2.28

or finally:

$$\begin{bmatrix} F_{YL} \\ F_{YR} \end{bmatrix} = \begin{bmatrix} P_{LL} & P_{LR} \\ P_{RL} & P_{RR} \end{bmatrix}_2 \begin{bmatrix} Y_L \\ Y_R \end{bmatrix} \qquad 2.29$$

where $$P_{LL} = \sum_{i=1}^{3} \frac{W_i}{(\tau - \tau_i)}$$

$$P_{RR} = \sum_{i=1}^{3} \frac{V_i^2}{(\tau - \tau_i)} \qquad 2.30$$

and $$P_{LR} = P_{RL} = \sum_{i=1}^{3} \frac{W_i V_i}{(\tau - \tau_i)}$$

$[P]$ is the general rotor receptance matrix at its journals.

2.2 - 3 Unbalanced flexible rotor on flexible supports.

If account is taken of the rotor mass eccentricities, the system is assumed stable and the rotor is supported on the type of bearings described in section 2.1 - 1, due to harmonic excitation caused by rotation, $D = i\omega$ and the equation corresponding to equation 2.17 is:

$$\frac{1}{\omega_*^2}\begin{bmatrix} r_1 \\ r_2 \\ r_3 \end{bmatrix} = \begin{bmatrix} \eta_{11} & \eta_{12} & \eta_{13} \\ \eta_{12} & \eta_{22} & \eta_{23} \\ \eta_{13} & \eta_{23} & \eta_{33} \end{bmatrix} \begin{bmatrix} M_1(r_1 + Y_1 + L_1 \sin(\omega_* t + \psi_1)) \\ M_2(r_2 + Y_2 + L_2 \sin(\omega_* t + \psi_2)) \\ M_3(r_3 + Y_3 + L_3 \sin(\omega_* t + \psi_3)) \end{bmatrix}$$

2.31

In this case the equation corresponding to equation 2.27 is :

$$\begin{bmatrix} F_{YL} \\ F_{YR} \end{bmatrix} = \begin{bmatrix} \left\{\frac{W_1^2}{\frac{1}{\omega_*^2}-\tau_1} + \frac{W_2^2}{\frac{1}{\omega_*^2}-\tau_2} + \frac{W_3^2}{\frac{1}{\omega_*^2}-\tau_3}\right\} & \left\{\frac{W_1V_1}{\frac{1}{\omega_*^2}-\tau_1} + \frac{W_2V_2}{\frac{1}{\omega_*^2}-\tau_2} + \frac{W_3V_3}{\frac{1}{\omega_*^2}-\tau_3}\right\} \\ \left\{\frac{W_1V_1}{\frac{1}{\omega_*^2}-\tau_1} + \frac{W_2V_2}{\frac{1}{\omega_*^2}-\tau_2} + \frac{W_3V_3}{\frac{1}{\omega_*^2}-\tau_3}\right\} & \left\{\frac{V_1^2}{\frac{1}{\omega_*^2}-\tau_1} + \frac{V_2^2}{\frac{1}{\omega_*^2}-\tau_2} + \frac{V_3^2}{\frac{1}{\omega_*^2}-\tau_3}\right\} \end{bmatrix} \begin{bmatrix} Y_L \\ Y_R \end{bmatrix}$$

$$+ \begin{bmatrix} W_1W_2W_3 \\ V_1V_2V_3 \end{bmatrix} \begin{bmatrix} \frac{1}{\frac{1}{\omega_*^2}-\tau_1} & 0 & 0 \\ 0 & \frac{1}{\frac{1}{\omega_*^2}-\tau_2} & 0 \\ 0 & 0 & \frac{1}{\frac{1}{\omega_*^2}-\tau_3} \end{bmatrix} \begin{bmatrix} \sqrt{M_1}\,S_{11} & \sqrt{M_2}\,S_{12} & \sqrt{M_3}\,S_{13} \\ \sqrt{M_1}\,S_{12} & \sqrt{M_2}\,S_{22} & \sqrt{M_3}\,S_{23} \\ \sqrt{M_1}\,S_{13} & \sqrt{M_2}\,S_{23} & \sqrt{M_3}\,S_{33} \end{bmatrix} \begin{bmatrix} L_1 \sin(\omega_* t + \psi_1) \\ L_2 \sin(\omega_* t + \psi_2) \\ L_3 \sin(\omega_* t + \psi_3) \end{bmatrix}$$

i.e.
$$\begin{bmatrix} F_{YL} \\ F_{YR} \end{bmatrix} = \begin{bmatrix} p_{LL} & p_{LR} \\ p_{RL} & p_{RR} \end{bmatrix} \begin{bmatrix} Y_L \\ Y_R \end{bmatrix} + \begin{bmatrix} q_{L1} & q_{L2} & q_{L3} \\ q_{R1} & q_{R2} & q_{R3} \end{bmatrix} \begin{bmatrix} L_1 \sin(\omega_* t + \psi_1) \\ L_2 \sin(\omega_* t + \psi_2) \\ L_3 \sin(\omega_* t + \psi_3) \end{bmatrix}$$

2.32

where $p_{LL} = \sum_{i=1}^{3} \frac{W_i^2}{(\frac{1}{\omega_i^2} - \tau_i)}$ and $q_{Lk} = \sqrt{M_k} \sum_{i=1}^{3} \frac{W_i S_{ki}}{(\frac{1}{\omega_i^2} - \tau_i)}$

$p_{RR} = \sum_{i=1}^{3} \frac{V_i}{(\frac{1}{\omega_i^2} - \tau_i)}$ ——————— 2 33

$p_{LR} = p_{RL} = \sum_{i=1}^{3} \frac{W_i V_i}{(\frac{1}{\omega_i^2} - \tau_i)}$ $q_{Rk} = \sqrt{M_k} \sum_{i=1}^{3} \frac{V_i S_{ki}}{(\frac{1}{\omega_i^2} - \tau_i)}$

$[p]$ is the rotor receptance matrix at its journals for harmonic motion.

2.3 Receptances of multi-span flexible rotors

The analysis is confined to rigidly coupled multi-mass, multi-span flexible rotors, free from imperfections and whirling freely on flexible bearings, such as the one shown diagrammatically in vertical projection in Fig. 2.5.

In Appendix 3 a summary is given of the application of the well known Moment Distribution method to the calculation of the influence coefficients of a rigidly coupled, multi-span rotor on flexible supports. There are other methods. What is relevant for the following analysis is that any method will produce a result of the following form:

$$\underset{\sim}{r} = [\eta]\underset{\sim}{F} + [\zeta]\underset{\sim}{Y} \qquad \text{2.34}$$

where

$\underset{\sim}{r}$ is the rotor elastic deflection vector

$[\eta]$ is the rotor flexibility matrix (defined in Appendix 3)

$\underset{\sim}{F}$ is the rotor inertia force vector

$[\zeta]$ is the journal displacement matrix (defined in Appendix 3)

$\underset{\sim}{Y}$ is the journal displacement vector

Now $$\underset{\sim}{F} = \frac{1}{\tau}\left([M]\ (\underset{\sim}{r} + \underset{\sim}{Y}_m)\right) \qquad \text{2.35}$$

where

$$\tau = -\frac{1}{D^2}$$

$[M]$ is the rotor mass matrix

$\underset{\sim}{Y}_M$ is the displacement vector describing displacements at the masses due directly to the journal displacements $\underset{\sim}{Y}$.

And $$\underset{\sim}{Y}_M = [\gamma]\underset{\sim}{Y} \qquad \text{2.36}$$

where $[\gamma]$ is a matrix describing the axial positions of the masses on the rotor shaft.

Substituting equation 2.36 and equation 2.35 into equation 2.34:

$$\underset{\sim}{r} = \frac{1}{\tau}[\eta]\left([M]\underset{\sim}{r} + [M][\gamma]\underset{\sim}{\chi}\right) + [\zeta]\underset{\sim}{\chi}$$

$$\therefore \tau\left(\underset{\sim}{r} - [\zeta]\chi\right) = [\eta]\left([M]\underset{\sim}{r} + [M][\gamma]\underset{\sim}{\chi}\right) \qquad \text{2.37}$$

Premultiply both sides of equation 2.37 by the diagonal matrix $[\sqrt{M}]$ corresponding to equation 2.12 and let

$$[\sqrt{M}]\underset{\sim}{r} = \underset{\sim}{s},$$

$$[\sqrt{M_j}]\,[\sqrt{M_k}]\,[\eta_{jk}] = [\tau_{jk}] \quad \text{etc.}$$

corresponding to equation 2.13. Then equation 2.37 becomes:

$$\tau\left(\underset{\sim}{s} - [\sqrt{M}][\zeta]\underset{\sim}{\chi}\right) = [\tau_{jk}]\left(\underset{\sim}{s} + [\sqrt{M}][\gamma]\underset{\sim}{\chi}\right)$$

$$\text{i.e. } \tau\left(\underset{\sim}{s} - [\sqrt{M}][\zeta]\underset{\sim}{\chi}\right) = [\tau_{jk}]\left(\underset{\sim}{s} - [\sqrt{M}][\zeta]\underset{\sim}{\chi} + [\sqrt{M}][\zeta+\gamma]\underset{\sim}{\chi}\right)$$

$$\qquad \text{2.38}$$

Then equation 2.38 is of the form

$$\tau[\underset{\sim}{S}] = [\tau_{jk}]\left(\underset{\sim}{S} + \underset{\sim}{U}\right)$$

where $[\underset{\sim}{S}] = \left(\underset{\sim}{s} - [\sqrt{M}][\zeta]\underset{\sim}{\chi}\right)$

and $[\underset{\sim}{U}] = [\sqrt{M}][\zeta+\gamma]\underset{\sim}{\chi}$

In this form, the coupled rotor solution corresponds to that already discussed for single-span rotors.

$[\tau_{jk}]$ is the mass/flexibility matrix corresponding to simple supports at the rotor journals and thus the first part of the solution of equation 2.38 is to solve for $\underset{\sim}{Y} = 0$. If the coupled rotors have been approximated by a large number of concentrated masses, the solution of the characteristic value problem, $\tau \underset{\sim}{S} = [\tau_{jk}]\underset{\sim}{S}$ may prove awkward. In this event the procedure outlined in Appendix 4 may be useful.

With the matrices corresponding to those in equation 2.22 the solution will be of the form:

$$\underset{\sim}{S} + \underset{\sim}{U} = [S_{jk}]\left[\frac{\tau}{\tau - \tau_i}\right][S_{jk}]\ \underset{\sim}{U} \qquad \text{2.39}$$

Corresponding to equation 2.16, the interspan force vector is thus given by

$$\underset{\sim}{F} = \frac{1}{\tau}\ [\overline{M}]\left(\underset{\sim}{S} + \underset{\sim}{U}\right) \qquad \text{2.40}$$

$$= [\overline{M}][S_{jk}]\left[\frac{1}{\tau - \tau_{jk}}\right][S_{jk}]\ [\overline{M}][\zeta + \gamma]\underset{\sim}{Y}$$

$$= [U][\zeta + \gamma]\ \underset{\sim}{Y} \qquad \text{2.41}$$

where $[U]$ has the same significance as equation 2.25.

Referring to Fig. 2.5, journal forces are expressible in terms of interspan forces and end moements. Thus

$$F_{ai} = \sum_{j=1}^{A}(1-\gamma_{aj})F_{aj} + \sum_{j=1}^{I}\gamma_{aj}F_{ij} - \frac{M_{oa}+M_{ai}}{l_a} + \frac{M_{ai}+M_{in}}{l_i} \qquad \text{2.42}$$

Using equation A 3.1 of Appendix 3 the end moments are expressible in terms of the interspan forces and journal displacements. Thus:

$$M_{ai} = \sum_{j=1}^{A} \omega_i \alpha_{aj} F_{aj} + \sum_{j=1}^{I} \omega_i \alpha_{ij} F_{ij} + \sum_{j=1}^{N} \omega_i \alpha_{nj} F_{nj} + \omega_i \beta_{oa} Y_{oa} + \omega_i \beta_{ai} Y_{ai} + \omega_i \beta_{in} Y_{in} + \omega_i \beta_{no} Y_{no} \qquad 2.43$$

Substituting equation 2.43 into equation 2.42 and collecting terms allows a journal force to be expressed in terms of all the interspan forces and journal displacements. Thus:

$$\underset{\sim}{F}_j = [V] \underset{\sim}{F} + [W] \underset{\sim}{Y}$$

where the $[V]$ and $[W]$ matrices are calculable in terms of the α, β, γ t erms as defined above. Substituting for $\underset{\sim}{F}$ from equation 2.41

$$\underset{\sim}{F}_j = [V][U][\zeta + \gamma] \underset{\sim}{Y} + [W] \underset{\sim}{Y}$$
$$= [P] \underset{\sim}{Y}$$

after addition. $[P]$ is then the general receptance matrix for the multi-span rotor.

Out-of-balance effects could be examined in a way similar to the single span case.

PART 2.

Synchronous oil whirl of flexible rotors.

CHAPTER 3

Theoretical study of synchronous oil whirl

Because of the invariable non coincidence of the mass axis and the rotational axis of a rotor, it has been shown in the preceding chapter that a rotating rotor will always experience synchronous forcing. When the rotor is supported in oil bearings, the forcing will result in a synchronous oil whirl, (also occasionally sub-harmonic whirl.) In practice the problem of minimising the effects of this whirl is usually tackled in both of the following ways.

1. Rotors are individually balanced as well as possible.

2. The frequency response of the assembled rotor system on its supports is designed to be such that the rotor operating speed does not coincide with a resonant condition.

The work of this chapter will suggest methods by which both of these approaches can be improved.

With respect to the first approach, Morrison has pointed out to the writer that the simple nature of the synchronous oil whirl of a rotor predicted by the theory at a rotor speed corresponding to a rotor natural frequency on simple supports suggests a useful method of

rotor balancing.

As far as the writer is aware, the design criteria that have up till now been used as the basis of the second approach are largely empirical. Until recently it would appear that the only resonance calculation carried out was that of the natural frequencies of the rotors on simple supports from which a rough estimate, on the basis of previous field experience, was made of the reduction of these frequencies in practice due to rotor support flexibility. Some attempt to calculate this reduction has since been made by assuming the oil film reaction to be simply that of a simple radial spring as described by Dollin (ref.37). Apart from the approximate nature of the results of this frequency calculation, it is realised that near the resonant conditions, which include the range of greatest interest, the corresponding calculated results of rotor displacement and inertia force are quite wrong due to omission of velocity terms in the oil film response. The work of the first two chapters makes it possible to take full account here of these terms.

In addition to contributing to the above approaches, it will be shown that the linear oil force theory should indicate the relative advantages of different bearing running conditions for the purposes of mitigating the

effects of synchronous forcing.

3.1 Brief historical notes

There has been remarkably little theoretical work in the literature on synchronous oil whirl.

Hagg in 1948 (ref.35) considered the synchronous whirl of a symmetrical, single mass, flexible rotor taking account of direct velocity oil force terms but omitting the cross-coupled displacement and cross-coupled velocity force terms.

Koenig in 1961 (ref.27) used the same bearing force form and also took account of housing mass and flexibility in an analysis of the synchronous whirl of multi-mass, multi-span rotors. The method of analysis is included in the transfer matrix method described by Pestel & Leckie (ref.26).

The effect of the cross-coupled oil force coefficients on synchronous whirl seems to have been considered first by Holmes (ref.15) in 1960 for the rigid rotor case.

The effect of the full oil force form on the synchronous whirl of symmetrical, single-mass, flexible rotors was analysed by Lund & Sternlicht (ref.17) and Morrison (ref.18) in 1962. Lund & Sternlicht's analysis is appropriate for this rotor form and for a calculation

procedure which cannot take account of cross-coupled terms. The cross-coupled terms were eliminated by expressing the equation of motion in terms of the principal axes of the rotor synchronous motion. The extension of the method to unsymmetrical rotor/bearing systems and multi-span systems would appear to be most inconvenient.

In Morrison's method, the motion is expressed very simply in terms of rotor and bearing characteristics so that the effect of modifications to either may be readily calculated. The method has been followed in the following section and extended to predict the motion of a system for which experimental results are given in the next chapter.

An authoritative description of the synchronous problem was included in Smith's paper in 1963 (ref.20) which concentrated on the influence of the bearing characteristics.

Recently Warner & Thoman (ref.36) have calculated the synchronous oil whirl response of symmetrical, single-span, two-mass flexible rotors using the full oil force form. The equations of motion were solved digitally and the paper includes a large number of response charts.

3.2 Solution of the symmetrical, single-span, single-disc flexible rotor taking account of shaft and journal mass

The following analysis is based on Morrison's (ref.18) which did not, however, take account of shaft and journal mass.

It is well known that, for the purposes of vibration calculations near the first natural frequency of a uniform rotor on simple supports, the rotor can be closely approximated by a massless flexible shaft with half the rotor mass concentrated at its centre. For the purposes of oil whirl analysis, journal inertia forces arising from the other half of the rotor mass should be taken account of. To a close approximation this mass, equally divided into two, can be considered as located in the planes of the journals.

3.2 - 1 Analysis

The system to which this analysis applies is diagrammatically illustrated in Fig. 3.1. To correspond to the experimental results of the next chapter, the rotor mass eccentricity is assumed to be confined to the central mass.

The rotor is shown rotating at ω_r^{rad}/sec about its geometric centre and simultaneously whirling at the same

frequency about its static equilibrium position in similar oil bearings at L and R. Because of the symmetry of the system its axial view is simply that given in Fig. 3.2. The equations of motion in terms of one symmetrical half of the rotor are:

$$F_x = -M_1 D^2 x + k(x_c - x) = -M_1 D^2 x - M_2 D^2 x_m \qquad \text{3.1}$$

$$F_y = -M_1 D^2 y + k(y_c - y) = -M_1 D^2 y - M_2 D^2 y_m$$

where F_x, F_y are components of the incremental oil force balancing the rotor inertia force. From the right hand side of equation 3.1:

$$x_c = \frac{k}{k+M_2 D^2} x - \frac{M_2 D^2}{k+M_2 D^2} L \cos \omega_+ t \qquad \text{3.2}$$

$$y_c = \frac{k}{k+M_2 D^2} y - \frac{M_2 D^2}{k+M_2 D^2} L \sin \omega_+ t$$

Substituting equation 3.2 into the middle of equation 3.1:

$$F_x + \left[M_1 D^2 + \frac{k M_2 D^2}{k+M_2 D^2} \right] x = -\frac{k M_2 D^2}{k+M_2 D^2} L \cos \omega_+ t \qquad \text{3.3}$$

$$F_y + \left[M_1 D^2 + \frac{k M_2 D^2}{k+M_2 D^2} \right] y = -\frac{k M_2 D^2}{k+M_2 D^2} L \sin \omega_+ t$$

Simplify equation 3.3 by the following processes:

1 Note that all stable solutions of equation 3.3 must be harmonic with circular frequency ω_+ and hence $D = i\omega_+$.

2 Use the α and β forms given in equation 1.9 to obtain synchronous oil force coefficients as follows:

$$\frac{c}{W} F_x = (\alpha_{xx} + i\beta_{xx})x + (\alpha_{xy} + i\beta_{xy})y = n_{xx}x + n_{xy}y$$

$$\frac{c}{W} F_y = (\alpha_{yx} + i\beta_{yx})x + (\alpha_{yy} + i\beta_{yy})y = n_{yx}x + n_{yy}y$$

3.4

The complex bearing coefficients n are plotted in Fig. 3.3 for the coefficients already plotted in Fig. 1.5 for $\frac{1}{d} = 0, \infty$.

3 Let $\frac{k}{M_1} = \omega_1^2$, $\frac{k}{M_2} = \omega_2^2$

4 Let $\frac{ck}{W}\left[\frac{\omega_+^2}{\omega_1^2} + \frac{\omega_+^2}{\omega_2^2 - \omega_+^2} \right] = p$

and $\frac{ck}{W}\left[\frac{\omega_+^2}{\omega_2^2 - \omega_+^2} \right] = p^1$

where $W = (M_1 + M_2)g$ is the static bearing load.

5 Let $\bar{L} = L \cos \omega_+ t$ be a general forcing action in which case $-i\bar{L} = L \sin \omega_+ t$.

With these steps equations 3.3 simplify to :

$$(n_{xx} - p)x + n_{xy} y = p^1 \bar{L}$$

$$n_{yx} x + (n_{yy} - p)y = - ip^1 \bar{L}$$

$$\therefore x = \frac{\begin{vmatrix} 1 & n_{xy} \\ -i(n_{yy}-p) & \end{vmatrix}}{\begin{vmatrix} (n_{xx}-p) & n_{xy} \\ n_{yx} & (n_{yy}-p) \end{vmatrix}} \qquad p^1\bar{L} = \frac{p^1(p_x-p)}{(p_1-p)(p_2-p)}\bar{L} = \frac{p^1}{p}\frac{p(p_x-p)}{(p_1-p)(p_2-p)}\bar{L}$$

$$\text{and} \quad y = -\frac{\begin{vmatrix} n_{xx}-p & i \\ n_{yx} & 1 \end{vmatrix}}{\begin{vmatrix} (n_{xx}-p) & n_{xy} \\ n_{yx} & (n_{yy}-p) \end{vmatrix}} ip^1\bar{L} = -\frac{p^1(p_y-p)}{(p_1-p)(p_2-p)}i\bar{L} = -\frac{p^1}{p}\frac{p(p_y-p)}{(p_1-p)(p_2-p)}i$$

3.5

where p_1 and p_2 are the solutions of

$$\begin{vmatrix} (n_{xx}-p) & n_{xy} \\ n_{yx} & (n_{yy}-p) \end{vmatrix} = 0$$

and $$p_x = n_{yy} + i\, n_{xy}$$

$$p_y = n_{xx} - i\, n_{yx}$$

The complex values p_1 p_2 p_x p_y, functions only of the bearing running conditions, have been calculated using the synchronous force coefficients of Fig. 3.3 and are plotted in Fig. 3.4.

Solution for $\bar{p} = 1$

For $\frac{M_1}{M_2} \rightarrow 0$, $p \rightarrow p^1$ and $\frac{p^1}{p} \rightarrow 1$. This is the system analysed by Morrison (ref. 18). Equations 3.5 become

$$x = \frac{p(p_x - p)}{(p_1-p)(p_2-p)} \bar{L} \qquad \text{3.6}$$

$$y = - \frac{p(p_y - p)}{(p_1-p)(p_2-p)} i\bar{L}$$

Equation 3.6 can be evaluated graphically from Fig. 3.4 using the method suggested by Morrison viz. for any p value, the amplitudes and phases of (p_x-p), (p_y-p), (p_1-p) and (p_2-p) are directly scaled off and substituted into equation 3.6. At this stage the solution is in the form:

$$x = x_o (\cos \theta_x + i \sin \theta_x) \bar{L}$$

$$y = - y_o (\cos \theta_y + i \sin \theta_y) i\bar{L}$$

From which, simply $x = x_o L \cos (\omega_r t + \theta_x)$ ——— 3.7

$$y = y_o L \sin (\omega_r t + \theta_y)$$

In the above fashion values of x_o, y_o, θ_x and θ_y have been calculated for a wide range of p, $\in$ and $\frac{l}{d}$

and are plotted in Figs 3.5. Although the abcissa p chosen for these and subsequent response diagrams may not present the results in the best form for direct design use, the diagrams are in a convenient form for concisely presenting the theoretical predictions and correlating the later experimental results of synchronous oil whirl.

From equation 3.3 with $M_1 = 0$ the journal forces are given by

$$\frac{c}{W} F_x = p \left[x + L \cos \omega_r t \right] \qquad \text{3.8}$$

$$\frac{c}{W} F_y = p \left[y + L \sin \omega_r t \right]$$

Using equation 3.7, equation 3.8 can be evaluated by calculation or more simply graphically to give:

$$\frac{c}{W} F_x = f_{xo} \cdot L \cos \left(\omega_r t + \theta_{fx} \right) \qquad \text{3.9}$$

$$\frac{c}{W} F_y = f_{yo} \cdot L \sin \left(\omega_r t + \theta_{fy} \right)$$

Values of $f_{xo}, f_{yo} \theta_{fx}$ and θ_{fy} graphically determined for a wide range of $p, \in$ and $\frac{1}{d}$ are plotted in Figs. 3.6. As $p \rightarrow \infty$ the values become indeterminate and the method described in the next section 3.2 - 2 was used. The axes of Figs. 3.6 are convenient, since for a given bearing running condition the ordinate allows a rapid

comparison to be made between the magnitude of the rotating oil forces F_x, F_y and the static load on the bearing W. At the same time, for x = y = o in equation 3.8.

$$\frac{1}{L}\ \frac{c}{W}\ F_x = p \cos \omega_+ t$$

$$\frac{1}{L}\ \frac{c}{W}\ F_y = p \sin \omega_+ t$$

Thus the lines $\frac{1}{L}\frac{c}{W} F_x = \frac{1}{L}\frac{c}{W} F_y = p$ correspond to rotating forces at the simple support type of bearing already discussed in Chapter 2 and described in equation 2.8. Comparison with these lines of the rotating oil film forces in ~~and~~ amplitude and phase gives a clear measure of the beneficial force attenuation properties of the oil film.

From equation 3.2 with $m_1 = o$, the rotor centre displacements are:

$$x_c = \frac{F_x}{k} + x \qquad \text{3.10}$$

$$y_c = \frac{F_y}{k} + y$$

Substituting into equation 3.10 from equation 3.8:

$$x_c = \frac{W}{ck} p \left[\frac{1 + \frac{W}{ck} p}{\frac{W}{ck} p} x + L \cos \omega_+ t \right] \qquad \text{3.11}$$

$$y_c = \frac{W}{ck} p \left[\frac{1 + \frac{W}{ck} p}{\frac{W}{ck} p} y + L \sin \quad t \right]$$

x_c, y_c are thus functions of $\frac{W}{ck}$ as well as p. For a given $\frac{W}{ck}$ it is probably simplest to evaluate x_c, y_c graphically from Figs. 3.5 and Figs. 3.6 using the following form of equation 3.10:

$$x_c = \frac{W}{ck} \frac{c}{W} F_x + x \qquad \text{3.12}$$

$$y_c = \frac{W}{ck} \frac{c}{W} F_y + y$$

Solution for $\frac{p^1}{p} \neq 1$

From equation 3.5 it is clear that for $\frac{p^1}{p} \neq 1$ the journal displacements corresponding to equation 3.6 are

$$x = \frac{p^1}{p} x_o L \cos (\omega_r t + \theta_x) \qquad \text{3.13}$$

$$y = \frac{p^1}{p} y_o L \sin (\omega_r t + \theta_y)$$

That is, the journal displacement phase relations for a particular value of p will be the same as that for the same value of p in the $\frac{p^1}{p} = 1$ case but in the present case the amplitudes will be multiplied by the factor $\frac{p^1}{p}$.

From equation 3.3, the journal forces are:

$$\frac{c}{W} F_x = p \left[x + \frac{p^1}{p} L \cos \omega_r t \right] \qquad \text{3.14}$$

$$\frac{c}{W} F_y = p \left[y + \frac{p^1}{p} L \sin \omega_r t \right]$$

Substituting equations 3.13 into equations 3.14 :

$$\frac{c}{W} F_x = \frac{p^1}{p} p \left[x_o L \cos(\omega_r t + \theta_x) + L \cos \omega_r t \right] \quad \text{3.15}$$

$$\frac{c}{W} F_y = \frac{p^1}{p} p \left[y_o L \sin (\omega_r t + \theta_y) + L \sin \omega_r t \right]$$

If equation 3.15 is compared with the result of substituting equation 3.7 into equation 3.8 it will be seen that, as for the journal displacements, the inertia force phase relations for a particular value of p will be the same as that for the same value of p in the $\frac{p^1}{p} = 1$ case but in the present case the amplitudes will be multiplied by the factor $\frac{p^1}{p}$.

The displacements at the rotor centre, from equation 3.2 are:

$$x_c = \frac{F_x}{k} + x \left(1 - \frac{\omega_r^2}{\omega_1^2}\right) \quad \text{3.16}$$

$$y_c = \frac{F_y}{k} + y \left(1 - \frac{\omega_r^2}{\omega_1^2}\right)$$

Substituting into equation 3.16 from equation 3.14:

$$x_c = \frac{W}{ck} p^1 \left[\frac{1 + \frac{W}{ck} p^1}{\frac{W}{ck} p^1} x + L \cos \omega_r t \right] \quad \text{3.17}$$

$$y_c = \frac{W}{ck} p^1 \left[\frac{1 + \frac{W}{ck} p^1}{\frac{W}{ck} p^1} y + L \sin \omega_r t \right]$$

x_c, y_c are thus functions of $\frac{W}{ck}$ and p^1 as well as p. For a particular case it is probably simplest to use equation 3.16.

3.2 - 2 Rotor running at simply supported natural frequency

As $\omega_s \longrightarrow \omega_1$, $p^1 \longrightarrow p \longrightarrow \infty$ and equation 3.5 shows that

$$x \longrightarrow -\bar{L} = -L\cos\omega_s t \qquad \text{3.18}$$

$$y \longrightarrow i\bar{L} = -L\sin\omega_s t$$

That is, when the rotor on oil bearings with mass eccentricity L is run at a frequency corresponding to its natural frequency on simple supports, the rotor journals move in a circle of radius L precisely 180^o out-of phase with the out-of-balance mass.

As pointed out to the writer by Morrison, this fact and the fact that other forms of rotor running at a natural frequency have a correspondingly simple motion suggests a simple direct method of improving the balance of flexible rotors. Unless other precautions were taken it would not normally be safe to run a poorly balanced rotor at such a speed and therefore a more conventional balancing method could be used first at a lower speed to achieve an appropriate degree of balance.

The oil force on the journal corresponding to its circular synchronous motion is readily obtained from equation 3.4 by substituting equation 3.18.

$$\frac{c}{W} F_x = \left[-(\alpha_{xx} + \beta_{xy}) + i\,(\alpha_{xy} - \beta_{xx})\right] \bar{L} \qquad \text{---} \quad 3.19$$

$$\frac{c}{W} F_y = \left[+\,(\alpha_{yy} - \beta_{yx}) + i\,(\alpha_{yx} + \beta_{yy})\right] i\bar{L}$$

The rotor centre deflections are then obtainable in the usual way.

3.3 General solution by receptance method

The forces required at the journals of a harmonically whirling rotor were expressed in receptance form in Chapter 2.

The oil force on a synchronously whirling journal according to the linear oil force theory is expressed in equation 3.4.

These two results are brought together in this section to show how the synchronous whirl behaviour of a system comprising both of these elements can be predicted. The analysisis illustrated with respect to a single-span rotor.

3.3 - 1 Equations of motion

Consider the out-of-balance rotor shown in Fig. 2.4 whirling in synchronisation with the rotor rotational frequency ω_+. Using equation 2.32 the journal forces are:

$$\begin{bmatrix} F_{xL} \\ F_{yL} \\ F_{xR} \\ F_{yR} \end{bmatrix} = \begin{bmatrix} p_{LL} & 0 & p_{LR} & 0 \\ 0 & p_{LL} & 0 & p_{LR} \\ p_{RL} & 0 & p_{RR} & 0 \\ 0 & p_{RL} & 0 & p_{RR} \end{bmatrix} \begin{bmatrix} X_L \\ Y_L \\ X_R \\ Y_R \end{bmatrix} + \left[\begin{array}{ccc|ccc} q_{L1} & q_{L2} & q_{L3} & 0 & 0 & 0 \\ 0 & 0 & 0 & q_{L1} & q_{L2} & q_{L3} \\ q_{R1} & q_{R2} & q_{R3} & 0 & 0 & 0 \\ 0 & 0 & 0 & q_{R1} & q_{R2} & q_{R3} \end{array}\right] \begin{bmatrix} \bar{L}_1 \\ \bar{L}_2 \\ \bar{L}_3 \\ -i\,\bar{L}_1 \\ -i\,\bar{L}_2 \\ -i\,\bar{L}_3 \end{bmatrix}$$

3.20

where $\bar{L}_i = L_i \cos(\omega_i t + \psi_i)$ are the forcing actions.

Using equation 3.4:

$$\begin{bmatrix} F_{xL} \\ F_{yL} \\ F_{xR} \\ F_{yR} \end{bmatrix} = \begin{bmatrix} \frac{W_L}{c_L} n_{xx} & \frac{W_L}{c_L} n_{xy} & 0 & 0 \\ \frac{W_L}{c_L} n_{yx} & \frac{W_L}{c_L} n_{yy} & 0 & 0 \\ 0 & 0 & \frac{W_R}{c_R} n_{xx} & \frac{W_R}{c_R} n_{xy} \\ 0 & 0 & \frac{W_R}{c_R} n_{yx} & \frac{W_R}{c_R} n_{yy} \end{bmatrix} \begin{bmatrix} X_L \\ Y_L \\ X_R \\ Y_R \end{bmatrix}$$

3.21

where $W_L = \sum_{i=1}^{3} \gamma_i m_i g$, $W_R = \sum_{i=1}^{3} (1-\gamma_i) m_i g$ are the static bearing loads at the left and right of the rotor respectively and c_L, c_R are the corresponding clearances.

Equating equation 3.20 and equation 3.21 the equation of motion is:

$$\begin{bmatrix} \left(\frac{W_L}{c_L} l^n_{xx} - p_{LL}\right) & \frac{W_L}{c_L} l^n_{xy} & -p_{LR} & 0 \\ \frac{W_L}{c_L} l^n_{yx} & \left(\frac{W_L}{c_L} l^n_{yy} - p_{LL}\right) & 0 & -p_{LR} \\ -p_{RL} & 0 & \left(\frac{W_R}{c_R} R^n_{xx} - p_{RR}\right) & \frac{W_R}{c_R} R^n_{xy} \\ 0 & -p_{RL} & \frac{W_R}{c_R} R^n_{yx} & \left(\frac{W_R}{c_R} R^n_{yy} - p_{RR}\right) \end{bmatrix} \begin{bmatrix} x_1 \\ y_1 \\ x_R \\ y_R \end{bmatrix} =$$

$$\begin{bmatrix} q_{L1} & q_{L2} & q_{L3} & 0 & 0 & 0 \\ 0 & 0 & 0 & q_{L1} & q_{L2} & q_{L3} \\ q_{R1} & q_{R2} & q_{R3} & 0 & 0 & 0 \\ 0 & 0 & 0 & q_{R1} & q_{R2} & q_{R3} \end{bmatrix} \begin{bmatrix} \bar{L}_1 \\ \bar{L}_2 \\ \bar{L}_3 \\ -i\bar{L}_1 \\ -i\bar{L}_2 \\ -i\bar{L}_3 \end{bmatrix} \qquad \text{3.22}$$

3.3 - 2 Solution of equations of motion

The solution requires inversion of the complex characteristic matrix on the left hand side of equation 3.22.

As a first step it will usually be convenient to rearrange the equation in order that the matrix to be

inverted is composed of real coefficients. This can be done simply by using a device described by Lanczos (ref. 38), which is apparently not widely known. The method is as follows:

Suppose a complex matrix

$$C = A + i B$$

occurs in an equation

$$Cz = c \quad \text{where } z = x + iy,\ c = a + ib.$$

Then the equation is

$$(A + iB)(x + iy) = a + ib$$

Hence

$$Ax - By = a$$

$$Bx + Ay = b$$

In matrix form

$$\begin{bmatrix} A & -B \\ B & A \end{bmatrix} \begin{bmatrix} x \\ y \end{bmatrix} = \begin{bmatrix} a \\ b \end{bmatrix}$$

Thus a nxn complex matrix can be re-arranged into the form of a 2n x 2n real matrix.

In the present case, the parts of equation 3.22 which correspond to the above illustration are:

$$A = \begin{bmatrix} \frac{W_L}{c_L}\alpha_{xx} & \frac{W_L}{c_L}\alpha_{xy} & 0 & 0 \\ \frac{W_L}{c_L}\alpha_{yx} & \frac{W_L}{c_L}\alpha_{yy} & 0 & 0 \\ 0 & 0 & \frac{W_R}{c_R}\alpha_{xx} & \frac{W_R}{c_R}\alpha_{xy} \\ 0 & 0 & \frac{W_R}{c_R}\alpha_{yx} & \frac{W_R}{c_R}\alpha_{yy} \end{bmatrix} - \begin{bmatrix} p_{LL} & 0 & p_{LR} & 0 \\ 0 & p_{LL} & 0 & p_{LR} \\ p_{RL} & 0 & p_{RR} & 0 \\ 0 & p_{RL} & 0 & p_{RR} \end{bmatrix}$$

$$B = \begin{bmatrix} \frac{W_L}{c_L}\beta_{xx} & \frac{W_L}{c_L}\beta_{xy} & 0 & 0 \\ \frac{W_L}{c_L}\beta_{yx} & \frac{W_L}{c_L}\beta_{yy} & 0 & 0 \\ 0 & 0 & \frac{W_R}{c_R}\beta_{xx} & \frac{W_R}{c_R}\beta_{xy} \\ 0 & 0 & \frac{W_R}{c_R}\beta_{yx} & \frac{W_R}{c_R}\beta_{yy} \end{bmatrix}$$

$$z = \begin{bmatrix} x_L \\ y_L \\ x_R \\ y_R \end{bmatrix} = \begin{bmatrix} x_{LO} & y_{LO} & x_{RO} & y_{RO} \end{bmatrix} \left(\begin{bmatrix} \cos\vartheta_{xL} \\ \cos\vartheta_{yL} \\ \cos\vartheta_{xR} \\ \cos\vartheta_{yR} \end{bmatrix} + i \begin{bmatrix} \sin\vartheta_{xL} \\ \sin\vartheta_{yL} \\ \sin\vartheta_{xR} \\ \sin\vartheta_{yR} \end{bmatrix} \right)$$

$$c = \left(\begin{bmatrix} q_{L1} & q_{L2} & q_{L3} \\ 0 & 0 & 0 \\ q_{R1} & q_{R2} & q_{R3} \\ 0 & 0 & 0 \end{bmatrix} - i \begin{bmatrix} 0 & 0 & 0 \\ q_{L1} & q_{L2} & q_{L3} \\ 0 & 0 & 0 \\ q_{R1} & q_{R2} & q_{R3} \end{bmatrix} \right) \begin{bmatrix} \bar{L}_1 \\ \bar{L}_2 \\ \bar{L}_3 \end{bmatrix}$$

Although the method has been described in terms of a single-span rotor, the analysis applies equally well to multi-span systems. Since the order of the real matrix to be inverted is four times the number of bearings in the system the largest sets in operation with about six rigidly coupled rotors would require the inversion of a 48 x 48 matrix for which appropriately fast digital facilities would be needed.

It can be argued that for the single span case, inversion of the 8 x 8 matrix is practicable using a desk calculating machine, especially if advantage is taken of the following method for inverting a partitioned matrix:

Given the partitioned matrix $\begin{bmatrix} Y_{11} & Y_{12} \\ Y_{21} & Y_{22} \end{bmatrix}$ the problem is to obtain its inverse $\begin{bmatrix} Z_{11} & Z_{12} \\ Z_{21} & Z_{22} \end{bmatrix}$

That is $$\begin{bmatrix} Z_{11} & Z_{12} \\ Z_{21} & Z_{22} \end{bmatrix} \begin{bmatrix} Y_{11} & Y_{12} \\ Y_{21} & Y_{22} \end{bmatrix} = \begin{bmatrix} I & 0 \\ 0 & I \end{bmatrix}$$

where Z is the pre- or post-inverse of Y. After multiplying out:

$$
\begin{aligned}
Z_{11} &= -Z_{12}\, Y_{22}\, Y_{12}^{-1} \\
Z_{12} &= \left[Y_{21} - Y_{22}\, Y_{12}^{-1}\, Y_{11}\right]^{-1} \\
Z_{22} &= -Z_{21}\, Y_{11}\, Y_{21}^{-1} \\
Z_{21} &= \left[Y_{12} - Y_{11}\, Y_{21}^{-1}\, Y_{22}\right]^{-1}
\end{aligned}
\qquad \text{3.23}
$$

This form is particularly suited to the inversion of the present characteristic matrix $\begin{bmatrix} A & -B \\ B & A \end{bmatrix}$

In this case equation 3.23 gives:

$$
\begin{bmatrix} A & -B \\ B & A \end{bmatrix}^{-1} = \begin{bmatrix} \left[AB^{-1}A + B\right]^{-1} AB^{-1} & \left[AB^{-1}A + B\right]^{-1} \\ -\left[AB^{-1}A + B\right]^{-1} & \left[AB^{-1}A + B\right]^{-1} AB^{-1} \end{bmatrix}
$$

Thus, given the 4 x 4 matrices A and B it will be found that the total number of operations with 4 x 4 matrices required for the inversion of the original 8 x 8 matrix is:

1 addition

3 multiplications

2 inversions

Since one of the inversions is simply of B, the bearing velocity force matrix which varies slowly relative to the rotor receptance matrix, it will not be required to invert it often. The final solution is then obtained by multiplying the right hand side of equation 3.22 by the inverted matrix.

CHAPTER 4

Experimental study of synchronous oil whirl.

In the past, information yielded by experimental investigation has played a vital part in the development of hydrodynamic bearing theory, classic examples being the work of Tower (ref. 1,2), Newkirk (ref. 42) and Ockvirk (ref. 7).

The development of the linear oil force theories has suggested valuable possibilities of oil whirl analyses but, although these analyses successfully predict most of the broad qualitative features of oil whirl observed in practice, they are as yet unsupported by specific experimental evidence. Accordingly the systematic experimental investigations described in this Chapter and in Chapter 6 have been designed on the basis of parameters suggested by the linear oil force theory to examine the characteristics of oil whirl and the extent to which these characteristics are adequately described by the theory.

In spite of efforts to cover practical ranges of the whirl parameters, the philosophy behind this experimental work, in common with all similar model experimental work, must be as follows. It cannot be expected that the rig behaviour will correspond precisely to that of a full size

rotor/oil film system, although the difference should not be large. The rig will rather be looked upon as a facility for applying a searching test to theories of the behaviour of full size systems for if the theories cannot adequately predict the behaviour of such simplified systems, the value of applying them to full size systems would seem to be limited to at least the same extent.

After describing the experimental rig, this Chapter presents the results of experiments with two simple flexible rotors during which the rotors were excited by a range of degrees of out-of-balance while supported in a wide variety of journal bearing pairs. Finally the results of the experiments are compared with the theoretical predictions of the previous Chapter and some design implications discussed.

4.1 Brief historical notes

The only published results of synchronous oil whirl experiments of which the writer is aware are those of Hagg & Sankey (refs. 43, 44) and Morrison (ref. 18).

The former authors systematically investigated the synchronous oil whirl of a single loaded journal. Since

the whirl measurements were made with respect to the major and minor axes of the synchronous whirl ellipse direct comparison between their results and those of the present work is not possible.

Morrison's rig comprised a symmetrical flexible rotor supported on similar oil bearings. His experimental results of synchronous oil whirl are confined to the typical behaviour of the rotor during two runs.

4.2 Experimental rig

4.2 - 1 Basis of rig design

Before embarking upon any experimental programme it is most useful to have to hand at least an approximate theoretical analysis of the problem to be studied. Such an analysis should not only suggest the phenomena to be encountered but also define the significant parameters of the system and thus enable the experimental programme to be designed to cover the ranges of practical interest of these parameters.

In the previous Chapter, the application of the linear oil force theory to the analysis of the synchronous oil whirl of a simple flexible rotor has shown that, apart from all being functions of the bearing running condition,

$\frac{x}{L}, \frac{y}{L}$ are functions only of p

$\frac{x_c}{L}, \frac{y_c}{L}$ are functions only of p & $\frac{ck}{W}$

and $\frac{F_x}{W}, \frac{F_y}{W}$ are functions only of p & $\frac{L}{c}$

Thus the theory predicts that the synchronous oil whirl behaviour of this system is describable only in terms of the bearing running condition and the parameters p, $\frac{ck}{W}$, $\frac{L}{c}$. It is relevant to consider what ranges of these parameters correspond to full size rotor operation.

p: With p, the range of interest is clearly extensive. Fig. 3.4 suggests the manner in which the whirl behaviour will change rapidly for a wide range of p from which it was decided that the range would be most efficiently covered by rotor speeds corresponding to the values, p = 1, 3, 6, 10, 20, 100 $\pm \infty$, -100 - 20, -10 -6 -3, -1, if they were attainable.

$\frac{ck}{W}$: The parameter $\frac{ck}{W}$ may be expressed as

$$\frac{ck}{W} = \frac{\text{radial clearance of bearing}}{\text{static deflection of rotor under bearing load}}$$

A physical consideration of this ratio shows that it is unlikely to be either very large or very small and cases outside the range $0.1 \prec \frac{ck}{W} \prec 10$ will be rare. The

majority of practical rotors will have values near the middle of this region and therefore it was decided to restrict the experimental investigation to about

$0.5 \prec \frac{ck}{W} \prec 3$

$\frac{L}{c}$: Practical interest is probably limited to about .1 or .2 but it was decided to cover as wide a range as possible, consistent with preventing rubbing of the journal on the bearing, to investigate the degree of linearity of the journal response.

Ockvirk Load Number N_L : Since it is general practice to operate the bearings of full size machines at fairly high load numbers it was decided to concentrate the experimental effort in the region $6 \prec N_L \prec 18$ corresponding to journal eccentricity ratios of about $.4 \prec \varepsilon \prec .7$ on Ockvirk's experimental curve.

4.2 - 2 Main assembly features

A general view of the experimental rig is given in the photograph, Fig. 4.1.

Drive: The drive was a 3 h.p. synchronous motor working through a hydraulic gear, the output speed of which was infinitely variable within the full motor range. The

gear output was stepped up by means of toothed pulleys to a maximum possible speed of about 8,000 rev/min. In order to interfere as little as possible with the transverse displacements of the experimental rotors, the final drive pulley was coupled to them by means of a $\frac{3}{16}$ in high-tensile steel quill, 8 in. long.

Foundation: The rig foundation consisted of a 12 in x 12 in I beam, the sides of which had been filled in with concrete to make the whole as massive as possible (over 1,000 lb) mounted on two transverse I beams. The possibilities of foundation resonances were investigated and practically eliminated by mounting the assembly on thin rubber pads.

Rotors: The dimensions of both rotors used and their approximating mass distribution are shown in Fig. 4.3.

Each rotor was constructed from a high tensile steel shaft on to which mild steel journals were bolted, the interface being a Morse taper. The journals were detachable to allow access to the shaft to load discs which gripped the shaft by means of tapered bushes. The circumference of each disc was tapped by four $\frac{1}{2}$ in. holes, equally spaced circumferentially, to allow the addition of out-of-balance weights in the form of filed $\frac{1}{2}$ in steel washers.

To find experimentally the natural frequencies of the rotors on simple supports they were excited by a 5 watt vibrator as shown in Fig. 4.4 . The resonance diagrams obtained are given in Fig. 4.5 . The excitation frequency was varied until the excitation and displacement signals were in quadrature. This condition appeared to coincide precisely with the peak displacement amplitude and was taken as the natural frequency condition.

The first natural frequency of Rotor 1 was found to correspond to 3130 rev/min for rotor centre vibration amplitudes of .005 in (peak to peak) and increased to 3160 rev/min for amplitudes of .001 in. Since the former rotor amplitudes were closer to those expected to be of most interest and since the lower frequency values suggested a more ideal support, the value of 3130 rev/min was adopted.

The corresponding values of the first and second natural frequency conditions of Rotor 2 were found to be 1605 rev/min and 5090 rev/min respectively.

In accordance with the suggestions of section 4.2 - 1, values for the rotor natural frequencies had already been obtained by calculation, following the methods of Chapter 2, since these values were the basis of the rotor designs. The value for Rotor 1 was designed to correspond to about

3,000 rev/min so that a wide range of p values could be obtained at realistic bearing running conditions. For this calculation the stiffening effect of the rotor discs could only be estimated and in fact the value obtained for Rotor 1 neglecting the stiffening effect was 2,980 rev/min. Comparing this value with the experimentally determined value of 3130 rev/min, the effective stiffening length of the discs appeared to be about 16% of what it would have been if the discs were integral with the shaft. Using the experimental frequency value and the mass distribution shown in Fig. 4.3, values of p and p^1 were calculated and are given in Fig. 4.6 where the ratio $\frac{p^1}{p}$ is also shown.

Rotor 2 was designed to allow investigation of whirling near a second natural frequency. By using the natural frequency values from the resonance test and the mass distribution given in Fig. 4.3 it was possible to solve for the appropriate flexibility coefficients in this case also. The calculated values of $p_{LL} = p_{RR}$ and $p_{LR} = p_{RL}$ using these results are given in Fig. 4.7.

Bearings: The range of bearing clearances used were chosen with respect to the suggested practical range of the parameter $\frac{ck}{W}$ in the previous section. For Rotor 1,

$$\omega_1^2 = \left(\frac{3130 \times 2\pi}{60}\right)^2 = 107,500$$

$$\therefore \frac{ck}{W} = \frac{\omega_1^2}{g} \cdot c = \frac{107,500}{386} \times c = \frac{c}{.00359}$$

The dimensions of the bearing pairs providing a practical range of $\frac{l}{d}$ values are given in the Table in Fig. 4.8.

The bearings were jig-bored while assembled in their respective housings where they were positively located at a conical interface as shown by the sectional diagram of a typical bearing in Fig. 4.9. All the bearings were 360^{o} cylindrical with an axial oil groove $\frac{1}{2}$ in wide x $\frac{1}{16}$ in deep at the tops coincident with the oil supply hole and running almost the full length of the bearings.

A special pair of alignment bearings were manufactured with a diametral clearance less than .001 in and $\frac{l}{d} = 1$. When each rotor was assembled in the rig for the first time it was supported in these bearings which were rigidly clamped inside their bearing housings. The positions of the housings relative to the foundation was adjusted until the rotor could be rotated freely in the bearings and this condition was maintained while the housings were rigidly bolted to the foundation. Since all the bearing pairs had been bored while clamped in the same position in the housings it was assumed that the alignment for all would be

better than $\tan^{-1}$ .0005.

Lubrication: To obtain the practical values of load number suggested in the previous section, lubricating oils with three different viscosity values were used:

	Absolute Viscosity (cp)	
	at 100°F	at 210°F
Mentor 28	3.7	1.3
Norpol 35	10	3
Norpol 55	90	7

The oils were circulated by a Monopump and supplied to the bearings via a steel tube fitted with a concentric 1½ K.W. immerser (simmerstat controlled), a pressure gauge and a bleed valve. Part or all of the pump output could be diverted to the sump by a relief valve. The lubricants could therefore be supplied to the bearings with a rather limited variation of temperature and pressure.

4.2 - 3 Instrumentation

Oil temperature measurement: The effective lubricant temperature was obtained from three thermocouples inserted in holes 60° apart in the loaded area of each bearing and just under the bearing surfaces. The viscosities used in calculating load numbers were obtained by relating the mean (as between bearings) of the highest temperatures obtained

in the bearings at each speed to the published data of the oil in use.

No attempt was made to measure directly the actual journal eccentricities attained. Such correlation as there is between the observed rotor behaviour and the bearing running condition is purely in terms of the Ockvirk load number which can in practice be calculated.

Rotor Speed measurement: A photo-electric transducer was used to scan sixty white stripes painted on a black back ground on one side of a rotor disc and hence to operate a digital electrical frequency meter. Since the meter displayed the number of pulses/sec received with an accuracy of $\pm$ 1 pulse/sec, the meter reading was a measure of rotor speed in rev/min with an accuracy of $\pm$1rev/min.

Rotor Whirl measurement: Since the writer was not aware of a suitable apparatus on the market for the rapid accurate measurement of the amplitude and phase of a whirling motion, he was forced to spend several weeks on the design, development and construction of one. The apparatus is described in detail in Appendix 5. Briefly, it allows the signals from each of six transducers either to be displayed in pairs to show rotor orbits, or to be displayed singly in

a manner which showed the phase of each signal relative to the out-of-balance excitation.

Recording rotor amplitude and phase: A 35 m.m. oscilloscope camera was used to record the amplitude and phase data obtained and approximately 300 ft of film were exposed and developed by the writer for this purpose. The three traces of the rotor orbits were recorded on the same frame of film by a triple exposure. To avoid superposition of the traces, the oscilloscope bias was used to move them to different positions on the screen. The same device was used for the three vertical signal phase circles and for the three horizontal signal phase circles.

To extract the data, the film negatives were projected on to the screen of a Baty projector. In the absence of graticule lights for the oscilloscope face, a special graticule had been made by the writer and etched with a luminous solution. However, the luminous effect was not strong enough to appear regularly in the negatives and therefore the screen of the Baty projector was aligned and calibrated by projecting on to it a negative of the oscilloscope face taken while it displayed bright vertical and horizontal traces. The projector lens used resulted

in a scale magnification of the oscilloscope face of about X 2.

The circumference of the $1\frac{1}{2}$ ft diameter projector screen was marked in degrees and could be rotated to measure the phase lag angles to a high degree of accuracy.

4.3 Rotor Balancing

For preliminary balancing at speeds low relative to the first natural frequency on simple supports the method described by den Hartog (ref. 45) was used. That is, the amplitude of the rotor motion while running in the oil bearings was noted at the same speed for at least four separate runs - one with only the rotor's inherent out-of-balance and the others with a deliberate out-of-balance in position at 90° to each other added to the inherent out-of-balance as excitation. From these readings a vector diagram could be drawn indicating the size and position of the required balancing weight. Rotor 1 was balanced in its central plane only while Rotor 2 was balanced in the two disc planes symmetrically situated about its centre.

At frequencies close to the first natural frequency of the rotors on simple supports the method suggested in section 3 was often used. The method was successful and

also much quicker than the other one since it only required one run and no calculation for each correction.

For balancing Rotor 2 near its second natural frequency a method similar to the first method was used with success, on this occasion the deliberate out-of-balance addition being a couple.

The mass eccentricity of both Rotor 1 and Rotor 2 after these balancing processes appeared to be better than .00015 in.

4.4 Experimental procedure

The experimental rig was clearly a comprehensive facility for the investigation of rotor oil whirl since a wide variety of combinations of rotor mass distribution and bearing characteristics were possible. However, in planning the preliminary experimental programme it was felt that the rotor should be kept as simple as possible and a wide variety of bearing oil films investigated in order that the influence of the films would emerge as clearly as possible. Rotor 1 was designed with this in mind and also so that then the comparison between the experimental results and the theoretical results of Chapter 3 would be as direct as possible. As there is considerable interest in the oil whirl behaviour of rotors near second natural frequencies,

Rotor 2 was designed to run at that condition and a short series of runs with it were fitted into the remaining time.

Throughout almost the whole of the speed ranges observed, the elliptical orbits of synchronous whirl of the rotors were clear and steady. However, different types of whirl were observed at either end of the speed range. On several occasions at rotor speeds corresponding to p values of 0.5 and less, mild resonant whirls were observed with both synchronous and precisely half speed frequencies. It is suspected that these whirls are a result of the non-linear characteristics of the oil film prominent because of the high journal eccentricities occurring at low speeds. Usually at the other end of the speed range indications of unstable oil whirl prevented further investigation of the synchronous whirl response.

4.4 - 1 Rotor 1

For each of fifteen pairs of bearings the whirling behaviour of Rotor 1 was observed while it ran through a variety of speeds carrying a variety of out-of-balance weights. For these runs the intermediate transducer probes were located in a plane about 4.5 in from the rotor centre, contacting the rotor shaft.

The speeds at which readings were taken were calculated beforehand to correspond to specific values of p and the values of the out-of-balance masses used were calculated to make the eccentricity from the rotor's rotational axis of the effective mass at the centre of the rotor one of the following values: 0.0005 in, 0.001 in, 0.0015 in and 0.002 in.

During some preliminary runs and on a number of subsequent occasions the oil supply pressure was varied from practically zero to often above 10 lbf/in^2 but no significant change in synchronous whirl behaviour was observed. The input pressure was therefore set at about 5 lb f/in^2 for all the experiments except the largest clearance cases where the large flow required reduced the maximum supply pressure to 2 lb f/in^2 or 3 lb f/in^2.

The immerser was used on a number of occasions to maintain a realistically large load number.

In a typical run, the rotor speed was increased from rest until it reached the speed corresponding to the first specific p value. After allowing the system about a minute to settle down, the following operations were completed in rapid succession:

i the six bearing thermocouple readings were taken

ii the three rotor orbit traces were consecutively displayed on the oscilloscope, appropriately attenuated and photographed.

iii the six rotor phase traces were consecutively displayed in two groups of three, modified to obtain circles and photographed.

The procedure was then repeated at the higher speeds corresponding to the pre-selected values of p.

Runs were completed with increasing degrees of out-of-balance until a mass eccentricity of .002 in had been reached or until there was evidence of rubbing of the journals on the bearings. Since each run was completed fairly quickly, the sump oil temperature and the bearing temperature altered little and thus the bearing running conditions were maintained from run to run.

4.4 - 2 Rotor 2

For each of three different bearing pairs the whirling behaviour of Rotor 2 was observed while it ran at a variety of speeds. Out-of-balance masses were used in the plane of only one of the discs which were calculated to make the eccentricity from the rotor rotational axis of the effective

mass in the plane of the disc either .001 in or .0015 in.

For these runs the intermediate pair of transducers were located in the centre plane of the rotor. The procedure used for recording the rotor motion was precisely as for Rotor 1.

Although the main object of the runs was to examine the synchronous oil whirl responses in the region of the second natural frequency (obtained on simple supports), on all but one of the runs the rotor became subject to unstable oil whirl before that speed was reached.

4.5 Analysis of experimental results

The systematic experimental data obtained for Rotor 1 is conveniently described under separate headings of journal displacement, rotor centre displacement and journal force.

In view of the small number of observations made of the synchronous whirl of Rotor 2 and the absence of a numerical evaluation of its theoretically predicted behaviour, the data collected for it is discussed in more general terms.

4.5 - 1 Rotor 1 - journal displacement

Figs. 4.10 present the experimental observations of journal displacement in the order in which they were obtained which corresponds to three groups of runs with a different oil used for each group.

Since the motion at one journal always corresponded closely with the motion at the other, the mean values of amplitude and phase have been taken as representative. The recorded amplitudes have been non-dimensionalised by dividing them by the eccentricity of the effective central mass from the rotor rotational axis.

The runs with the smallest clearances i.e. those of R 1.5. R 1. 9 and R 1.10, do not agree well with the others but do agree well between themselves, especially R 1.5 and R 1. 9 which operated at fairly similar load numbers. The abnormally large non-dimensional journal and rotor centre displacements in themselves suggest reasons for the abnormal behaviour.

Firstly, for the mass eccentricity used in these cases (.0005 in), the journal amplitudes are so large relative to the bearing clearance that the oil forces are certain to be quite non-linear. Because of the rotor flexibility, the effective rotor inertia force at the journals when they are

restrained in this way could be expected to be much larger than if the oil force characteristics had remained linear for those amplitudes. To complete a case of circular causation, the increased journal forces transmitted to the oil film would encourage the non-linear condition.

Secondly, the associated large rotor centre displacements would result in slight misalignment of the journals in the bearing.

The two most striking features of the other journal responses are the linearity for a given bearing pair and the similarity of the runs for different bearing pairs.

With respect to the linearity feature, the effect of small degrees of oil force non-linearity is too complex to be adequately explained in the same simple way as the abnormal behaviour of the runs with small clearance bearings. Thus it is fortunate to find the remarkable degree of amplitude linearity and phase similarity between the runs with a given bearing pair. The agreement between the results for the higher mass eccentricities is particularly good, the greater variation of the .0005 in eccentricity results being no doubt due in part to the greater percentage effect of the residual out-of-balance in those cases.

For further analysis it is convenient to refer to the theory of sect. 3.2 - 1 since only then can all the known variables be taken account of meaningfully. In fact, the similarity between the results for different bearings is evident largely because they have been plotted in terms of the main controlling parameter of the problem, p, and because the other two most relevant theoretical parameters, $\frac{p}{p}1$ and the bearing running condition have been designed to be fairly constant over the range of interest. To obtain a direct comparison of the journal displacements for all the runs independently of the variation of these last two parameters, they are replotted in Figs. 4.14 (on twice the vertical scale) where they have been grouped in ranges of load number and the magnitudes multiplied by $\frac{p}{p}1$ in accordance with the theory. Only one representative value was taken for each bearing condition, where possible the mean between the two higher mass eccentricity values. It can be seen that both amplitude and phase points correlate well with each other with the exception of the abnormal small clearance cases already noted.

Comparing Figs 4.14 with each other the grouping into load number ranges does not reveal that this variable has a significant effect in the range covered even allowing that only a few points were obtained on either side of the main range of interest, $6 < N_L < 18$, and that these points lie close to that range. Similarly $\frac{1}{d}$ ratio appears to have a

negligible effect on the response.

4.5 - 2 Rotor 1 - rotor centre displacement.

In Figs 4.11 the observed rotor centre displacements have been plotted in the same way as for the journal displacements and the same remarks apply about the behaviour of R 1.5, R 1.9 and R 1.10.

The linearity of the responses is not quite as good as for the journal displacements, the differences being apparent both in amplitude and phase.

The theoretical relationship between the rotor centre displacement and the other system variables does not lend itself to a convenient form for correlation purposes. The results have therefore been used for a separate correlation - that of the rotating oil force.

4.5 - 3 Rotor 1 - rotating oil force

A force can only be measured if it is allowed to move through a calibrated displacement and thus the rotating forces at bearings are usually monitored by load cells built into the bearing housings. In the present case the simple rotor mass distribution and the rotor flexibility allows the rotating oil forces to be readily calculated from the measurement of journal displacement and rotor centre

displacement. The relevant relationship is obtainable from equation 3.16.

$$F_x = k\left[x_c - x\left(1 - \frac{\omega_r^2}{\omega_1^2}\right)\right]$$

$$F_y = k\left[y_c - y\left(1 - \frac{\omega_r^2}{\omega_1^2}\right)\right]$$

or in non-dimensional form:

$$\frac{c}{L}\frac{F_x}{W} = \frac{ck}{W}\left[\frac{x_c}{L} - \frac{x}{L}\left(1 - \frac{\omega_r^2}{\omega_1^2}\right)\right]$$

$$\frac{c}{L}\frac{F_y}{W} = \frac{ck}{W}\left[\frac{y_c}{L} - \frac{y}{L}\left(1 - \frac{\omega_r^2}{\omega_1^2}\right)\right]$$

If $\frac{\omega_r^2}{\omega_1^2}$ was negligible (i.e. if the journal masses were negligible) the rotating oil forces at the journals would simply be proportional to the shaft deflection. Since the stiffness of the shaft is accurately known it could thus be regarded as a conveniently situated rotating spring balance. In fact for Rotor 1 the effective journal mass is such that values of $\left(1 - \frac{\omega_r^2}{\omega_1^2}\right)$ as high as 0.5 are obtained for the highest speeds of interest. The non-dimensional force terms $\frac{c}{L}\frac{F_x}{W}$ and $\frac{c}{L}\frac{F_y}{W}$ were thus calculated by multiplying the journal displacements by $\left(1 - \frac{\omega_r^2}{\omega_1^2}\right)$ and then subtracting them vectorially from the corresponding values of rotor centre displacement. After the resultant vectors were multiplied by $\frac{ck}{W}$, the

amplitudes and phases were plotted in Fig. 4.12. The results are collected in groups of load number in Fig. 4.15 with the amplitudes multiplied by $\frac{p}{p_1}$ for correlation purposes as suggested by the theory.

The results correlate reasonably with each other suggesting an equally good correlation for the rotor centre displacement results.

4.5 - 4 Rotor 2

Figs. 4.13 present the experimental whirling results of Rotor 2 in the order in which they were observed, two pairs of runs with a different oil for each pair. The displacements have been non-dimensionalised by dividing them by the effective eccentricity of the out-of-balance rotor disc and are plotted in terms of $\frac{c}{W} p_{LL} = \frac{c}{W} p_{RR}$, the p values being obtainable from Fig. 4.7.

In spite of a variation of load numbers between the runs a definite pattern emerges. In the absence of a numerical evaluation of the predicted motion, discussion of the results will be confined to qualitative features of the pattern.

The displacements of both journals at the lowest

frequencies and in the region of the first natural frequency (obtained on simple supports) compare with the corresponding behaviour of the journals of Rotor 1. The rotor centre displacement appears relatively larger than that for Rotor 1, no doubt due to the greater flexibility of Rotor 2.

At values of $\frac{c}{W}p_{LL} = \frac{c}{W}p_{RR} = 0$, both the journal amplitudes and the rotor centre amplitude are small indicating about the smallest rotating forces recorded during the runs. The corresponding phase lag of all three displacements are close to 180^{o}. Clearly this would be a desirable operating position for smooth running.

With further increase in speed the three displacement amplitudes grow and the phase lag values at the two journals draw apart significantly for the first time.

Finally, with reference only to Fig. 4.13 (c), at the second natural frequency (obtained on simple supports), the three displacement amplitudes reduce. The phase lag of the journal at the eccentric mass end of the rotor becomes 180^{o} out-of-phase with the mass eccentricity while the journal at the other end of the rotor has returned to a position in which it is in phase with the mass eccentricity.

4.6 Comparison of theoretical and experimental results.

4.6 - 1 Rotor 1 - journal displacement : circular orbit at natural frequency.

It is convenient to begin by comparing the particular theoretical prediction described in sect.3.2-2, namely, that at a rotor running frequency corresponding to the first natural frequency of the rotor on simple supports ($p = p^1 = \infty$) the rotor journals move in a circle with a radius equal in magnitude and precisely 180^o out-of-phase with the mass eccentricity.

At first sight the experimental results do not appear to provide good confirmation of this prediction. However, on closer examination it becomes clear that the predicted journal behaviour does occur but at higher rotor speeds than expected. Thus, returning to Figs. 4.10, the higher speed at which the vertical amplitude of a journal response is equal to the mass eccentricity is quite sharply defined due to its relatively rapid rate of change in that vicinity. When the horizontal amplitude and the phase magnitudes corresponding to this defined speed are checked it is found that in every case observed, including the otherwise abnormal small clearance cases, the journal motion conforms to that predicted to a high degree of accuracy.

Because of the large change in p values for small changes in rotor rotational frequency near the rotor natural frequency, the diagrams exaggerate the apparent difference between the experimentally observed and theoretically predicted speeds at which the condition occurs. In fact, for bearing pairs other than those with the three smallest clearances, the condition is observed at speeds ranging from about 3250 rev/min to about 3330 rev/min with an average value of about 3290 rev/min for the twelve runs. This compares with the value of 3130 rev/min obtained from the static resonance test. For the three smallest clearances the values ranged from about 3,350 rev/min to about 3,400 rev/min.

It is difficult to wholly explain the discrepancy, either in terms of reduction of rotor span (calculated to be about .8 in - ten times the possible error), or in terms of the flexibility of the supposed simple supports used in the resonance test.

Apart from the slightly higher speeds at which the condition was observed for the three smallest clearances, there does not appear to be significant correlation between the slighly different speeds at which the condition was observed and obvious variables.

4.6 - 2 Rotor 1 - journal displacement : general form of response.

Since it has been found that neither a variation of $\frac{l}{d}$ ratios nor of load numbers in the regions of main interest have in themselves a significant effect on the journal response, the points plotted in Figs. 4.14 (c,d) will be taken as representative of the experimental values obtained and will be compared with the corresponding theoretical values in Fig. 3.5 (c,d).

It appears that the experimental values have a slight shift to the right relative to the theoretical ones, an observation corresponding to the discrepancy between the experimental and theoretical speeds for circular whirl discussed above. Thus, although the agreement between the results as plotted is fair it would be improved by moving the experimental points to the left by an amount sufficient to cancel the discrepancy between the observed and predicted speeds of journal circular whirl.

In that case the observed amplitude and phase of the y values would appear to lie closely between the predicted $\frac{l}{d}$ = 0 curves of ϵ = .4 and ϵ = .7. Also in that case, the agreement between the observed and predicted x values would not be quite so good, the observed values of amplitude and phase being slightly less than predicted.

However, the $\frac{1}{d}$ = 0 curves of ϵ = .4 and ϵ = .7 still describe the behaviour remarkably well.

4.6 - 3 Rotor 1 - rotating oil force.

For the same reasons as Figs. 4.14 (c,d) were considered as representative of the journal displacement observations, Figs. 4.15 (c,d) are taken as representative of the rotating oil force observations and will be compared with Fig. 3.6 (c,d).

The most striking difference between the experimental and theoretical results occurs for both the phases and amplitudes of the x force components for values of p in the range 1 to 20. In fact the discrepancy is understandable when it is realised that the method of calculation of the theoretical values is inaccurate for journal displacement components which are close in amplitude to and close to 180^{o} out-of-phase with the mass eccentricity. Referring to Fig. 3.5 it can be seen that this is the situation for the x displacement components within the range of p from about 1 to 20 for journal eccentricity ratios of .4, .7 and .9.

With this proviso, the agreement between theory and experiment is good. For positive values of p, the experimental points agree well with the theoretical $\frac{1}{d}$ = 0, ϵ = .4 curve but the experimental phase points are

only in fair agreement. For negative values of p_1 the experimental points appear to lie largely between the $\frac{1}{d} = 0$ and $\frac{1}{d} = \infty$ curves for both eccentricities ratios of .4 and 17.

Throughout, the y amplitudes, and to a lesser extent the y phase lags, appear to be slightly smaller than predicted and agree least well with the $\frac{1}{d} = 0$, $\in =$ .7 curves.

The shift of experimental points to the right of theoretical points observed in the journal displacement results does not seem to be repeated and indeed, for negative values of p there appears to be a slight shift to the left.

4.6 - 4 Rotor 2

The theoretical predictions of rotor motion in Chapter 3 have not been evaluated numerically for Rotor 2. However it is possible and of some practical interest to consider the form of the theoretical predictions for $\frac{c}{W}p_{LL} = \frac{c}{W}p_{RR} =$ 0, the condition at which Rotor 2 was observed to run remarkably smoothly. In fact the condition corresponds to zero for the diagonal terms of the rotor receptance matrix and a minimum value for the cross receptance term

(see Fig. 47) both of which factors would indeed seem to suggest an optimum running condition. Clearly of equal interest in analyses of smooth running is the form of the matrix operator $[q]$. More work is required to evaluate the importance of these factors.

4.7 Use of synchronous whirl data

The linearity of the experimental results and their close agreement with the theoretical predictions based on the linear oil force theory provide strong support for the linear oil force theory and for the method of simple rotor synchronous whirl analysis set out in Chapter 3.

4.7 - 1 Values of the oil force coefficients.

If the form of the theory based on eight oil force coefficients is applicable then these coefficients can be regarded as the unknowns of the present experimental work and since eight readings were taken at each whirling condition, in theory it should be possible to calculate the values of the coefficients from the experimental observations. However, in view of the number of variables involved which are difficult to measure accurately, and the extensive calculations that would be required, the determinations are impracticable and the experimental

results were never intended to be used in this way. Nevertheless the present correlation obtained between theory and experiment confirms the practicability and desirability of experimental methods of coefficient determination using more specialised rigs. A rig, such as that being run by my colleague Mr. L. Paterson, which is based on the excitation of a rotating journal at frequencies much higher than its rotational frequency (to make the velocity force coefficients dominant), or one which excited a rotating journal at frequencies much lower than its rotational frequency (to make the displacement force coefficients dominant) are possible methods.

Thus the conclusion of the present experimental work with respect to linear oil force coefficients is that they can be used successfully for synchronous oil whirl predictions and that for this purpose the given theoretical values for $\frac{l}{d} = 0$: $\Theta = .4$ and $\Phi = .7$, have been found fairly satisfactory.

4.7 - 2 Total displacement and force

For many purposes it will be useful to obtain the total journal displacement and the total journal force and this can be simply done as for the particular case shown in Fig. 4.16 where, for Rotor 1, the relative orbits of the journals, rotor geometric centre and rotor mass centre are

shown .

4.7 - 3 Some design implications

The work suggests two simple, useful generalisations for rotors with their mass concentrated near the centre running at load numbers $6 \prec N_L \prec 20$ on oil films which have linear force characteristics.

1 The maximum journal amplitude is close to $1\frac{1}{2}$ x the rotor mass eccentricity.

2 The maximum rotating oil force is close to that given by the expression $F = 6 \frac{L}{c} W$. Thus for a value of rotor mass eccentricity equal to a twelfth of the bearing radial clearance, the maximum rotating force will be equal to half the bearing load.

No attempt has been made to re-arrange the results into a more convenient form for design purposes. However, some implications of the results for design will be briefly indicated.

Bearings: For the ranges covered it has been found that $\frac{l}{d}$ ratio and oil inlet pressure have little effect on synchronous whirl. Also, provided that the smallest

clearance between journal and bearing is large enough relative to the rotor mass eccentricity for the oil force response to be reasonably linear, load number has little effect for the range covered.

Bearing clearance appears to have at least two significant effects. Firstly, for a constant load number, decreasing clearance clearly increases the chances of unfavourable non-linear behaviour and rubbing. The second effect is through the parameter p. Thus for a given rotor and reasonably linear behaviour of the oil film, small clearance bearings will result in a 'peakier' (though not larger) amplitude response with respect to speed and it could therefore be argued that if it was unavoidable to run a rotor near one of its natural frequencies (obtained on simple supports), smoother running may be obtained with a small clearance than with a large one. However, the improvement is not large for the normal range of clearances employed and the smallest clearances are subject to the above non-linear objection.

Rotors: By indicating the width of the resonant condition, the work should be useful in helping to decide to what values of natural frequency on simple supports a rotor can be designed in order to avoid resonant conditions when running on oil bearings.

By indicating the amplitude of the resonant response, the work should be useful in helping to decide the degree of balancing that is necessary to obtain smooth running.

With respect to balancing, the circular journal orbit motion would appear to be a basis for a potentially most useful balancing method.

Finally there is evidence that further study of the interaction of rotor receptances and bearing force coefficients would lead to the recognition of optimum conditions for smooth running.

PART 3

Unstable oil whirl of flexible rotors.

CHAPTER 5

Theoretical study of unstable oil whirl

Unstable oil whirl results from a condition in which the oil films supporting a rotor, far from controlling the tendency of the rotor to whirl as they do for synchronous whirl rather encourage the build up of a large amplitude unstable whirl.

The instability has attracted much attention, mainly because of its significance for turbine engineers, but though many hypotheses have been put forward to explain the mechanism of the whirl's self-excitation, as yet none of these has been accepted as reliable. Therefore, with respect to this problem especially, turbine engineering practice has developed almost entirely on the results of field experience and of a few experimental investigations of the problem with models. Together these have suggested at least two ways in which the instability can be avoided.

Firstly, when unstable whirls have been observed during the commissioning of a set they have usually been successfully countered by modifying the journal bearing shells by grooving, lobing etc. There is a limit to the extent that bearings can be so modified and still perform satisfactorily with respect to other factors of major importance such as low power absorption and

reliability.

Secondly, an early empirical design criterion which is still commonly observed suggests that for stability the rotor running frequency be kept lower than twice the first rotor natural frequency (calculated on simple supports).

Although the above means have been successful in the past, more accurate and reliable data about unstable oil whirl on which design decisions may be based is clearly desirable, especially because of new factors being introduced by the rapidly increasing size of turbo-alternators.

A reliable criterion can only come from a satisfactory explanation of the whirl mechanism and it is here suggested that the recent instability criteria obtained by using the linear oil force theory provide a satisfactory explanation. The experimental work described in the next chapter contributes some support to this suggestion. Both chapters include and extend a report of that part of the writer's work which has already been published in a joint paper with Dr. D. Morrison (ref. 19).

In the present chapter, after consideration of simple symmetrical rotor/bearing systems, attention is turned to

unsymmetrical and multi-span systems and a method is suggested for the instability analysis of the most usual form of these systems.

5.1 Brief historical notes .

While investigating large vibrations of model rotors in oil bearings, Newkirk & Taylor in 1925 (ref.42) first discovered that a rotor instability could arise for which the oil film was responsible. For an authoritative account of the efforts which took place between 1925 and 1957 to explain the mechanism of the instability and to find a cure for it, the reader is referred to the review paper by Newkirk (ref. 46). Although the emergence of a satisfactory instability criterion could not be reported, Newkirk wrote "In view of the important role of the quasi-elastic and damping of the oil film it is desirable that they be investigated further."

In fact, as described in Chapter 1, a linear oil force theory has developed since 1957 and the application of it to unstable oil whirl analysis is the subject of this chapter.

An altogether different instability hypothesis has been implied by the work of Cole (ref. 47), Milne (ref. 22) and Hughes (ref. 48) at N.E.L. The implication is that "a complete film is associated with whirl, and a cavitated film with stability." It can easily be shown that the experimental work of both Cole and Hughes agrees with the linear oil force stability analyses. However, the analyses suggest that it is unsafe to use the second part of the above implication as an instability criterion because the rigs only covered a range of the parameter $\frac{W}{mcW_r^2}$ (the significance of which will be described later in this chapter) which is well above those values of the parameter that the linear oil force analysis predicts would result in unstable conditions. The 'initial value' calculations of Milne neglect journal mass and indicate stability for all such journals on cavitated oil films. Since in this case the value of the parameter $\frac{W}{mcW_r^2}$ is infinitely large, once more the linear oil force stability analyses agree with the calculations but not with the inference that all cavitated oil films are stable. The theory confirms that a complete oil film is inherently unstable.

Reference has already been made (ref. sect. 1.3 - 3) to a group of papers concerned with the instability implications of the non-linear characteristics of oil films. The preliminary investigations suggest that

non-linear modes of instability are quite possible. More work is required, however, before any firm conclusions can be drawn. If these analyses do locate and reliably predict non-linear modes of instability for such simple systems as a journal with mass, they would probably be of considerable direct use for the design of small rigid rotors. However, for the whirl analysis of a turbo-alternator set with complicated rotor and foundation characteristics, it is a matter of considerable numerical difficulty to include even the terms of the linear oil force theory. Thus it is difficult to imagine that for the purposes of turbo-alternator design, the non-linear analyses of simplified systems can lead to anything more valuable than a suggestion of the qualitative nature of the effect of the non-linear force characteristics.

5.2 Application of the linear oil force theory to the conventional stability analysis of simplified rotor/bearing systems

The equations of free motion of the simplest flexible rotor on oil films which are representable in terms of the linear oil force theory are obtained by equating equation 2.7 to the equation corresponding to equation 1.9 :

$$\begin{bmatrix} F_x \\ F_y \end{bmatrix} = \frac{W}{c}\begin{bmatrix} (\alpha_{xx} + \beta_{xx}\frac{D}{w_r}) & (\alpha_{xy} + \beta_{xy}\frac{D}{w_r}) \\ (\alpha_{yx} + \beta_{yx}\frac{D}{w_r}) & (\alpha_{yy} + \beta_{yy}\frac{D}{w_r}) \end{bmatrix}\begin{bmatrix} x \\ y \end{bmatrix} = \frac{-k^D{}^2}{\omega_1^2 + D^2}\begin{bmatrix} x \\ y \end{bmatrix} \qquad 5.1$$

The corresponding frequency equation is:

$$\gamma_1 G^6 + \left[\gamma_2 + \frac{w_1^2}{w_p^2}\gamma_3\right] G^5 + \left[\left(\frac{w_1}{w_p}\right)^4 + \left(\frac{w_1}{w_p}\right)^2\gamma_5 + \gamma_4 + 2\left(\frac{w_1}{w_r}\right)^2\gamma_1\right] G^4 + \left[\left(\frac{w_1}{w_p}\right)^2\left(\frac{w_1}{w_r}\right)^2\gamma_3 + 2\left(\frac{w_1}{w_r}\right)^2\gamma_2\right] G^3$$
$$+ \left[\left(\frac{w_1}{w_p}\right)^2\left(\frac{w_1}{w_r}\right)^2\gamma_5 + 2\left(\frac{w_1}{w_r}\right)^2\gamma_4 + \left(\frac{w_1}{w_r}\right)^4\gamma_1\right] G^2$$
$$+ \left(\frac{w_1}{w_r}\right)^4\gamma_2 G + \left(\frac{w_1}{w_r}\right)^4\gamma_4 = 0, \qquad 5.2$$

where $G = \frac{D}{w_r}$, is expressed in terms of five compound oil film coefficients (which seem to have been first used by Morrison (ref. 18) and are plotted in Fig. 5.1 using the force coefficients from Fig. 1.5):

$$\gamma_1 = \beta_{xx}\beta_{yy} - \beta_{xy}\beta_{yx}$$
$$\gamma_2 = \alpha_{xx}\beta_{yy} + \alpha_{yy}\beta_{xx} - \alpha_{xy}\beta_{yx} - \alpha_{yx}\beta_{xy}$$
$$\gamma_3 = \beta_{xx} + \beta_{yy}$$
$$\gamma_4 = \alpha_{xx}\alpha_{yy} - \alpha_{xy}\alpha_{yx}$$
$$\gamma_5 = \alpha_{xx} + \alpha_{yy}$$

and in terms of three characteristic phase velocities:

ω_r rotor angular velocity

$\omega_1 = \sqrt{\frac{k}{m}}$ phase velocity of elastic vibration of rotor on simple supports.

$\omega_p = \sqrt{\frac{W}{mc}} = \sqrt{\frac{g}{c}}$ phase velocity of the rotor oscillating pendulum-wise in the bearing clearance which is characteristic not because of any pendular motion, but because $\frac{W}{c}$ is a measure of the scale of magnitude of the oil film stiffness.

Before discussing the motion of the full system a brief description of the behaviour of special cases of it will be given.

5.2 - 1 Static Instability

When a rotating journal moves so slowly transversely that the incremental velocity dependent oil forces exerted on it are negligible, the incremental oil force on it will be expressible in terms of the displacement coefficients only:

$$\begin{bmatrix} F_x \\ F_y \end{bmatrix} = \frac{W}{c} \begin{bmatrix} \alpha_{xx} & \alpha_{xy} \\ \alpha_{yx} & \alpha_{yy} \end{bmatrix} \begin{bmatrix} x \\ y \end{bmatrix} \qquad 5.3$$

If the equations are taken separately then the conditions under which each component force is zero are given by:

$$\text{for } F_x = 0, \frac{x}{y} = -\frac{\alpha_{xy}}{\alpha_{xx}} = \tan\theta_x$$

$$F_y = 0, \frac{x}{y} = -\frac{\alpha_{yy}}{\alpha_{yx}} = \tan\theta_y$$

where θ_x, θ_y for a variety of relative values of the displacement coefficients are given in Fig. 5.2. Thus:

in Fig. 5.2a : $-\frac{\alpha_{yy}}{\alpha_{yx}} > -\frac{\alpha_{xy}}{\alpha_{xx}}$ or $\gamma_4 > 0$

$$\therefore \tan\theta_y > \tan\theta_x$$

$$\theta_y > \theta_x$$

It can be seen that no matter the position of the journal, it always experiences a net restoring force. There is only one point of equilibrium - where the two zero force lines intersect.

in Fig. 5.2b: $\gamma_4 = 0$

In this case there exists a line of equilibrium

in Fig. 5.2c: $\gamma_4 < 0$

In this case there exists a zone, shaded in Fig. 5.2c, in which the journal experiences a net force away from the origin.

Thus, depending on the value of γ_4, the force system results in static stability, neutral stability or static instability respectively.

A different way of describing this possibility of instability has been given by Smith (ref. 20) who showed that if a point orbited the origin of the force system of Fig. 5.2c it would gain an amount of energy proportional to γ_4 and the area of the orbit.

The orientation of the $F_x = 0$ and $F_y = 0$ lines for the case of the short and long bearing coefficients being used in this work are shown in Fig. 5.2d where they are superposed on an assumed semi-circular journal centre equilibrium locus. From this figure or from the corresponding values of γ_4 plotted in Fig. 5.1 it can be seen that the static stability condition is well satisfied for these cases.

5.2 - 2 Dynamic Instability

Without velocity force coefficients : If Hummel's oil force form equation 5.4 is used for the dynamic analysis of the motion of the simplest rigid rotors or of the simplest flexible rotors, solutions of the corresponding frequency equations using the coefficient values in Fig.

1.5 show that the system is always positively damped and that for $\gamma_4 > \left(\frac{\gamma_5}{2}\right)^2$ the roots are oscillatory. The frequency of oscillation is not a function of the rotor running frequency except in so far as it determines the displacement force coefficients. By consulting Fig. 5.1 it will be seen that the inequality is only satisfied for eccentricity ratios less than about .7. Non-oscillatory roots are obtained above this value. Predictions of rotor motion on the basis of this analysis have been made by Parszewski & Cameron (ref. 49).

With velocity force coefficients : If the journal mass is negligible, equation 5.1 reduces to:

$$G^2 + \frac{\gamma_2}{\gamma_1} G + \frac{\gamma_4}{\gamma_1} = 0$$

$$\text{i.e.} \quad G = \frac{D}{w_r} = -\frac{\gamma_2}{2\gamma_1} \pm \sqrt{\left(\frac{\gamma_2}{2\gamma_1}\right)^2 - \frac{\gamma_4}{\gamma_1}}$$

Once again the motion is predicted to be stable for the coefficient values in Fig. 1.5. If the square root is evaluated it is found that oscillatory roots are obtained for all eccentricities. A feature from the point of view of half speed or unstable oil whirl is that not only is the oscillation now expressed as a direct function of the rotor running frequency but the frequency ratio is found to be close to a half for small eccentricities.

If journal mass is considered, equation 5.1 reduces to

$$\left(\frac{\omega_r}{\omega_p}\right)^4 G^4 + \gamma_3\left(\frac{\omega_r}{\omega_p}\right)^2 G^3 + \left[\gamma_1 + \left(\frac{\omega_r}{\omega_p}\right)^2 \gamma_5\right] G^2 + \gamma_2 G + \gamma_4 = 0 \qquad 5.4$$

Fourth order equations are solvable by algebraic formulas but the numerical computation involved is large. For the present purposes, the chief interest in the above equation has been to discover whether or not bearing conditions exist for which the equation yields unstable roots. Using the Routh-Hurwitz criterion Korovchinski (ref. 8) and Holmes (ref.15) have found that instability is indicated unless, in the present notation, the following condition is satisfied

$$\frac{W}{mc\omega_r^2} = \frac{\omega_p^2}{\omega_r^2} \geqslant \frac{1}{P} \qquad 5.5$$

where $$P = \frac{\gamma_1 \gamma_2 \gamma_3}{\gamma_2^2 - \gamma_5 \gamma_3 \gamma_2 + \gamma_4 \gamma_3^2} \qquad 5.6$$

An alternative approach to the instability analysis is by Leonhard's method as described by Morrison (ref. 18). This method also allows the unstable frequency ratio corresponding to the boundary of instability indicated by equation 5.5 to be quickly found by putting $G = i\lambda\omega_r$ in equation 5.4 and solving the imaginary terms only to obtain

$$\lambda^2 = \left(\frac{\omega_b}{\omega_r}\right)^2 = \frac{\gamma_2}{\gamma_3} \quad \frac{W}{mcW^2}$$

Thus at the stability limit, substituting for $\frac{W}{mcW^2}$ from inequality 5.5:

$$\lambda^2 = \left(\frac{\omega_b}{\omega_r}\right)^2 = \frac{Q}{P} \qquad \text{5.7}$$

$$\text{where} \quad Q = \frac{\gamma_2}{\gamma_3} \qquad \text{5.8}$$

It is of interest to note that the possibility of dynamic instability only arises for the bearing characteristics considered when both journal mass and oil velocity dependent forces are taken account of.

The stability of the simplest flexible rotor case on oil films representable by the linear oil force theory (described in equation 5.1 and equation 5.2 in the present notation) has been investigated by several authors. Although the stability criteria arrived at are apparently dissimilar, it is shown in Appendix 6 that they are all expressible in the form

$$\left(\frac{\omega_r}{\omega_p}\right)^2 \leqslant P \left(\frac{\omega_1}{\omega_r}\right)^2 - Q \qquad \text{5.9}$$

where P and Q have the same significance as in equation 5.6 and in equation 5.8 respectively. Moreover, it is found that for this case the unstable frequency ratio is the same as that given in equation 5.7 where it can be seen that the ratio is a function only of the bearing

running condition. Hence ω_b, the whirl phase velocity, is a fourth characteristic phase velocity of the system in addition to those defined after equation 5.2.

5.2 - 3 Discussion of instability criteria

Values of P and Q, obtained as described in Appendix 6, are plotted together in Fig. 5.3. It can be seen that there are wide numerical differences between the results, presumably due to the different assumptions for bearing operation.

Bounding values of the results have been used to plot stability boundaries in logarithmic form which are compared in the stability chart Fig. 5.4. It is apparent that the three full theoretical treatments C, D and E give results of identical general form while the approximating treatments A and B give the asymptotes of the fuller theory.

A shaded area is shown which indicates the region occupied by experimental points which will be discussed in the next chapter.

5.3 Problems associated with the application of the linear oil force theory to the conventional instability analysis of realistic rotor/bearing systems

Although the instability criteria for the simple symmetrical flexible rotor case can probably be taken as a good guide towards the instability characteristics of symmetrical single-span rotor/bearing systems in general, it is of some importance to be able to extend the analysis to unsymmetrical and multi-span systems. To examine the possiblities, the problem of ascertaining the instability characteristics of the rotor shown in Fig. 2.4 while it is supported on dissimilar bearings will be considered. From equation 1.9 and equation 2.29 the required equation of motion is:

$$\begin{bmatrix} \frac{W_L}{c_L}\left(\alpha_{xx}+i_L\beta_{xx}D\right)-P_{LL} & \frac{W_L}{c_L}\left(\alpha_{xy}+i_L\beta_{xy}D\right) & -P_{LR} & 0 \\ \frac{W_L}{c_L}\left(\alpha_{yx}+i_L\beta_{yx}D\right) & \frac{W_L}{c_L}\left(\alpha_{yy}+i_L\beta_{yy}D\right)-P_{LL} & 0 & -P_{LR} \\ -P_{RL} & 0 & \frac{W_R}{c_R}\left(\alpha_{xx}+i_R\beta_{xx}D\right)-P_{RR} & \frac{W_R}{c_R}\left(\alpha_{xy}+i\beta_{xy}D\right) \\ 0 & -P_{RL} & \frac{W_R}{c_R}\left(\alpha_{yx}+i_R\beta_{yx}D\right) & \frac{W_R}{c_R}\left(\alpha_{yy}+i_R\beta_{yy}\right)-P_{RR} \end{bmatrix} \begin{bmatrix} x_L \\ y_L \\ x_R \\ y_R \end{bmatrix} = 0 \qquad 5.10$$

The approach to the conventional stability analyses used in section 5.2. is to multiply out the frequency determinant and test the roots of the resulting frequency equation for positive real parts. Thus the order of the frequency equation in the present case is of interest.

The order of frequency equations corresponding to the form of equation 5.10 can be simply determined by calculating the first and last terms of the expression that would be got by multiplying out the product of the diagonal terms of the frequency determinant. When the last term is rationalised, so also are all the other terms of the full frequency equation and this process will always make either the first term that of the highest order or the last term part of the term with the highest order. For an unsymmetrical flexible rotor, with n interspan masses, supported on N dissimilar bearings the order of the frequency equation is found to be $N(4n + 2)$. Thus if the rotor is symmetrical and is supported on two similar bearings the order is 6 which checks with equation 5.2.

In the present 3-mass unsymmetrical case the indicated order of the frequency equation is 28. The examination of the roots of such a high order frequency equation would seem to be quite impracticable by any other means than by trial and error for which purpose an extension of an analysis by Morrison (ref. 50) may be useful. Writing with respect to the simple symmetrical flexible rotor case already discussed, Morrison considered the form of the frequency determinant corresponding to a

forcing frequency which was a fraction of the rotor running frequency. It was found that the frequency determinant was zero for a frequency ratio of close to one half and that this condition corresponded to the unstable oil whirl prediction by the conventional means. Thus the condition for which the frequency determinant was zero for a real frequency ratio, a condition defining a stability boundary, could be found by trial and error. The extension of the process to unsymmetrical and multi-span systems would appear to require no further justification.

Thus for the present 3-mass case, p_{LL}, $p_{LR} = p_{RL}$, p_{RR} could be substituted for P_{LL}, $P_{LR} = P_{RL}$, P_{RR} in equation 5.10 except that they would be regarded as functions of $\lambda\omega_r$, where λ is real, and not of ω_r. Curves of p_{LL}, $p_{LR} = p_{RL}$, p_{RR} may be available in terms of ω_r for the purposes of synchronous whirl analysis as in Fig. 4.6 and Fig. 4.7 . Since unstable oil whirl isusually observed to have a frequency just less than half of rotor rotational frequency and in the region of the rotors first natural frequency on simple supports, the following trial and error procedure suggests itself:

i Let $\lambda = \frac{1}{2}$ and vary p_{LL}, $p_{LR} = p_{RL}$, p_{RR} by varying ω_+ close to $2\omega_1$ to obtain a minimum value for the frequency determinant.

ii Vary λ to improve the minimum.

iii Vary p_{LL}, $p_{LR} = p_{RL}$, p_{RR} to improve the minimum. Repeat ii and iii until satisfied that the determinant is close enough to zero when ω_+ will correspond to a threshold of instability.

Since the determinant has complex coefficients, the above calculations would be lengthy and for this reason it is not known to what extent the method is practical. For appropriate cases, the technique for dealing with unsymmetrical and multi-span rotors described in section 5.6 - 2 is recommended.

5.4 Spring-like behaviour of oil films at the stability boundary

The simplest derivation of the condition of unstable oil whirl for a single bearing oil film is in extension of a concept advanced by Marsh (ref. 51). It can be argued that at the stability boundary, where theoretically harmonic vibration of constant amplitude could persist, the bearing oil film must be representable by a simple spring-like element. If, additionally, the system

apart from the oil film is axially symmetric, then the spring equivalence of the oil film must amount to a simple radial stiffness. It is supposed that this radial stiffness is given by $k^1 = \rho \frac{W}{c}$ and that this condition only occurs at a particular whirl frequency ω_b where ρ and ω_b/ω_r are functions of the bearing running condition. Then, putting

$$\frac{D}{\omega_r} = i \frac{\omega_b}{\omega_r} = i\lambda \quad \text{where} \quad \lambda = \frac{\omega_b}{\omega_r}$$

in equation corresponding to equation 1.9

$$\begin{bmatrix} F_x \\ F_y \end{bmatrix} = \frac{W}{c} \begin{bmatrix} (\alpha_{xx} + i\lambda \beta_{xx})(\alpha_{xy} + i\lambda \beta_{xy}) \\ (\alpha_{yx} + i\lambda \beta_{yx})(\alpha_{yy} + i\lambda \beta_{yy}) \end{bmatrix} \begin{bmatrix} x \\ y \end{bmatrix} = \frac{W}{c} \begin{bmatrix} \rho & 0 \\ 0 & \rho \end{bmatrix} \begin{bmatrix} x \\ y \end{bmatrix}$$

From which the frequency determinant is

$$\begin{vmatrix} (\alpha_{xx} + i\lambda \beta_{xx} - \rho) & (\alpha_{xy} + i\lambda \beta_{xy}) \\ (\alpha_{yx} + i\lambda \beta_{yx}) & (\alpha_{yy} + i\lambda \beta_{yy} - \rho) \end{vmatrix} = 0$$

Expanding this determinant and separating real and imaginary parts:

$$i\lambda \left\{ \alpha_{xx}\beta_{yy} + \alpha_{yy}\beta_{xx} - \alpha_{xy}\beta_{yx} - \alpha_{yx}\beta_{xy} - \rho(\beta_{xx} + \beta_{yy}) \right\} = 0$$

$$\alpha_{xx}\alpha_{yy} - \alpha_{xy}\alpha_{yx} - \rho(\alpha_{xx} + \alpha_{yy}) + \rho^2 - \lambda^2(\beta_{xx}\beta_{yy} - \beta_{xy}\beta_{yx}) = 0$$

From which, using the symbols given at the beginning of section 5.2:

$$\rho = \frac{\gamma_2}{\gamma_3} \qquad \text{5.11}$$

and $$\lambda^2 = \frac{\rho^2 - \rho\gamma_5 + \gamma_4}{\gamma_1} \qquad \text{---------- 5.12}$$

Substituting for ρ in equation 5.12 from equation 5.11

$$\lambda^2 = \frac{\gamma_2^2 - \gamma_5\gamma_3\gamma_2 + \gamma_4\gamma_3^2}{\gamma_1\gamma_2\gamma_3} \cdot \frac{\gamma_2}{\gamma_3} \qquad 5.13$$

Comparing equation 5.11 and equation 5.13 with equation 5.8 and equation 5.7 respectively it is found that

$$\rho = \frac{c}{W} k^1 = Q \qquad \text{---------- 5.14}$$

and $$\lambda^2 = \left(\frac{\omega_b}{\omega_r}\right)^2 = \frac{Q}{P} \qquad \text{---------- 5.15}$$

where Q and P are the values that have already been plotted in Fig. 5.3.

5.5 Application to rotor stability analysis of the spring-like behaviour of the oil film at a stability boundary.

The concept of the spring-like behaviour of the oil film at a stability boundary allows the stability boundaries of certain rotor/oil film systems to be simply deduced. After illustrating its application to the case of a rotor of the type used for the experimental work described in the next chapter, the treatment of more

practical rotor systems is considered.

5.5 - 1 Instability of a symmetrical flexible rotor taking account of journal mass

The rotor considered is of the type shown in Fig. 3.1 which is considered to be supported in similar bearings. The frequency equation describing its motion is of eighth order which means that an investigation of the nature of its stability by conventional means would be extremely awkward.

If the rotor, rotating at phase velocity ω_r whirls symmetrically in the bearings at a phase velocity ω_b such that each oil film behaves like a spring of stiffness $k^1 = \rho \frac{W}{c}$, the rotor/oil film system can be represented by the equivalent mass/spring system shown in Fig. 5.5 for which the following relationship holds:

$$\omega_b^4 - \left(\frac{k}{m_2} + \frac{k+k^1}{m_1}\right) \omega_b^2 + \frac{kk^1}{m_1 m_2} = 0 \qquad \text{5.16}$$

Simplify this equation by

i multiplying through by $\frac{m_1}{m_1+m_2} \cdot \frac{1}{\omega_r^4}$

ii letting $\frac{k}{m_2} = \omega_1^2$, $\frac{g}{c} = \omega_p^2$

iii putting $\frac{\omega_b}{\omega_r} = \lambda$

Then equation 5.16 becomes

$$\left(\frac{m_1}{m_1+m_2}\right)\lambda^4 - \left[\left(\frac{\omega_1}{\omega_r}\right)^2 + \rho\left(\frac{\omega_p}{\omega_r}\right)^2\right]\lambda^2 + \left(\frac{\omega_1}{\omega_r}\right)^2\left(\frac{\omega_p}{\omega_r}\right)^2\rho = 0$$

After some manipulation this can be put into the form

$$\left(\frac{\omega_1}{\omega_p}\right)^2 = \frac{\left[\left(\frac{\omega_1}{\omega_r}\right)^2 \frac{1}{\lambda^2} - 1\right]\rho}{\left[1 - \frac{m_1}{m_1+m_2}\frac{\lambda^2}{\left(\frac{\omega_1}{\omega_p}\right)^2}\right]}$$

Substituting in the top line for $\rho = Q$ from equation 5.14 and $\lambda^2 = \frac{Q}{p}$ from equation 5.15

$$\left(\frac{\omega_1}{\omega_p}\right)^2 = \frac{p\left(\frac{\omega_1}{\omega_r}\right)^2 - Q}{\left[1 - \frac{m_1}{m_1+m_2}\frac{\lambda^2}{\left(\frac{\omega_1}{\omega_r}\right)^2}\right]} \qquad 5.17$$

As should be expected, for $m_1 \ll m_2$ equation 5.17 corresponds to inequality 5.9 while for $m_1 \gg m_2$, equation 5.17 corresponds to inequality 5.5.

Using the oil film spring concept, an investigation of the effect of bearing foundation flexibility on rotor stability has recently been published by Lund (ref. 52).

5.5 - 2 Instability of any rotationally symmetric single span or multi-span rotor running on oil film bearings with the same load numbers.

It is general turbo-alternator practice to design bearings on the basis of a common load number. For this case, the concept of the spring equivalence of an oil film at a stability limit can be applied to the stability analysis of the system.

As an illustration, consider the unsymmetrical rotor in Fig. 2.4 supported in bearings running at the same load number. If the rotor whirls at the unstable whirl frequency ratio $\lambda = \frac{\omega_b}{\omega_r}$,

$$\begin{bmatrix} {}_L n_{xx} & {}_L n_{xy} \\ {}_L n_{yx} & {}_L n_{yy} \end{bmatrix} = \begin{bmatrix} {}_R n_{xx} & {}_R n_{xy} \\ {}_R n_{yx} & {}_R n_{yy} \end{bmatrix} = \begin{bmatrix} \rho & 0 \\ 0 & \rho \end{bmatrix} \quad \text{5.18}$$

Substituting this result into the equation for the system equation 5.10 and also substituting p_{LL}, $p_{LR} = p_{RL}$, p_{RR} for P_{LL}, $P_{LR} = P_{RL}$, P_{RR} where p_{LL}, $p_{LR} = p_{RL}$, p_{RR} are treated as functions of $\lambda\omega_r$ and not of ω_r, equation 5.10 becomes:

$$\begin{bmatrix} \frac{W_L}{c_L}\rho - p_{LL} & 0 & -p_{LR} & 0 \\ 0 & \frac{W_L}{c_L}\rho - p_{LL} & 0 & -p_{LR} \\ -p_{RL} & 0 & \frac{W_R}{c_R}\rho - p_{RR} & 0 \\ 0 & -p_{RL} & 0 & \frac{W_R}{c_R}\rho - p_{RR} \end{bmatrix} \begin{bmatrix} x_L \\ y_L \\ x_R \\ y_R \end{bmatrix} = 0 \qquad 5.19$$

for which the corresponding frequency equation is

$$\left[\left(\frac{W_L}{c_L}\rho - p_{LL}\right)\left(\frac{W_R}{c_R}\rho - p_{RR}\right) - p_{LR}p_{RL}\right]^2 = 0 \qquad 5.20$$

Thus the following sequence of steps should allow the calculation of the rotor rotational frequency for unstable conditions:

i Find ρ from equation 5.14

ii Find λ^2 from equation 5.15

iii From the plotted values of p_{LL}, $p_{LR} = p_{RL}$, p_{RR} estimate, initially by inspection, when equation 5.20 is satisfied.

iv Hence obtain ω_r by using ii and the value of $\lambda\omega_r$ which satisfies equation 5.20.

CHAPTER 6

Experimental study of unstable oil whirl

In contrast to the considerable activity on the theoretical front there has been little experimental work on the problem of unstable oil whirl. No doubt this has been largely due to the bewildering number of variables which would have to be taken account of in a comprehensive phenomenological approach.

As described in the previous chapter, the recent application of the linear oil force theory to the problem has suggested characteristic dynamic parameters of the system and pointed the way for a rational experimental programme which is the subject of the present chapter. The bulk of this work has already been reported in the writer's joint paper with Dr. D. Morrison (ref. 19) but since that publication, a new correlation between the experimental results has been found. Also, by taking account of the effective journal mass, the experimentally defined stability criterion has been found to be slightly more restrictive than previously reported.

6.1 Brief historical notes

An authoritative review of early experimental work on unstable oil whirl is contained in Newkirk's 1957 review paper (ref. 46). There the subject is traced from a paper describing experimental work which resulted in the discovery that the oil films were responsible for unstable oil whirl (ref. 42) to subsequent papers by Pinkus (ref. 53, 54) and Newkirk & Grobel (ref. 55) describing work which primarily set out to find a practical cure for the problem in the form of 'elliptical,' 'lobed' or 'self-loaded' bearings, rather than to understand the unstable oil whirl mechanism. Reference was also made to a group of papers (ref. 56,57 , 58) which describe a systematic experimental investigation of the influence of plain journal bearing parameters on unstable oil whirl during which one end of a symmetrical flexible rotor was supported in the specimen journal bearing while the other end rested on a ball bearing race. The conclusions of this experimental investigation were of a qualitative nature. In fact the results obtained can be shown to agree well with the linear oil force stability criterion but, on account of the small clearances of the specimen bearings and the use of the ball bearing race, the results cover a narrow and relatively uninteresting range of the dominant parameter of the problem as suggested by the linear oil force theory, $\left(\frac{\omega_1}{\omega_p}\right)^2$.

More recently the experimental work of Cole (ref 47) and Hughes (ref. 48) has implied that a cavitated oil film is inherently stable. The limitations of their results have already been mentioned in sect. 5.1.

Hori (ref. 14) gives a qualitative description of an experimental investigation of unstable oil whirl which provides little specific support for his theoretical instability criterion.

Recent experimental work at Loughborough (ref 5, 16) has concentrated on the unstable oil whirl of a short rigid rotor on 360° film journal bearings. This type of bearing is rarely met with in practice but it was chosen for ease of comparison of the results with theoretical analyses of non-linear oil force effects.

6.2 Experimental rig

6.2 - 1 Basis of rig design

The unstable oil whirl analysis of the previous chapter for a flexible rotor with its mass concentrated near the centre suggests that for that case the unstable oil whirl criterion can be expressed as a function of the bearing running condition and of two frequency ratios, $\left(\frac{\omega_1}{\omega_p}\right)^2$ and $\left(\frac{\omega_1}{\omega_+}\right)^2$. It is clearly desirable to base the

experimental programme on ranges of these parameters of practical interest.

$\left(\frac{\omega_1}{\omega_p}\right)^2 = \frac{ck}{W}$: The significance of the parameter $\frac{ck}{W}$ has already been discussed in sect. 4.2 - 1 where it was decided that the range of greatest practical interest is about $0.5 < \frac{ck}{W} < 3$. Referring to the theoretical stability chart Fig. 5.4 it can be seen that this range is just the region in which the 'break' in the various stability boundaries occurs and is thus by inference the region in which real systems are not closely approximated by either of the limiting hypotheses A or B.

$\left(\frac{\omega_1}{\omega_r}\right)^2$: The stability chart Fig. 5.4 and the results of previous observations of unstable oil whirl suggested that rotor rotational frequencies above twice the simply supported rotor natural frequency may be required for instability in some cases. Consideration of this factor, of the maximum safe speed of the rig and of realistic bearing running conditions suggested the choice of a rotor natural frequency corresponding to about 3,000 rev/min.

Load number: Both theory and experiment suggested that bearing load number has a considerable influence on unstable oil whirl and it was therefore resolved to cover as wide a range as possible.

6.2 - 2 Main assembly features

A photograph of the experimental rig used is given in Fig. 4.2. The rig employed the same foundations, bearing housings, drive, speed measurement device and oil temperature measurement device as were used for the synchronous whirl experiments and described in Chapter 4. The instability rig was different, however, in the following respects.

Rotor: On the basis of the above reasoning the rotor shown in Fig. 6.1was designed. Constructed from a single shaft with a shrunk on disc, the rotor was machined all over and weighed 50 lb f. To estimate the effective journal mass, half of the mass of the shaft was divided equally between the journals where it was added to the journal masses, while the other half of the shaft mass was added to the mass of the central disc. This method gives $\frac{m_1}{m_1+m_2} = .193$.

By means of a resonance test similar to that described in sect. 4.2-2 the natural frequency of the rotor on simple supports was found to correspond to 2,880 rev/min. Thus

$$\omega_1^2 = \left(\frac{2880 \times 2\pi}{60}\right)^2 = 91,000 \qquad \text{6.1}$$

Bearings: The bearing clearances were chosen on the basis of the above reasoning. Thus

$$\omega_p^2 = \frac{g}{c} = \frac{386}{c} \qquad \text{6.2}$$

Hence, using equations 6.1 and 6.2,

$$\left(\frac{\omega_1}{\omega_p}\right)^2 = \frac{91000\ c}{386} = \frac{c}{.00425} \qquad \text{6.3}$$

The desired practical range of $\left(\frac{\omega_1}{\omega_p}\right)^2$ values was obtained by using a variety of bearing diametral clearances (nominally .005, .008, .010, .015, .020, .025 in). The bearings were the same ones as those used for the synchronous whirl experiments except that they had been machined to a slightly different bore diameter and that initially they had no axial oil groove. The same range of $\frac{1}{d}$ ratio was used.

Lubricants: To obtain a variety of bearing operating conditions for the same rotor/bearing combination, oils with three different viscosity characteristics were used:

	Absolute viscosity (cp) at 100°F	at 210°F
Norpol 35	10	2
Norpol 45	40	4.8
Norpol 55	90	7

The oil was gravity fed from a tank (about 8 ft head) to the bearing surfaces initially through a single oil hole which was graded according to the bearing lengths ($\frac{5}{16}$, $\frac{3}{8}$, $\frac{7}{16}$, $\frac{1}{2}$ in). Later tests were completed with an axial oil groove $\frac{1}{2}$ in wide and 1/16 in. deep coincident with the oil hole.

6.2 - 3 Unstable whirl detection and measurement

The system used for unstable whirl observation is shown diagrammatically in Fig. 6.2. The motion of one of the rotor journals relative to its bearing was monitored by two moving coil transducers attached to the bearing housing with their probes contacting the journal in the same way as for the synchronous whirl observations and shown in the photograph in Fig. A 5.2.

The signals from the transducers were integrated by vibration meters which gave an approximate display of whirl amplitude. After a fixed amplification of about x 40, the signals were connected to the x and y terminals of an oscilloscope to obtain a trace of the whirl orbit.

After some practice, the frequency of small unstable whirls at the threshold of full instability was obtainable

using a lissajous figure technique. The small unstable whirls were usually of an unsteady amplitude which tended to grow, but with a constant frequency for a given system.

In order to prevent the masking of the small unstable whirl signals by small synchronous signals caused either by the residual out-of-balance of the rotor or by pulses transmitted to the transducer probes by minute irregularities on the journal bearing surface, the synchronous signals were much attenuated by a tunable filter which was switched into series with one of the transducer outputs. The efficient tuning of the filter was greatly assisted by referring to a large waveform display oscilloscope which provided a valuable method of distinguishing the 'half speed' whirl signal.

Thus modified, the transducer signal was compared with a strong, variable frequency signal from an oscillator and when a steady lissajous figure was obtained by synchronisation of the oscillator signal, the oscillator frequency could be read off from a four figure digital counter.

6.3 Experimental phenomena and procedure

6.3 - 1 Effect of variable frequency external excitation on rotor close to instability.

The nature of the stability boundary was initially investigated with caution. Mainly for safety reasons it was hoped that close to instability, the rotor response to external excitation would provide a useful method of defining the instability boundary by extrapolation from a stable condition. The reasoning is based on an analysis by Morrison (ref. 50).

Accordingly, a 5 watt variable frequency exciter was bolted to the foundation at the free end of the rotor. It was coupled by means of a small ball bearing race to a short quill located co-axially in the rotor. A series of tests were completed in which, for a rotor speed just below instability, the response of the rotor journal was noted to a variety of excitation powers and frequencies. It was found that the response was resonant at an excitation frequency equal to that of the self-excited small whirls usually occurring near the stability limit. The procedure was repeated for rotor speeds closer to the stability boundary when, for the same excitation power, the resonant amplitude increased while the resonant frequency remained almost constant. After further

repetitions the unstable speed could be extrapolated as shown for a particular case in Fig. 6.3. This speed corresponded well with that obtained by increasing the rotor speed until full instability developed.

It was felt that this method could provide a comprehensive indication of the degree of sensitivity and of the unstable frequency characteristics of the system as it approached instability. Difficulties were present, however. To measure resonant amplitude accurately, the excitation usually had to be in phase as well as synchronised with any self-excited small whirls which was awkward because of the unsteady nature of the whirls. Also, due to small synchronous signals, large levels of excitation were often required and the accuracy of the extrapolation suffered correspondingly.

6.3 - 2 Nature of the stability boundary

After several preliminary runs a pattern of rotor behaviour emerged which was confirmed by the subsequent experimental programme.

A typical rotor response is given in Fig. 6.4. On increasing rotor speed from rest, the rotor experienced a resonant synchronous whirl of small amplitude at a running

frequency close to the rotor's simply supported natural frequency, the whirl amplitude decreasing as the running frequency was increased above that value.

On further acceleration to some higher speed, the rotor suddenly became unstable, the fully developed unstable whirl being close in form to the circle dictated by the bearing clearance and with a frequency slightly less than half of the running frequency. Broadly speaking two forms of transition from stable to unstable motion was observed.

(i) With an unstable running frequency not far above the rotor natural frequency on simple supports the transition was by means of a double looping of the original synchronous whirling orbit. With increased speed, one of the loops decreased in size relative to the other and began to move around the inside of the larger one while it remained stationary. Corresponding to further increases in speed, the smaller loop continued to decrease in size and moved round more rapidly inside the larger one which then began to expand and move round in the same direction until eventually the small loop disappeared and the rapidly rotating large loop burst into the fully developed instability. This sequence was observed on many occasions.

(ii) With an unstable running frequency well above the rotor natural frequency on simple supports, the rotor was steady immediately before instability. From almost a point, the journal centre trace suddenly opened out in a spiralling elliptical path to the fully developed instability. Often small amplitude unstable whirls were impossible to observe in these circumstances. Although a less violent instability than (i) this type had a smaller transition speed range.

On a few occasions only, corresponding to load numbers higher than 25, the rotor was still stable at the rig speed limit of about 7,000 rev/min. In this condition the rotor was often unsteady without becoming fully unstable. On two of these occasions, with bearing pairs of 1 x .020 in and .667 x .010 in, the whirl frequency was observed to be locked onto a fraction of exactly $\frac{1}{3}$ of the rotor running frequency, the whirl frequency in both cases being close to 1920 rev/min, or $\frac{2}{3}$ of the rotor's natural frequency on simple supports. On about four other occasions, at lower speeds, mildly resonant whirls were observed with a locked frequency ratio of exactly $\frac{1}{2}$. These were in some cases difficult to distinguish from the unstable oil whirls and occurred at whirl frequencies of 1660, 1820, 2100 and 2550 rev/min.

These 'locked' frequency ratios are almost certainly a result of non-linear characteristics of the oil film since these would provide a coupling between sub-harmonic motion of the rotor and the synchronous out-of-balance forcing effect.

When the rotor speed was reduced from the fully unstable state in order to regain stability it was always necessary to make the reduction to a speed rather lower than that at which the instability had occurred. This 'hysteresis effect' varied from as much as 600 rev/min down to practically zero. Although for each run the speed at which stability was regained was quite consistent, no meaningful correlation with other factors was observed except that the effect increased with clearance.

On the occasions on which speed was increased several hundred rev/min during a fully developed instability the whirl amplitude tended to increase and no inclination to pull through the large whirl was observed. Although the fully developed unstable whirl resulted in large rotating forces the rig was safe in the sense that practically no metal to metal contact was observed.

6.3 - 3 Experimental procedure

For each experimental point, the rotor was accelerated until unstable whirling occurred. The speed was then reduced until whirling ceased and reset to about 100 rev/min below the unstable speed. The rotor was run at this condition for about one hour in order to reach thermal equilibrium. During this period the unstable whirl was often considerably effected by the decrease in lubricant viscosity with increase in temperature. It was observed that below a load number of about 5 the warming decreased the unstable speed but it had the opposite effect for higher load numbers.

After thermal equilibrium was reached the relevant condition was determined by measuring:

1. the bearing temperatures;

2. the frequency of small amplitude (i.e. incipient) unstable whirl where this was observable, as it usually was;

3. the rotor speed at the onset of large amplitude unstable whirl. Six readings of this speed were taken for each point and the mean value used. These speeds were repeatable to about $\pm$ 20 rev/min in each test run.

6.4 Analysis of experimental results

A selection of the results obtained at the stability boundary is given in the Table in Fig. 6.5.

Two almost independent methods of analysis of the results were used.

6.4 - 1 Evaluation of P and Q primarily from observed values of ω_r

From equation 5.17:

$$\left[1 - \frac{m_1}{m_1+m_2} \frac{\lambda^2}{\left(\frac{\omega_1}{\omega_r}\right)^2}\right] \left(\frac{\omega_1}{\omega_p}\right)^2 = P \left(\frac{\omega_1}{\omega_r}\right)^2 - Q \qquad \text{6.4}$$

Grouping the points into ranges of load number, that is 0 - 1.5, 1.5 - 3, 3 - 6 and 6 - 20, values of $\left[1 - \frac{m_1}{m_1+m_2} \frac{\lambda^2}{\left(\frac{\omega_1}{\omega_r}\right)^2}\right] \left(\frac{\omega_1}{\omega_p}\right)^2$ have been plotted against $\left(\frac{\omega_1}{\omega_r}\right)^2$ in Fig. 6.6. In Fig. 6.6 (a, b, c, d) the oil corresponding to each point can be distinguished while for Fig. 6.6 (p, q, r, s) the $\frac{1}{d}$ ratio for each point can be distinguished. In both sets of figures the points corresponding to grooved bearings have been circled.

A line has been drawn in each figure which is considered representative of the right hand boundary of the points and from the slope and intercept of these lines,

values can be deduced for P and Q respectively.

6.4 - 2 Evaluation of P and Q primarily from observed values of W_b

From equation 5.7

$$P = \frac{Q}{\left(\frac{W_b}{W_r}\right)^2} \qquad \text{6.5}$$

Substituting equation 6.5 into equation 6.4 it can readily be shown that

$$Q = \frac{\left(\frac{W_1}{W_p}\right)^2 \left[1 - \frac{m_1}{m_1+m_2}\left(\frac{W_b}{W_1}\right)^2\right]}{\left[\left(\frac{W_1}{W_b}\right)^2 - 1\right]} \qquad \text{6.6}$$

These relationships may be used to determine P and Q for each experimental point as a function of load number. Plots of P and Q obtained in this way are shown in Fig. 6.7 and Fig 6.8 respectively where, as for Fig. 6.6, $\frac{1}{d}$ ratio, oil and grooving can be distinguished. Lower boundaries are drawn which are considered as representative of the experimental points and the stepped function obtained by the method of section 6.4 - 1 is also given for comparison.

6.4 - 3 Significance of the scatter of experimental P and Q values.

It is immediately clear from Fig. 6.6 (a, b, c, d), Fig. 6.7 (a) and Fig. 6.8 (a) that there is a strong correlation between the boundaries of the scatter regions and those points that were obtained with the thinnest oil, Norpol 35. The correlation is particularly striking in the P and Q diagrams where it can be seen that the points corresponding to the ungrooved bearings with the medium oil form a group behind the ungrooved thin oil points while those points obtained with the thickest oil and ungrooved bearings form a group still further away from the boundary.

The grooving appears to have improved the correlation with the boundary of the thickest oil group of points, to have scarcely altered the position of the medium oil group and to have somewhat reduced the correlation of the thin oil group.

Fig. 6.6 (p, q, r, s), Fig. 6.7 (b) and Fig. 6.8 (b) suggest that the points corresponding to large $\frac{l}{d}$ ratios agree rather better with the boundary than those corresponding to the small $\frac{l}{d}$ ratios but there are

notable exceptions with the thickest oil.

Although there are no doubt a variety of possible explanations of the significance of the above correlations, the following is offered as the most likely one.

During a fully developed unstable oil whirl the pumping action of the journal is observed to be much greater than for steady operation at the same speed. Therefore if the supply of oil to the bearing is such that it cannot meet the volume requirement of a fully unstable condition, presumably the system cannot become fully unstable. Since the situation was little improved by the grooving, it would seem that in the present case the supply system behind the inlet is responsible. In fact, it is probable that the resistance of the thickest oils in the $\frac{3}{4}$ in diameter supply tubes was sufficiently large to considerably reduce the effective pressure head at the bearing. It is therefore suggested that the results with the thinnest oil correspond most closely to the ideal supply assumptions of the theory and that more consistent results would have been obtained with the thicker oils if a pressurised oil supply had been used.

6.5 Comparison of theoretical and experimental results

For comparison, values of P and Q corresponding to the stepped functions obtained in Fig. 6.6, to the lower boundaries of the points in Fig. 6.7 and Fig. 6.8 and to representative theoretical values have been plotted in Fig. 6.9 and Fig. 6.10 respectively. The theoretical values which are plotted in terms of journal eccentricity have been related to the experimental results which are plotted in terms of load number by using Ockvirk's experimental curve (ref. 7).

6.5 - 1 P values.

The lower boundary of the experimental values of P is lower than any of the theoretical values except those of Hori. However, since Hori's assumption of bearing boundary conditions is not a practical one (.e.g. see discussion of long bearing boundary condition in Appendix 1) his corresponding numerical stability criterion is unlikely to be accurate. Therefore, remembering that it is low values of P which are critical for instability, the lower boundary of the experimental P values is suggested as the most practical for instability calculations Apart from the high values of Pinkus & Sternlicht the remaining theoretical values are in fair agreement with the suggested practical curve, the agreement being good for high load numbers. For the lowest load numbers, where few experimental points were obtained, the

recommended curve has been drawn to take account of the theoretical treatments which agree best with the experimental curve for the higher load numbers.

6.5 - 2 Q values

Bearing in mind that for a given P value high values of Q are the most critical for instability, it is of some importance to consider the significance of the spread of the points corresponding to the thicker oils to high Q values. In fact it must be remembered that the high Q values correspond to P values which are also abnormally high and that for $Q > \frac{P}{4}$ a whirl frequency of greater than half of the running frequency is implied but in fact was never observed in the experiments and rarely has been in the history of the subject. Hence an upper limit in the Q chart is provided by the curve $Q = \frac{P}{4}$ as deduced from the recommended curve of P values in Fig. 6.9. By referring back to Fig. 6.8 it can be seen that the $Q = \frac{P}{4}$ curve closely follows the Q values obtained experimentally using the thin oil. The curve encloses the practical theoretical Q values except at load numbers higher than about 10. Since the whirl frequency ratio was observed to be less for high load numbers than for low ones, the experimental curve which lies between the $\frac{P}{4}$ curve and the majority of the theoretical

values is preferred for that region. The theoretical values of Q are only in fair agreement with the proposed practical Q curve.

6.6 Use of unstable whirl data

6.6 - 1 Single-span symmetrical rotors with mass concentrated in the centre.

A stability chart, derived from the practical values of P and Q given in Fig. 6.9 and Fig. 6.10 respectively, is given in Fig. 6.11 and may be used to check the stability of a proposed rotor design as described by Morrison (ref. 18).

Alternatively the P and Q values may be used as suggested by Martin in his contribution to the discussion of reference 19. In that form the effect on rotor stability of modifications to bearing design may be readily estimated.

6.6 - 2 Practical rotors

In appropriate cases the values of P and Q can also be used for the instability analysis of more practical rotor systems in the manner suggested in section 5.5.

As a simple example of this application, the stability of the type of rotor which was assumed to approximate the rotor used in the experiments will be considered at a load number of 3 (which seems to correspond to about the most unstable bearing running condition.) For $\frac{m_1}{m_1+m_2} = 0$ the stability boundary corresponds to the $N_L = 3$ boundary of Fig. 6.11 and is replotted in Fig. 6.12. The stability boundary for intermediate values of $\frac{m_1}{m_1+m_2}$ of 0.1 and 0.4 have been obtained by substituting these values and the recommended values of P and Q into equation 6.4. It is found that for a greater distribution of mass but the same clearance, bearing load, bearing running condition and rotor natural frequency (i.e. same rotor static deflection - implying a reduction of shaft stiffness), the stability is improved. The condition $\frac{m_1}{m_1+m_2} = 1$ is the bounding case of a rigid rotor.

CONCLUSION

An advantage of the linear oil force theory relative to earlier oil film theories used for oil whirl is that, because of the linearisation which is the basis of the theory, for whirl, the dynamic characteristics of hydrodynamic oil films and the dynamic characteristics of whirling rotors may be considered independently. Also due to the linearisation, the equations of whirling motion of combined rotor/oil film systems are of a simple form. It is clear, however, that analyses based on these equations cannot be regarded as reliable until it has been shown that the linearisation itself is reliable in practice. Although ideally this check ought to be made with full size machines, the remarkably good correlation between the experimental results of the present investigations with model rotors when the results are plotted in terms of parameters suggested by the linear oil force theory provides strong support for the theory.

The correlation between the numerical whirl predictions and the experimental whirl results is also good. However, this comparison highlights the desirability of obtaining accurate evaluations of the set of oil force coefficients. Since a variety of analytical solutions of the coefficients are available which yield different numerical values, experimental determinations of the coefficients would be of

interest.

On the basis of the good correlation between the theory and the experiment of this thesis, it is suggested that the given theoretical and experimental results can be regarded as reliable guides to the behaviour of simple, practical rotor/oil film systems. Furthermore, since the application of the receptance theory for rotors has shown that the same form of whirl analysis used for the simple rotor/oil film system applies to systems with axially unsymmetrical rotors or with co-axially coupled rotors, it is also suggested that in the latter cases the application of the linear oil force theory will yield reliable oil whirl results. Since the detailed solution of the whirling of most practical systems involves lengthy calculations, the importance of both qualitative analytical approaches and model rotor experiments should be considered for the investigation of design criteria.

Although the work of this thesis has been based on the assumptions of immovable bearing housings and relatively ideal rotors, the justification of the use of the linear oil force theory and, in part, the rotor receptance theory are logical steps in the development of analyses which take account of other system variables.

A P P E N D I X I

A 1.1 To find simple relations between the velocity force coefficients and displacement force coefficients of a long bearing

Morrison (ref.18) not only deduced simple explicit relations between the velocity and displacement force coefficients of a short bearing but also showed that these relations should be independent of film extent. That is, the relations were functions only of the oil film equations and not of the circumferential end conditions.

Following a method similar to Morrison's, the writer has found that for the long bearing case the same simple explicit relations hold for three of the four velocity force coefficients but that no simple relation is apparent for the fourth coefficient.

Extensive preliminary investigations of the problem were hampered by an incorrect choice of dynamic circumferential boundary conditions. To emphasise the effect of this choice, the results of an early analysis based on it are given.

A 1.1 - 1 Reynold's equation for the dynamic long bearing case - derivation of circumferential pressure gradient.

Referring to Fig. 1.1 and making the usual assumptions:

Continuity equation: $\frac{1}{R}\frac{\partial q}{\partial \theta} = -\frac{\partial h}{\partial t}$ ——— A1.1

Force equation: $\frac{1}{R}\frac{\partial p}{\partial \theta} = \eta \frac{\partial^2 u}{\partial y^2}$ ——— A1.2

Integrating equation A1.2 twice with respect to y, putting

$$u = 0 \quad \text{at} \quad y = 0$$

$$u = R\omega_s \quad \text{at} \quad y = h$$

$$u = \frac{1}{2\eta R}\frac{\partial p}{\partial \theta} y(y - h) + \frac{R\omega_s y}{h}$$

$$\therefore \quad q = \int_0^h u \, dy = -\frac{1}{12\eta R}\frac{\partial p}{\partial \theta} h^3 + \frac{R\omega_s h}{2} \quad \text{——— A1.3}$$

With displacements r and s defined in Fig. 1.6,

$$h = c + e\cos\theta + r\cos\theta - s\sin\theta \quad \text{——— A1.4}$$

Substituting equation A1.4 into equation A1.1 and integrating w.r.t. θ,

$$q = -R(\dot{r}\sin\theta + \dot{s}\cos\theta) + C_1 \quad \text{——— A1.5}$$

where the dot notation indicates differentiation w.r.t. time and C_1 is constant w.r.t. θ.

Then from equation A1.3 and equation A1.5:

$$-\frac{1}{12\eta R}\frac{dp}{d\theta}h^3 + \frac{R\omega h}{2} + R(\dot{r}\sin\theta + \dot{s}\cos\theta) = C_1 \qquad \text{A1.6}$$

This equation may be obtained directly from the long bearing form of Reynold's equation 1.1 after one integration. It has been derived here to obtain the flow relations equation A1.3 and equation A1.5 which will be used to discuss boundary conditions.

Re-arranging A1.6:

$$\frac{dp}{d\theta} = 6\eta R^2\omega_+\left[\frac{(e + r + \frac{2}{\omega_+}\dot{s})\cos\theta - (s - \frac{2}{\omega_+}\dot{r})\sin\theta + c - C_1}{h^3}\right] \qquad \text{A1.7}$$

$$\text{Hence } p = 6\eta R^2\omega_+\left[(e + r + \frac{2}{\omega_+}\dot{s})\int\frac{\cos\theta\,d\theta}{h^3} - (s - \frac{2}{\omega_+}\dot{r})\int\frac{\sin\theta\,d\theta}{h^3} + (c - C_1)\int\frac{d\theta}{h^3} + C_2\right] \qquad \text{A1.8}$$

Let $p = o$ at $\theta = \theta_1$ in equation A1.8

$$\therefore\ p = 6\eta R^2\omega_+\left[e\int_{\theta_1}^{\theta_2}\frac{\cos\theta}{h^3}d\theta + (r + \frac{2}{\omega_+}\dot{s})\int_{\theta_1}^{\theta_2}\frac{\cos\theta\,d\theta}{h^3} - (s - \frac{2\dot{r}}{\omega_+})\int_{\theta_1}^{\theta_2}\frac{\sin\theta}{h^3}d\theta + (c - C_1)\int_{\theta_1}^{\theta_2}\frac{d\theta}{h^3}\right] \qquad \text{A1.9}$$

Also let p = o at $\theta = \theta_2$ in equation A1.8. Then

$$(c - C_1) = -(e + r + \frac{2}{\omega_+}\dot{s}) \frac{\int_{\theta_1}^{\theta_2} \frac{\cos\theta\, d\theta}{h^3}}{\int_{\theta_1}^{\theta_2} \frac{d\theta}{h^3}} + (s - \frac{2}{\omega_+}\dot{r}) \frac{\int_{\theta_1}^{\theta_2} \frac{\sin\theta\, d\theta}{h^3}}{\int_{\theta_1}^{\theta_2} \frac{d\theta}{h^3}}$$

i.e. $(c - C_1) = -(e + r + \frac{2}{\omega_+}\dot{s}) \frac{K}{I} + (s - \frac{2}{\omega_+}\dot{r})\frac{J}{I}$ ———— A1.10

where $I = \int_{\theta_1}^{\theta_2} \frac{d\theta}{h^3}$, $K = \int_{\theta_1}^{\theta_2} \frac{\cos\theta\, d\theta}{h^3}$, $J = \int_{\theta_1}^{\theta_2} \frac{\sin\theta\, d\theta}{h^3}$

Substituting equation A1.10 into equation A1.7

$$\frac{dp}{d\theta} = 6\eta R^2 \omega_+ \left[\frac{(e+r+\frac{2}{\omega_+}\dot{s})(\cos\theta - \frac{K}{I}) - (s - \frac{2}{\omega_+}\dot{r})(\sin\theta - \frac{J}{I})}{h^3}\right]$$

———— A1.11

A 1.1 - 2 Definition of oil pressure forces.

Referring to Fig.1.1, the components of the total oil pressure force in the r and s directions are:

$$Q_r = - Rl \int_{\theta_1}^{\theta_2} p \cos\theta \; d\theta$$

$$Q_s = Rl \int_{\theta_1}^{\theta_2} p \sin\theta \; d\theta$$

Integrating by parts:

$$Q_r = - Rl \left[p \sin\theta \Big|_{\theta_1}^{\theta_2} - \int_{\theta_1}^{\theta_2} \frac{dp}{d\theta} \sin\theta \; d\theta \right]$$

$$Q_s = Rl \left[- p \cos\theta \Big|_{\theta_1}^{\theta_2} + \int_{\theta_1}^{\theta_2} \frac{dp}{d\theta} \cos\theta \; d\theta \right]$$

Since p at θ_1 = p at θ_2 = 0,

$$\therefore \quad Q_r = Rl \int_{\theta_1}^{\theta_2} \frac{dp}{d\theta} \sin\theta \; d\theta$$

$$Q_s = Rl \int_{\theta_1}^{\theta_2} \frac{dp}{d\theta} \cos\theta \; d\theta$$

A1.12

Definition of oil force coefficients.

On the basis that r, s, $\frac{2}{\omega_r}\dot{r}$, $\frac{2}{\omega_r}\dot{s}$ are small relative to e, let

$$Q_r = Q_{ro} + \frac{\partial Q_r}{\partial r} r + \frac{\partial Q_r}{\partial \dot{s}} \dot{s} + \frac{\partial Q_r}{\partial s} s + \frac{\partial Q_r}{\partial \dot{r}} \dot{r}$$

$$Q_s = Q_{so} + \frac{\partial Q_s}{\partial r} r + \frac{\partial Q_s}{\partial \dot{s}} \dot{s} + \frac{\partial Q_s}{\partial s} s + \frac{\partial Q_s}{\partial \dot{r}} \dot{r}$$

Where the oil force components Q_{ro}, Q_{so} balance the static load on the bearing. The remaining force components are assumed proportional to displacements and velocities of the journal centre. The constants of proportionality are the displacement force coefficients, a, and the velocity force coefficients, b, referred to in

equation 1.8 where here

$$a_{rr} = \frac{\partial Q_r}{\partial r} \qquad a_{rs} = \frac{\partial Q_r}{\partial s}$$

$$a_{sr} = \frac{\partial Q_s}{\partial r} \qquad a_{ss} = \frac{\partial Q_s}{\partial s}$$

$$b_{rr} = \frac{\partial Q_r}{\partial \dot{r}} \qquad b_{rs} = \frac{\partial Q_r}{\partial \dot{s}}$$

$$b_{sr} = \frac{\partial Q_s}{\partial \dot{r}} \qquad b_{ss} = \frac{\partial Q_s}{\partial \dot{s}}$$

A1.13

A 1.1 - 3 Differentiation of an integral.

For a function $f_1(r) = \int_{\theta_1=a(r)}^{\theta_2=b(r)} f_2(r,\theta)\, d\theta$ where

both a (r) and b(r) are continuous and differentiable functions of r for $u \leq r \leq v$; and for $f_2(r,\theta)$ to be a continuous function of r and θ where $\theta_1 \leq \theta \leq \theta_2$, $u \leq r \leq v$, it can be shown that

$$\frac{d}{dr} f_1(r) = -f_2(\theta_1, r) \frac{d\theta_1}{dr} + \int_{\theta_1}^{\theta_2} \frac{d f_2(r,\theta)}{dr} d\theta + f_2(\theta_2, r) \frac{d\theta_2}{dr}$$

If it can be assumed that the integral term is much larger than the other two, the above equation reduces to:

$$\frac{d}{dr} f_1(r) = \int_{\theta_1}^{\theta_2} \frac{d}{dr} f_2(r,\theta)\, d\theta \qquad \text{A1.14}$$

A 1.1 - 4 Evaluation of oil force coefficients.

Using the result equation A1.14, the oil force coefficients defined in A1.13 can be evaluated by differentiating the oil forces expressed in A1.12 after substituting for $\frac{dp}{d\theta}$ from A1.11. Now

$$\frac{1}{6\eta R^2\omega_+}\frac{d}{dr}\left(\frac{dp}{d\theta}\right) = \frac{(\cos\theta - \frac{K}{I})}{h^3} - \frac{e\frac{d}{dr}\left(\frac{K}{I}\right)}{h^3} - \frac{3e\,(\cos\theta - \frac{K}{I})\cos\theta}{h^4}$$

and similarly for $\frac{d}{d\dot{r}}\left(\frac{dp}{d\theta}\right)$ and $\frac{d}{ds}\left(\frac{dp}{d\theta}\right)$ and $\frac{d}{d\dot{s}}\left(\frac{dp}{d\theta}\right)$

Also

$$\frac{d}{dr}\left(\frac{K}{I}\right) = \frac{d}{dr}\;\frac{\int_{\theta_1}^{\theta_2}\frac{\cos\theta\,d\theta}{h^3}}{\int_{\theta_1}^{\theta_2}\frac{d\theta}{h^3}}$$

$$= \frac{-3}{I}\left[\int_{\theta_1}^{\theta_2}\frac{\cos^2\theta\,d\theta}{h^4} - \frac{K}{I}\int_{\theta_1}^{\theta_2}\frac{\cos\theta\,d\theta}{h^4}\right]$$

$$= -\frac{3}{I}\int_{\theta_1}^{\theta_2}\frac{(\cos\theta - \frac{K}{I})\cos\theta}{h^4}\,d\theta$$

Similarly $\frac{d}{ds}\left(\frac{K}{I}\right) = \frac{3}{I}\int_{\theta_1}^{\theta_2}\frac{(\cos\theta - \frac{K}{I})}{h^4}\sin\theta\,d\theta$

and correspondingly for $\frac{d}{d\dot{r}}\left(\frac{J}{I}\right)$ and $\frac{d}{d\dot{s}}\left(\frac{J}{I}\right)$.

Collecting these results, the displacement and velocity force coefficients can be expressed as follows:

$$
\begin{aligned}
a_{rr} &= 6\eta R^3 1\omega_+ \left[\int_{\theta_1}^{\theta_2} \frac{(\cos\theta - \frac{K}{I})\sin\theta\, d\theta}{h^3} - 3e\int_{\theta_1}^{\theta_2} \frac{(\cos\theta - \frac{K}{I})(\sin\theta - \frac{J}{I})\cos\theta\, d\theta}{h^4}\right] \\
a_{sr} &= 6\eta R^3 1\omega_+ \left[\int_{\theta_1}^{\theta_2} \frac{(\cos\theta - \frac{K}{I})\cos\theta\, d\theta}{h^3} - 3e\int_{\theta_1}^{\theta_2} \frac{(\cos\theta - \frac{K}{I})^2\cos\theta\, d\theta}{h^4}\right] \\
a_{rs} &= 6\eta R^3 1\omega_+ \left[\int_{\theta_1}^{\theta_2} \frac{(\sin\theta - \frac{J}{I})\sin\theta\, d\theta}{h^3} + 3e\int_{\theta_1}^{\theta_2} \frac{(\cos\theta - \frac{K}{I})(\sin\theta - \frac{J}{I})\sin\theta\, d\theta}{h^4}\right] \\
a_{ss} &= 6\eta R^3 1\omega_+ \left[\int_{\theta_1}^{\theta_2} \frac{(\sin\theta - \frac{J}{I})\cos\theta\, d\theta}{h^3} + 3e\int_{\theta_1}^{\theta_2} \frac{(\cos\theta - \frac{K}{I})\sin\theta\, d\theta}{h^4}\right]
\end{aligned}
$$

$$
\begin{aligned}
b_{rr} &= 6\eta R^3 1\omega_+ \frac{2}{\omega_+} \int_{\theta_1}^{\theta_2} \frac{(\sin\theta - \frac{J}{I})\sin\theta\, d\theta}{h^3} \qquad \text{Al.15} \\
b_{sr} &= 6\eta R^3 1\omega_+ \frac{2}{\omega_+} \int_{\theta_1}^{\theta_2} \frac{(\sin\theta - \frac{J}{I})\cos\theta\, d\theta}{h^3} \\
b_{rs} &= 6\eta R^3 1\omega_+ \frac{2}{\omega_+} \int_{\theta_1}^{\theta_2} \frac{(\cos\theta - \frac{K}{I})\sin\theta\, d\theta}{h^3} \\
b_{ss} &= 6\eta R^3 1\omega_+ \frac{2}{\omega_+} \int_{\theta_1}^{\theta_2} \frac{(\cos\theta - \frac{K}{I})\cos\theta\, d\theta}{h^3}
\end{aligned}
$$

$$
\begin{aligned}
b_{rs} &= 6\eta R^3 1\omega_+ \frac{2}{\omega_+} \int_{\theta_1}^{\theta_2} \frac{(\cos\theta\sin\theta - \frac{K}{I}\sin\theta)\, d\theta}{h^3} \\
&= 6\eta R^3 1\omega_+ \frac{2}{\omega_+} \int_{\theta_1}^{\theta_2} \frac{(\cos\theta\sin\theta - \frac{J}{I}\cos\theta)\, d\theta}{h^3}
\end{aligned}
$$

$\therefore \quad b_{rs} = b_{sr}$ — Al.16

Referring back to equation A1.11 and equation A1.12, if $r = s = \dot{r} = \dot{s} = 0$,

$$Q_{ro} = 6\eta R^3 l \omega_+ \left[e \int_{\theta_1}^{\theta_2} \frac{(\cos\theta - \frac{K}{I}) \sin\theta}{h^3} \, d\theta \right] = W \cos\phi$$

$$Q_{so} = 6\eta R^3 l \omega_+ \left[e \int_{\theta_1}^{\theta_2} \frac{(\cos\theta - \frac{K}{I}) \cos\theta}{h^3} \, d\theta \right] = W \sin\phi$$

A1.17

where W is the static load on the bearing and ϕ is the attitude angle of the journal line of centres.

As shown by Morrison (ref.18)

$$a_{ss} = \frac{W \cos\phi}{e}, \qquad a_{rs} = -\frac{W \sin\phi}{e}$$ A1.18

Substituting equation A1.17 and equation A1.18 into equation A1.15 and using equation A1.16:

$$b_{sr} = b_{rs} = \frac{2}{\omega_+} a_{ss}$$

$$b_{ss} = -\frac{2}{\omega_+} a_{rs}$$ A1.19

Attempts to obtain a simple relation between the fourth velocity coefficient b_{rr} and the displacement coefficients were made by trying to make use of the fact that the first of the two terms on the right hand side of the displacement expressions in A1.15 correspond to the velocity terms. The attempts were unsuccessful.

A 1.2 'Zero pressure gradient' boundary condition for static case

Equating equation AL3 and equation AL5 for the static case,

$$q = -\frac{1}{12\eta R}\frac{dp}{d\theta}h^3 + \frac{R\omega_4 h}{2} = c_1 \qquad \text{AL.20}$$

(pressure flow) (shear flow)

For laminar flow it can be seen that the total flow is made up of a continuous shear component and a pressure component which therefore must also be continuous. If it is assumed that the oil pressure cannot become negative (cavitation), it follows that to avoid flow discontinuity at the end of the pressure profile, the pressure flow and hence the pressure gradient will be zero. The boundary conditions indicated are therefore

$$\begin{aligned} p &= 0 \quad \text{at} \quad \theta = \theta_1 \\ p = \frac{dp}{d\theta} &= 0 \quad \text{at} \quad \theta = \theta_2 \end{aligned} \qquad \text{AL.21}$$

Although it is clear that the second order Reynold's equation for a long bearing can only satisfy two independent boundary conditions, it can be shown - as by Pinkus & Sternlicht (ref. 4) - that the last two conditions of equation AL.21 are not necessarily independent. Calculated pressure profiles satisfying all three conditions of equation AL.21 are in good

agreement with experimental evidence and Pinkus & Sternlicht have assembled several tables of bearing running data based on these conditions.

A 1.3 Incorrect simple relations between the velocity force coefficients and displacement force coefficients of a long bearing based on the static 'zero pressure gradient' boundary condition

If it is assumed that the boundary conditions equation A1.21 are at least approximately true for the dynamic case, equation A1.7 becomes

$$\frac{dp}{d\theta} = 6\eta R^2 \omega_+ \left[(e+r+\frac{2}{\omega_+}\dot{s})\frac{(\cos\theta - \cos\theta_2)}{h^3} - (s-\frac{2}{\omega_+}\dot{r})(\sin\theta - \sin\theta_2) \right] \qquad \text{A1.22}$$

After a procedure similar to that described in section A 1.1, the following simple relation was found between the velocity and displacement force coefficients:

$$b_{rs} = \frac{2}{\omega_+} a_{ss}$$

$$b_{ss} = \frac{-2}{\omega_+} a_{rs}$$

$$b_{sr} = \frac{-2}{\omega_+} a_{rr}$$

$$b_{rr} = \frac{2}{\omega_+} \left[2 \epsilon^2 a_{rs} + (1 - \epsilon^2) a_{sr} \right]$$

The relations for the two coefficients b_{rs} and b_{sr} agree with those found in the previous analysis equation A1.19. The relations for the other two coefficients are quite different from the previous analysis and trial stability calculations using them have yielded predictions which are far removed from observed behaviour.

A 1.4 Incompatibility of the 'zero pressure gradient' type of boundary condition for the dynamic case

By adopting the two boundary conditions

$$p = 0 \quad \text{at} \quad \theta = \theta_1$$

and $$p = K \frac{dp}{d\theta} \quad \text{at} \quad \theta = \theta_2 \qquad \text{A1.23}$$

Pinkus & Sternlicht (ref. 4) were able to show that there existed a condition for which

$$p = \frac{dp}{d\theta} = 0 \quad \text{at} \quad \theta = \theta_2 \qquad \text{A1.24}$$

independently of the value of K. In the present notation, the condition was expressible in the form

$$I \cos\theta_2 = K \qquad \text{A1.25}$$

When the same end conditions equation A1.23 are tried for the dynamic case, to satisfy the requirements equation A1.24, in addition to the condition equation A1.25, a second condition was found:

$$I \sin\theta_2 = J \qquad \text{A1.26}$$

The conditions could be deduced by comparing equation A1.22 with A1.11.

An oil pressure profile satisfying equation A1.26 is quite incompatible with those observed experimentally. Hence it must be concluded that a 'zero pressure gradient' condition is not satisfied in the dynamic case.

Attempts to incorporate a modified 'zero pressure gradient' condition were not successful.

A P P E N D I X 2

Orthogonal properties of the characteristic deflection modes.

The characteristic equation 2.13 can be written

$$\tau \begin{bmatrix} s_1 \\ s_2 \\ s_3 \end{bmatrix} = \begin{bmatrix} \tau_{11} & \tau_{12} & \tau_{13} \\ \tau_{12} & \tau_{22} & \tau_{23} \\ \tau_{13} & \tau_{23} & \tau_{33} \end{bmatrix} \begin{bmatrix} s_1 \\ s_2 \\ s_3 \end{bmatrix} \qquad \text{A 2.1}$$

Let the roots of the frequency determinant corresponding to equation A 2.1, τ_1, τ_2, τ_3 be different from each other (this will always be the case for a single span rotor) and let the characteristic deflection modes corresponding to each root be expressed as $s'_{11}\ s'_{21}\ s'_{31}$, $s'_{12}\ s'_{22}\ s'_{32}$, $s'_{13}\ s'_{23}\ s'_{33}$ respectively where the shape but not the scale factor of each mode is known. The following identity then follows from equation A 2.1:

$$\begin{bmatrix} s'_{11} & s'_{12} & s'_{13} \\ s'_{21} & s'_{22} & s'_{23} \\ s'_{31} & s'_{32} & s'_{33} \end{bmatrix} \begin{bmatrix} \tau_1 & 0 & 0 \\ 0 & \tau_2 & 0 \\ 0 & 0 & \tau_3 \end{bmatrix} = \begin{bmatrix} \tau_{11} & \tau_{12} & \tau_{13} \\ \tau_{12} & \tau_{22} & \tau_{23} \\ \tau_{13} & \tau_{23} & \tau_{33} \end{bmatrix} \begin{bmatrix} s'_{11} & s'_{12} & s'_{13} \\ s'_{21} & s'_{22} & s'_{23} \\ s'_{31} & s'_{32} & s'_{33} \end{bmatrix} \qquad \text{A2.2}$$

Premultiply the j^{th} column of equation A 2.2 by the k^{th} deflection mode $\begin{bmatrix} s'_{1k} & s'_{2k} & s'_{3k} \end{bmatrix}$

$$\tau_j \begin{bmatrix} s'_{1k} & s'_{2k} & s'_{3k} \end{bmatrix} \begin{bmatrix} s'_{1j} \\ s'_{2j} \\ s'_{3j} \end{bmatrix} = \begin{bmatrix} s'_{1k} & s'_{2k} & s'_{3k} \end{bmatrix} \begin{bmatrix} \tau_{11} & \tau_{12} & \tau_{13} \\ \tau_{12} & \tau_{22} & \tau_{23} \\ \tau_{13} & \tau_{23} & \tau_{23} \end{bmatrix} \begin{bmatrix} s'_{1j} \\ s'_{2j} \\ s'_{3j} \end{bmatrix}$$

Transposing both sides:

$$\tau_j \begin{bmatrix} s'_{1j} & s'_{2j} & s'_{3j} \end{bmatrix} \begin{bmatrix} s'_{1k} \\ s'_{2k} \\ s'_{3k} \end{bmatrix} = \begin{bmatrix} s'_{1j} & s'_{2j} & s'_{3j} \end{bmatrix} \begin{bmatrix} \tau_{11} & \tau_{12} & \tau_{13} \\ \tau_{12} & \tau_{22} & \tau_{23} \\ \tau_{13} & \tau_{23} & \tau_{33} \end{bmatrix} \begin{bmatrix} s'_{1k} \\ s'_{2k} \\ s'_{3k} \end{bmatrix}$$

$$= \tau_k \begin{bmatrix} s'_{1j} & s'_{2j} & s'_{3j} \end{bmatrix} \begin{bmatrix} s'_{1k} \\ s'_{2k} \\ s'_{3k} \end{bmatrix}$$

ie $(\tau_j - \tau_k) \begin{bmatrix} s'_{1j} & s'_{2j} & s'_{3j} \end{bmatrix} \begin{bmatrix} s'_{1k} \\ s'_{2k} \\ s'_{3k} \end{bmatrix} = 0$

Hence $\begin{bmatrix} s'_{1j} & s'_{2j} & s'_{3j} \end{bmatrix} \begin{bmatrix} s'_{1k} \\ s'_{2k} \\ s'_{3k} \end{bmatrix} = 0$ since $\tau_j \neq \tau_k$

When the product of two deflection modes is zero as above, the modes are said to be orthogonal.

Since the modes have an arbitrary scale factor, the following conditions imply no loss of generality:

$$\begin{bmatrix} S_{ij} & S_{2j} & S_{3j} \end{bmatrix} \begin{bmatrix} S_{1j} \\ S_{2j} \\ S_{3j} \end{bmatrix} = 1 \quad \text{for } j = 1 \rightarrow n \qquad \text{A 2 4}$$

Modes subject to this condition are called normalised modes and their components will be written as S_{jk}. In the present case, because of the symmetry of the $[\mathcal{C}_{jk}]$ matrix in A 2.1, the normalised modal matrix is symmetric and the orthogonal property can therefore be simply expressed as

$$\begin{bmatrix} S_{11} & S_{12} & S_{13} \\ S_{12} & S_{22} & S_{23} \\ S_{13} & S_{23} & S_{33} \end{bmatrix} \begin{bmatrix} S_{11} & S_{12} & S_{13} \\ S_{12} & S_{22} & S_{23} \\ S_{13} & S_{23} & S_{33} \end{bmatrix} = \begin{bmatrix} 1 & 0 & 0 \\ 0 & 1 & 0 \\ 0 & 0 & 1 \end{bmatrix} \qquad \text{A 2 5}$$

Thus if the modal matrices in equation A 2.2 were normalised and then both sides of the equation post-multiplied by the normalised modal matrix the following result is obtained:

$$\begin{bmatrix} \tau_{11} & \tau_{12} & \tau_{13} \\ \tau_{12} & \tau_{22} & \tau_{23} \\ \tau_{13} & \tau_{23} & \tau_{33} \end{bmatrix} = \begin{bmatrix} s_{11} & s_{12} & s_{13} \\ s_{12} & s_{22} & s_{23} \\ s_{13} & s_{23} & s_{33} \end{bmatrix} \begin{bmatrix} \tau_1 & 0 & 0 \\ 0 & \tau_2 & 0 \\ 0 & 0 & \tau_3 \end{bmatrix} \begin{bmatrix} s_{11} & s_{12} & s_{13} \\ s_{12} & s_{22} & s_{23} \\ s_{13} & s_{23} & s_{33} \end{bmatrix}$$

A 2.6

A P P E N D I X 3

Moment Distribution method for calculating the influence coefficients of a rigidly coupled, multi-span rotor on flexible supports.

The Moment Distribution method is an iterative process with the following procedure (which will refer to Fig. 2.5):

A rotational restraint is put on the rotor at its journals before any inter-span loads or journal displacements are allowed. After the rotor has been loaded and any journal displacements have taken place, the imposed rotational restraint is removed from one journal. The opposing moments set up at the journal by the loading and displacements are equalised and the moments at the restrained journals on either side of the released journal are adjusted until equilibrium is established. The rotational restraint is then re-applied at this journal. The process is repeated several times for each journal until equilibrium is maintained without the rotational restraints.

Referring to Fig 2.5, for simplicity it is assumed that for each rotor the transverse bending stiffness at all sections are equal. Then the fixing moments required at each journal due to inter-span forces and journal displacements are shown in Fig. A 3.1a and Fig. A 3.1b respectively.

The ratio in which to distribute an unbalanced moment at a journal when the rotational restraint is removed is

shown in Fig. A 3.2.

When the fixed moments have been completely distributed, a typical balanced journal moment will be of the form:

$$M_{ai} = \sum_{j=1}^{A} {}_{ai}\alpha_{aj} F_{aj} + \sum_{j=1}^{I} {}_{ai}\alpha_{ij} F_{ij} + \sum_{j=1}^{N} {}_{ai}\alpha_{nj} F_{nj} + {}_{ai}\beta_{oa} y_{oa} + {}_{ai}\beta_{ai} y_{ai} + {}_{ai}\beta_{in} y_{in} + {}_{ai}\beta_{no} y_{no} \quad \text{A 3.1}$$

where ${}_{ai}\alpha_{aj}$ etc. are the interspan force coefficients

${}_{ai}\beta_{oa}$ etc. are the journal displacement coefficients

The effect of the end moments and the interspan forces on the rotor elastic deflection is shown in Fig. A 3.3a and Fig. A 3.3b respectively.

Fig. A 3.3c shows a typical span with all interspan forces and moments present. The total effect can be expressed as

$$r_{ik} = {}_{ig}g_{ai} M_{ai} - {}_{ik}g_{in} M_{in} + \sum_{j=1}^{I} {}_{ik}h_{ij} F_{ij} \quad \text{A 3.2}$$

Substituting into A3.2 from A 3.1

$$\begin{aligned} r_{ik} = {} & \sum_{j=1}^{A} \left({}_{ik}g_{ai}\, {}_{ai}\alpha_{aj} - {}_{ik}g_{in}\, {}_{in}\alpha_{aj} \right) F_{aj} \\ & + \sum_{j=1}^{I} \left({}_{ik}g_{ai}\, {}_{ai}\alpha_{ij} - {}_{ik}g_{in}\, {}_{in}\alpha_{ij} + {}_{ik}h_{ij} \right) F_{ij} \\ & + \sum_{j=1}^{N} \left({}_{ik}g_{ai}\, {}_{ai}\alpha_{nj} - {}_{ik}g_{in}\, {}_{in}\alpha_{nj} \right) F_{nj} \\ & + \left({}_{ik}g_{ai}\, {}_{ai}\beta_{oa} - {}_{ik}g_{in}\, {}_{in}\beta_{oa} \right) y_{oa} \\ & + \left({}_{ik}g_{ai}\, {}_{ai}\beta_{ai} - {}_{ik}g_{in}\, {}_{in}\beta_{ai} \right) y_{ai} \\ & + \left({}_{ik}g_{ai}\, {}_{ai}\beta_{in} - {}_{ik}g_{in}\, {}_{in}\beta_{in} \right) y_{in} \\ & + \left({}_{ik}g_{ai}\, {}_{ai}\beta_{no} - {}_{ik}g_{in}\, {}_{in}\beta_{no} \right) y_{no} \end{aligned} \quad \text{A 3.3}$$

i.e. $\underset{\sim}{r} = [\mathcal{C}]\,\underset{\sim}{F} + [\mathcal{G}]\,\underset{\sim}{\dot{x}}$ ——————— A 3.4

A P P E N D I X 4

Diagonalisation of the flexibility matrix of a rigidly coupled multi-span rotor.

It has been explained in Section 2.2 - 1 that the diagonalisation of a high order matrix is awkward. The following solution for a multi-span rotor is in terms of the diagonalisations of the flexibility matrices of the individual rotors when uncoupled. In practice it is probable that the individual diagonalisations would be done in any case (partly to assist in the balancing procedure of the individual rotors).

Consider the rigidly coupled rotor on simple supports shown diagrammatically in Fig. A 4.1.

Let the deflections $\underset{\sim}{Y}_a$, $\underset{\sim}{Y}_b$ and the journal transverse rotations θ_{oa}, θ_{ob} result from the mutual moments M_a, M_b only.

Let the deflections $\underset{\sim}{r}_a$, $\underset{\sim}{r}_b$ and the journal transverse rotations $(\theta_a - \theta_{oa})$, $(\theta_b - \theta_{ob})$ result only from the interspan inertia forces $\underset{\sim}{F}_a$ $\underset{\sim}{F}_b$ respectively. Then:

$$\tau \underset{\sim}{r}_a = [\tau_a][M_a](\underset{\sim}{r}_a + \underset{\sim}{Y}_a) \qquad \text{A 4.1}$$

$$\tau \underset{\sim}{r}_b = [\tau_b][M_b](\underset{\sim}{r}_b + \underset{\sim}{Y}_b)$$

The equations A 4.1 are of the form of equation 2.17 and upon being diagonalised like it lead to the equations:

$$\underset{\sim}{F}_a = [U_a]\ \underset{\sim}{Y}_a \qquad \text{A 4.2}$$

$$\underset{\sim}{F}_b = [U_b]\ \underset{\sim}{Y}_b$$

where $[U]$ is defined in equation 2.25 and equation 2.26.

In the present case,

$$\underset{\sim}{Y}_a = [\alpha_a]\,\theta_{oa} \qquad \text{A 4.3}$$

$$\underset{\sim}{Y}_b = [\alpha_b]\,\theta_{ob}$$

where $[\alpha_a]$ and $[\alpha_b]$ are displacement slope matrices.

Hence:

$$\underset{\sim}{F}_a = [U_a][\alpha_a]\,\theta_{oa} \qquad \text{A 4.4}$$

$$\underset{\sim}{F}_b = [U_b][\alpha_b]\,\theta_{ob}$$

$$\text{Let } (\theta_a - \theta_{oa}) = [\delta_a]\underset{\sim}{F}_a \qquad \text{A 4.5}$$

$$(\theta_b - \theta_{ob}) = [\delta_b]\underset{\sim}{F}_b$$

where $[\delta_a]$ and $[\delta_b]$ are slope force matrices. Substituting from equation A 4.4 into equation A 4.5:

$$\theta_a = (1 + [\delta_a][U_a][\alpha_a])\,\theta_{oa} \qquad \text{A 4.6}$$

$$\theta_b = (1 + [\delta_b][U_b][\alpha_b])\,\theta_{ob}$$

$$\text{If } M_a = \xi_{fa}\,\theta_{oa} \qquad \text{A 4.7}$$

$$\text{and } M_b = \xi_{fb}\,\theta_{ob}$$

where ξ_a and ξ_b are moment slope coefficients, then there are two compatibility conditions at the common support:

$$\theta_a = \theta_b \qquad \text{A 4.8}$$

$$M_a = -M_b$$

Using equation A 4.7 the second compatibility condition gives

$$\theta_{oa} = -\frac{\xi_b}{\xi_a}\,\theta_{ob} \qquad \text{A 4.9}$$

Substituting A 4.9 into A 4.6 and using the first compatibility condition:

$$-\frac{\xi_b}{\xi_a}\left(1 + [\delta_a][U_a][\alpha_a]\right) = \left(1 + [\delta_b][U_b][\alpha_b]\right)$$

$$\therefore \frac{\xi_b}{\xi_a}[\delta_a][U_a][\alpha_a] + [\delta_b][U_b][\alpha_b] = -\left(\frac{\xi_b}{\xi_a} + 1\right) \qquad \text{A 4.10}$$

When the matrices of equation A 4.10 are multiplied out and terms collected, the following form of frequency equation can be obtained:

$$\frac{\xi_b}{\xi_a}\frac{a1\,V_a}{\tau-\tau_{a1}} + \cdots\cdots + \frac{\xi_b}{\xi_a}\frac{aAV_a}{\tau-\tau_{aA}} + \frac{b1\,V_b}{\tau-\tau_{b1}} + \cdots\cdots + \frac{bB\,V_b}{\tau-\tau_{bB}} = -\left(\frac{\xi_b}{\xi_a} + 1\right) \qquad \text{A 4.11}$$

where ${}_{a1}V_a$ etc. are the collected terms from the above matrix multiplication after $[U_a]$, $[U_b]$ have been expressed as shown in equation 2.26.

This frequency equation is in a relatively simple form for solution.

Now $$\begin{bmatrix} \underset{\sim}{F}_a & \underset{\sim}{F}_b \end{bmatrix} = \frac{1}{\mathcal{C}} \begin{bmatrix} [M_a] & 0 \\ 0 & [M_b] \end{bmatrix} \begin{bmatrix} Y_a + r_a \\ Y_b + r_b \end{bmatrix} \qquad \text{A 4.12}$$

corresponding to equation 2.16.

Also from equation A 4.4 and using equation A 4.9

$$\begin{bmatrix} \underset{\sim}{F}_a & \underset{\sim}{F}_b \end{bmatrix} = \begin{bmatrix} U_a & 0 \\ 0 & U_b \end{bmatrix} \begin{bmatrix} \alpha_a . - \frac{\xi_{jb}}{\xi_{ja}} \\ \alpha_b \end{bmatrix} \theta_{ob} \qquad \text{A 4.13}$$

Equating equation A 4 - 12 and equation A 4 - 13

$$\begin{bmatrix} \underset{\sim}{Y}_a + \underset{\sim}{r}_a \\ \underset{\sim}{Y}_b + \underset{\sim}{r}_b \end{bmatrix} = \begin{bmatrix} [M_a]^{-1} & 0 \\ 0 & [M_b]^{-1} \end{bmatrix} \begin{bmatrix} U_a & 0 \\ 0 & U_b \end{bmatrix} \begin{bmatrix} \alpha_a . - \frac{\xi_{jb}}{\xi_{ja}} \\ \alpha_b \end{bmatrix} \theta_{ob} \qquad \text{A 4.14}$$

Thus the modal shapes corresponding to the solutions of the frequency equation A 4 - 11 can be obtained by substituting those solutions into equation A 4 - 14.

The treatment could be extended to deal with several rigidly coupled rotors.

A P P E N D I X 5

Apparatus for rotor whirl measurement

A photograph of the integrating console and the oscilloscope with camera is given in Fig. A 5.1. A photograph of the arrangement of a pair of moving coil transducers relative to a journal is given in Fig A 5.2.

Amplitude measurement: The conversion factor of the moving coil transducers is quoted as .302 $^{mV}/_{cm/sec}$. To obtain a useful measure of small amplitudes it is therefore necessary to integrate the transducer's outputs with respect to time and to amplify them. Each of the two channels of the circuit shown diagrammatically in Fig. A 5.3. was designed to fulfil both of these functions using a solid state operational amplifier. The design factors are given in Fig. A 5.4.

For each of the control switch positions A, B, C the signals from each pair of transducers were integrated, amplified and connected to the corresponding terminals of an X - Y oscilloscope. Thus, after calibration, the amplitudes of the orbital motion of the rotor in the three transducer planes could be measured from the displays on the oscilloscope screen. In fact the actual measurements were made from magnified projections of filmed records of

the displays.

Phase measurement: The remaining six positions of the control switch allowed a determination of the phase of the displacement at each transducer relative to the deliberate rotor out-of-balance. The mode of operation will be illustrated for position A_y, corresponding to the vertical probe at plane A.

The transducer signal was integrated and amplified by channel Y and then connected to the Y terminal of the oscilloscope as for the amplitude measurements. The output signal from the Y channel was also connected to the input of channel X and after a second integration and amplification was connected to the X terminal of the oscilloscope. When the original signal was simple harmonic, at the oscilloscope the 'X' signal was in quadrature with the 'Y' signal and therefore the oscilloscope trace was an ellipse, the principal axes of which coincided with the horizontal and vertical directions of the oscilloscope axes. When the trace components were made equal (coarse control on oscilloscope, fine control on the variable potentiometer of the integrating circuit), a circle was obtained. The modification of the brightness of this circle by pulses from a photo-electric transducer scanning tapes aligned with the position of the deliberate

out-of-balance provided the required phase reference. The relative position of the out-of-balance weight, the tapes and the photo-electric transducer are shown in Fig. A 5.5 from which it can be seen that the same phase datum was chosen as for the theoretical results, namely the x direction. The sequence of the uneven tape widths indicated the direction in which the lag angles should be measured. As for the amplitude measurements, the phase angles were measured from magnified projections of filmed records of the displays.

Calibration: The calibration of the system was done by a direct method and checked by two indirect methods.

The direct calibration was done as follows. The surface of an aluminium rod was 'turned' by a clamped tool while the rod was gripped by and rotated with the tool chuck of a jig borer. After 'turning,' the rod was traversed 0.005 in radially by a calibrated screw normally used for setting cuts on the borer (the eccentricity was also checked independently with a clock gauge), and then rotated about the borer axis so as to communicate a simple harmonic motion to the contacting probe of a transducer. With the transducer signal passing through the console and displayed on the

oscilloscope, the calibrating potentiometer in the integrating circuit was adjusted to give an oscilloscope trace amplitude of 2 in (peak to peak) for an oscilloscope setting of 5 $\frac{mV}{cm}$. The gain switch of the oscilloscope then allowed a wide range of overall amplitude gains of up to x 10,000. The outputs of all six transducers were compared and no difference was found between them.

Immediately after the direct calibration, an oscillator was coupled across the input terminals of a channel of the console while a transducer was also connected across them. The oscillator output voltage and frequency were accurately measured while they were varied throughout the ranges of interest, while the corresponding console output was measured. By this means the linearity of the measuring system was proved and, using the transducer conversion factor of .302 $\frac{mV}{cm/sec}$ the calibration was cross-checked.

Finally, a .5 mV square wave was available at the oscilloscope for its calibration. The form of the triangular wave which resulted when it was integrated by the console provided a further check on the integrity of the integration. The amplitude of the triangular wave was noted after the system had been calibrated by the direct method and this served as a quick calibration

check which was used on numerous occasions during the experiments.

A P P E N D I X 6

Analytical equivalence and numerical comparison of instability criteria.

A.6 - 1 A. Stable conditions below twice first natural frequency.

Possibly the earliest proposed criterion of stability of a flexible rotor was that the running frequency should not exceed twice the first rotor natural frequency (calculated on simple supports). The ratio $\left(\frac{\omega_1}{\omega_p}\right)^2$ in the stability relationship can be interpreted physically as

$$\left(\frac{\omega_1}{\omega_p}\right)^2 = \frac{ck}{W} = \frac{\text{radial clearance of bearing}}{\text{static deflection of rotor due to bearing load}}$$

For a rotor supported in bearings with a clearance much smaller than the static deflection of the centre mass of the rotor, as can easily be the case in model rotors, the left hand side of equation 5.9 is practically zero and the criterion reduces to

$$0 \lessdot P\left(\frac{\omega_1}{\omega_r}\right)^2 - Q \qquad \text{A 6.1}$$

For a wide range of bearing conditions (Fig. 5.3) $\frac{Q}{P} \doteq \frac{1}{4}$. Then inequality A6.1 becomes

$$0 < \left(\frac{\omega_1}{\omega_r}\right)^2 - \frac{1}{4}$$

$$\text{or } \omega_r < 2\,\omega_1$$

which is the above stability criterion.

A.6 - 2 Rigid Rotor analyses

A rigid rotor is the limiting case of ω_1 becoming very large and hence in criterion 5.9 the effect of the constant Q becomes negligible. The criterion reduces to:

$$\left(\frac{\omega_1}{\omega_p}\right)^2 \ll P\left(\frac{\omega_1}{\omega_r}\right)^2$$

$$\text{or} \quad \left(\frac{\omega_p}{\omega_r}\right)^2 \gg \frac{1}{P}$$

which is the same as equation 5.5.

B Holmes (ref. 15) Correlating notations from Fig. A 6.1, values of $\frac{1}{P}$ are obtainable directly from Holmes' Fig. 3. Three values of Q are also obtainable from his Fig. 3 using the three points for which corresponding values of frequency ratio and $\frac{1}{P}$ are given by substituting into equation 5.7. Alternatively, to obtain Q values for a wider range of bearing conditions, use can be made of a later diagram given by Holmes (ref. 59), and

the following form of inequality at the stability limit:

$$Q = \left(\frac{\omega_1}{\omega_r}\right)^2\left[p - \frac{1}{\left(\frac{\omega_p}{\omega_r}\right)^2}\right]$$

Korovchinskii's Fig. 5 (ref. 8) corresponds to Holme's Fig. 3 and takes account of the effect of $\frac{1}{d}$ ratio.

A.6 - 3 Flexible rotor analyses

C Hori (ref. 14)

Hori arrived at a stability criterion of the form

$$\frac{1}{\omega^2}\ \frac{F}{m\delta} > K_1(\kappa_o)\left[K_2(\kappa_o) + \frac{1}{\omega_1^2}\ \frac{F}{m\delta}\right] \qquad \text{A 6.2}$$

the notation being as defined in Fig. A 6.1. The calculated results are given in a chart showing critical values of $\frac{1}{\omega^2}\ \frac{F}{m\delta} = \left(\frac{\omega_p}{\omega_r}\right)^2$ in terms of the eccentricity ratio κ_o with $\frac{1}{\omega_1^2}\ \frac{F}{m\delta} = \left(\frac{\omega_p}{\omega_1}\right)^2$ as a parameter.

Writing equation A 6.2 in the present notation

$$\left(\frac{\omega_p}{\omega_1}\right)^2 > K_1(\kappa_o)\left[K_2(\kappa_o) + \left(\frac{\omega_p}{\omega_1}\right)^2\right]$$

Multiplying through by $\left(\frac{\omega_1}{\omega_p}\right)^2$ and rearranging gives

$$\left(\frac{\omega_1}{\omega_p}\right)^2 < \frac{1}{K_1(\kappa_0)K_2(\kappa_0)} \left(\frac{\omega_1}{\omega_r}\right)^2 \quad - \quad \frac{1}{K_2(\kappa_0)}$$

which is precisely the general form being used.

D Pinkus & Sternlicht (ref. 4).

Immediately preceding their final equation 8.44, the following expression is found:

$$s^2 \frac{\zeta}{s}\left(\frac{\nu}{s}\right)^2 - s A\left(\frac{\nu}{s}\right)^2 + \frac{\zeta}{s} = 0 \qquad \text{A 6.3}$$

The term $\frac{A}{s}$ may be identified not by the definition given in equations 8.39 but rather by inference between equations 8.36 and 8.38 as

$$\frac{A}{s} = \frac{kc}{\lambda\omega}$$

a factor of 2 being dropped to allow for the fact that the analysis is apparently based on the stiffness k for the whole shaft (two halves) and only on one bearing.

By reference to equation 8.3 and tables 8.1 and 8.2, $\lambda\omega = W/_{fo}$ where W is the load on each journal. It can also be shown that fo is the reciprocal of the Sommerfeld number. Hence

$$\frac{A}{s} = f_o \frac{kc}{W} = f_o \left(\frac{\omega_1}{\omega_p}\right)^2$$

in the present notation. Thus, rewriting equation A 6.3 and noting that $\frac{1}{s}\,2 = \left(\frac{\omega_1}{\omega_r}\right)^2$ we have

$$\frac{\zeta}{s}\left(\frac{\nu}{s}\right)^2 - fo\left(\frac{\nu}{s}\right)\left(\frac{\omega_1}{\omega_p}\right) + \frac{\zeta}{s}\left(\frac{\omega_1}{\omega_r}\right)^2 = 0$$

That is $\left(\frac{\omega_1}{\omega_p}\right)^2 = P\left[\left(\frac{\omega_1}{\omega_r}\right)^2 - \frac{Q}{P}\right]$

where $P = \dfrac{\frac{\zeta}{s}}{fo\left(\frac{\nu}{s}\right)^2}$ and $Q = -\dfrac{\frac{\zeta}{s}}{fo}$

E Morrison (ref. 18)

Morrison's stability criterion was expressed in the form

$$\frac{ck}{W} \leqslant \frac{\gamma_1\gamma_2\gamma_3}{\gamma_2^2 - \gamma_5\gamma_3\gamma_2 - \gamma_4\gamma_3^2} - \frac{\gamma_2}{\gamma_3}$$

This translates directly to

$$\left(\frac{\omega_1}{\omega_p}\right)^2 \leqslant P\left(\frac{\omega_1}{\omega_r}\right)^2 - Q$$

F Someya (ref. 25)

Someya's linear stability criterion is expressed in the form

$$\frac{\omega}{\omega_k} < \frac{1}{\sqrt{\frac{m\,S(\epsilon)}{\mu} + n}}$$

where $\frac{\omega}{\omega_k} = \frac{\omega_r}{\omega_1}$ and $\mu = \left(\frac{\omega_o}{\omega_k}\right)^2 = \left(\frac{\omega_p}{\omega_1}\right)^2$ in the present notation. Rearranging after squaring:

$$\left(\frac{\omega_1}{\omega_p}\right)^2 < \frac{1}{m.\,S(\epsilon)}\left[\left(\frac{\omega_1}{\omega_r}\right)^2 - n\right]$$

where $P = \frac{1}{m\,S(\epsilon)}$ and $Q = \frac{n}{m\,S(\epsilon)}$

Perhaps the simplest method of obtaining P and Q values from Someya's stability chart is to read off corresponding values of $\frac{\omega}{\omega_k}$ and μ for a particular eccentricity. If then $\frac{1}{\mu}$ is plotted against $\left(\frac{\omega_k}{\omega}\right)^2$ (i.e. in present notation $\left(\frac{\omega_1}{\omega_p}\right)^2$ is plotted against $\left(\frac{\omega_1}{\omega_r}\right)^2$)the slope and intercept of the straight line obtained are the required values of P and Q respectively. The values given in Fig. 5.4 were obtained in this way.

REFERENCES

1. TOWER, B. 'First report on friction experiments,' Proc. Instn. Mech. Engrs, Lond. 1883, 34, 632.

2. TOWER, B. 'Second report on friction experiments,' Proc. Instn. Mech. Engrs., Lond, 1885, 36, 58.

3. REYNOLDS, O. 'On the theory of lubrication and its application to Mr. Beauchamp Towers experiments, including an experimental determination of the viscosity of olive oil' Trans. Roy. Soc. Lond. 1886, 177, 157.

4. PINKUS, O. and STERNLICHT, B. 'Theory of hydrodynamic lubrication' 1961 (McGraw-Hill Book Co., New York and London).

5. MITCHELL, J.R., HOLMES, R. and BYRNE, J. 'Oil whirl of a rigid rotor in 360° journal bearings: further Characteristics.' to be published in Proc. Instn. Mech. Engrs. Lond. 1965-66, 180 Part 1.

6. SOMMERFELT, A 'Zur hydrodynamischen theorie der schmiermittelreibung,' Z. Math. Phys. 1904, 50, 97.

7. OCKVIRK, F.W. 'Analytical derivation and experimental evaluation of short-bearing approximation for full journal bearings' 1953 N.A.C.A. report 1157.

8. KOROVCHINSKII, M.V. 'Friction and wear in machinery' 1956, 11, 248 (Translation from the Russian published by A.S.M.E., New York).

9. MOTOSH, N. 'Cylindrical journal bearings under constant load, the influence of temperature and pressure on viscosity' 1964 Lub. & Wear Conv. Instn. Mech. Engrs. London. Paper 24.

10. CARL, T.E. 'An experimental investigation of a cylindrical journal bearing under constant and sinusoidal loading' 1964 Lub. & Wear Conv. Instn. Mech. Engrs. London. Paper 19.

11. HUMMEL, C.H. 1926 Forsh.-Arb. Ing.-Wes. No. 287 as quoted in BIEZENO, C.B. and GRAMMEL, R. 'Engineering dynamics, vol 3, Steam turbines,' 1954 (Blackie and Son Ltd., London and Glasgow).

12. HAGG, A.C. 'The influence of oil film journal bearings on the stability of rotating machines,' Trans. A.S.M.E. 1946, 68, A-211.

13. PORITSKY, H. 'Contribution to the theory of oil whip' Trans. A.S.M.E. 1953, 75, 1153.

14. HORI, Y. 'A theory of oil whip.' Trans. A.S.M.E. 1959, 81, 189.

15. HOLMES, R. 'The vibration of a rigid shaft on short sleeve bearings.' J. Mech. Eng. Sci. 1960, 2, 337.

16. HOLMES, R. 'Oil whirl characteristics of a rigid rotor in 360° journal bearings' 1962 Instn. Mech. Engrs. London P11/63.

17. LUND, J.W. and STERNLICHT, B. 'Rotor bearing dynamics with emphasis on attenuation' J. Basic Eng. T.A.S.M.E. 1962, 84, 491.

18. MORRISON, D. 'The influence of plain journal bearings on the whirling action of an elastic rotor,' Proc. Instn. Mech. Engrs., London 1962 176, 542.

19. MORRISON, D. and PATERSON, A.N. 'Criteria for unstable oil whirl of flexible rotors' Lub. & Wear Conv. Inst. Mech. Engrs. London 1965, Paper 14.

20. SMITH, D.M. 'Dynamic characteristics of turbine journal bearings' Lub. & Wear Conv. Inst. Mech. Engrs. London 1963, p. 72.

21. REDDI, M.M. and TRUMPLER, P.R. 'Stability of the high speed journal bearing under steady load.' J. Engng. Ind. T.A.S.M.E. 1962, 84 (Series B) 351.

22. MILNE, A.A. 'Theoretical studies of the performance of dynamically loaded journal bearings' 1962 N.E.L. Report 70.

23. JENNINGS, U.D. and OCKVIRK, F.W. 'The simulation of bearing whirl on an electronic analogue computer' J. Basic Engng. T.A.S.M.E. 1962, 503.

24. HUGGINS, N.J. 'Non-linear modes of vibration of a rigid rotor in short bearings' Lub & Wear Conv. Inst. Mech. Engrs. London 1964, Paper 18.

25. SOMEYA, T. 'Stability of a balanced shaft running in cylindrical journal bearings' Lub & Wear Conv. Instn. Mech. Engrs. London 1964. Paper 21.

26. PESTEL, E.C. and LECKIE, F.A. 'Matrix methods in elastomechanics' 1963 (McGraw-Hill Book Co. New York and London).

27. KOENIG, E.C. 'Analysis for calculating lateral vibration characteristics of rotating systems with any number of flexible supports' J. Appl. Mech. 1961, 28 (No. 4), 585.

28. BISHOP, R.E.D. and GLADWELL, G.M.L. 'The vibration and balancing of an unbalanced flexible rotor' J. Mech. Eng. Sci. 1959, 1, 66.

29. GLADWELL, G.M. Land BISHOP, R.E.D. 'The receptances of uniform and non-inform rotating shafts' J. Mech. Engng. Sci. 1959, 1, 78.

30. GLADWELL, G.M.L. and BISHOP, R.E.D. 'The vibration of rotating shafts supported in flexible bearings' J. Mech. Engng. Sci., 1959, 1, 195.

31. PARKINSON, A.G. and BISHOP, R.E.D. 'Vibration and balancing of rotating continuous shafts' J. Mech. Engng. Sci. 1961, 3, 200.

32. MORRIS, J. 'The escalator method in engineering vibration problems' 1947 (Chapman and Hall Ltd. London).

33. MYKLESTAD, N.O. 'A new method of calculating natural modes of uncoupled bending vibration of airplane wings and other types of beams' J. Aero. Sci. 1944, 11, No. 2, 153.

34. BISHOP, R.E.D., GLADWELL, G.M.L. and MICHAELSON, S. 'The matrix analysis of vibration.' 1965 (Cambridge University Press).

35. HAGG, A.C. 'Some vibration aspects of lubrication' 1948 Lub. Engng. 166.

36. WARNER, P.C. and THOMAN, R.J. 'The effect of 150° partial journal bearings on rotor unbalance vibration' 1964 J. Basic Engng. T.A.S.M.E. Series D 86, 337.

37. DOLLIN, F. 'Some design problems arising in the development of very large high-speed turbines' 1963 Proc. Instn. Mech. Engrs. London 177, 221.

38. LANCZOS, C. 'Applied Analysis' 1957 (Pitman London)

39. BARWELL, F.T. 'Bearing data : can they be made more useful to designers?' Lub & Wear Conv. Instn. Mech. Engrs., London 1965, Paper 23.

40. CAMERON, A. and WOOD, W.L. 'The full journal bearing' Proc. Instn. Mech. Engrs. London 1949, 161, 59.

41. SASSENFELD, H. and WALTHER, A. 'Journal bearing calculations' V.D.I. Forschungsheft, Edition A, 1954 20, 441.

42. NEWKIRK, B.L. and TAYLOR, H.D. 'Shaft whipping due to oil action in journal bearings' General Electric Rev., 1925, 559.

43. HAGG, A.C. and SANKEY, G.O. 'Some dynamic properties of oil film journal bearings with reference to the unbalance vibration of rotors' J. Appl. Mech. A.S.M.E. 1956, 23, 302.

44. HAGG, A.C. and SANKEY, G.O. 'Elastic and damping properties of oil film journal bearings for applicatio to unbalance vibration calculations.' J. Appl. Mech. A.S.M.E. 1958, 25, 141.

45. DEN HARTOG J.P. 'Mechanical Vibrations' 1956 4th Ed. (McGraw Hill Book Co. London and New York).

46. NEWKIRK, B.L. (Journal bearing instability' Proc. Conf. Lub. & Wear. Instn. Mech. Engrs. London 1957, 179.

47. COLE, J.A. 'Film extent and whirl in complete journal bearings.' Proc. Conf. Lub. & Wear. Instn. Mech. Engrs. London 1957, 186.

48. HUGHES, C.J. 'The behaviour of a rigid rotor carried in hydrodynamic bearings' 1964 N.E.L. Report No. 126.

49. PARSZEWSKI, Z. and CAMERON, A. 'Oil whirl of flexible rotors' Proc. Instn. Mech. Engrs. London 1962, 176, 523.

50. MORRISON, D. Reply to discussion of ref (18) in Proc. Instn. Mech. Engrs. London 1962, 176, 599.

51. MARSH, H., Ph.D. Thesis, University of Cambridge, 1963.

52. LUND, J.W. 'The stability of an elastic rotor in journal bearings with flexible, damped supports' J. Appl. Mech. A.S.M.E. 1965, 911.

53. PINKUS, O. 'Note on oil whip' J. Appl. Mech. A.S.M.E. 1953, 20, 450.

54. PINKUS, O. 'Experimental investigation of resonant whip' Trans. A.S.M.E. 1956, 78, 975.

55. NEWKIRK, B.L. and GROBEL, L.P. 'Oil film whirl - a non-whirling bearing' Trans. A.S.M.E. 1934, 56, 607.

56. NEWKIRK, B.L. and LEWIS, J.F. 'An investigation of disturbances due to oil films in journal bearings' 1954. W.A.D.C. Tech. Rep. 54 - 188.

57. LEWIS, J.F. and FULTON, G.B. 'A further investigation of disturbances due to oil films in journal bearings' 1956. W.A.D.C. Tech. Rep. 56 - 259.

58. LEWIS, J.F. and FULTON, G.B. 'Continued studies of fluid film whirl' 1957 W.A.D.C. Tech. Rep. 57 - 737.

59. HOLMES, R. Contribution to ref. 18.

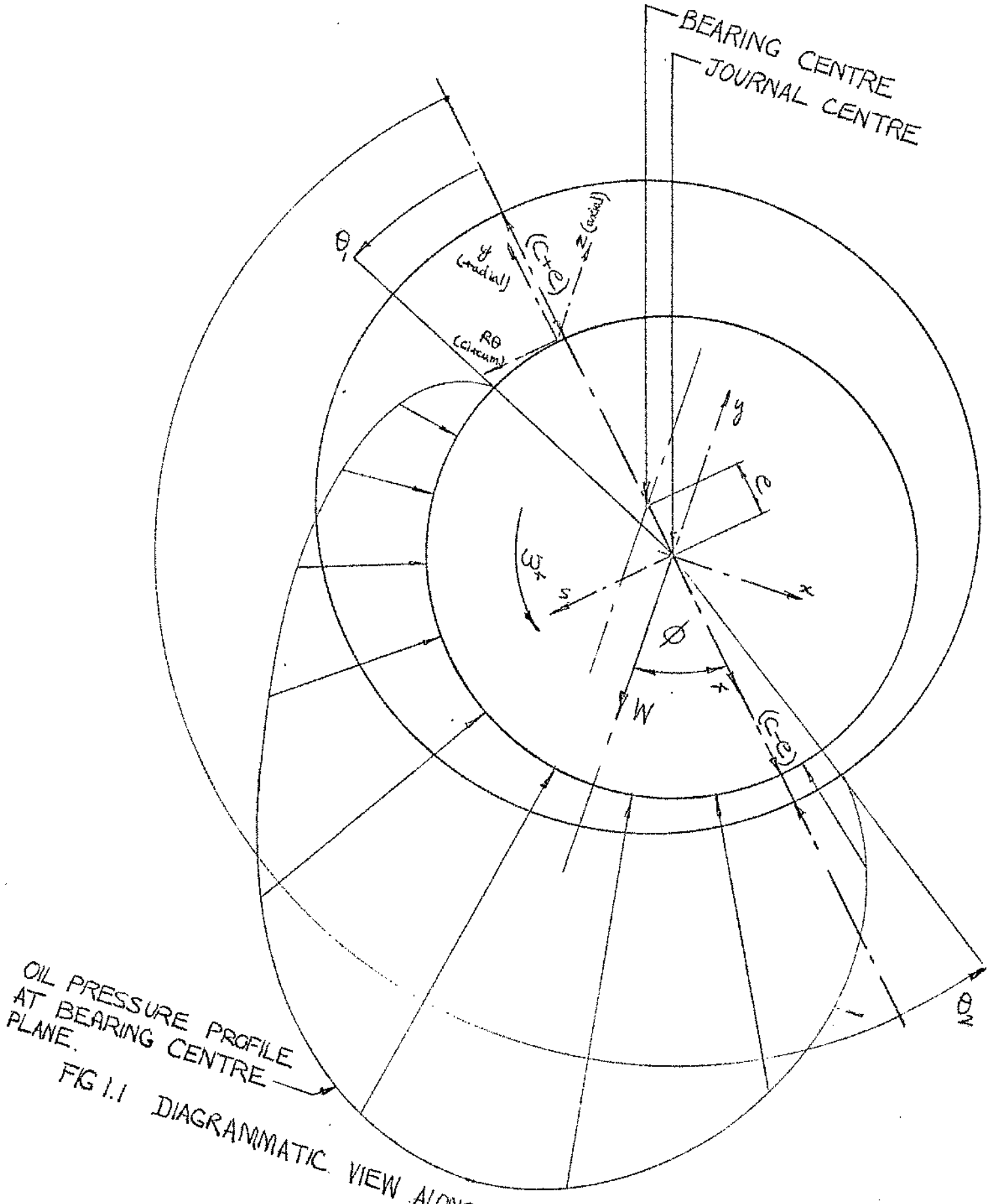

FIG 1.1 DIAGRAMMATIC VIEW ALONG AXIS OF JOURNAL BEARING.

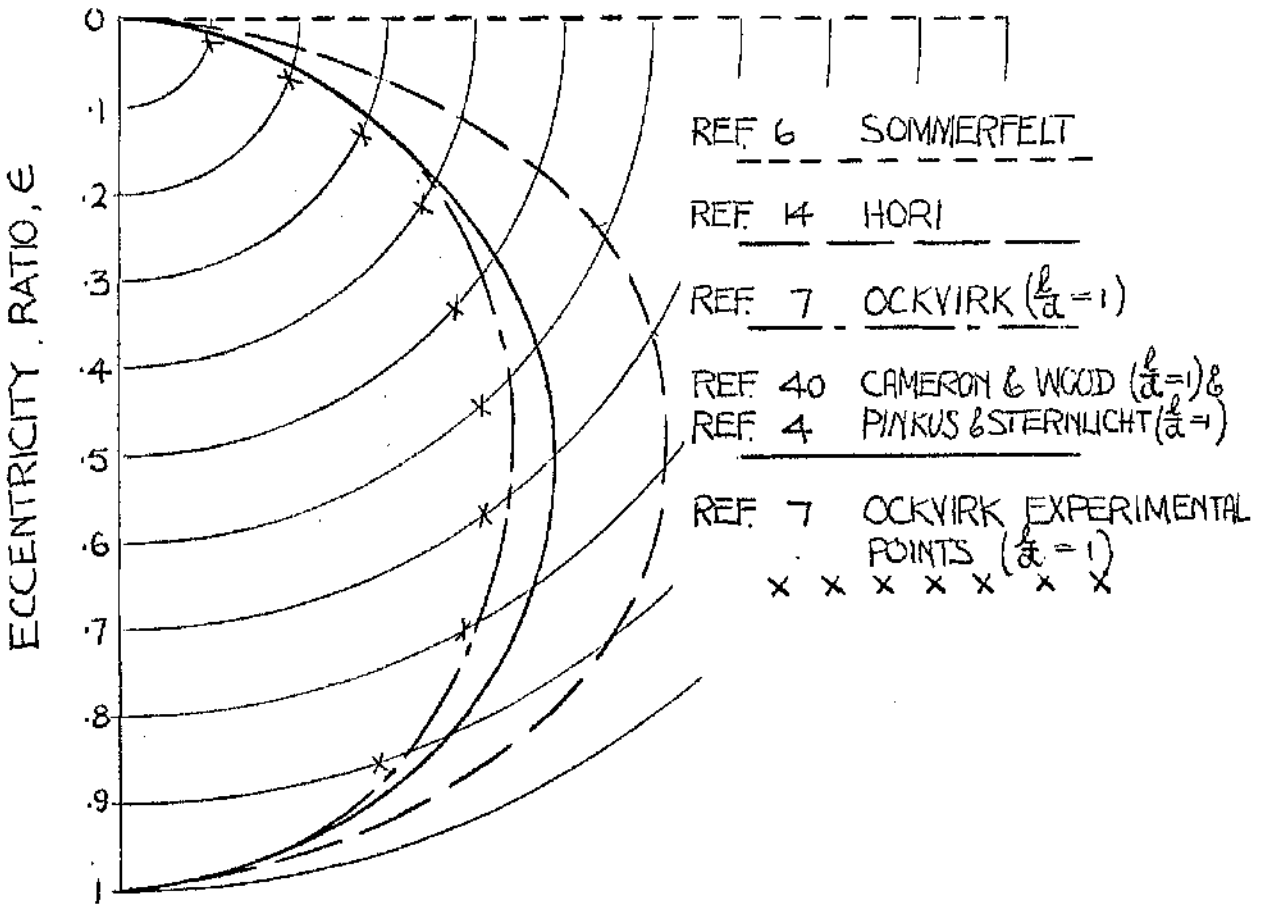

FIG 1.2 ATTITUDE / ECCENTRICITY CURVES

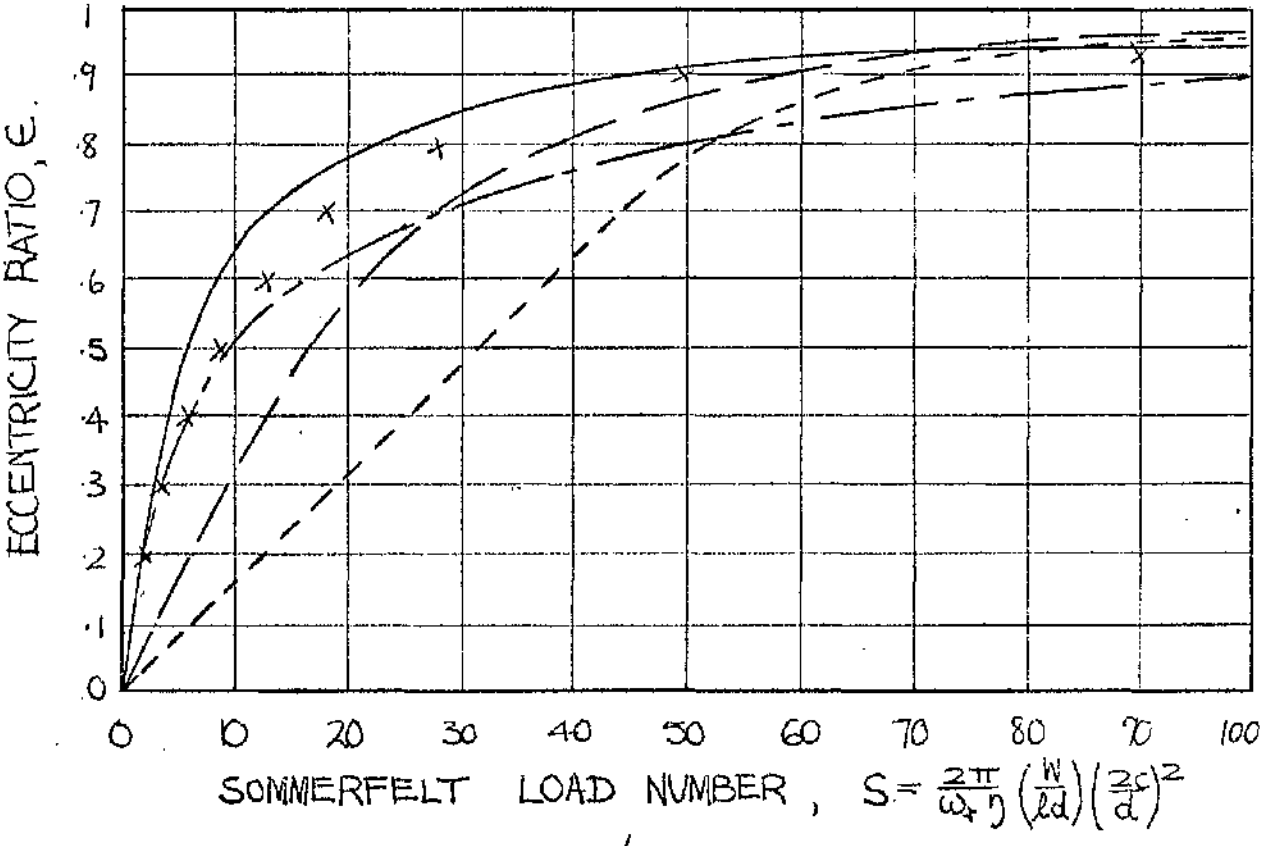

FIG 1.3 LOAD NUMBER / ECCENTRICITY CURVES

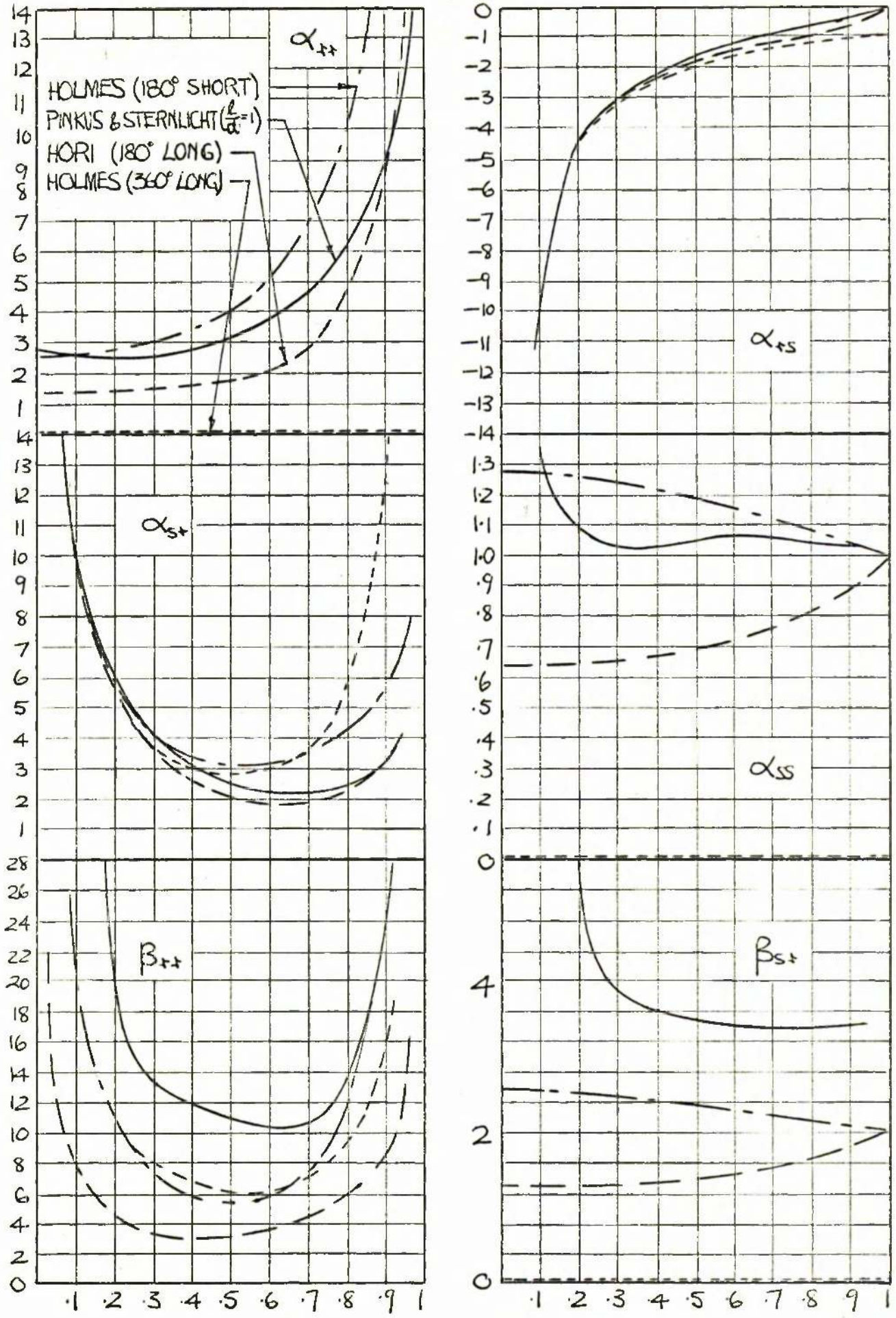

FIG 1.4 COMPARISON OF BEARING FORCE COEFFICIENTS

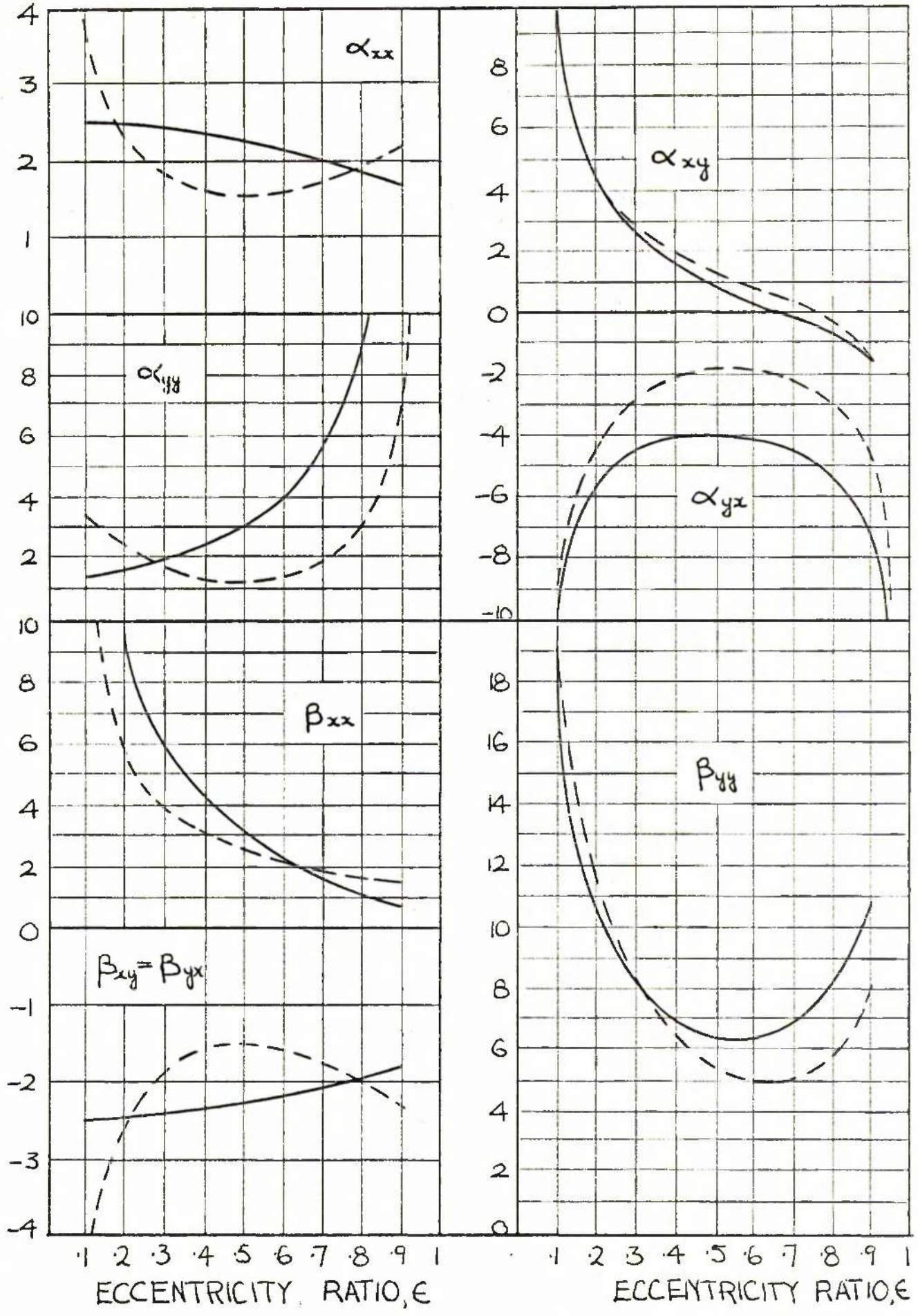

FIG 1.5 LIMITING BEARING FORCE COEFFICIENTS.
(——— $\frac{l}{d} = 0$, - - - - - $\frac{l}{d} = \infty$).

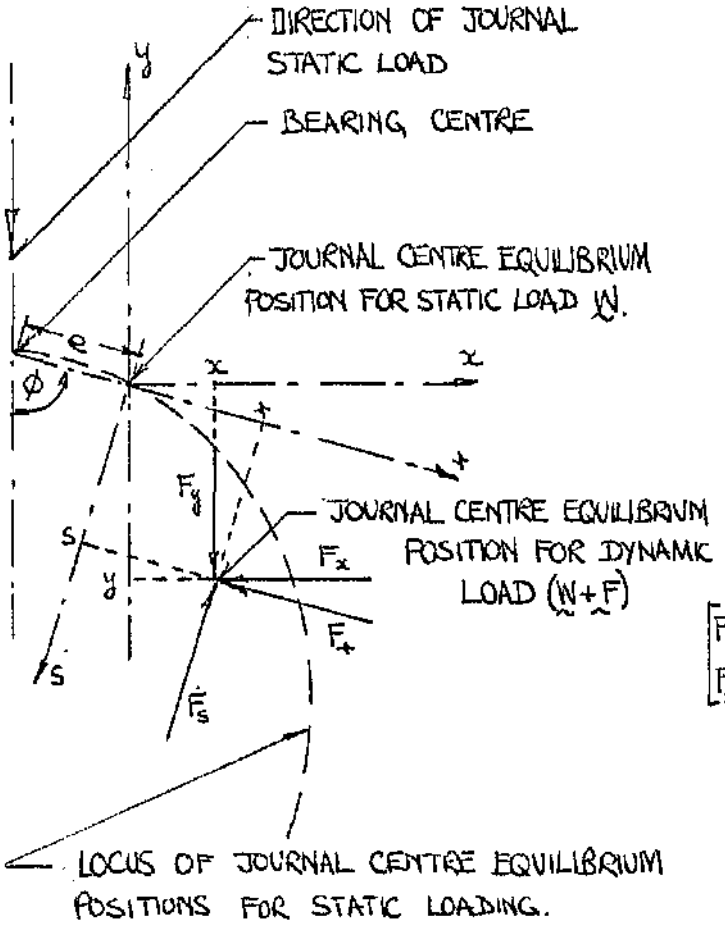

$$\begin{bmatrix} F_t \\ F_s \end{bmatrix} = \begin{bmatrix} A & B \\ C & D \end{bmatrix} \begin{bmatrix} t \\ s \end{bmatrix}$$

$$\begin{bmatrix} F_t \\ F_s \end{bmatrix} = \begin{bmatrix} -\cos\phi & \sin\phi \\ -\sin\phi & -\cos\phi \end{bmatrix} \begin{bmatrix} F_y \\ F_x \end{bmatrix}$$

$$\begin{bmatrix} t \\ s \end{bmatrix} = \begin{bmatrix} -\cos\phi & \sin\phi \\ -\sin\phi & -\cos\phi \end{bmatrix} \begin{bmatrix} y \\ x \end{bmatrix}$$

$$\begin{bmatrix} F_y \\ F_x \end{bmatrix} = \begin{bmatrix} \cos\phi & \sin\phi \\ -\sin\phi & \cos\phi \end{bmatrix} \begin{bmatrix} A & B \\ C & D \end{bmatrix} \begin{bmatrix} \cos\phi & -\sin\phi \\ \sin\phi & \cos\phi \end{bmatrix} \begin{bmatrix} y \\ x \end{bmatrix}$$

Fig 1.6 REFERENCE AXES, WITH TRANSFORMATIONS, FOR FORCE COEFFICIENTS.

AUTHORS	FORM OF REYNOLD'S EQUATION	CIRCUMFERENTIAL END CONDITIONS
SOMMERFELT (ref. 6)	LONG BEARING EQUATION	360° FILM
HORI (ref 14)	LONG BEARING EQUATION	180° CONVERGENT FILM
OCKVIRK (ref 7)	SHORT BEARING EQUATION	180° CONVERGENT FILM
CAMERON & WOOD (ref 40)	FULL EQUATION	$p=0$ at $\theta=0$. $p=\frac{dp}{d\theta}=0$ at $\theta=\theta_2$
PINKUS & STERNLICHT (ref 4)	FULL EQUATION	$p=0$ at $\theta=0$. $p=\frac{dp}{d\theta}=0$ at $\theta=\theta_2$
SOMEYA (ref 25)	FULL EQUATION	360° FILM
HOLMES (ref 15)	SHORT BEARING EQUATION	180° CONVERGENT FILM
HOLMES (ref. 16)	SHORT BEARING EQUATION	360° FILM
HOLMES (ref 16)	LONG BEARING EQUATION	360° FILM
MORRISON (ref 18)	SHORT BEARING EQUATION	$\frac{\text{VELOCITY}}{\text{DISPLACEMENT}}$ PURE RATIO INDEPENDENT
KOROVCHINSKII (ref 8)	LONG BEARING WITH AXIAL FLOW	VARIOUS.

Fig 1.7 TABLE OF OIL FILM ASSUMPTIONS.

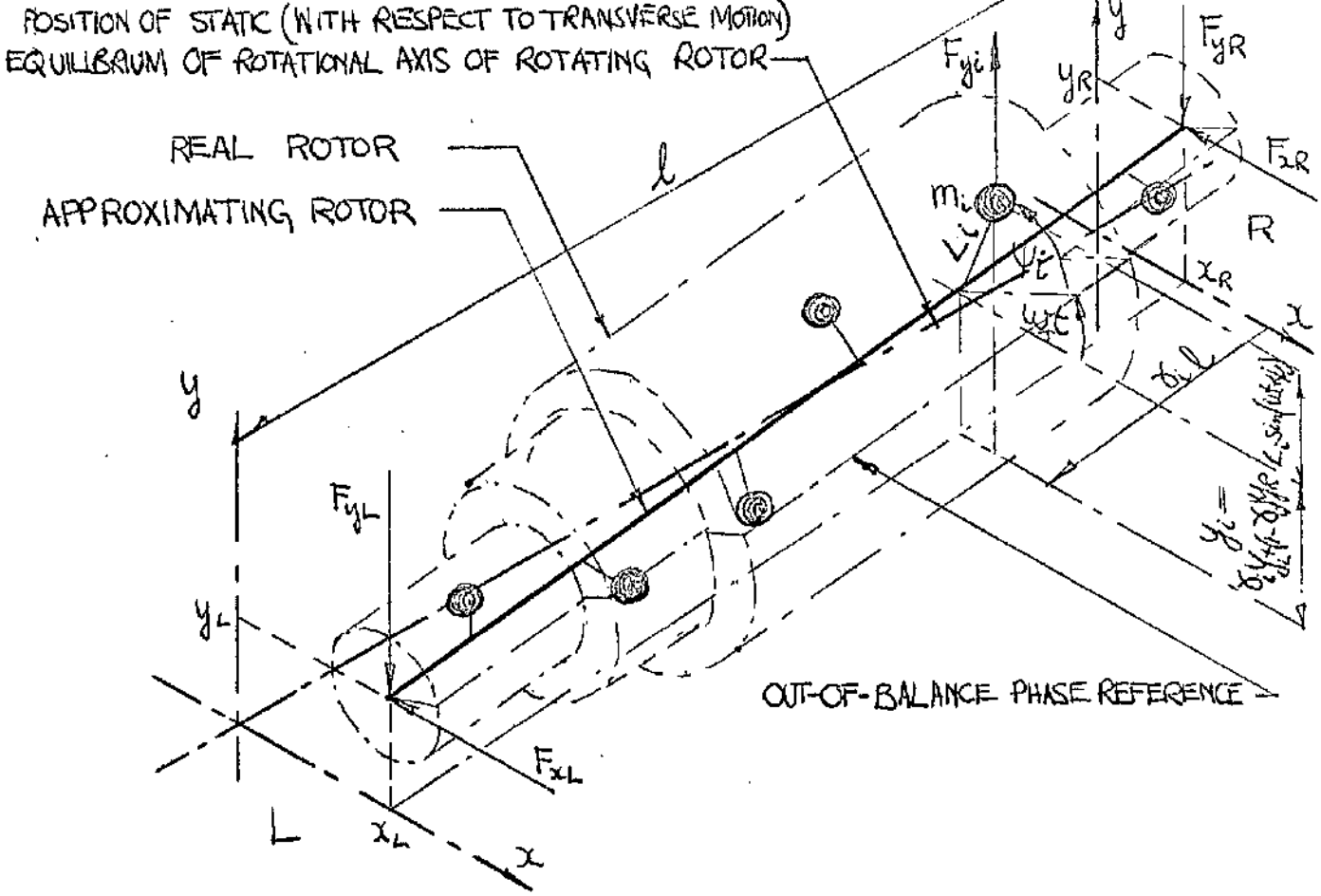

Fig 2.1 WHIRLING RIGID ROTOR

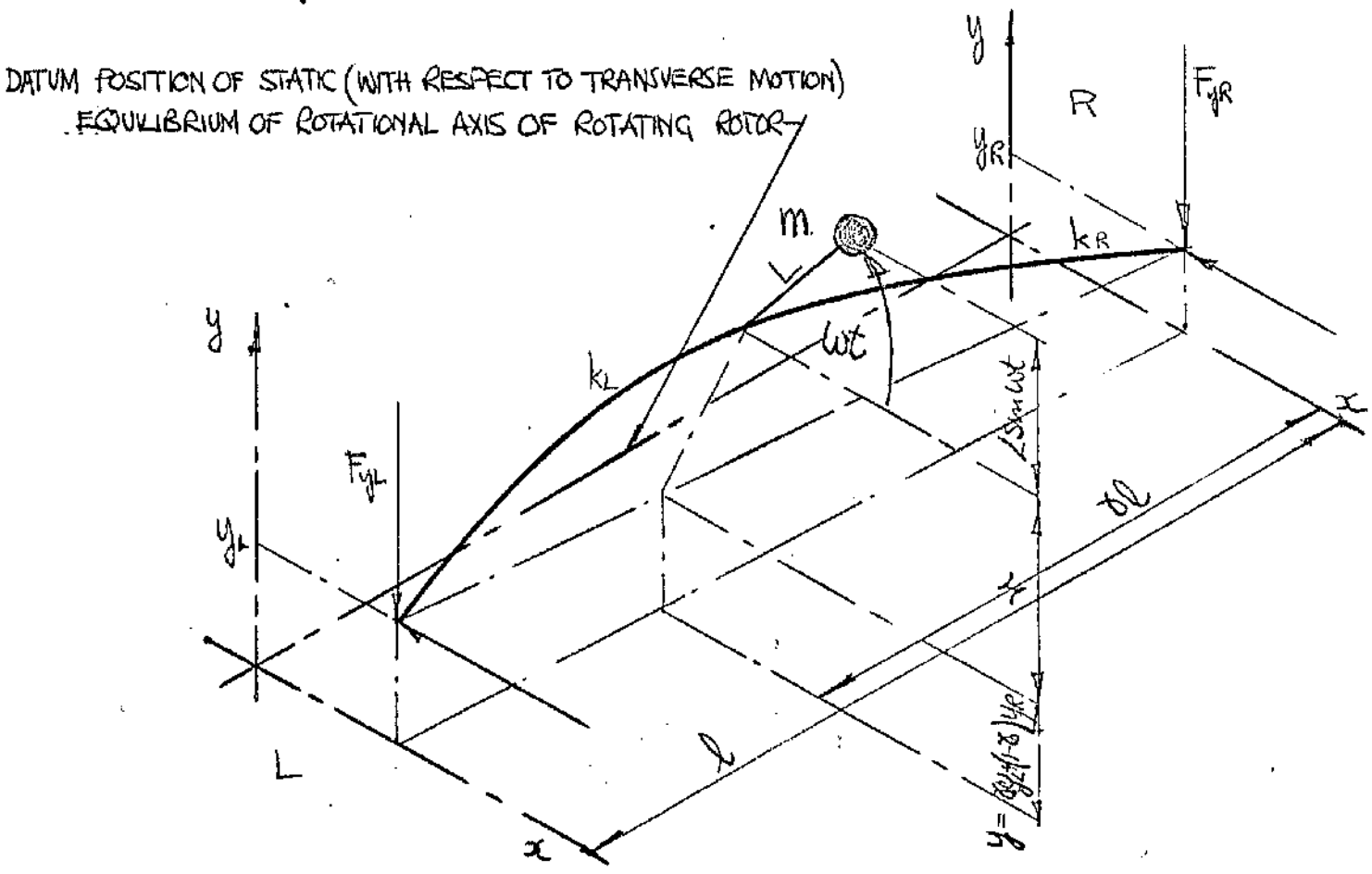

Fig. 2.2 WHIRLING SINGLE MASS FLEXIBLE ROTOR ON FLEXIBLE SUPPORTS.

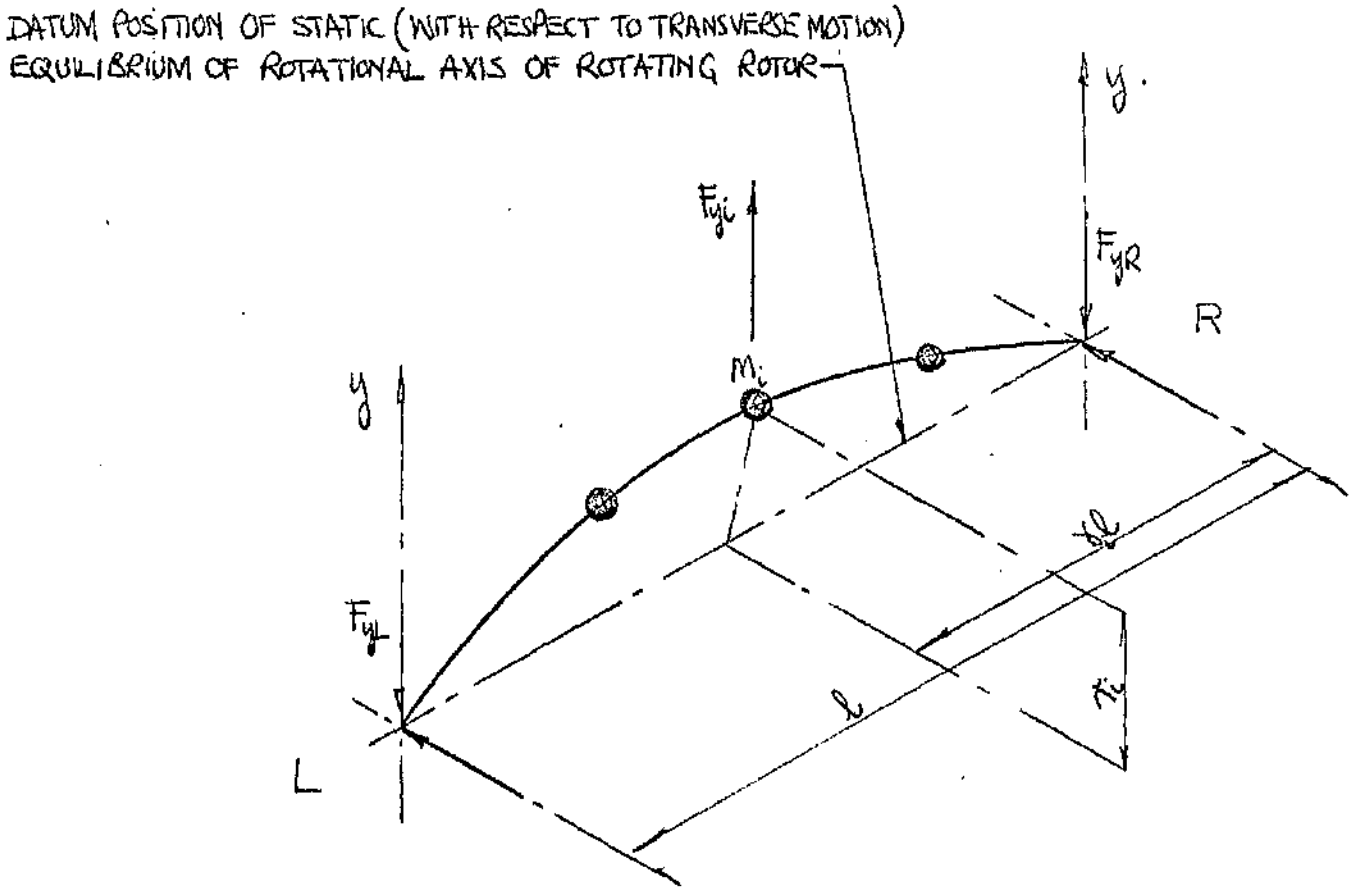

Fig 2.3 WHIRLING THREE MASS FLEXIBLE ROTOR ON SIMPLE SUPPORTS.

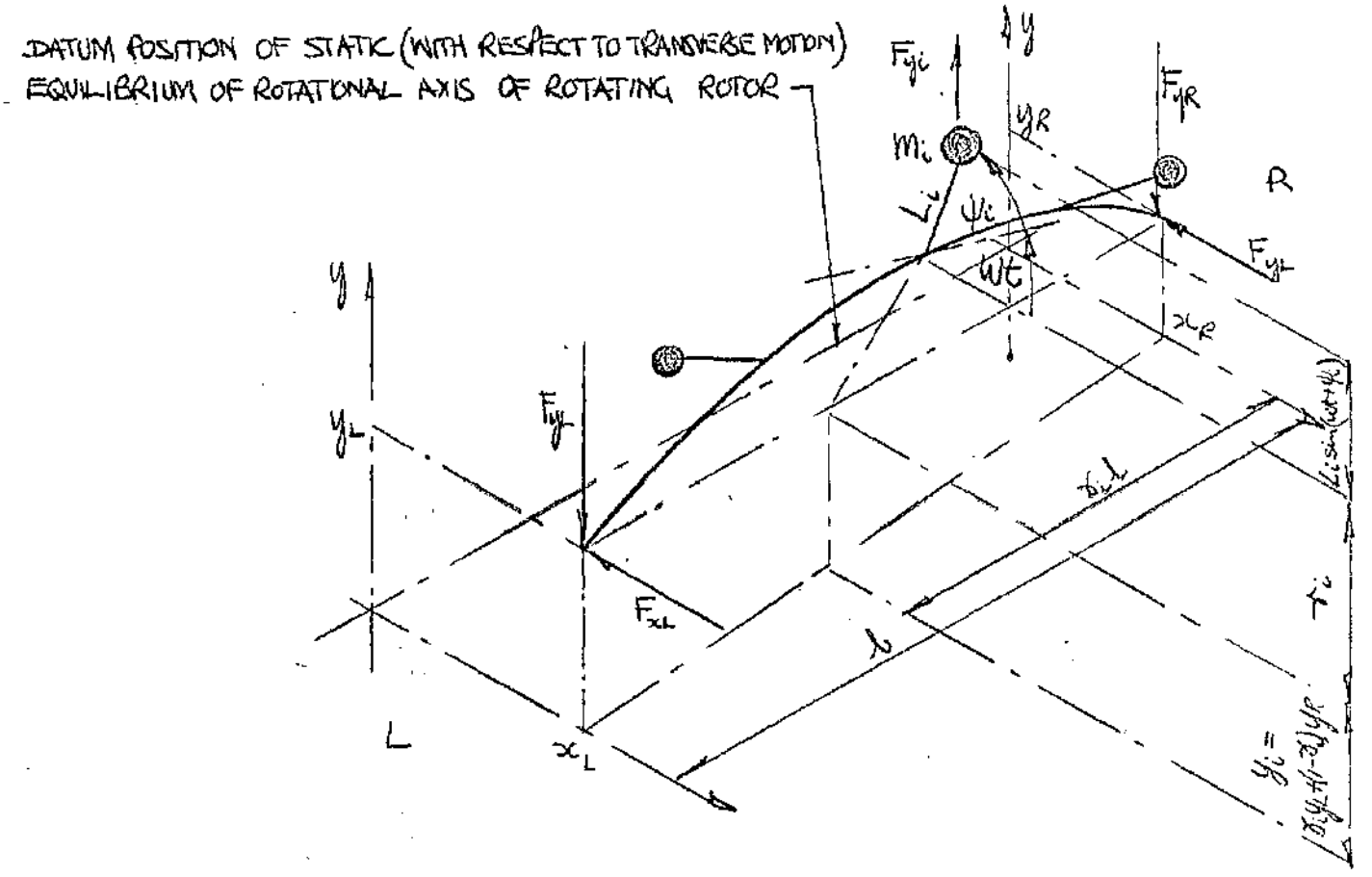

Fig 2.4 WHIRLING THREE MASS FLEXIBLE ROTOR ON FLEXIBLE SUPPORTS.

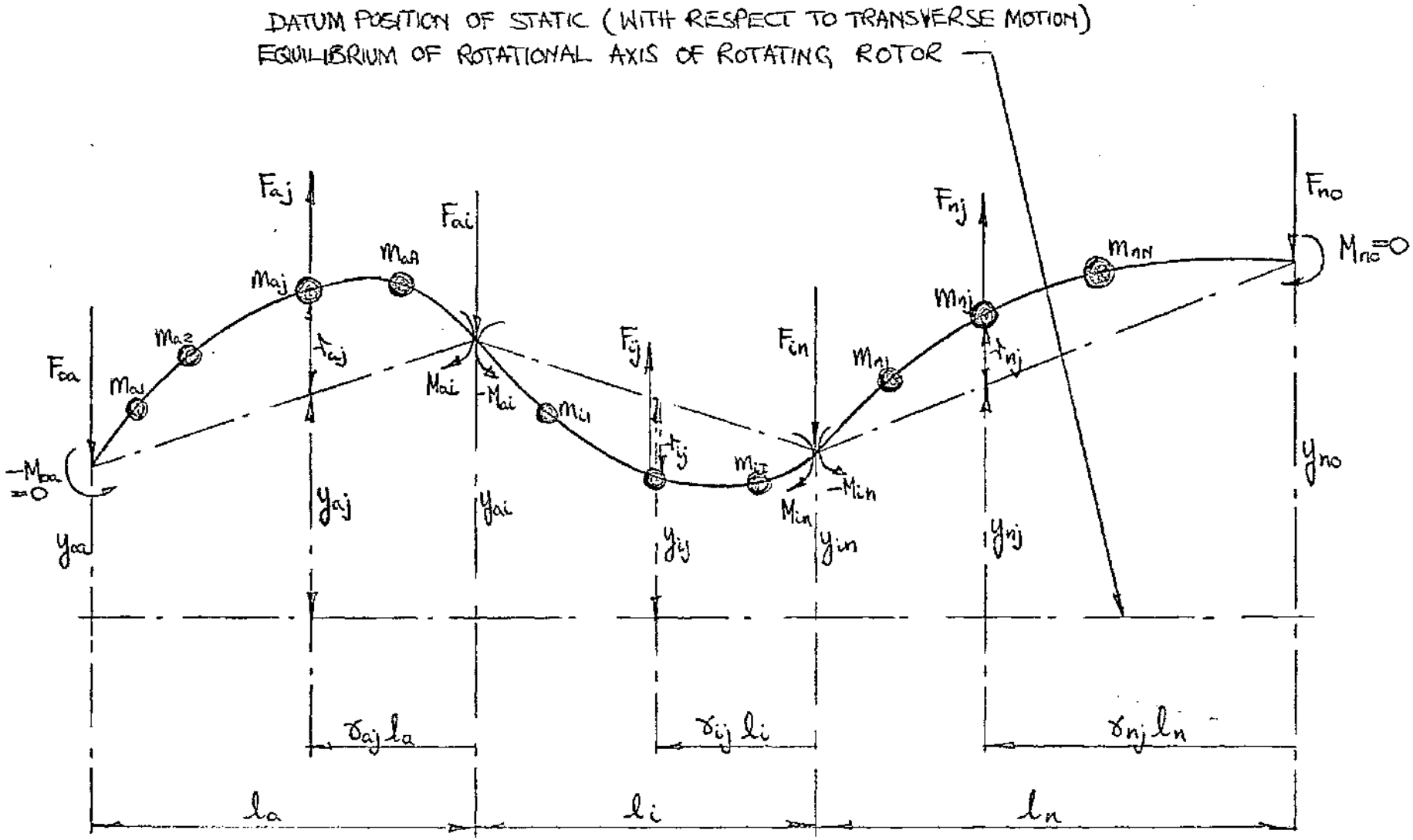

Fig 2.5 WHIRLING MULTI-MASS, MULTI-SPAN FLEXIBLE ROTOR ON FLEXIBLE SUPPORTS.

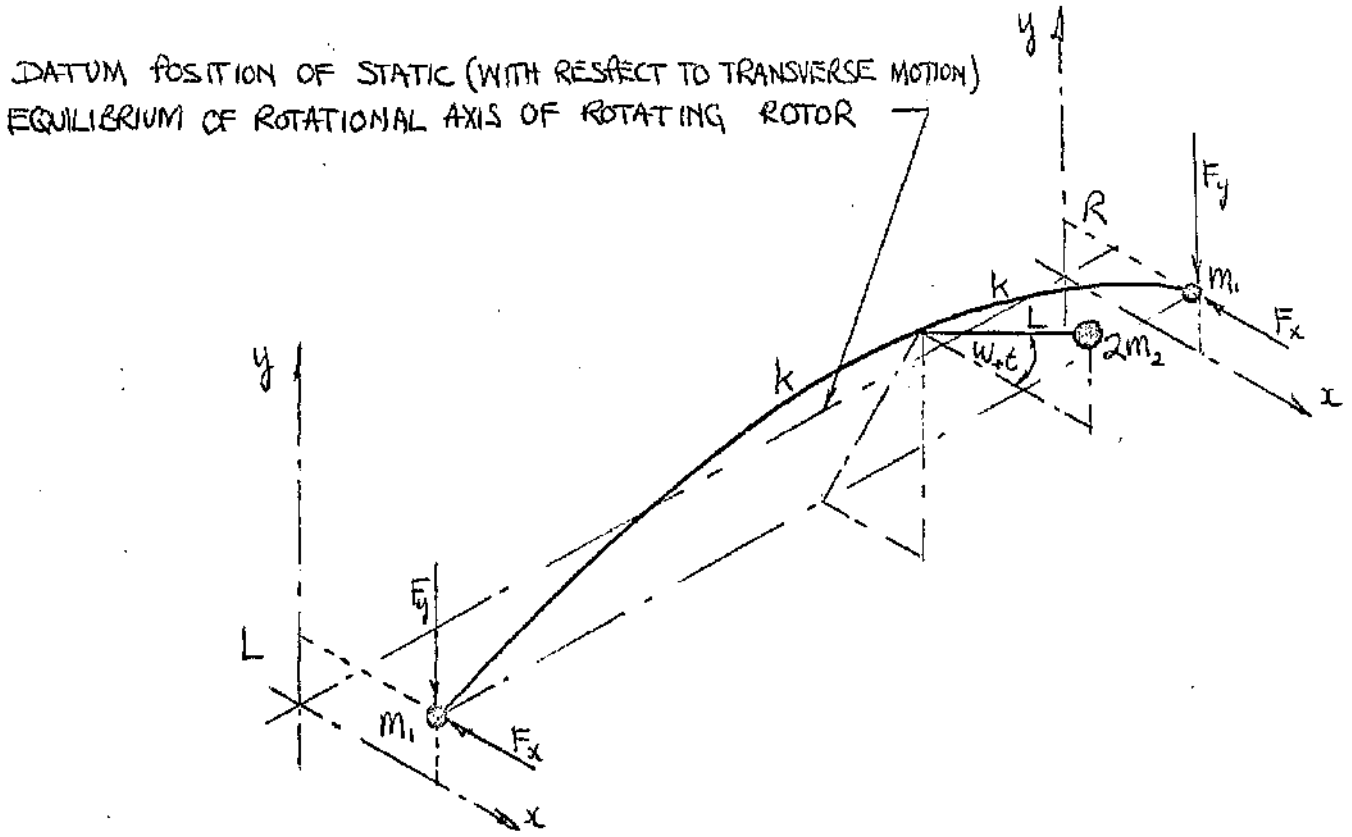

Fig 3.1 WHIRLING SYMMETRICAL FLEXIBLE ROTOR ON SIMILAR FLEXIBLE SUPPORTS.

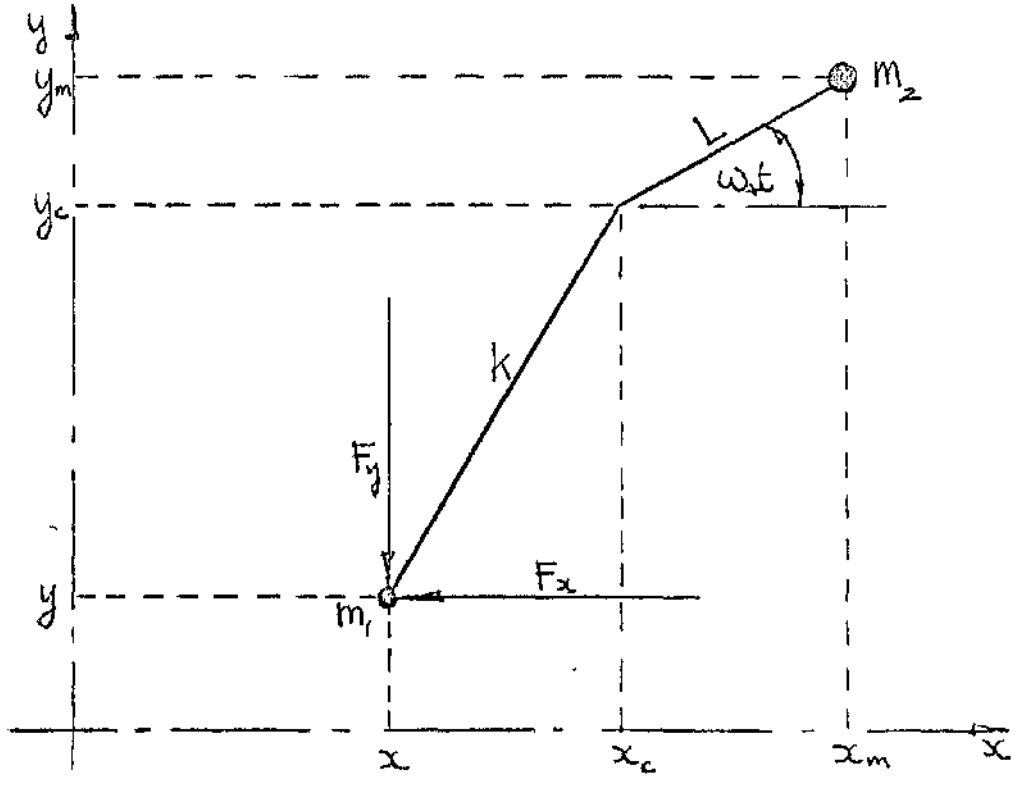

Fig 3.2 AXIAL VIEW OF HALF OF SYMMETRICAL FLEXIBLE ROTOR WHIRLING ON SIMILAR FLEXIBLE SUPPORTS.

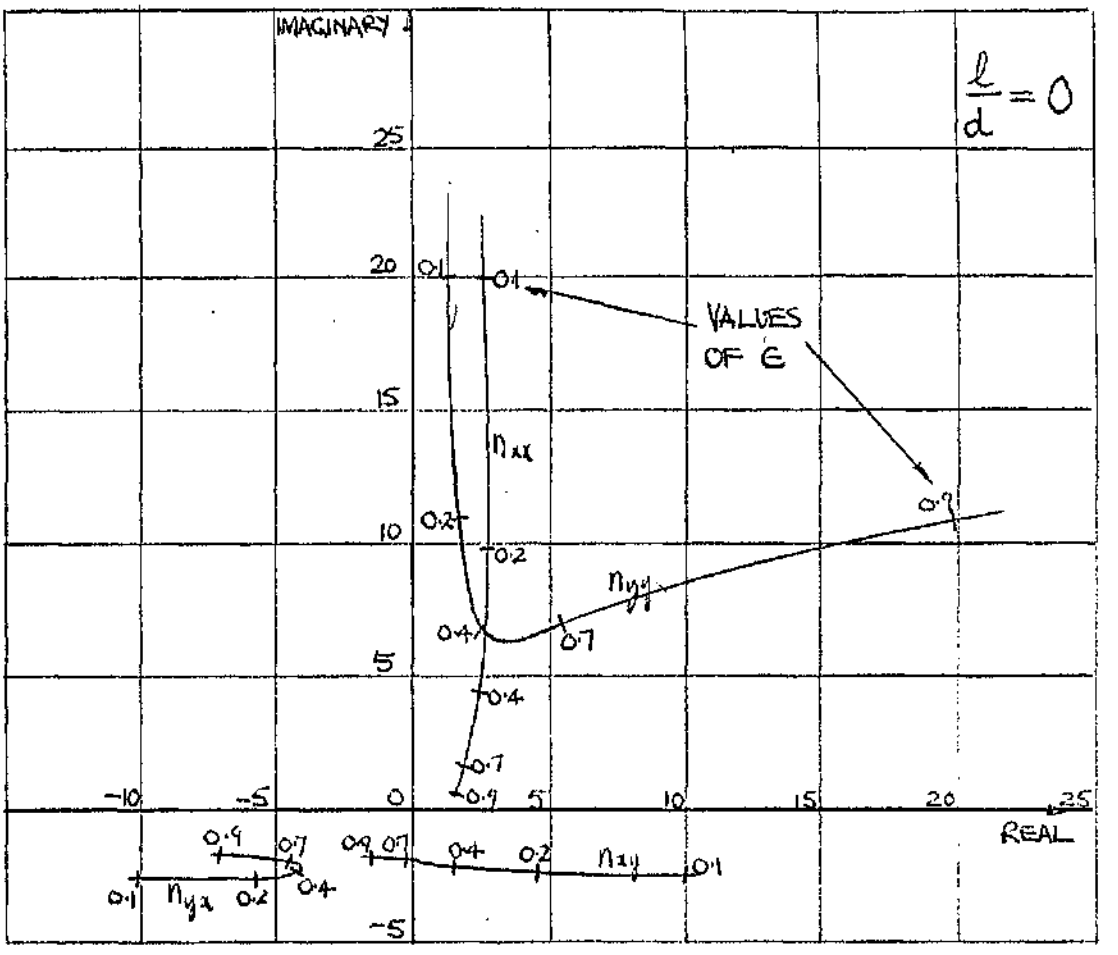

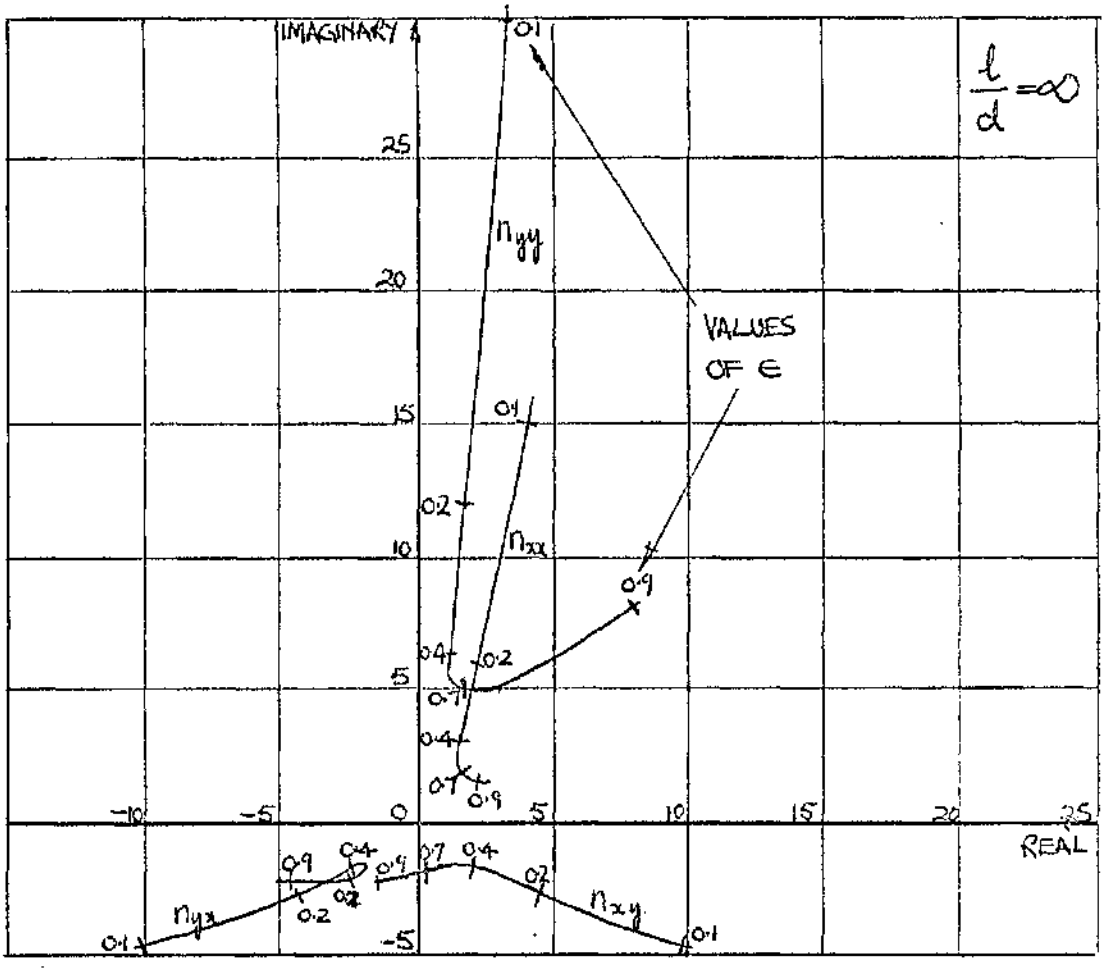

Fig 33 COMPLEX OIL FORCE COEFFICIENTS FOR SYNCHRONOUS WHIRL $\left(\frac{l}{d}=0, \frac{l}{d}=\infty\right)$

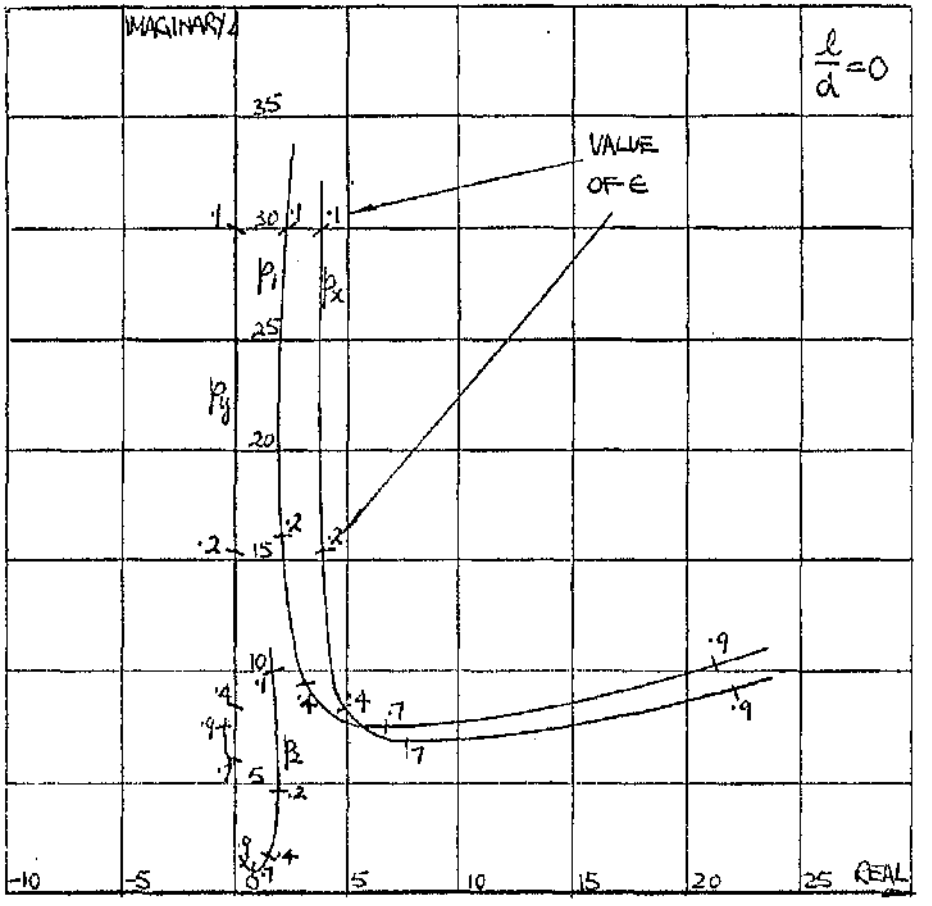

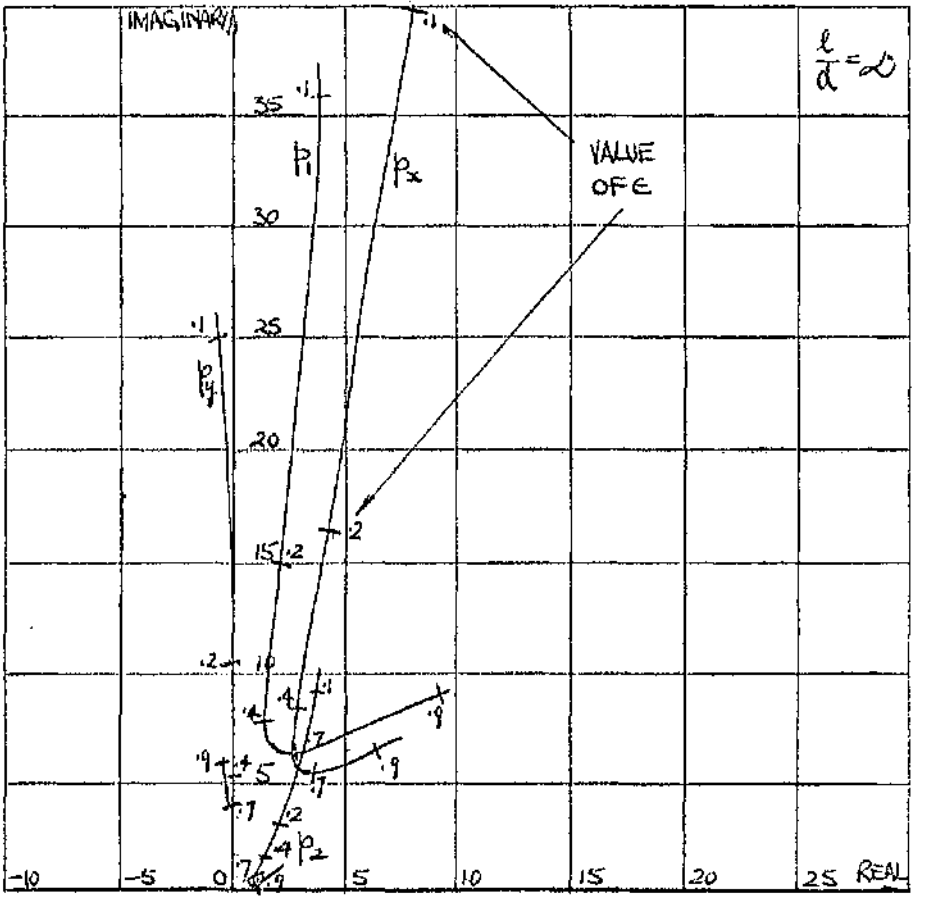

Fig 34 VALUES OF p_1, p_2, p_x, p_y FOR $\frac{l}{d}=0$, $\frac{l}{d}=\infty$.

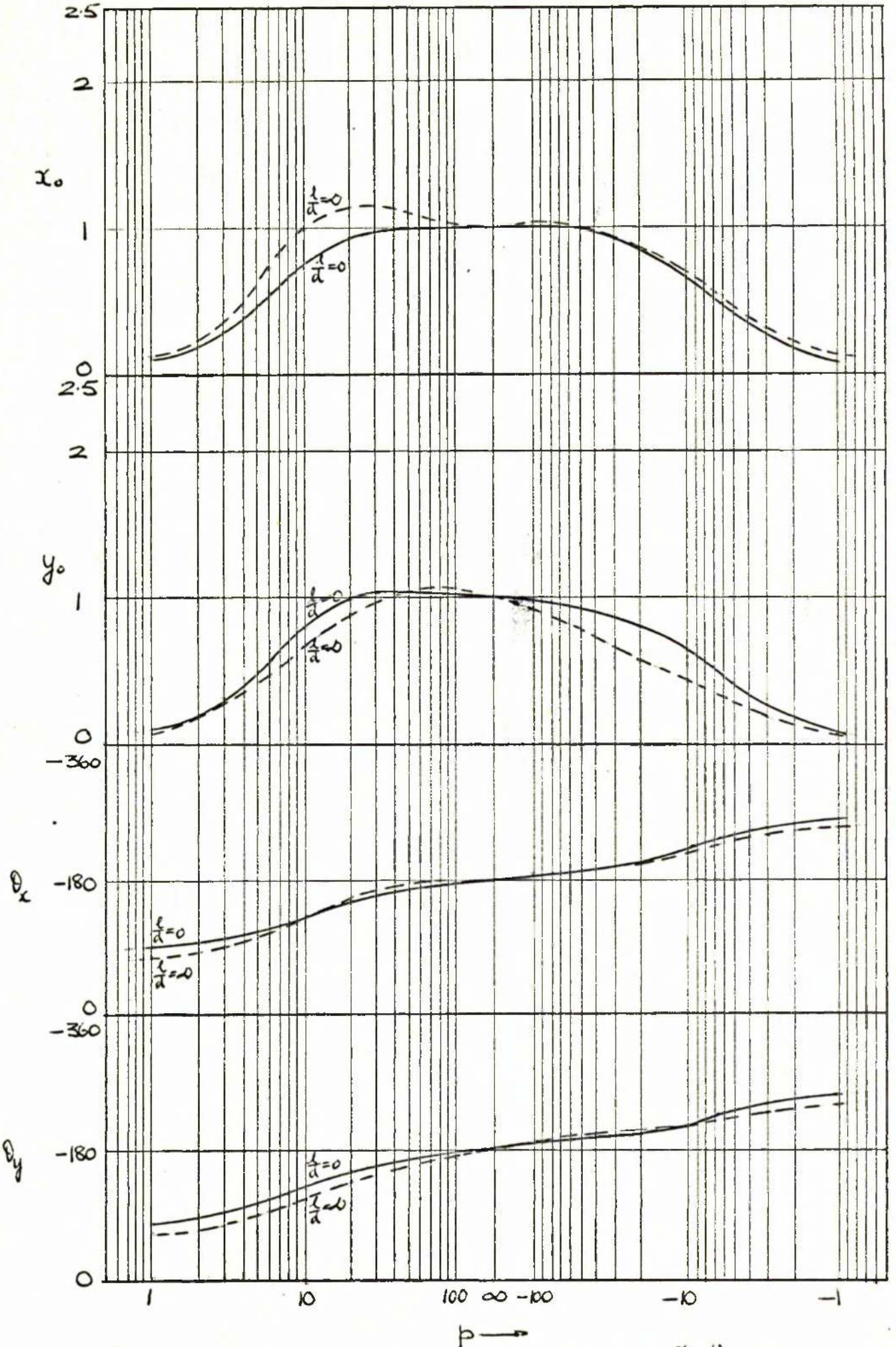

Fig 3.5(a) THEORETICAL PREDICTIONS OF JOURNAL DISPLACEMENT $\frac{x}{L}, \frac{y}{L}$ FOR $\epsilon = \cdot 1$

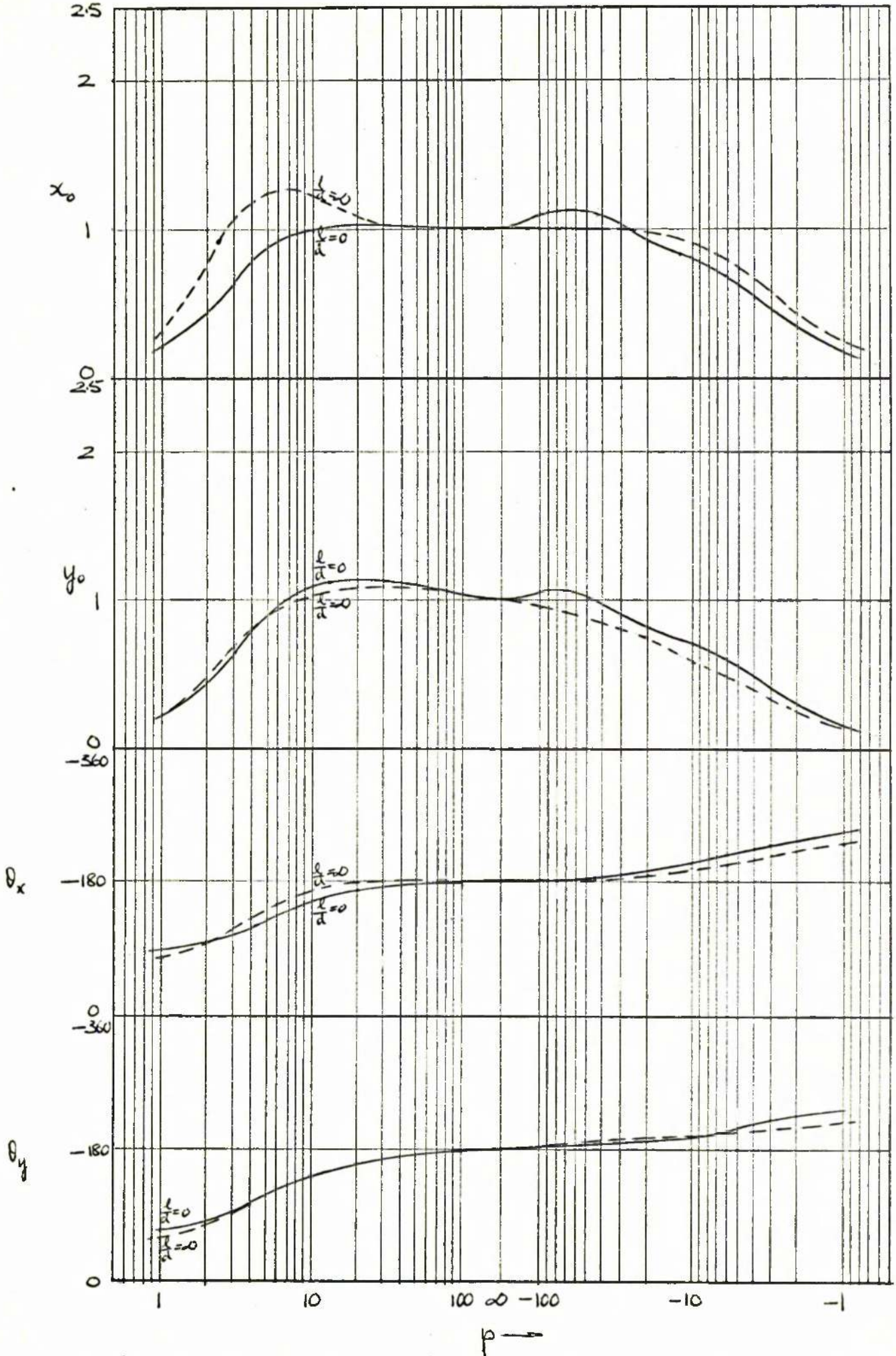

Fig 35(b) THEORETICAL PREDICTIONS OF JOURNAL DISPLACEMENT $\frac{x}{c}, \frac{y}{c}$ FOR $\epsilon = \cdot 2$

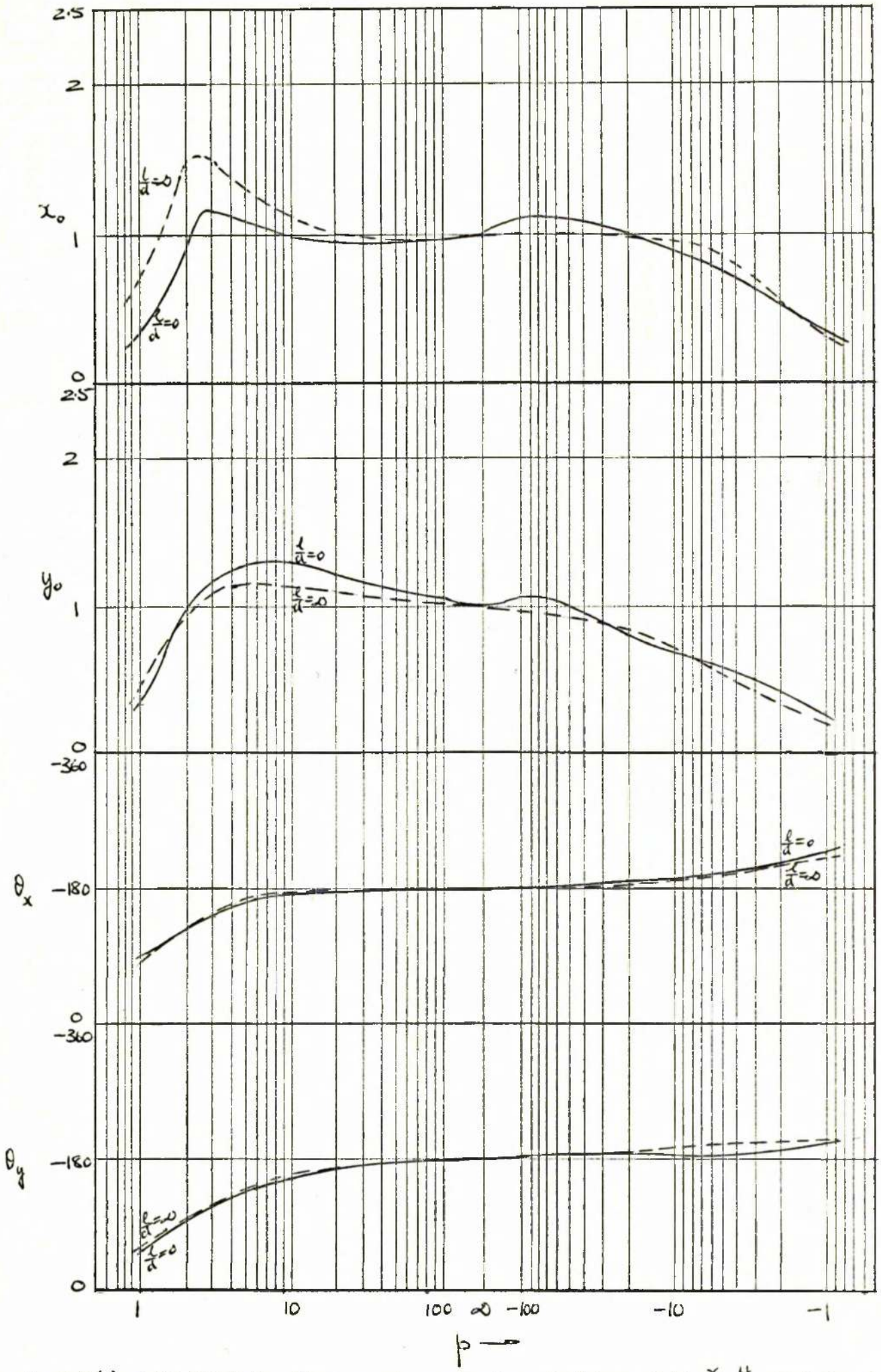

Fig 3.5(c) THEORETICAL PREDICTIONS OF JOURNAL DISPLACEMENT $\frac{x}{L}, \frac{y}{L}$ FOR $\epsilon = .4$

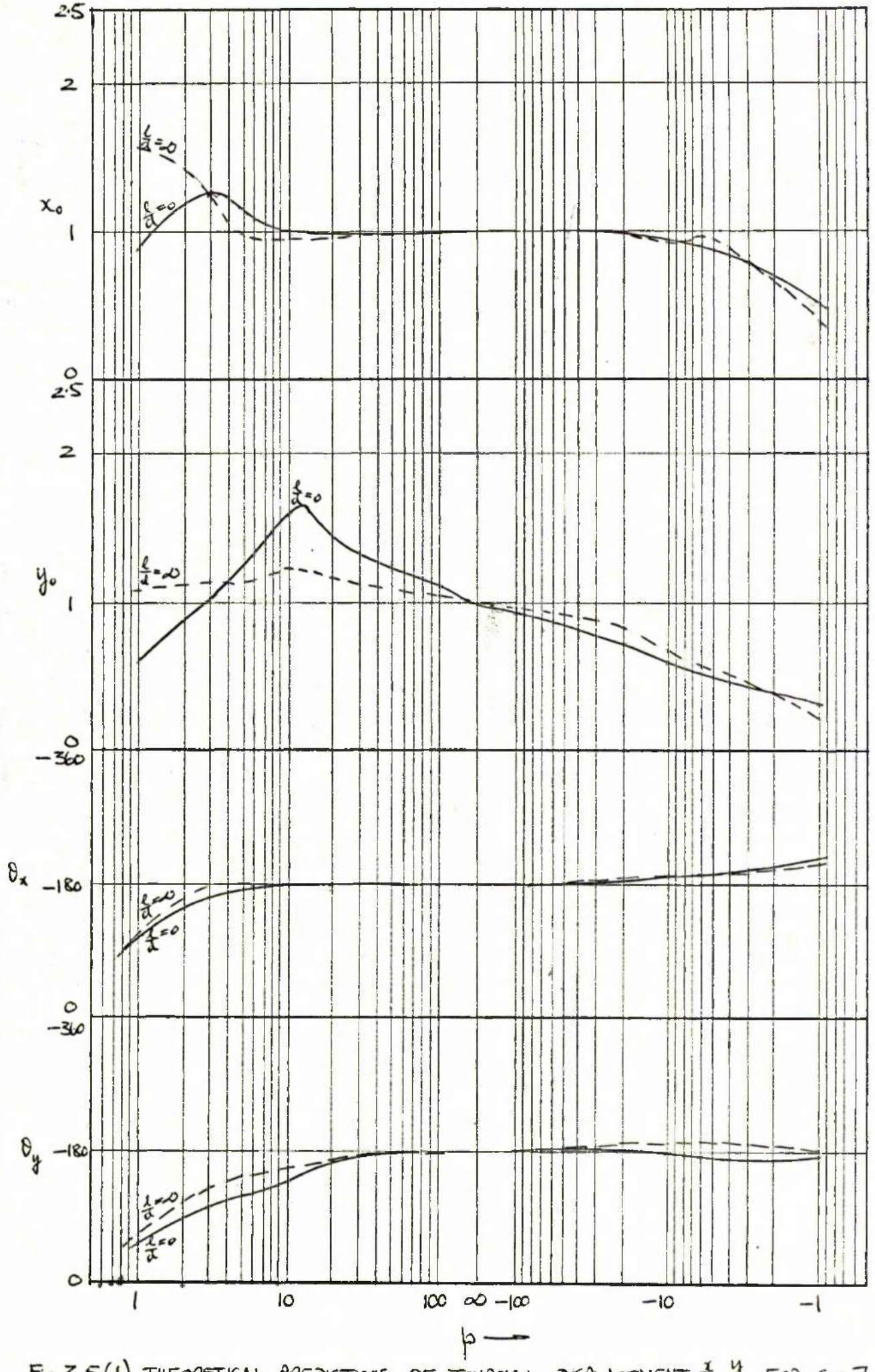

Fig 3.5(d) THEORETICAL PREDICTIONS OF JOURNAL DISPLACEMENT $\frac{x}{L}, \frac{y}{L}$ FOR $\epsilon=.7$

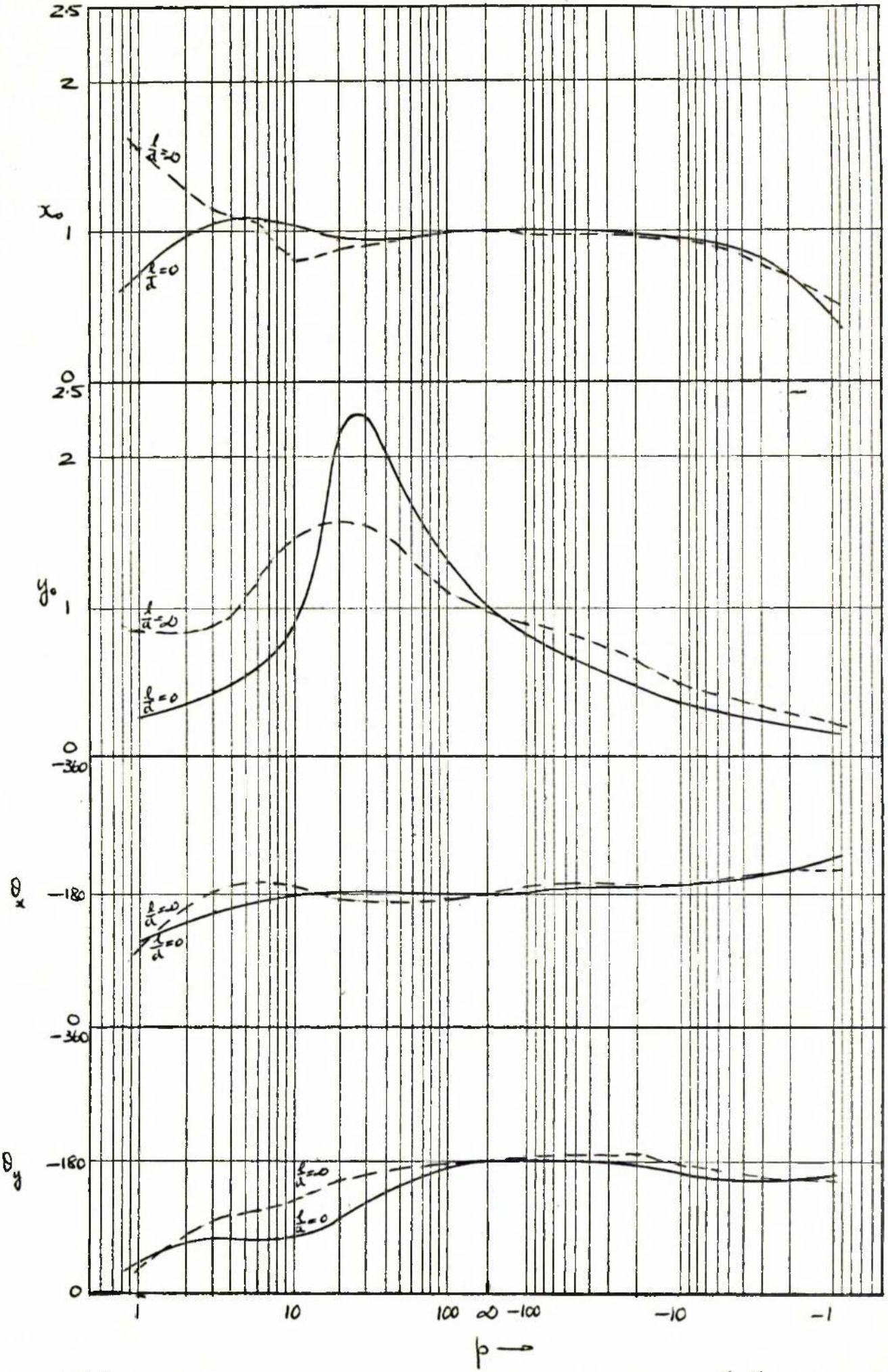

Fig 3.5 (e) THEORETICAL PREDICTIONS OF JOURNAL DISPLACEMENT $\frac{x}{L}, \frac{y}{L}$ FOR $\epsilon = \cdot 9$

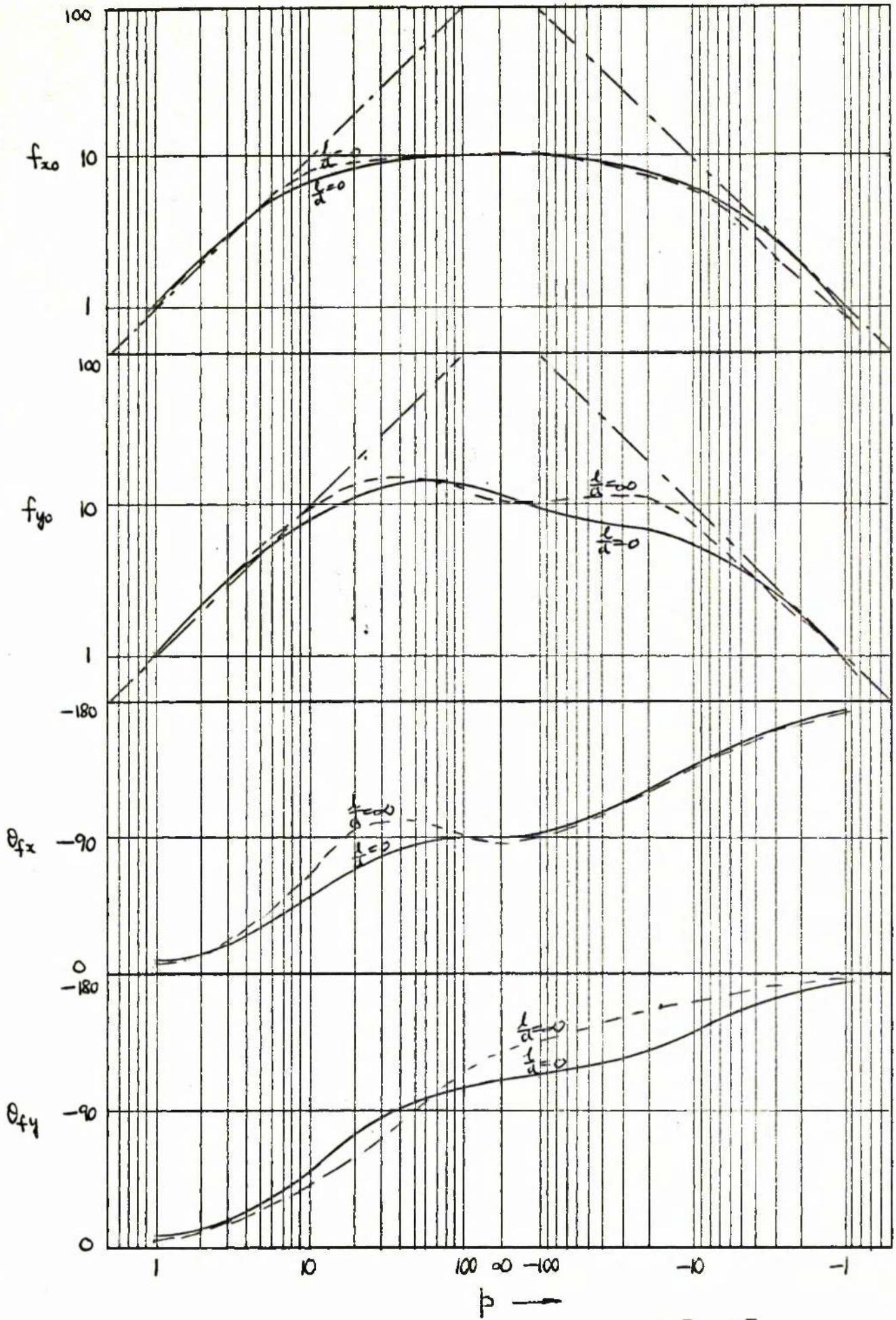

Fig 36(a) THEORETICAL PREDICTIONS OF OIL FORCE ON JOURNAL $\frac{c}{L}\frac{F_x}{W}$, $\frac{c}{L}\frac{F_y}{W}$ FOR $\epsilon = \cdot 1$

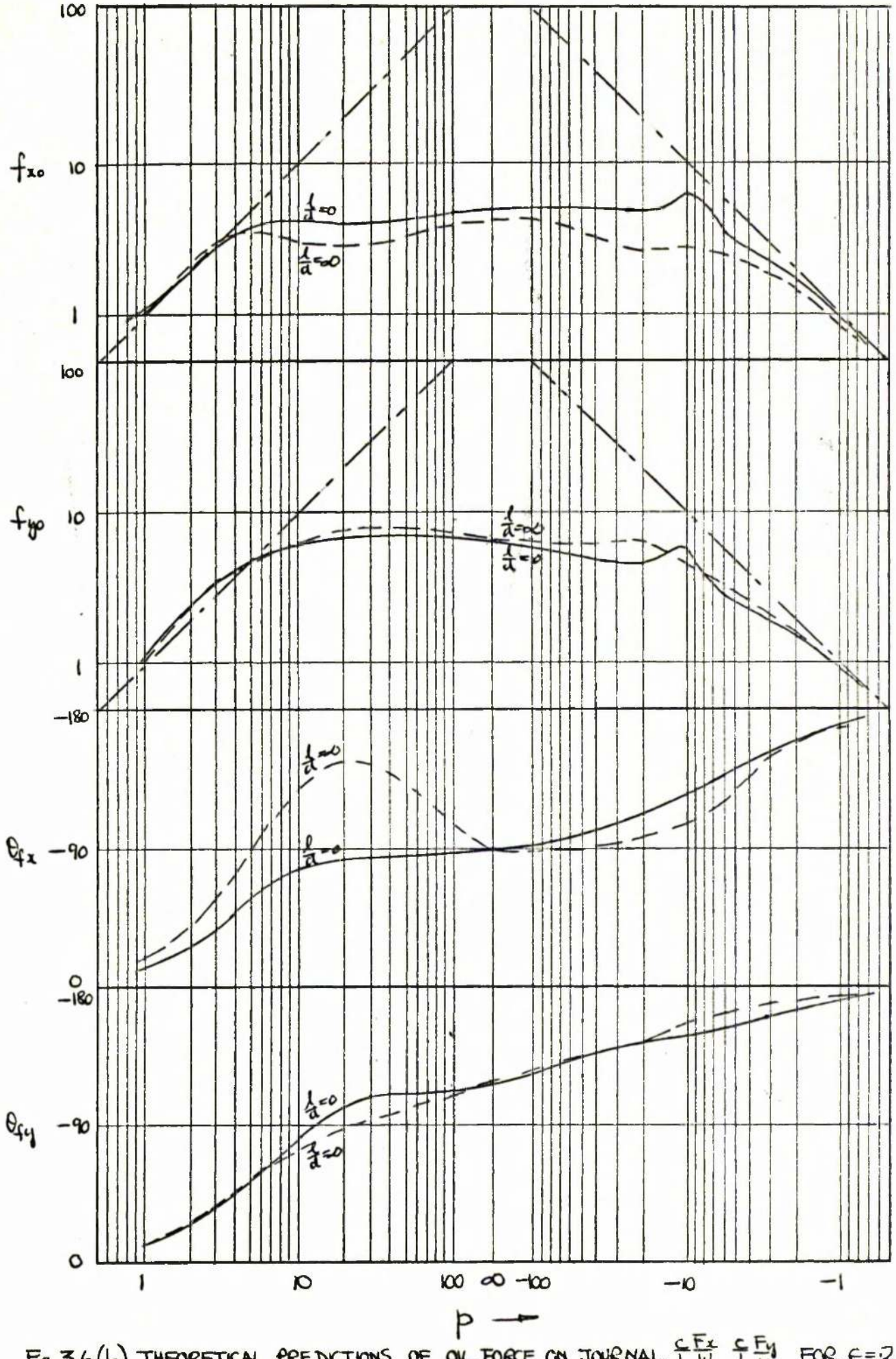

Fig 3.6(b) THEORETICAL PREDICTIONS OF OIL FORCE ON JOURNAL $\frac{c}{L}\frac{F_x}{W}$, $\frac{c}{L}\frac{F_y}{W}$ FOR $\epsilon=2$.

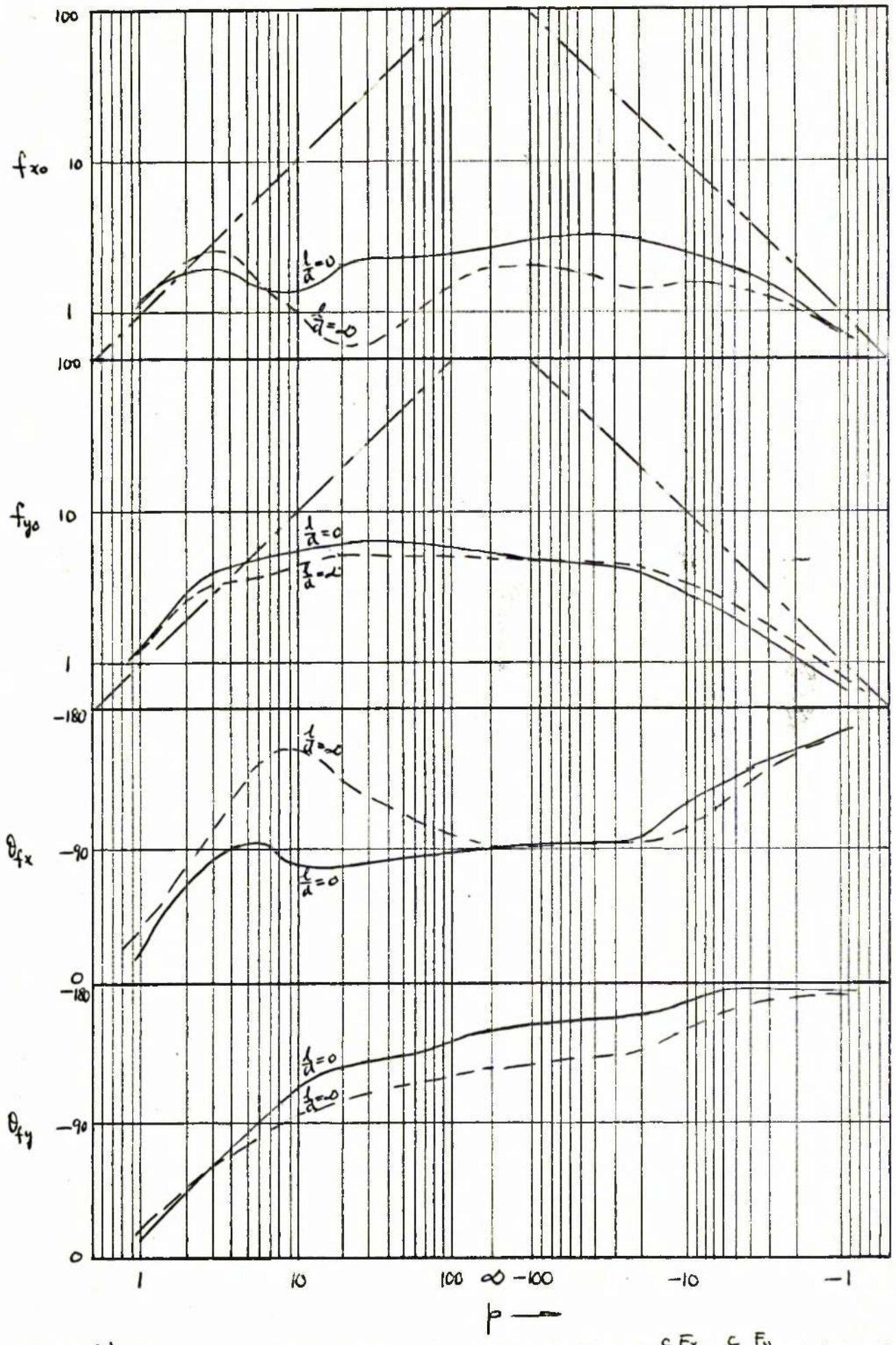

Fig 3.6(c) THEORETICAL PREDICTIONS OF OIL FORCE ON JOURNAL $\frac{c}{L}\frac{F_x}{W}$, $\frac{c}{L}\frac{F_y}{W}$ FOR $\epsilon = \cdot 4$

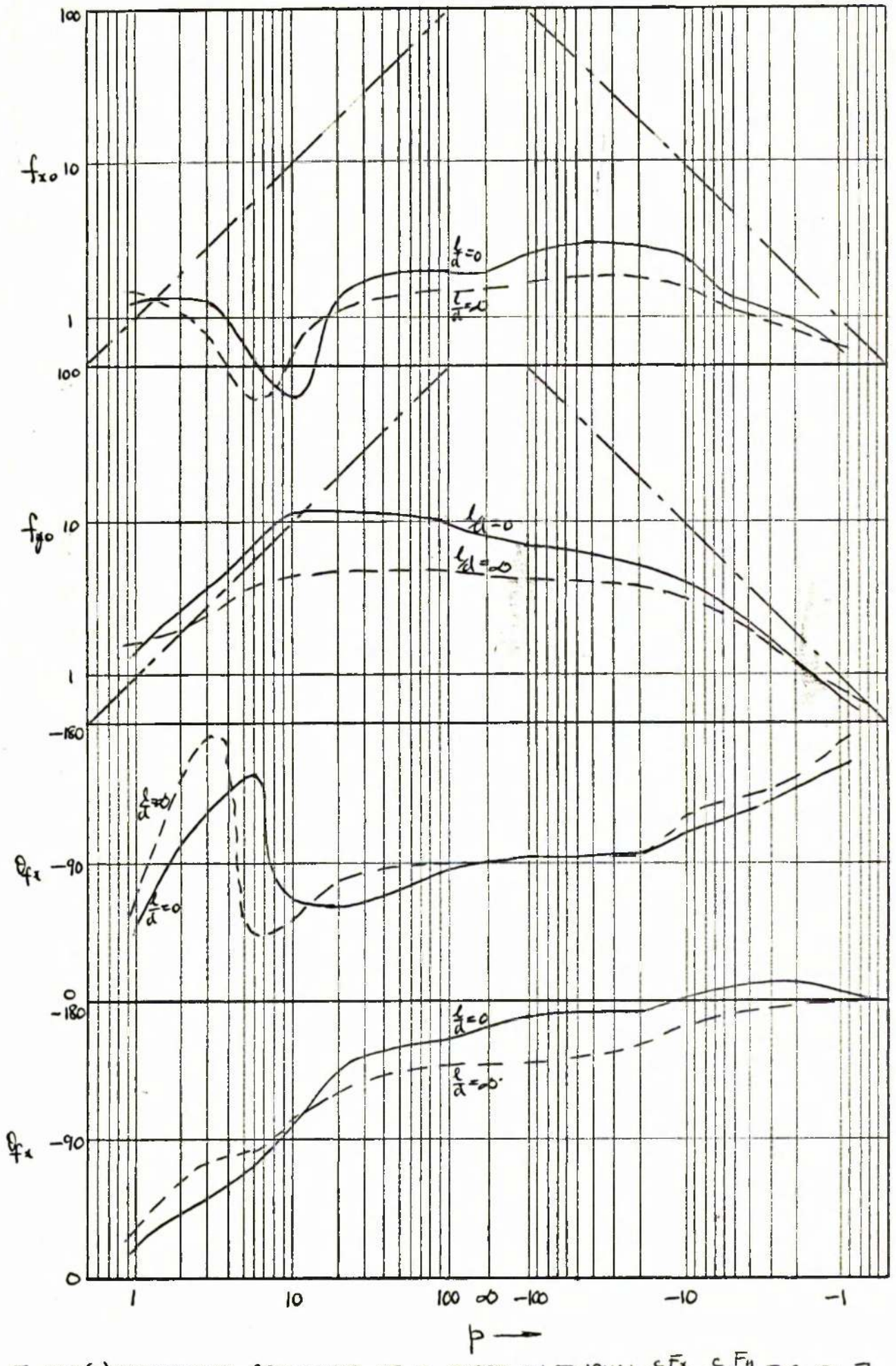

Fig 3.6(a) THEORETICAL PREDICTIONS OF OIL FORCE ON JOURNAL $\frac{c}{L}\frac{F_x}{N}$, $\frac{c}{L}\frac{F_y}{N}$ FOR $\epsilon = .7$

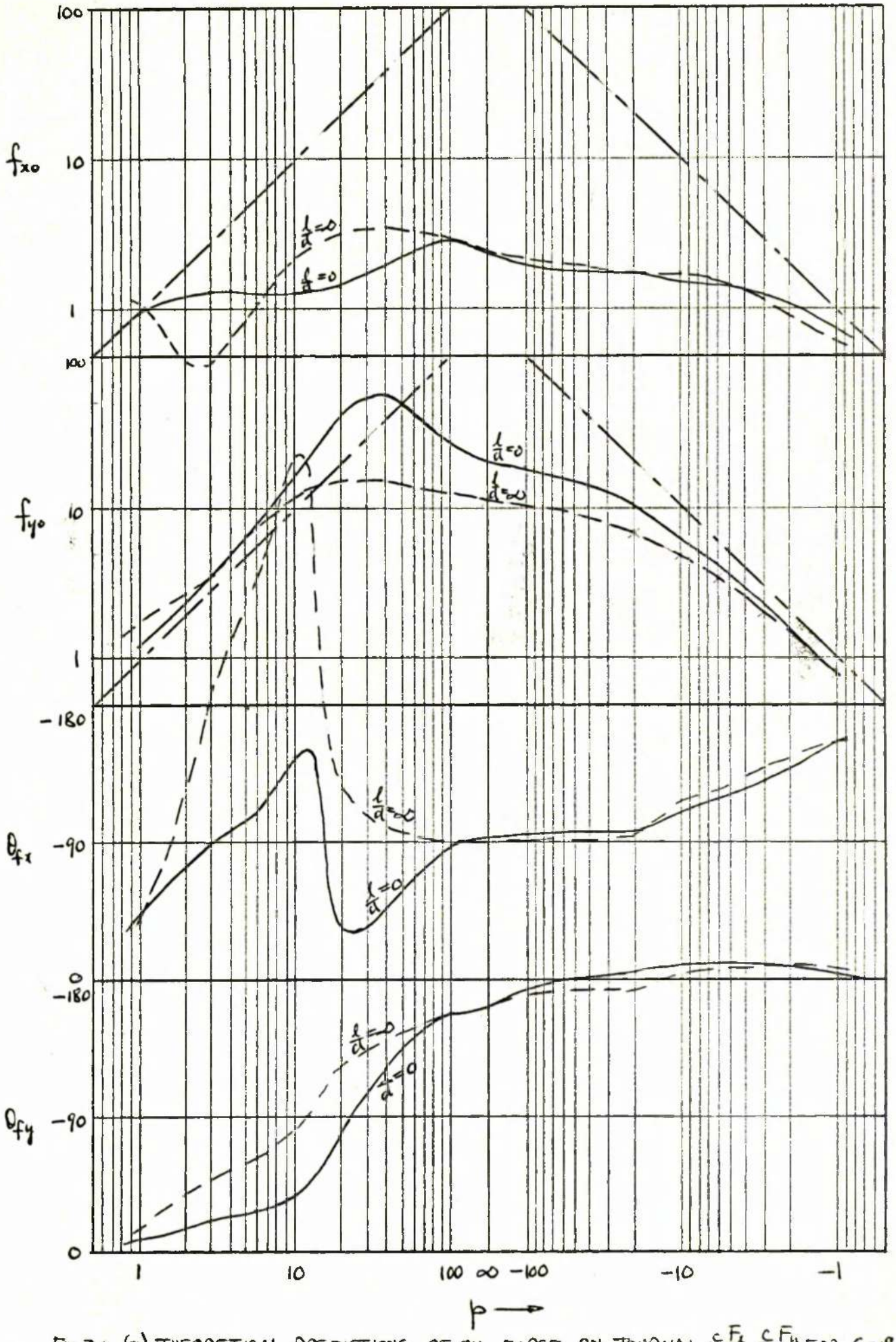

Fig 3.6 (e) THEORETICAL PREDICTIONS OF OIL FORCE ON JOURNAL $\frac{c}{LW}\frac{F_x}{}$, $\frac{c}{LW}\frac{F_y}{}$ FOR $\epsilon = 0.9$

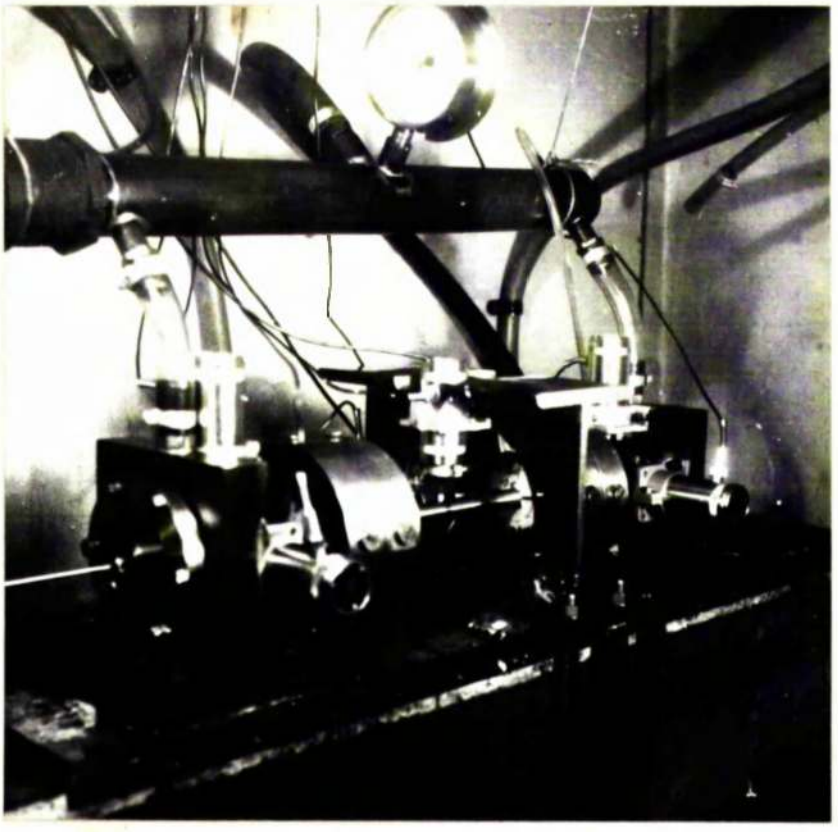

Fig 4.1 RIG SET UP FOR SYNCHRONOUS OIL WHIRL EXPERIMENTS

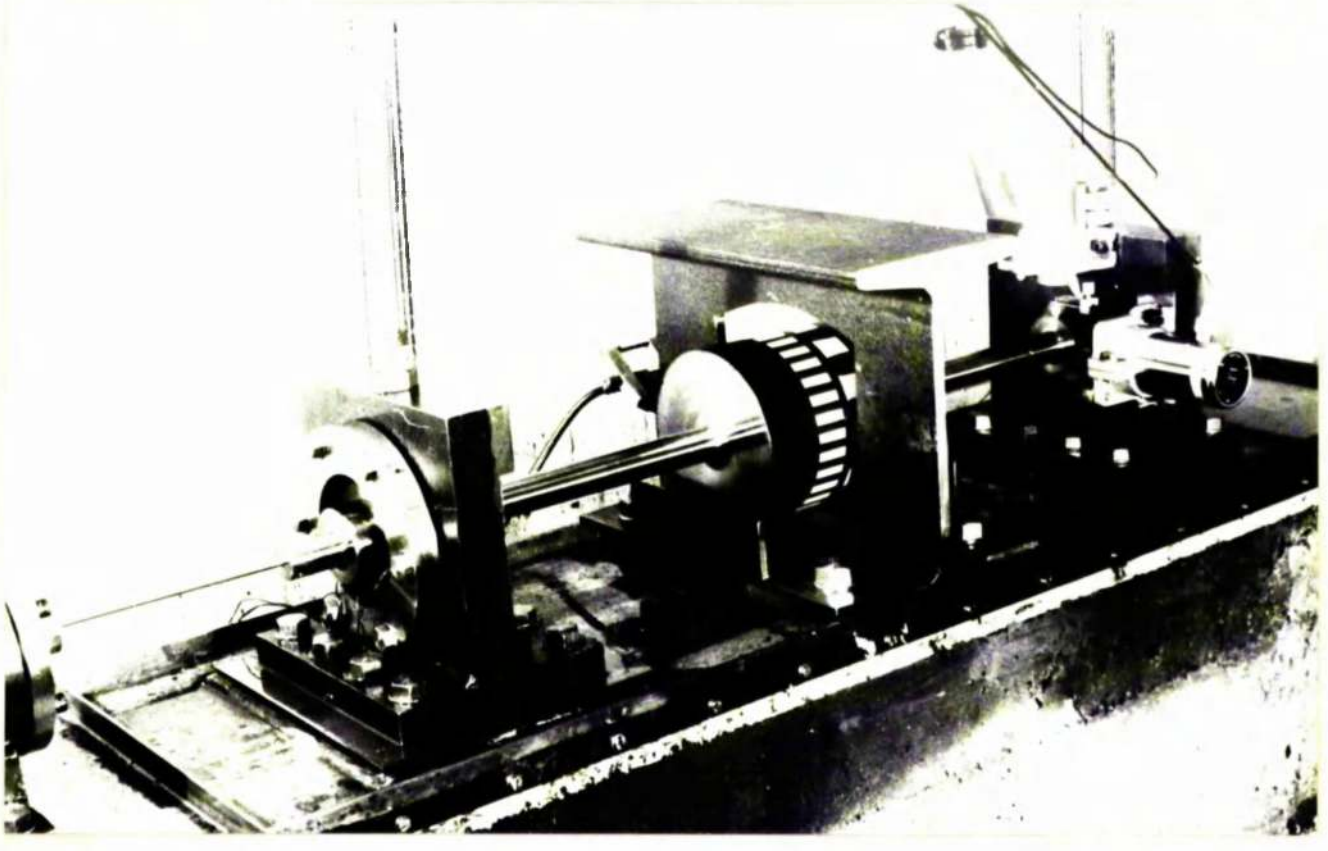

Fig 4.2 RIG SET UP FOR UNSTABLE OIL WHIRL EXPERIMENTS.

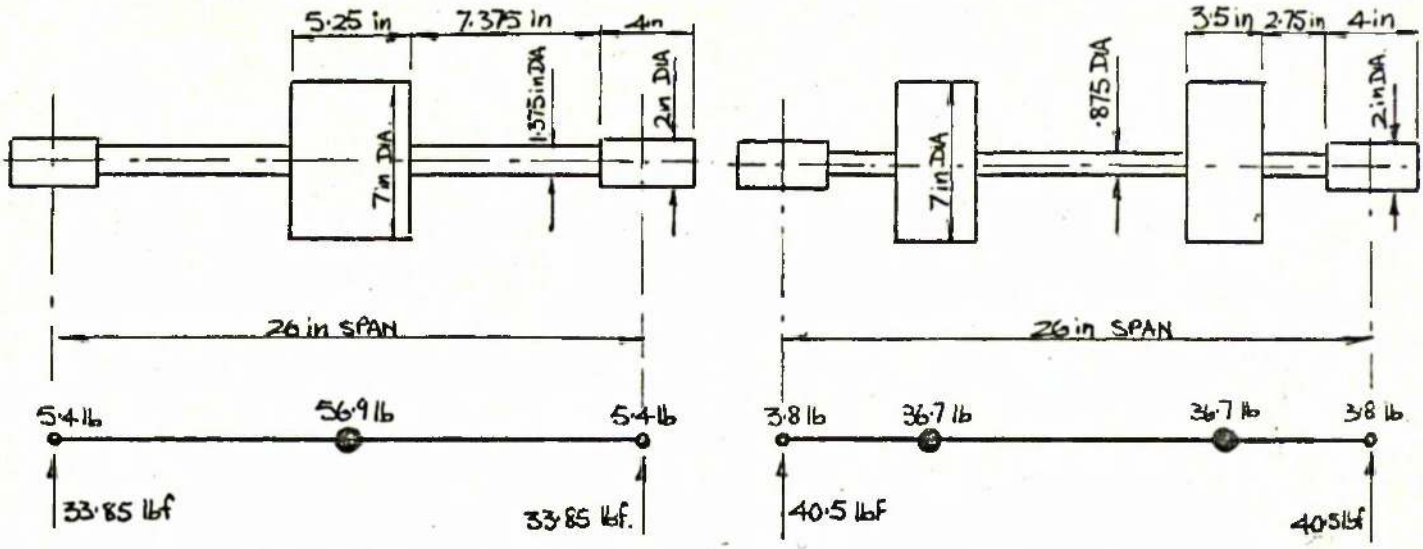

F.g 4.3 ROTOR DIMENSIONS AND MASS DISTRIBUTIONS.

F.g 4.4 ARRANGEMENT FOR ROTOR RESONANCE

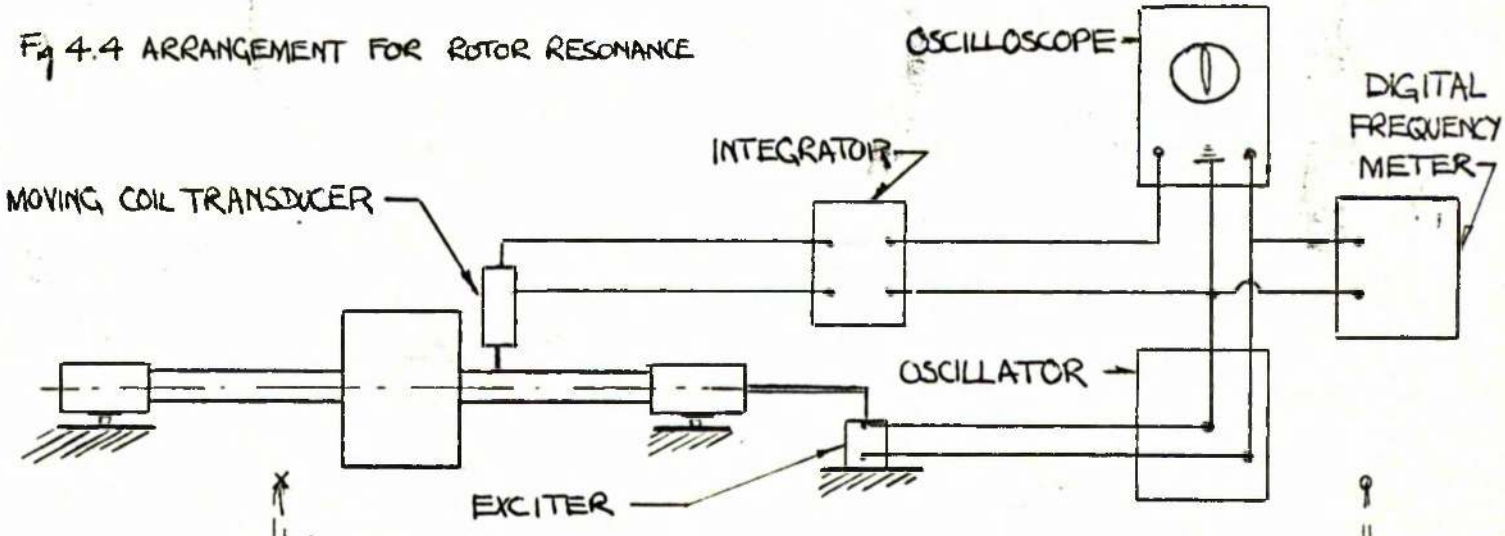

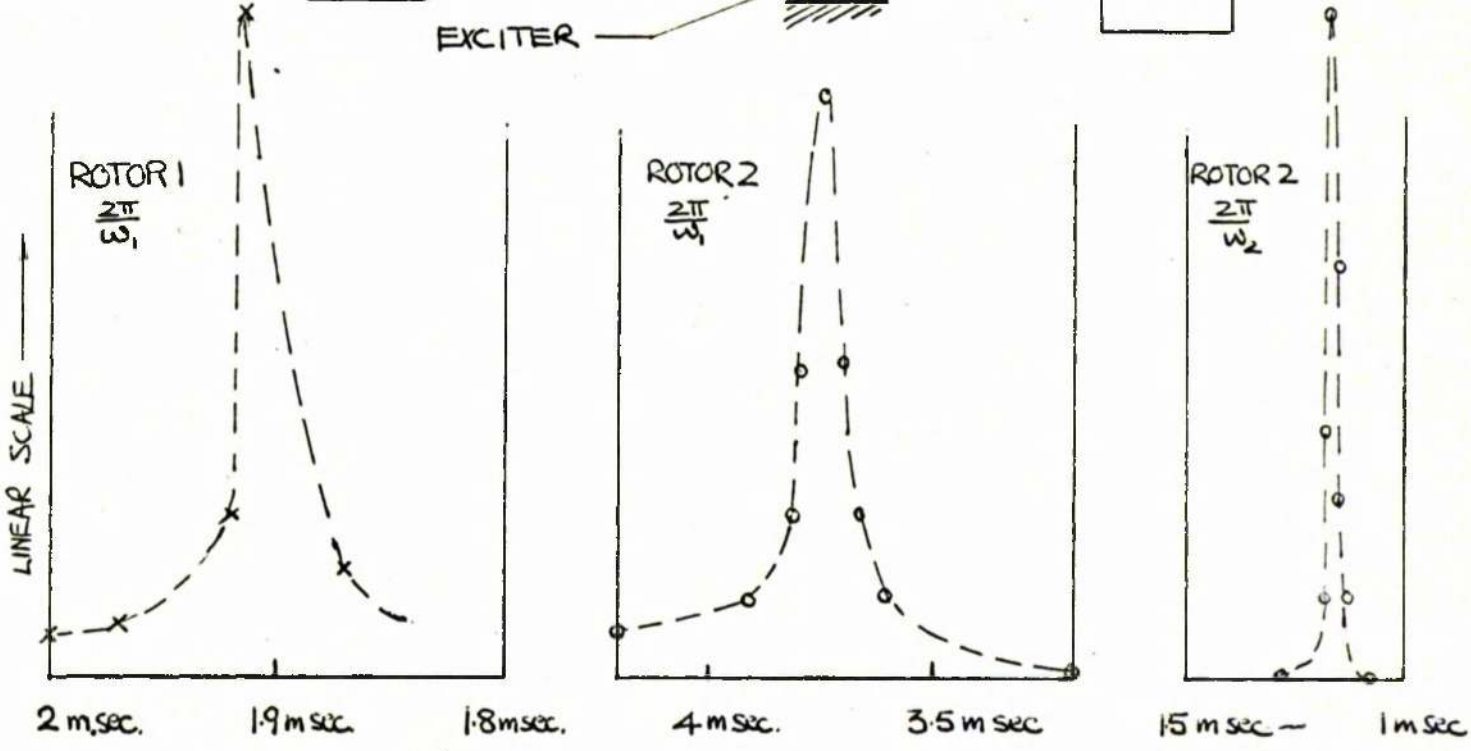

F.g 4.5 ROTOR RESONANCE DIAGRAMS.

Fig 4.6 RECEPTANCE COEFFICIENTS FOR ROTOR 1.

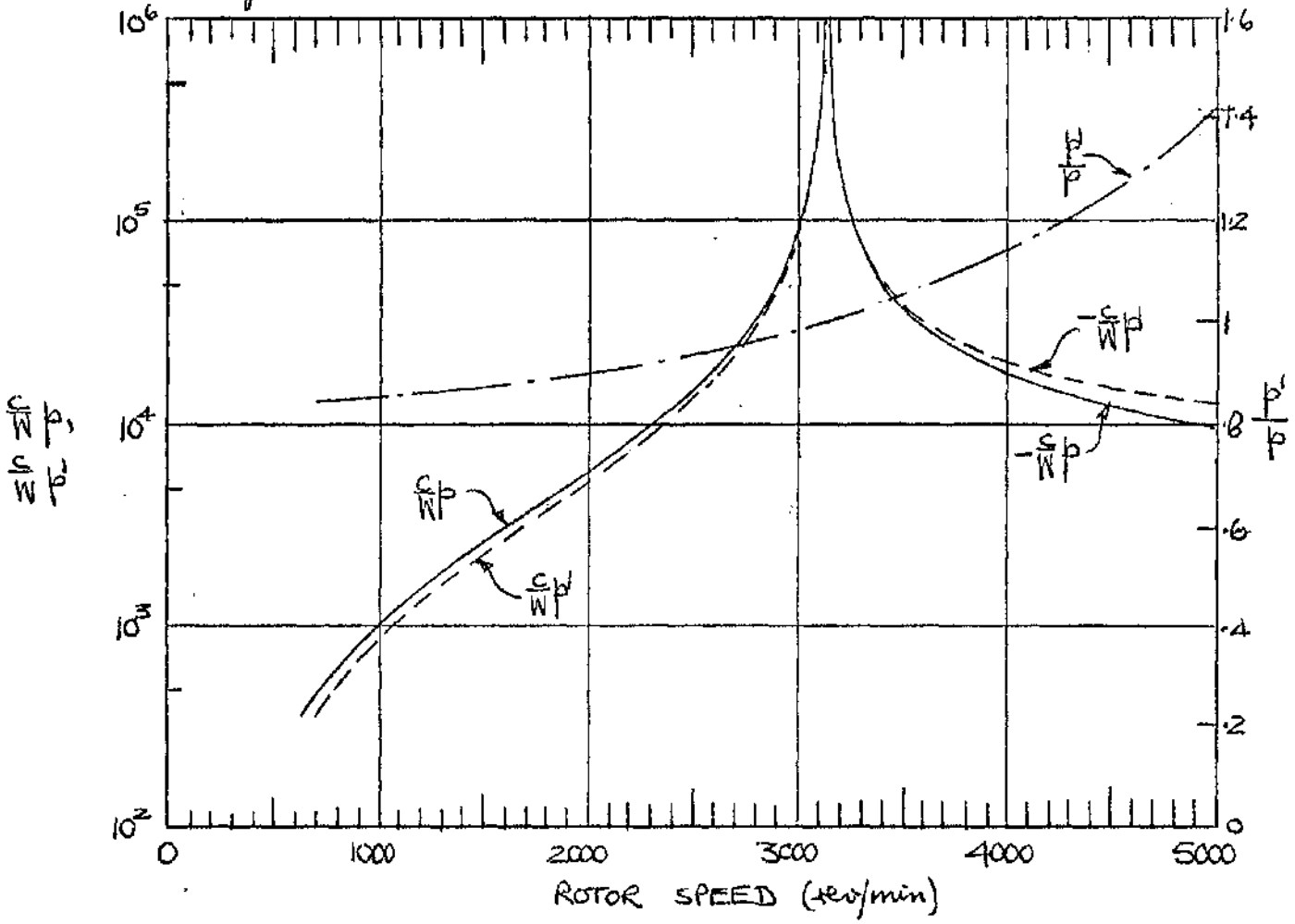

Fig 4.7 RECEPTANCE COEFFICIENTS FOR ROTOR 2.

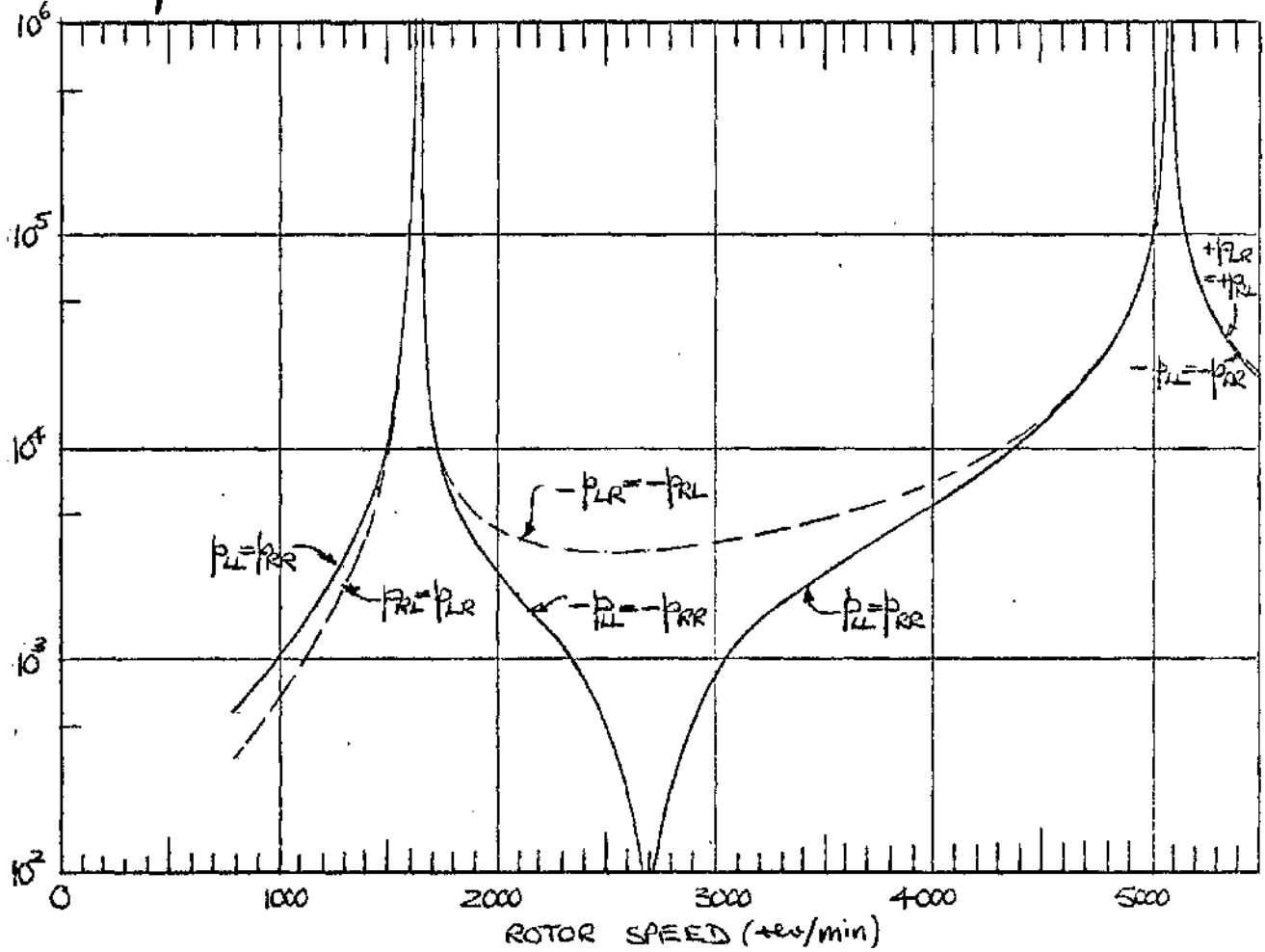

2c, BEARING CLEARANCE (in/1000)	l, BEARING LENGTH (in)			
	2·0	1·5	1·0	·667
		4·9	3·9	4·5
		11·3	9·7	12·4
	15·0	15·5	15·5	
	22·3	22·3	22·3	
	30·5	27·6	27·7	

Fig 4.8 TABLE OF BEARING DIMENSIONS.

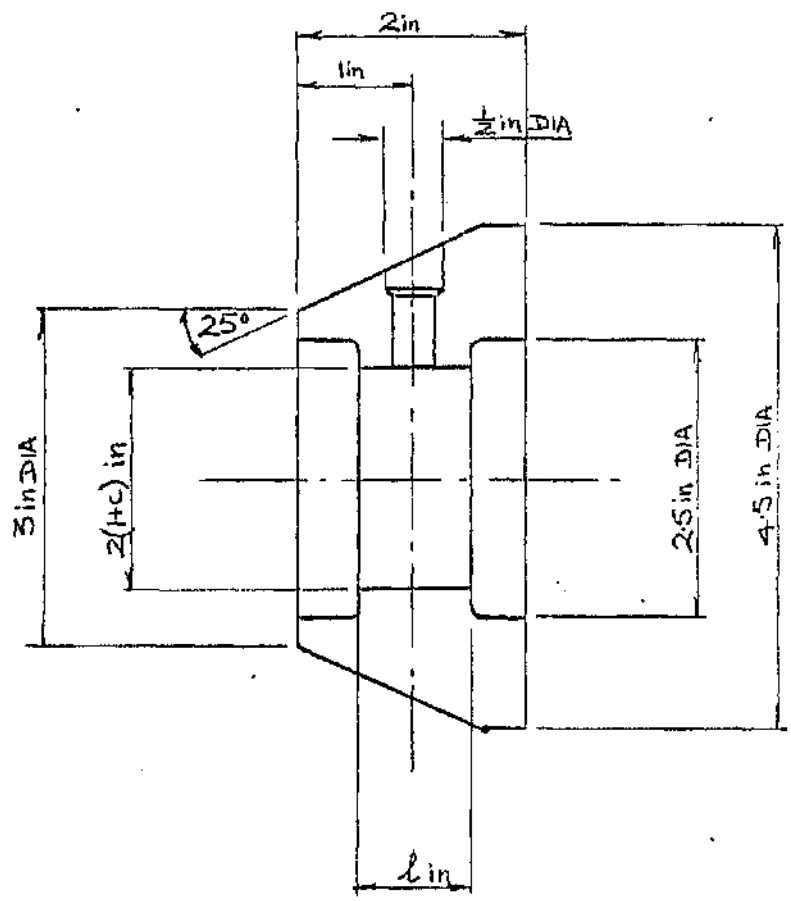

Fig 4.9 SECTIONAL VIEW OF SPECIMEN BEARING.

Fig. 4.10(a) EXPERIMENTAL OBSERVATIONS OF JOURNAL DISPLACEMENT
ROTOR: 1 BEARINGS: 1·5in x ·0223in OIL: NORPOL 35 (ASSEMBLY R1.1)

Fig 4.10(b) EXPERIMENTAL OBSERVATIONS OF JOURNAL DISPLACEMENT
ROTOR: 1 BEARINGS: 2 in × ·0305 in OIL: NORPOL 35 (ASSEMBLY R1.2)

Fig 4.10(c) EXPERIMENTAL OBSERVATIONS OF JOURNAL DISPLACEMENT
ROTOR : 1 BEARINGS : 1 in x ·0097 in OIL: NORPOL 35 (ASSEMBLY R1.3)

Fig 4.10(d) EXPERIMENTAL OBSERVATIONS OF JOURNAL DISPLACEMENT.
ROTOR: 1 BEARINGS: 1·5 in × ·0155 in OIL: NORPAL 35 (ASSEMBLY R1.4)

Fig 4.10(e) EXPERIMENTAL OBSERVATIONS OF JOURNAL DISPLACEMENT
ROTOR: 1 BEARINGS: ·667 in x ·0045 in OIL: NORPOL 35 (ASSEMBLY R1.5)

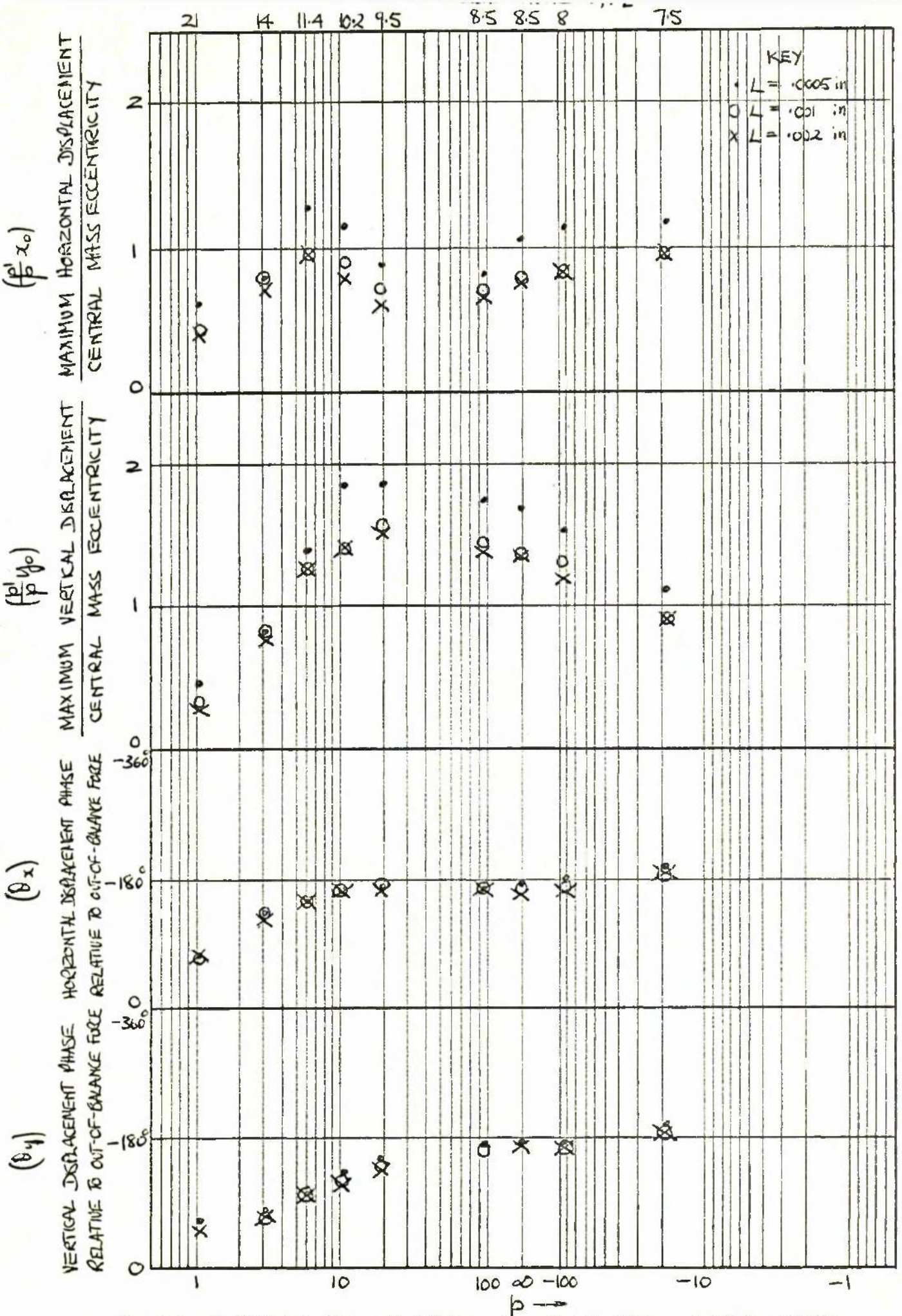

Fig 4.10(f) EXPERIMENTAL OBSERVATIONS OF JOURNAL DISPLACEMENT.
ROTOR: 1 BEARINGS: 2 in x ·0223 in OIL: NORPOL 35 (ASSEMBLY R1.6)

Fig 4.10(g) EXPERIMENTAL OBSERVATIONS OF JOURNAL DISPLACEMENT.
ROTOR: 1 BEARINGS: 1·5 in × ·0113 in OIL: MENTOR 28 (ASSEMBLY R1.7)

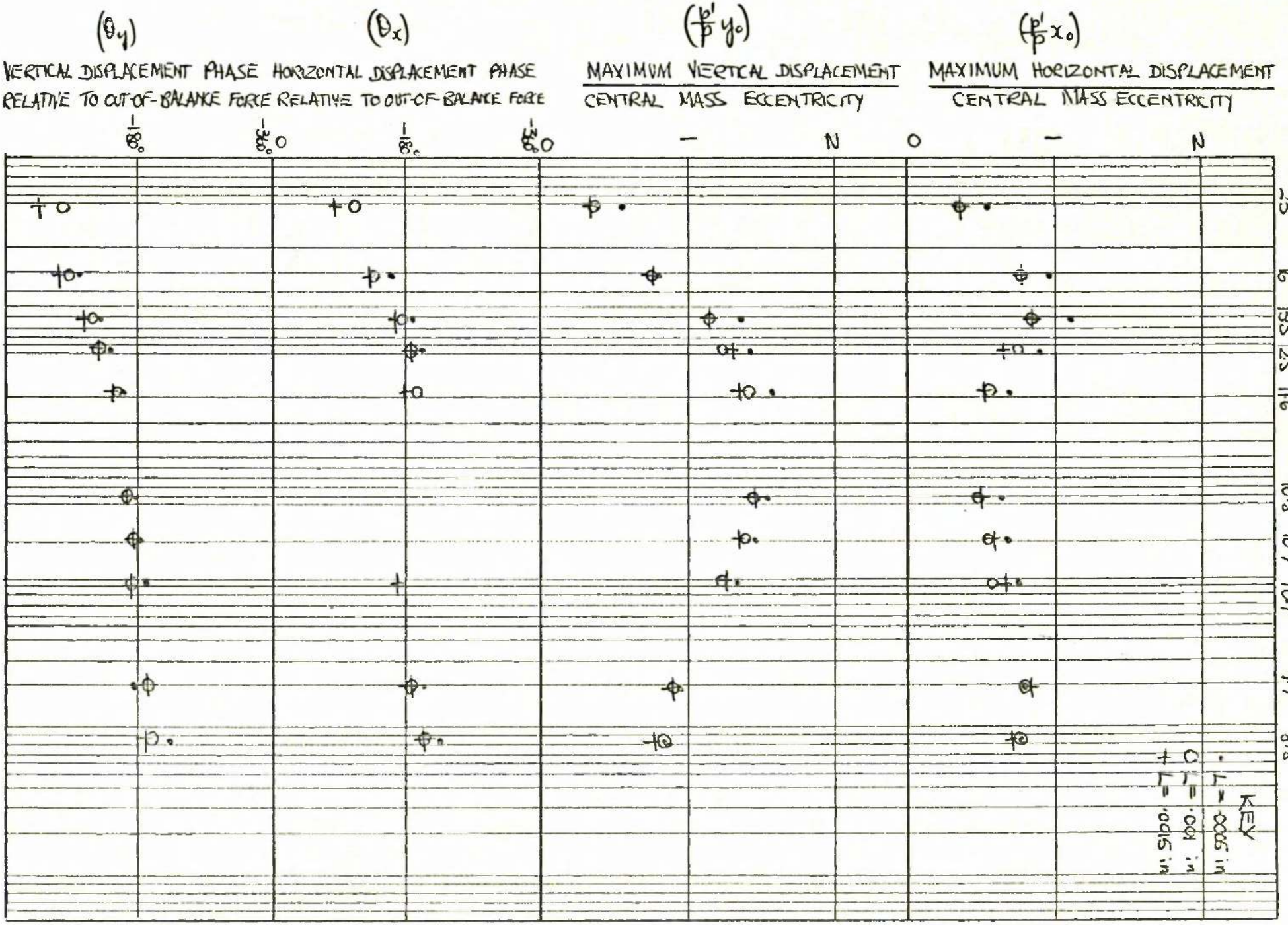

Fig 4.10(h) EXPERIMENTAL OBSERVATIONS OF JOURNAL DISPLACEMENT
ROTOR: 1 BEARINGS: 2 in x .015 in OIL: MENTOR 28 (ASSEMBLY R1.8)

Fig 4.10(i) EXPERIMENTAL OBSERVATIONS OF JOURNAL DISPLACEMENT.
ROTOR: 1 BEARINGS: 1 in x ·0039 in OIL: MENTOR 28 (ASSEMBLY R1.9)

Fig 4.10(j) EXPERIMENTAL OBSERVATIONS OF JOURNAL DISPLACEMENT.
ROTOR : 1 BEARINGS : 1·5 in × ·0049 in OIL : MENTOR 28 (ASSEMBLY R1.10)

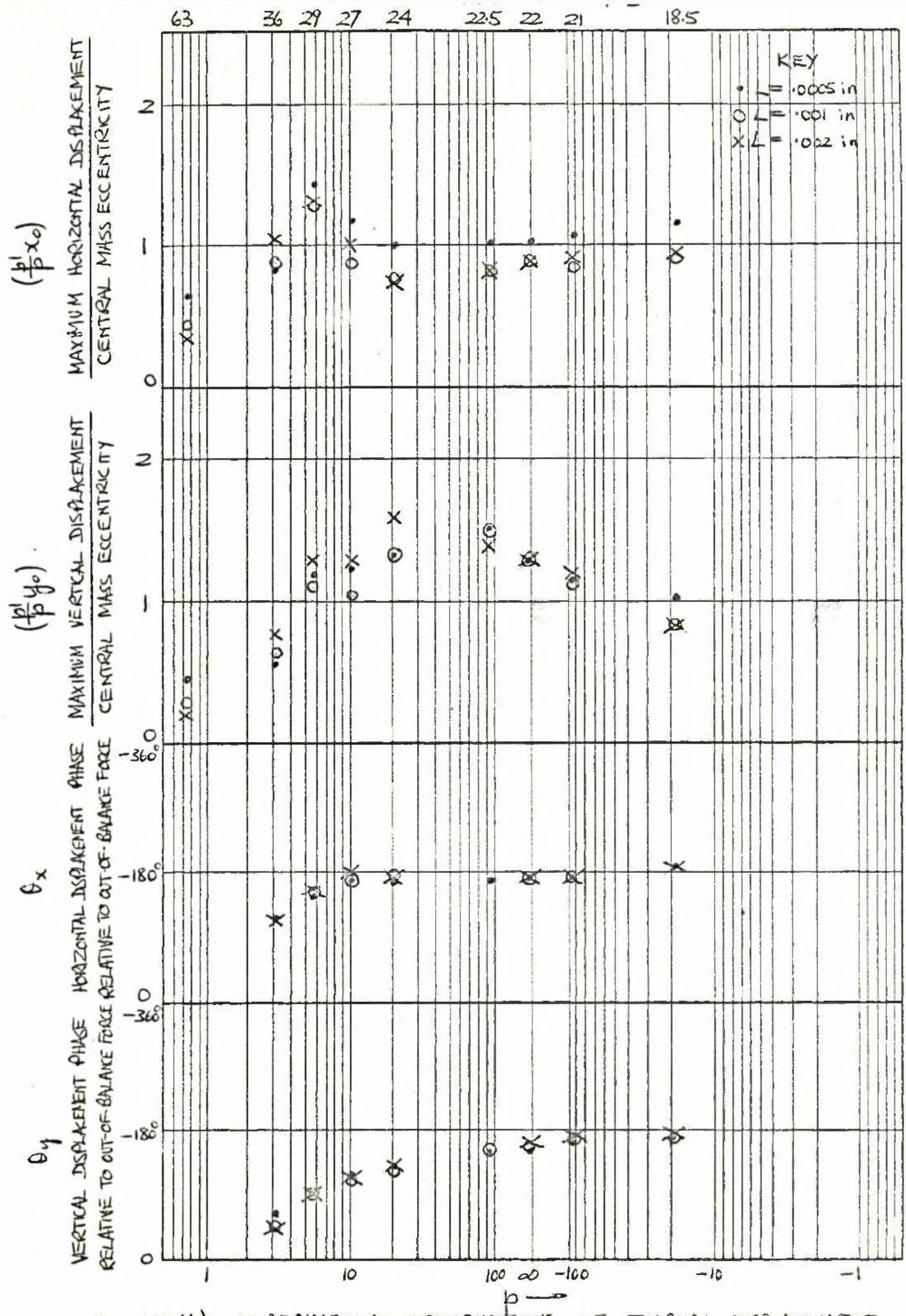

Fig 4.10(k) EXPERIMENTAL OBSERVATIONS OF JOURNAL DISPLACEMENT
ROTOR: 1 BEARINGS: 1 in x ·0277 in OIL: NORPOL 55 (ASSEMBLY R1.11)

Fig 4.10 (ℓ) EXPERIMENTAL OBSERVATIONS OF JOURNAL DISPLACEMENT.
ROTOR : 1 BEARINGS : ·667 in x ·0124 in OIL : NORPOL 55 (ASSEMBLY R1.12)

Fig 4.10(m) EXPERIMENTAL OBSERVATIONS OF JOURNAL DISPLACEMENT.
ROTOR: 1 BEARINGS: 1 in x ·0223 in OIL: NORPOL 55 (ASSEMBLY R1.B)

Fig 4.10 (n) EXPERIMENTAL OBSERVATIONS OF JOURNAL DISPLACEMENT
ROTOR: 1 BEARINGS: 1 in x ·015 in OIL: NORPOL 55 (ASSEMBLY R1.14)

Fig 4.10 (c) EXPERIMENTAL OBSERVATIONS OF JOURNAL DISPLACEMENT
ROTOR: 1 BEARINGS: 1·5in x ·0276in OIL: NORAL 55 (ASSEMBLY R1.1S)

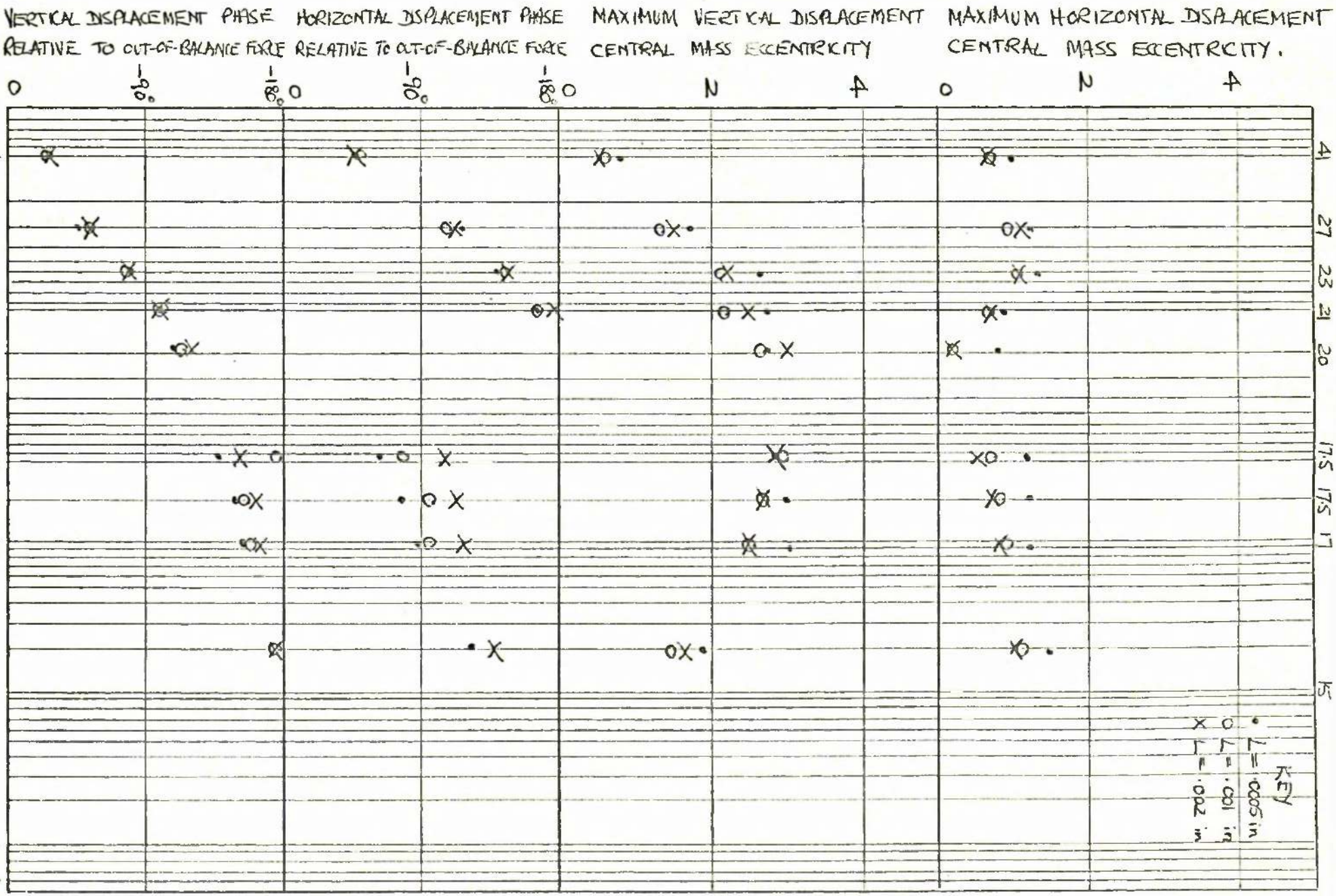

Fig 4.11(a) EXPERIMENTAL OBSERVATIONS OF ROTOR CENTRE DISPLACEMENT
ROTOR: 1
BEARINGS: 1 Sin x .022 in OIL: NORAL 35 (ASSEMBLY R.1)

Fig 4.11(b) EXPERIMENTAL OBSERVATIONS OF ROTOR CENTRE DISPLACEMENT
ROTOR: 1 BEARINGS: 2in x ·0305in OIL: NORPOL 35 (ASSEMBLY R1.2)

Fig 4.11 (c) EXPERIMENTAL OBSERVATIONS OF ROTOR CENTRE DISPLACEMENT.
ROTOR · 1 BEARINGS : 1 in x ·0097 in OIL : NORPOL 35 (ASSEMBLY R1.3)

Fig 4.11 (a) EXPERIMENTAL OBSERVATIONS OF ROTOR CENTRE DISPLACEMENT
ROTOR: 1 BEARINGS: 1·5 in × ·0155 in OIL: NORPOL 35 (ASSEMBLY R14

Fig 4.11 (c) EXPERIMENTAL OBSERVATIONS OF ROTOR CENTRE DISPLACEMENT
ROTOR: 1 BEARINGS: ·667 in x 0045 in OIL: NORPOL 35 (ASSEMBLY R1.5)

Fig 4.11 (f) EXPERIMENTAL OBSERVATIONS OF ROTOR CENTRE DISPLACEMENT
ROTOR: 1 BEARINGS: 2 in x ·0223 in OIL: NORPOL 35 (ASSEMBLY R1.6)

Fig 4.11(g) EXPERIMENTAL OBSERVATIONS OF ROTOR CENTRE DISPLACEMENT
ROTOR : 1 BEARINGS : 1·5 in x ·0113 in OIL : MENTOR 28 (ASSEMBLY R1.7)

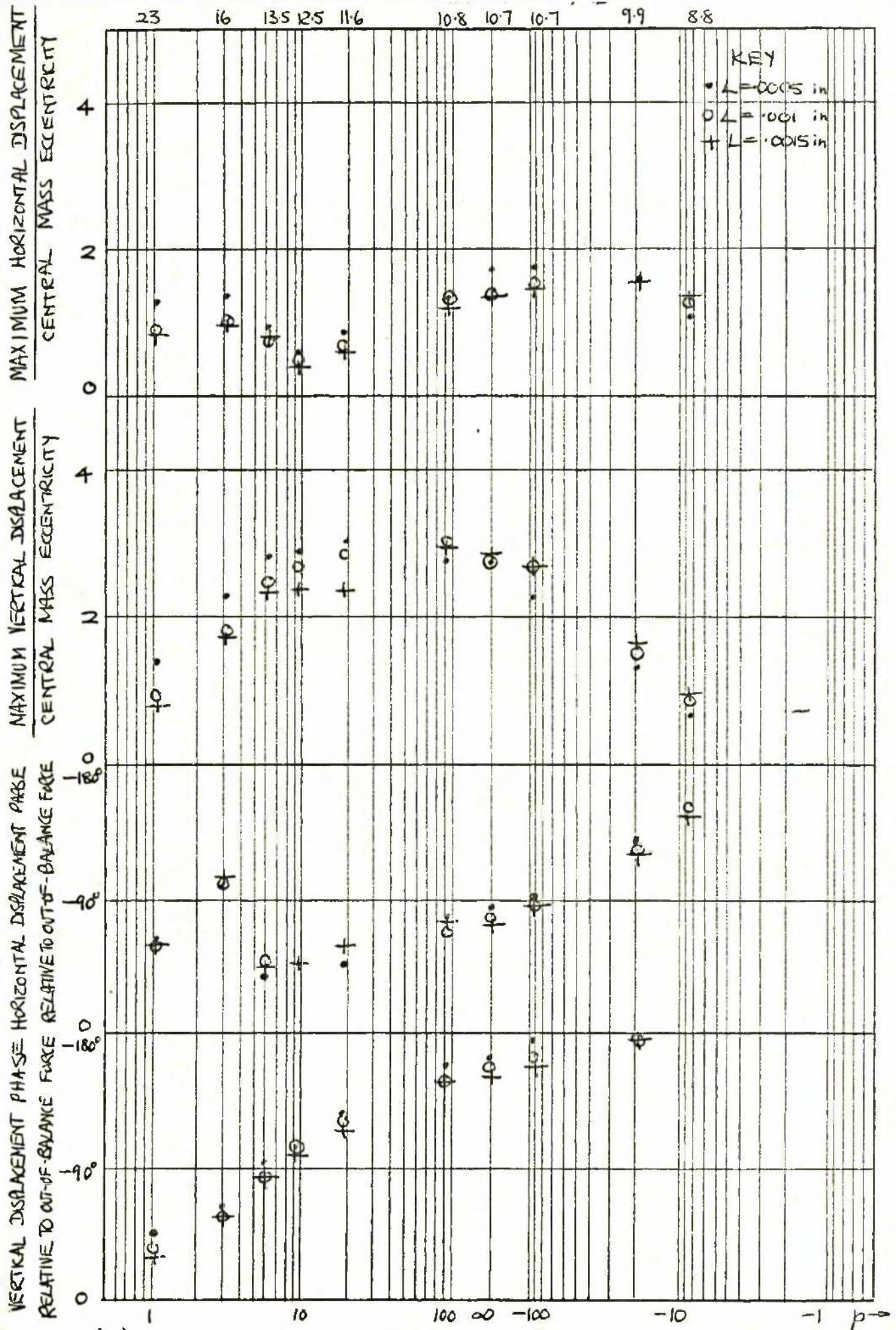

Fig 4.11 (h) EXPERIMENTAL OBSERVATIONS OF ROTOR CENTRE DISPLACEMENT

ROTOR: 1 BEARINGS: 2 in x ·015 in OIL: MENTOR 28 (ASSEMBLY R1.8)

Fig 4.11(i) EXPERIMENTAL OBSERVATIONS OF ROTOR CENTRE DISPLACEMENT
ROTOR: 1 BEARINGS: 1 in x ·0039 in OIL: MENTOR 28 (ASSEMBLY R1.9)

Fig 4.11 (j) EXPERIMENTAL OBSERVATIONS OF ROTOR CENTRE DISPLACEMENT
ROTOR: 1 BEARINGS: 1·5 in × ·0049 in OIL: MENTOR 28 (ASSEMBLY R1.10)

Fig 4.11(k) EXPERIMENTAL OBSERVATIONS OF ROTOR CENTRE DISPLACEMENT
ROTOR : 1 BEARINGS : 1 in x ·0277 in OIL : NORPAL 55 (ASSEMBLY R1.11)

Fig 4.11(1) EXPERIMENTAL OBSERVATIONS OF ROTOR CENTRE DISPLACEMENT.
ROTOR : 1 BEARINGS : ·667 in x ·0124 in OIL : NORPOL 55 (ASSEMBLY R1.12)

Fig 4.11 (m) EXPERIMENTAL OBSERVATIONS OF ROTOR CENTRE DISPLACEMENT
ROTOR: 1 BEARINGS: 1in x ·0223in OIL: NORPOL 55 (ASSEMBLY R1.13)

Fig 4.11 (n) EXPERIMENTAL OBSERVATIONS OF ROTOR CENTRE DISPLACEMENT
ROTOR: 1 BEARINGS: 1 in x ·0155 in OIL: NORPOL 55 (ASSEMBLY R1.14)

Fig 4.11(a) EXPERIMENTAL OBSERVATIONS OF ROTOR CENTRE DISPLACEMENT
ROTOR: 1 BEARINGS: 1·5 in × ·0276 in OIL: NORPOL 55 (ASSEMBLY R1.1S)

Fig 4.12 (a) VALUES OF OIL FORCE DEDUCED FROM THE EXPERIMENTAL RESULTS OF Fig 4.10(a), Fig 4.11(a)
ROTOR: 1 BEARINGS: 1·5 in × ·0223 in OIL: NORPOL 55 (ASSEMBLY R1.1).

Fig 4.12 (b) VALUES OF OIL FORCE DEDUCED FROM THE EXPERIMENTAL RESULTS OF Fig 4.10(b), Fig 4.11(b)
ROTOR: 1 BEARINGS: 2in x .0305in OIL: NORPOL 35 (ASSEMBLY RI. 2)

Fig 4.12(c) VALUES OF OIL FORCE DEDUCED FROM THE EXPERIMENTAL RESULTS OF Fig 4.10(K) & Fig 4.11
ROTOR: 1 BEARINGS: 1 in x ·0097 in OIL: MOBILMOL 35 (ASSEMBLY R1. 3)

Fig 4.12(d) VALUES OF OIL FORCE DEDUCED FROM THE EXPERIMENTAL RESULTS OF Fig 4.10(d), Fig 4.11(d)
ROTOR: 1 BEARINGS: 1·5 in x 0·5 in OIL: NORPOL 35 (ASSEMBLY R1·4).

Fig 4.12(e) VALUES OF OIL FORCE DEDUCED FROM THE EXPERIMENTAL RESULTS OF Fig 4.10(e), Fig 4.11(e)
ROTOR: 1 BEARINGS: ·667 in × ·0045 in OIL: NORPOL 35 (ASSEMBLY R1.5)

Fig. 4.12(f) VALUES OF OIL FORCE DEDUCED FROM THE EXPERIMENTAL RESULTS OF Fig 4.10(f), Fig 4.11(f).
ROTOR: 1 BEARINGS: 2 in x .0223 in. OIL: NORPOL 35 (ASSEMBLY R1.6)

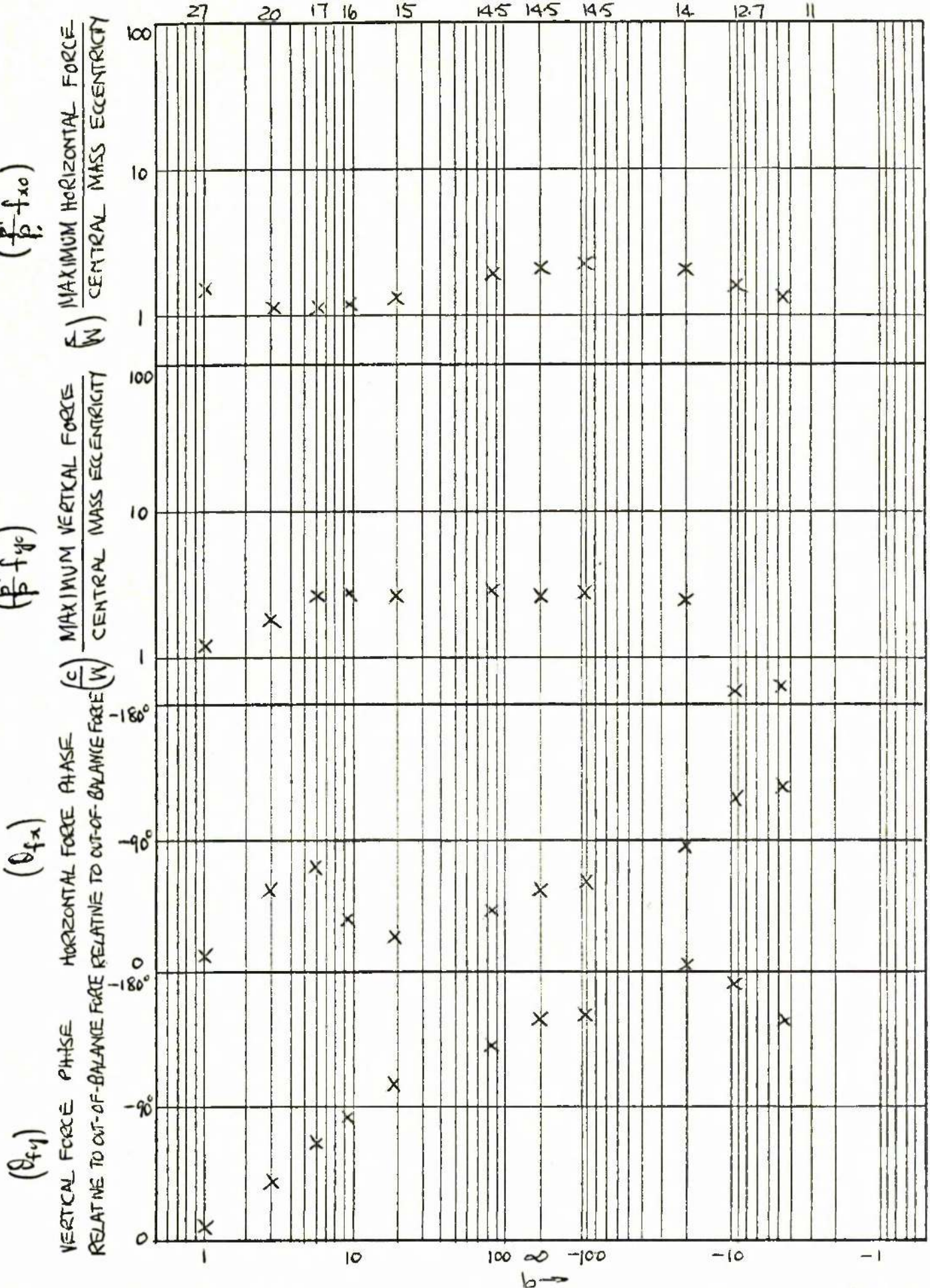

Fig 4.12(g) VALUES OF OIL FORCE DEDUCED FROM THE EXPERIMENTAL RESULTS OF Fig 4.10(g), Fig 4.11(g)
ROTOR: 1 BEARINGS: 1.5 in x .0113 in OIL: MENTOR 28 (ASSEMBLY R1.7)

Fig 4.12(h) VALUES OF OIL FORCE DEDUCED FROM THE EXPERIMENTAL RESULTS OF Fig 4.10(h), Fig 4.11(h)
ROTOR: 1 BEARINGS: 2in x .015 in OIL: MENTOR 28 (ASSEMBLY RI. 8)

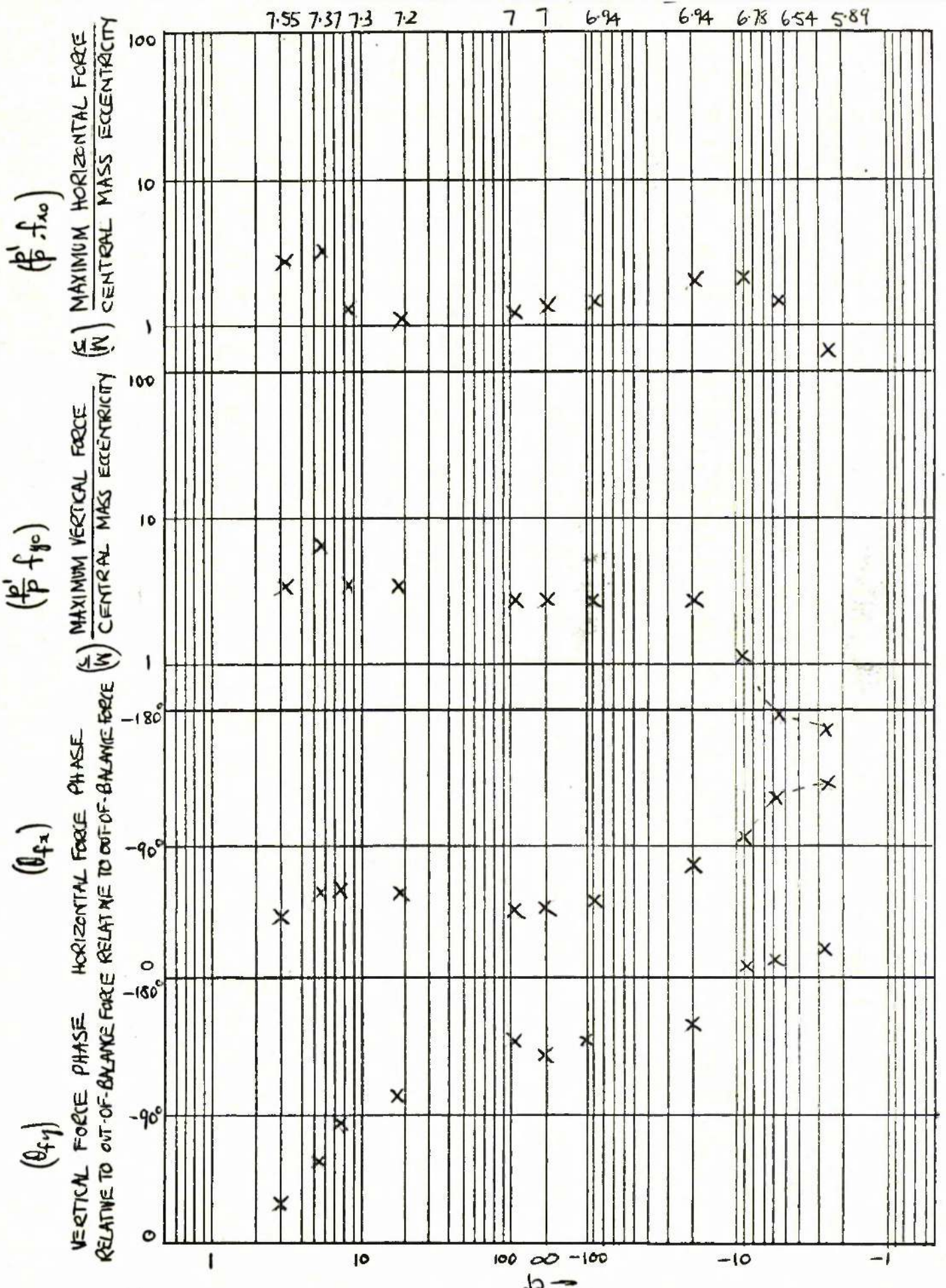

Fig 4.12(i) VALUES OF OIL FORCE DEDUCED FROM THE EXPERIMENTAL RESULTS OF Fig 4.10(i), Fig 4.11(i)
ROTOR: 1 BEARINGS: 1 in × ·0039 in OIL: MENTOR 28 (ASSEMBLY R1.9)

Fig 4.12(j) VALUES OF OIL FORCE DEDUCED FROM THE EXPERIMENTAL RESULTS OF Fig 4.10(j), Fig 4.11(j)
ROTOR: 1 BEARINGS: 1·5 in × ·0049 in OIL: MENTOR 28 (ASSEMBLY R. 10)

Fig 4.12(k) VALUES OF OIL FORCE DEDUCED FROM THE EXPERIMENTAL RESULTS OF Fig 4.10(k), Fig 4.11(k
ROTOR: 1 BEARINGS: 1 in x .0277 in OIL: NORPOL 55 (ASSEMBLY R1.11)

Fig 4.12(l) VALUES OF OIL FORCE DEDUCED FROM THE EXPERIMENTAL RESULTS OF Fig 4.10(l), Fig 4.11(l)
ROTOR: 1 BEARINGS: ·667 in × ·012 in OIL: NORPOL 55 (ASSEMBLY RI. 12)

Fig 4.12 (m) VALUES OF OIL FORCE DEDUCED FROM THE EXPERIMENTAL RESULTS OF Fig 4.10(m), Fig 4.11(m)
ROTOR: 1 BEARINGS: 1 in x ·0223 in OIL: NORPOL 55 (ASSEMBLY R.1.13)

Fig 4.12(n) VALUES OF OIL FORCE DEDUCED FROM THE EXPERIMENTAL RESULTS OF Fig 4.10(n), Fig 4.11(n)
ROTOR: 1 BEARINGS: 1 in x 0.55 in OIL: NORPOL 55 (ASSEMBLY R1.1a)

Fig 4.12 (a) VALUES OF OIL FORCE DEDUCED FROM THE EXPERIMENTAL RESULTS OF Fig 4.10(a) Fig 4.11(a)
ROTOR: 1 BEARINGS: 1·5 in × ·0278 in OIL: NORPOL 35 (ASSEMBLY R1. 6)

4.13(a) EXPERIMENTAL OBSERVATIONS OF ROTOR DISPLACEMENT
ROTOR: 2 BEARINGS: 1 in x ·0223 in OIL: NORPOL 55 L(PART MASS): ·001 in (ASSEMBLY R2.1)

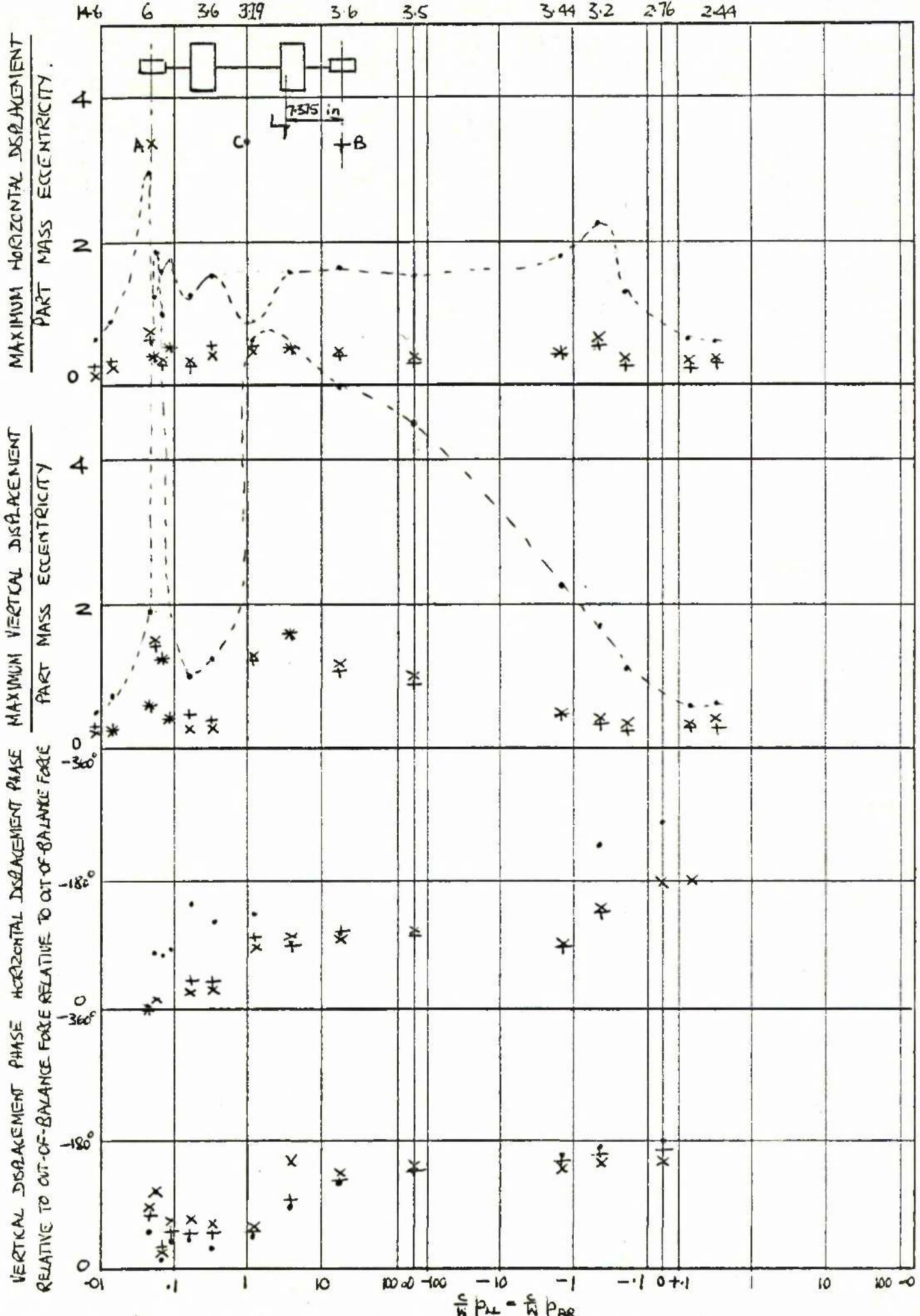

Fig 4.13 (b) EXPERIMENTAL OBSERVATIONS OF ROTOR DISPLACEMENT.
ROTOR: 2 BEARINGS: 1 in x ·0097 in OIL: NORPOL 55 L(PART MASS): ·001 in (ASSEMBLY R22)

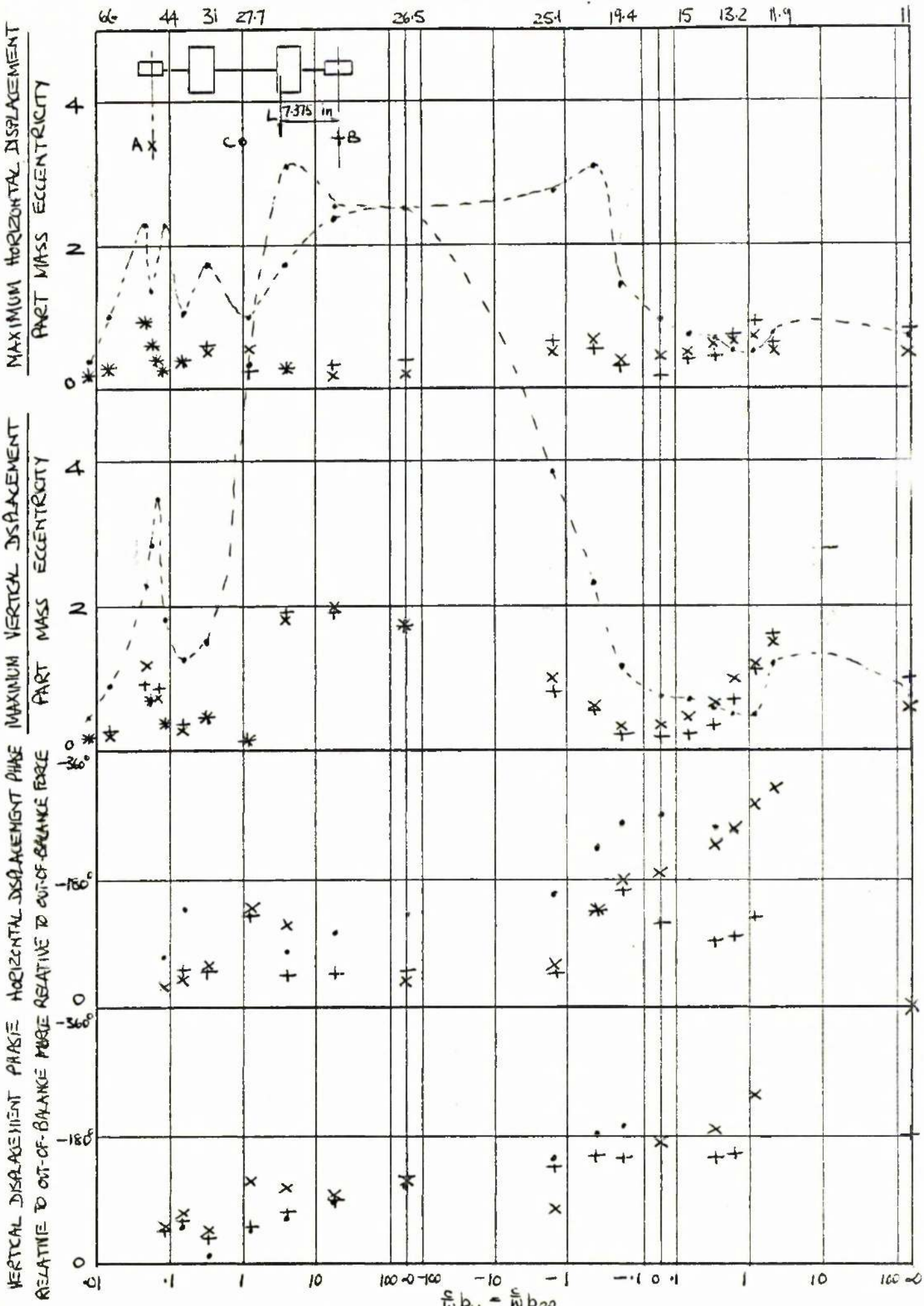

Fig 4.13 (c) EXPERIMENTAL OBSERVATIONS OF ROTOR DISPLACEMENT
ROTOR: 2 BEARINGS: 1 in × ·0097 in OIL: NORPOL 35 L (PART MASS): ·01 in (ASSEMBLY 123)

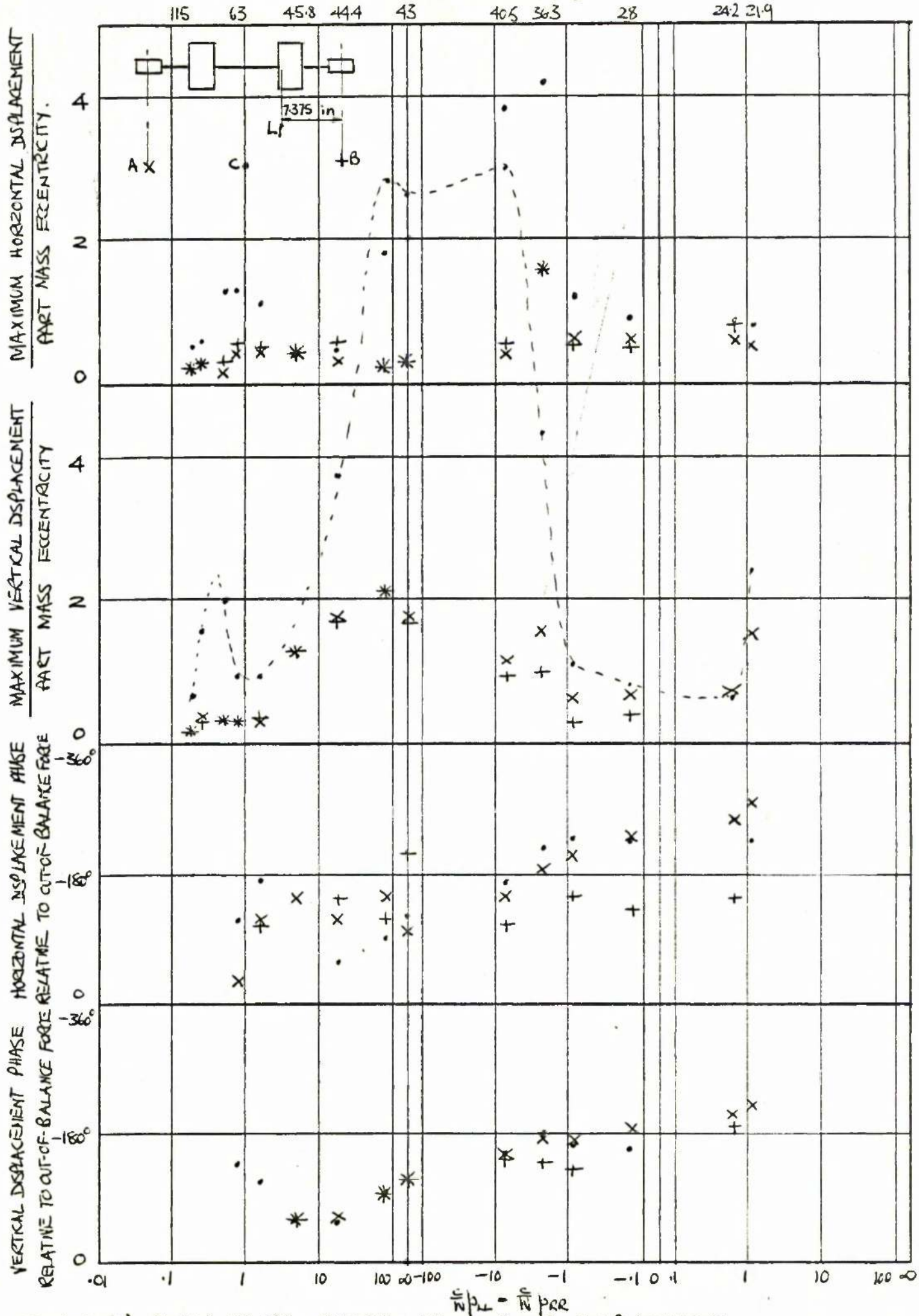

Fig 4.13 (d) EXPERIMENTAL OBSERVATIONS OF ROTOR DISPLACEMENT

ROTOR: 2 BEARINGS: 1·5 in × ·0223 in OIL: NORTOL 35 L(PART MASS): ·015 in (ASSEMBLY R2.4)

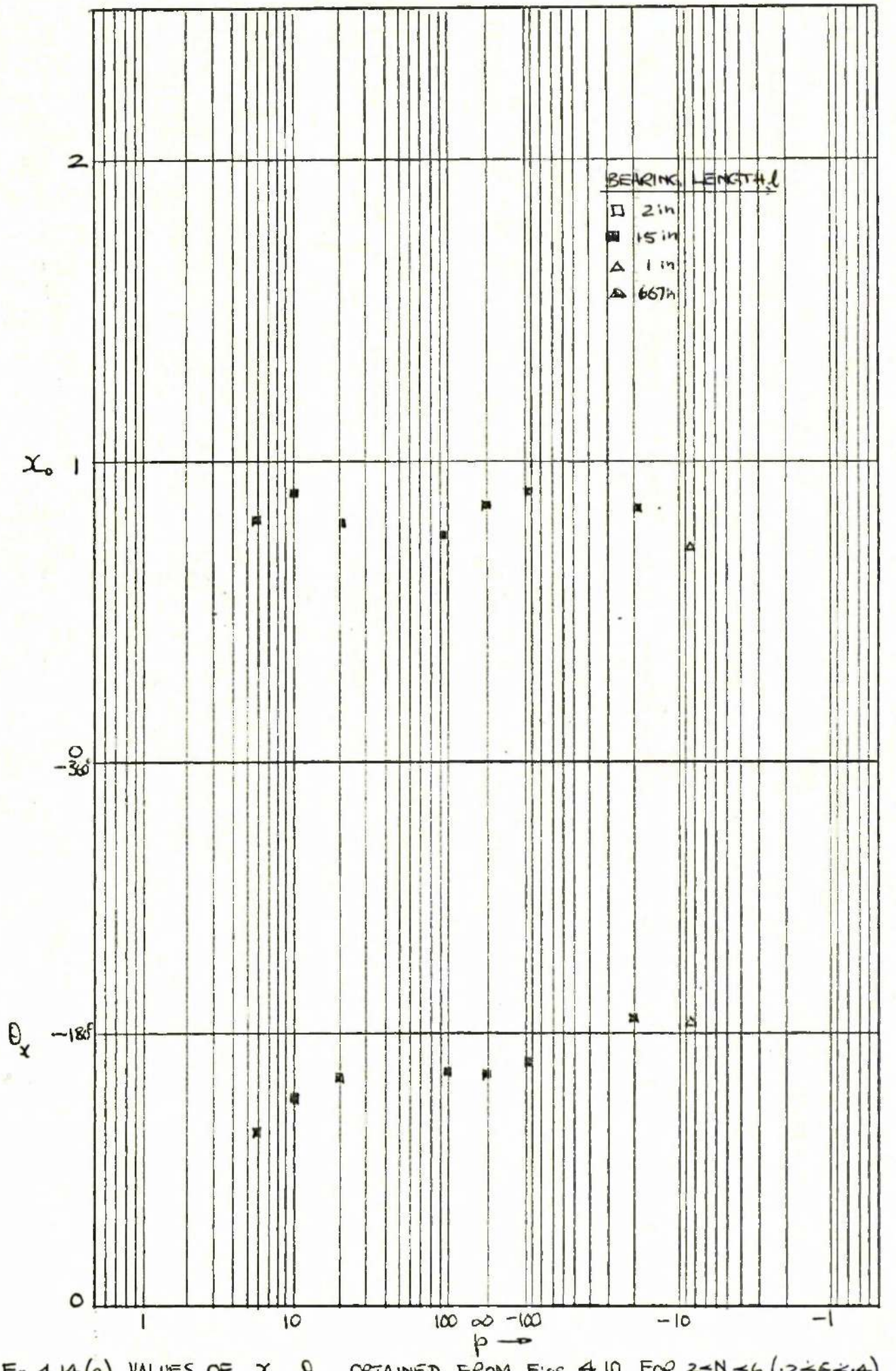

Fig 4.14(a) VALUES OF x_o, θ_x OBTAINED FROM Figs 4.10 FOR $2 < N_L < 6$. $(.2 \div E \div .4)$

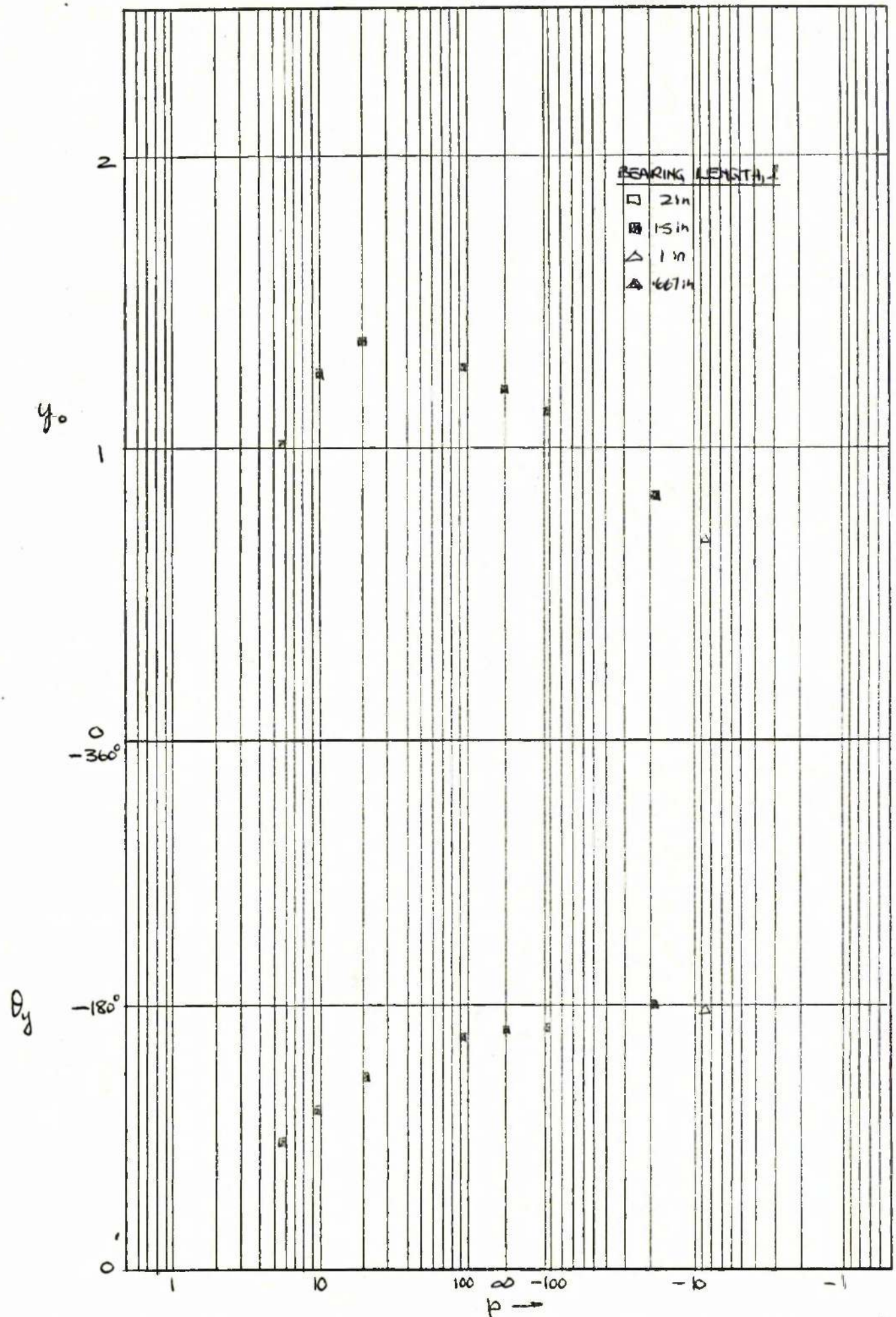

Fig 4.14(b) VALUES OF y_o, θ_y OBTAINED FROM Figs 4.10 FOR $2 < N_L < 6$ $(.2 \div \epsilon \div .4)$

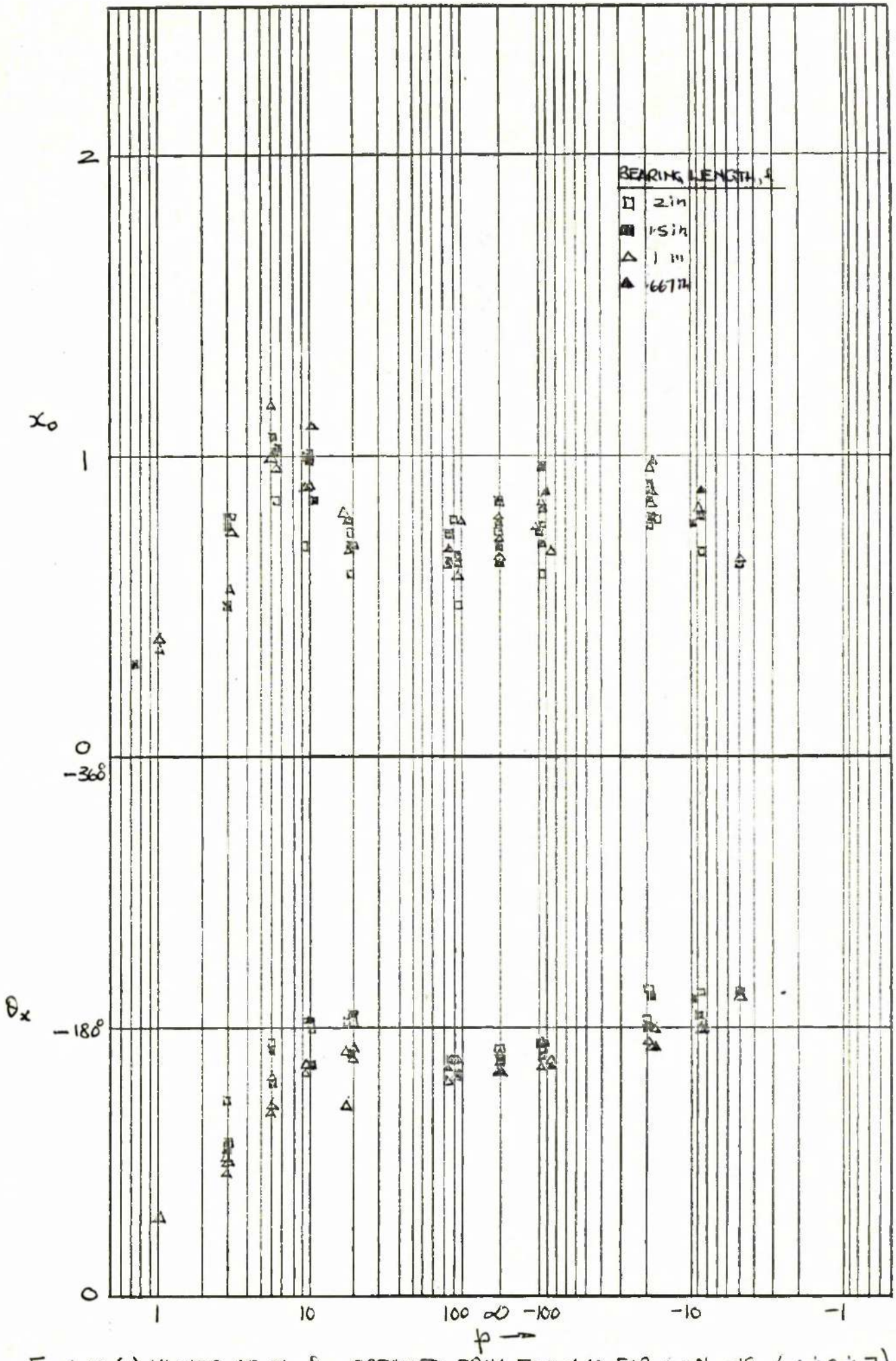

Fig 4.14 (c) VALUES OF x_o, θ_x OBTAINED FROM Figs 4.10 FOR $6 < N_L < 18$ $(.4 \div \epsilon \div .7)$

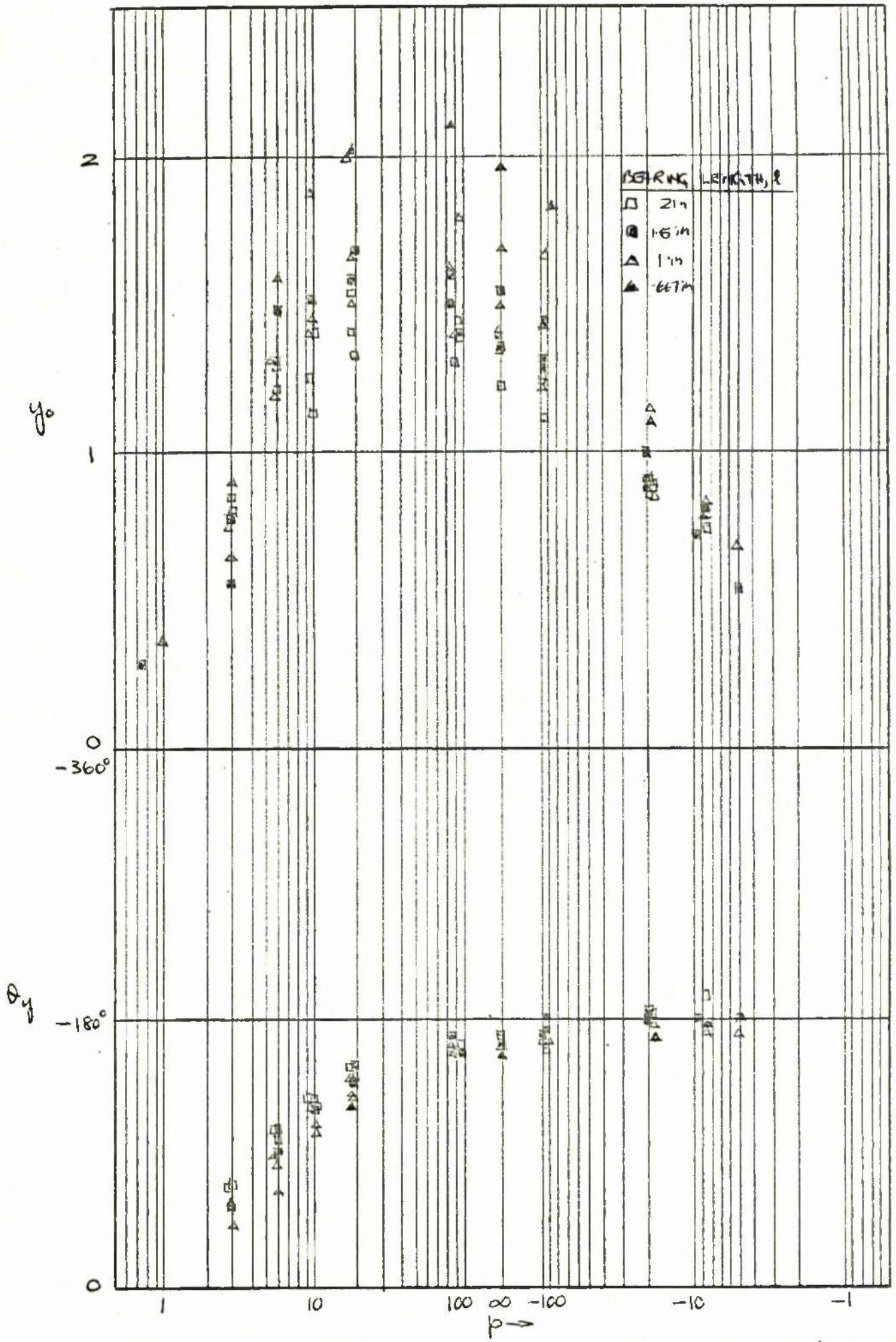

Fig 4.14(a) VALUES OF y_o, θ_y OBTAINED FROM Figs 4.10 FOR $6 \leq N_L \leq 18$ ($4 \div E \div 7$)

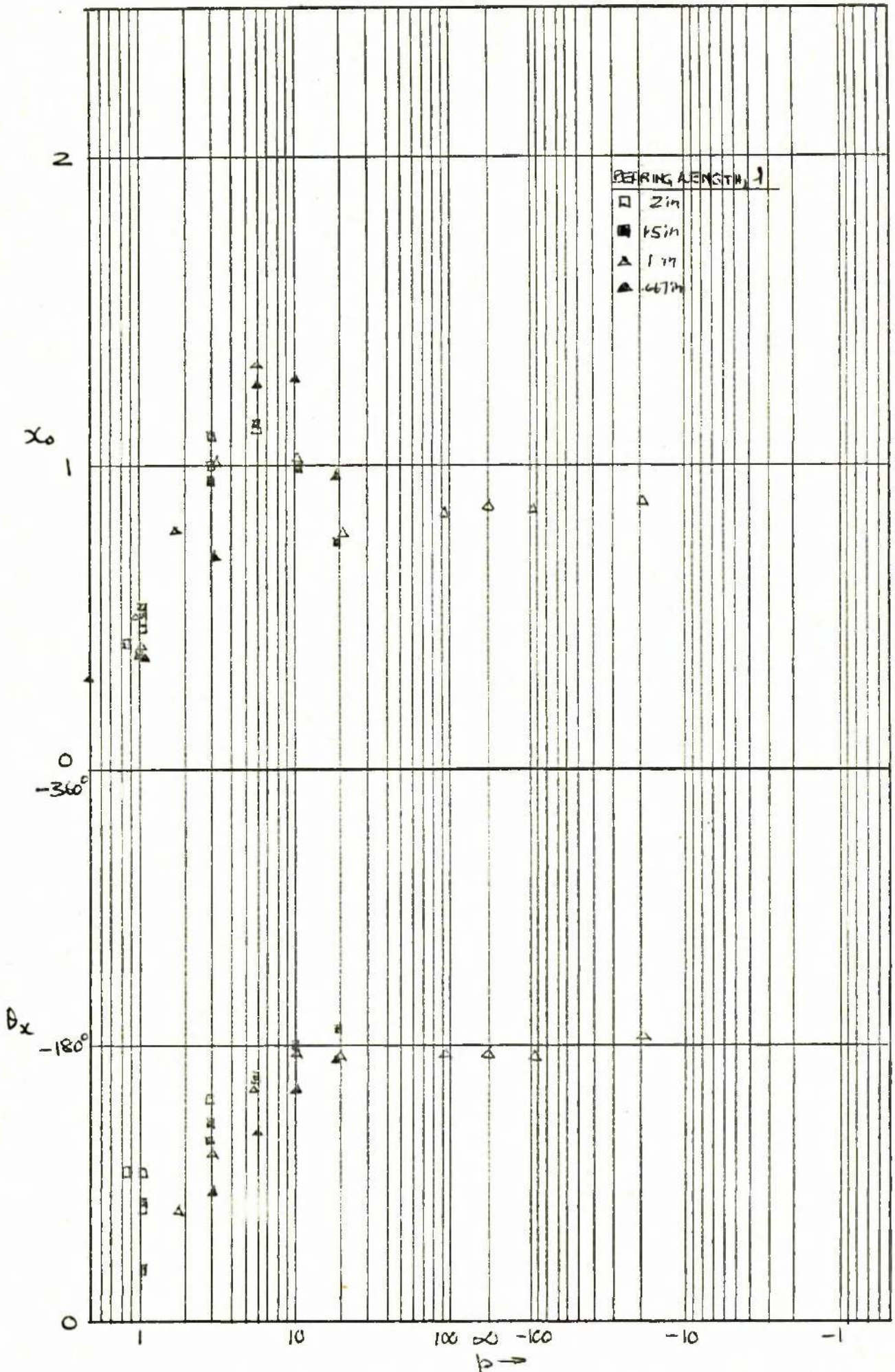

Fig 4.14 (e) VALUES OF x_o, θ_x OBTAINED FROM Figs 4.10 FOR $18 \leq N_L \leq 55$ $(.7 \div \epsilon \div .9)$

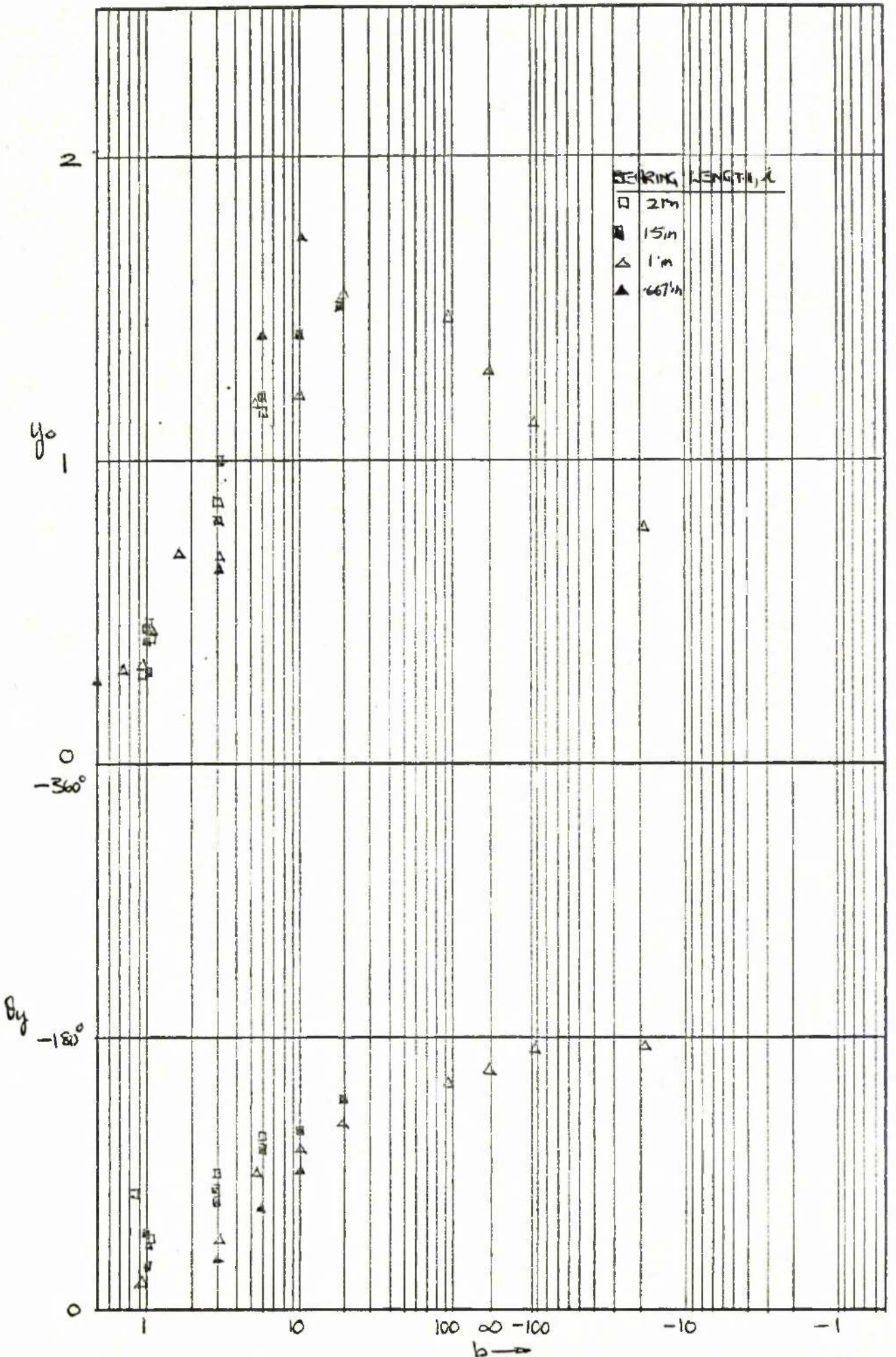

Fig 4.14(f) VALUES OF y_o, θ_y OBTAINED FROM Figs 4.10 FOR $18 < N_L < 55$ $(.7 \div \epsilon \div .9)$

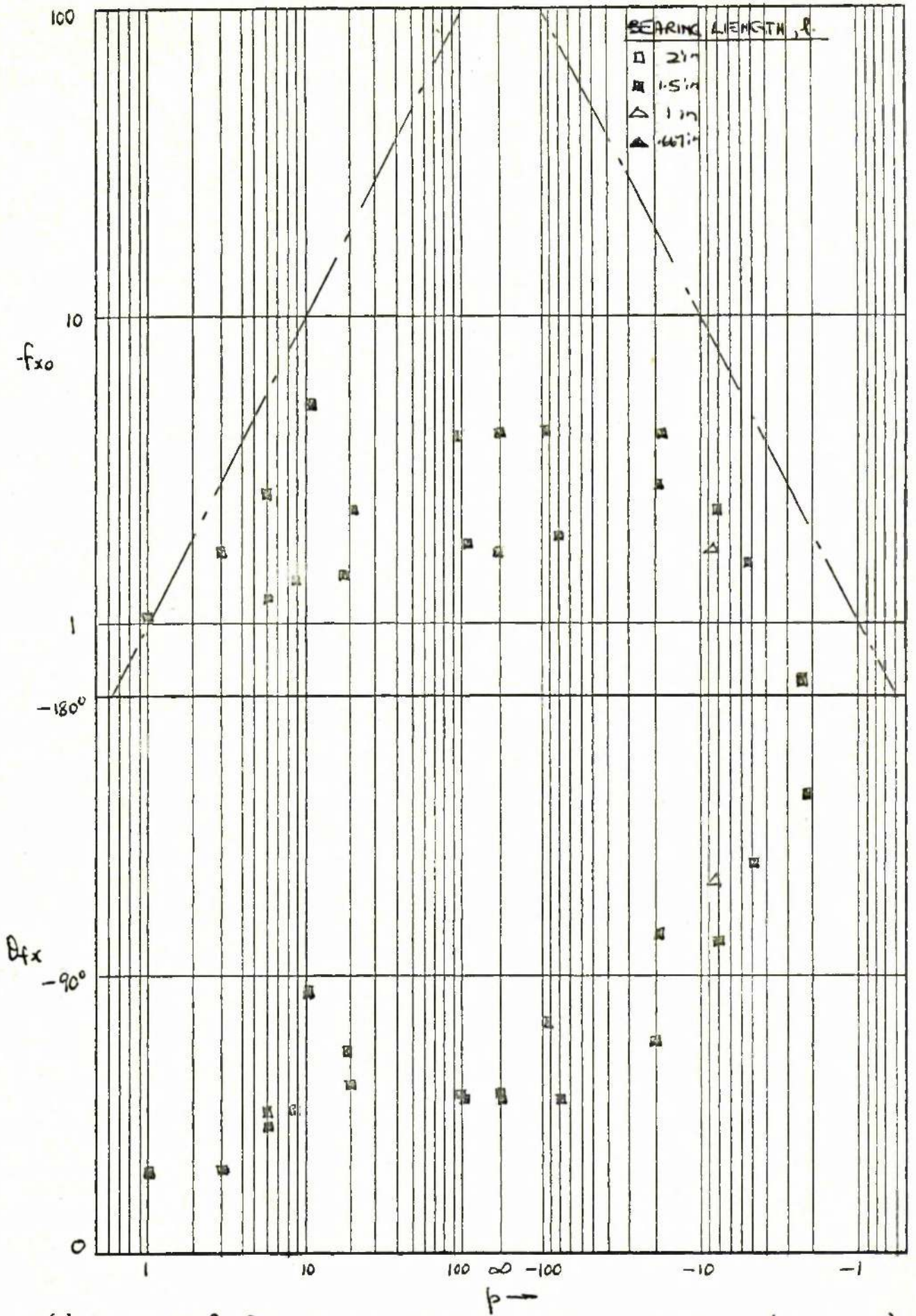

Fig 4.15(a) VALUES OF f_{xo}, θ_{fx} OBTAINED FROM Figs 4.12 FOR $2 < N_L < 6$ $(.2 \div \epsilon \div .4)$

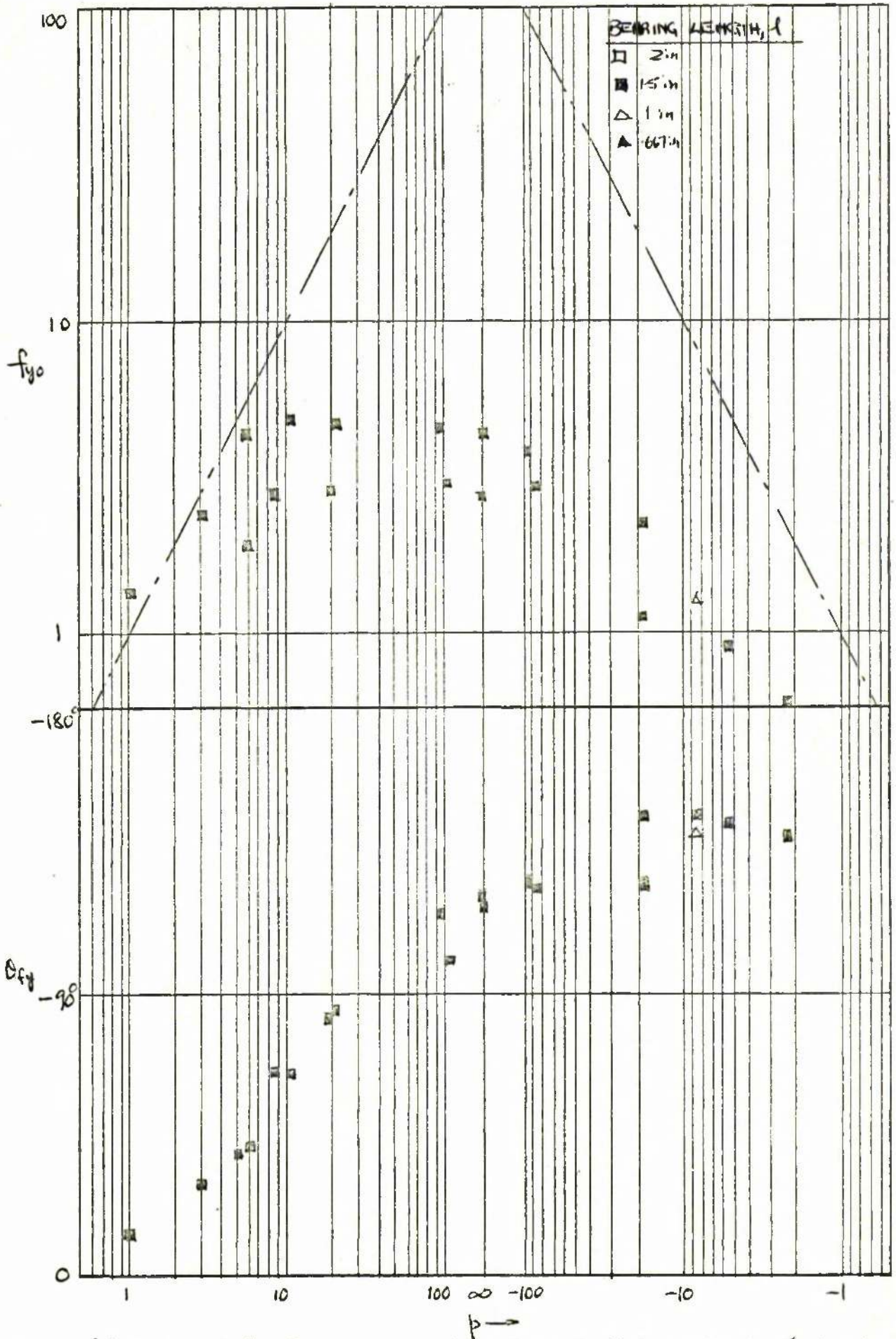

Fig 4.15 (b) VALUES OF f_{yo}, θ_{fy} OBTAINED FROM Figs 4.12 FOR $2 < N_L < 6$ $(.2 \div \epsilon \div .4)$

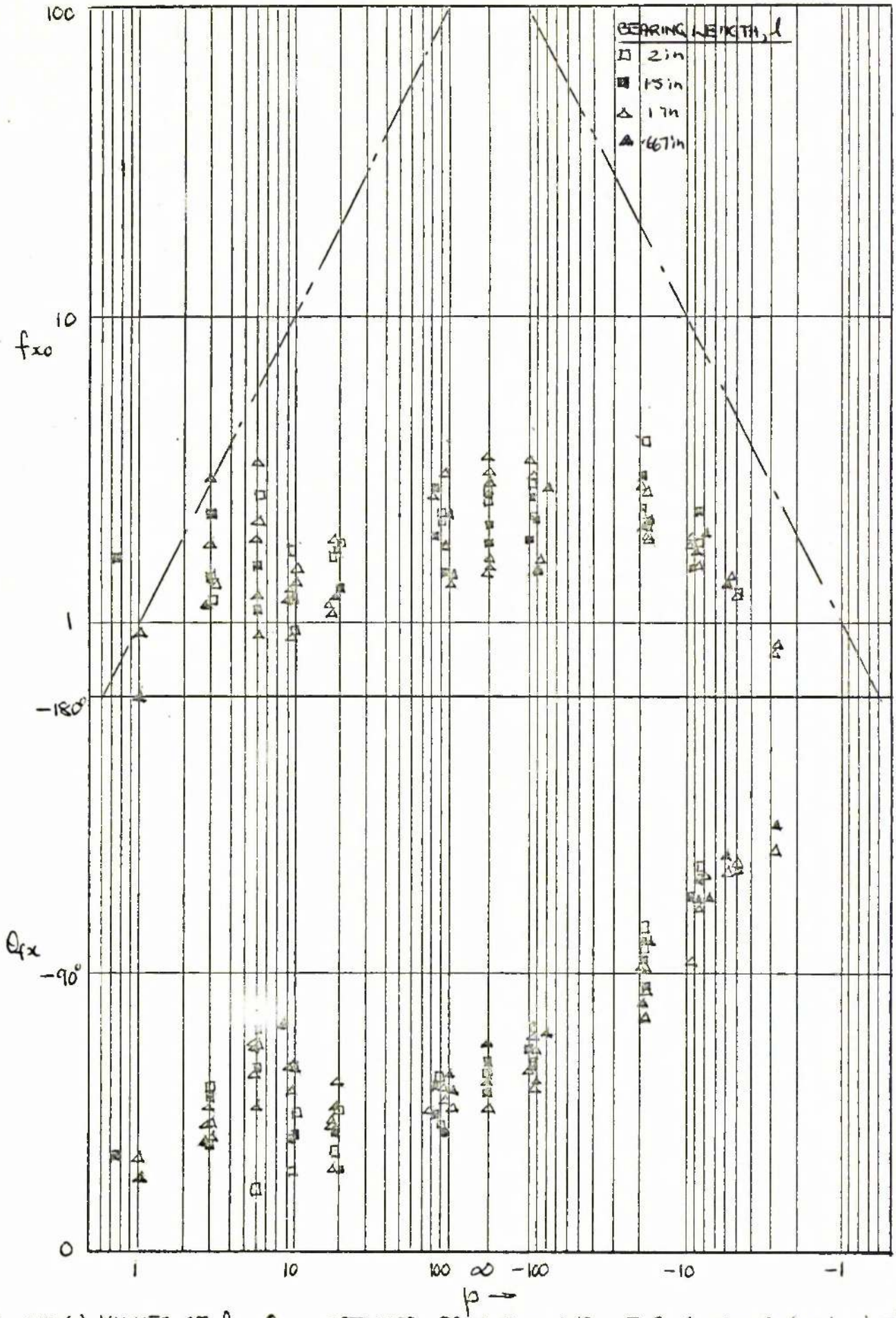

Fig 4.15 (c) VALUES OF f_{xo}, θ_{fx} OBTAINED FROM Figs 4.12 FOR $6 < N_L < 18$ $(.4 \leq \epsilon \leq .7)$

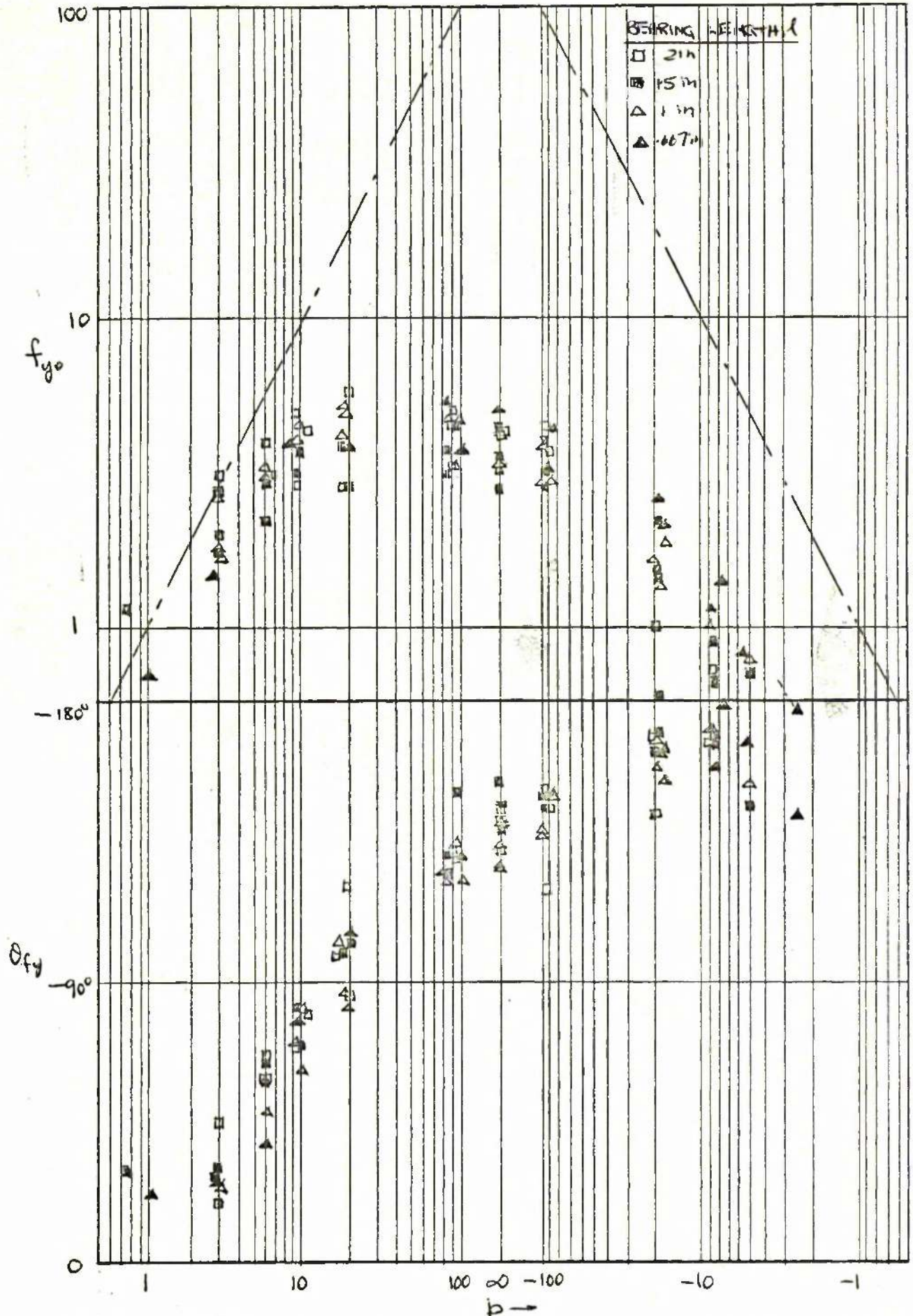

Fig 4.15 (d) VALUES OF f_{yo}, θ_{fy} OBTAINED FROM Figs. 4.12 FOR $6 < N_L < 18$ $(.4 \div \epsilon \div .7)$

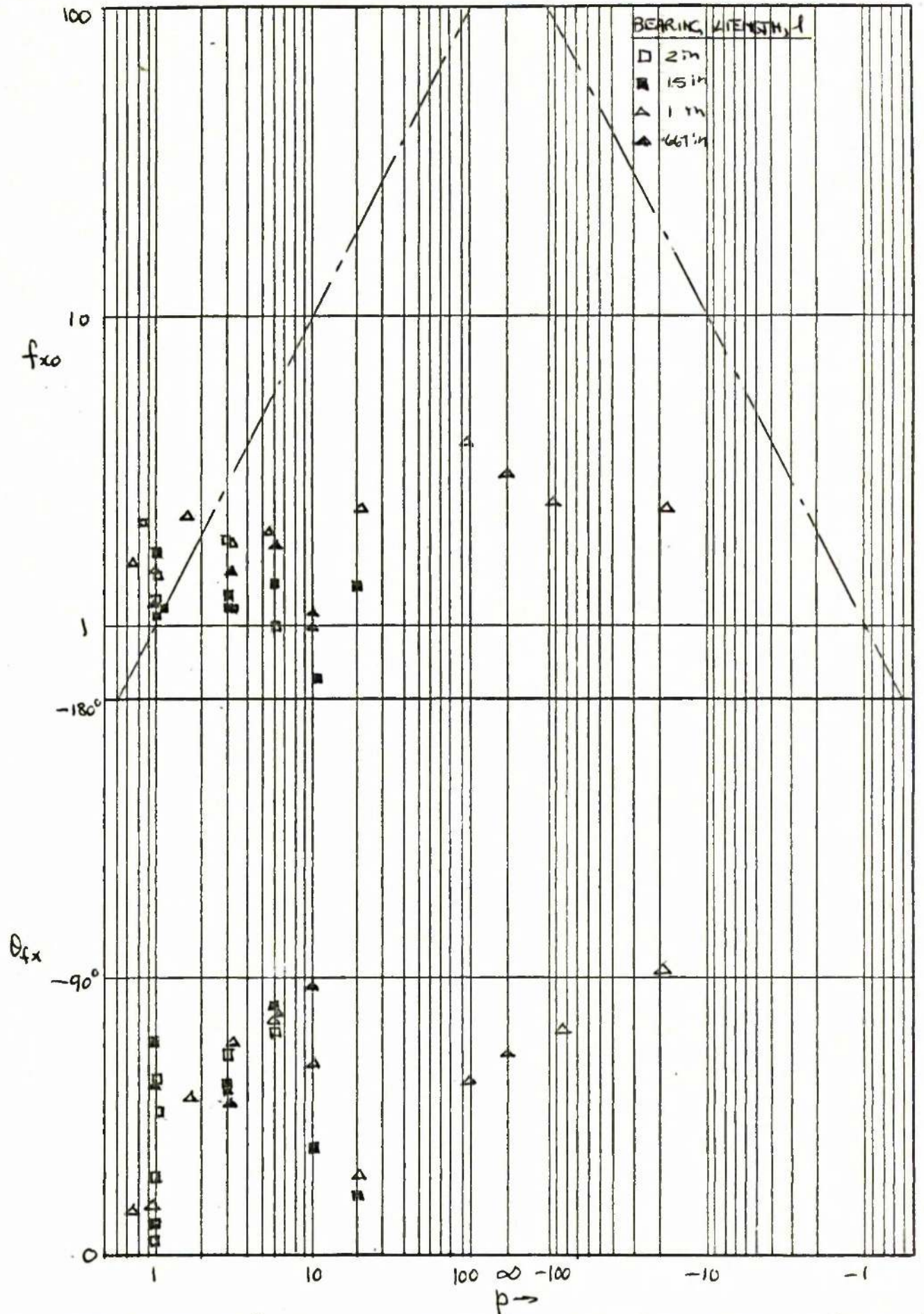

Fig 4.15 (e) VALUES OF f_{xo}, θ_{fx} OBTAINED FROM Figs 4.12 FOR $18 < N_L < 55$ $(.7 \div \epsilon \div .9)$

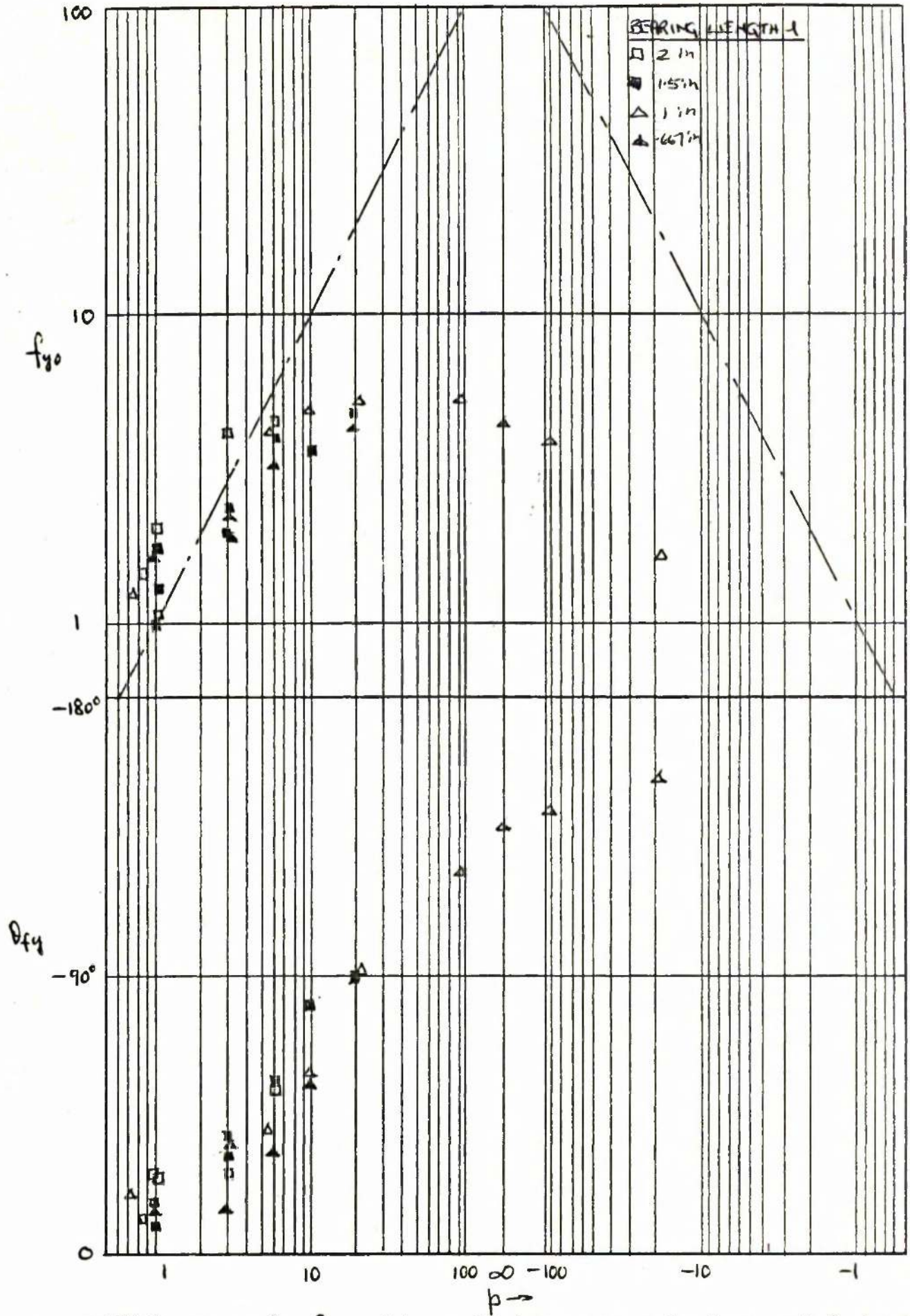

Fig 4.15 (f) VALUES OF f_{yo}, θ_{fy} OBTAINED FROM Figs 4.12 FOR $18 < N_L < 55$ ($.7 \div E \div .9$

ROTOR 1

$L = .002$ in $p = 10$ $N_L = 11.4$ $(\epsilon \div .58)$

x_o	θ_x	y_o	θ_y	x_{co}	θ_{xc}	y_{co}	θ_{yc}
.719	159°	1.469	113°	.75	103°	2.94	92°

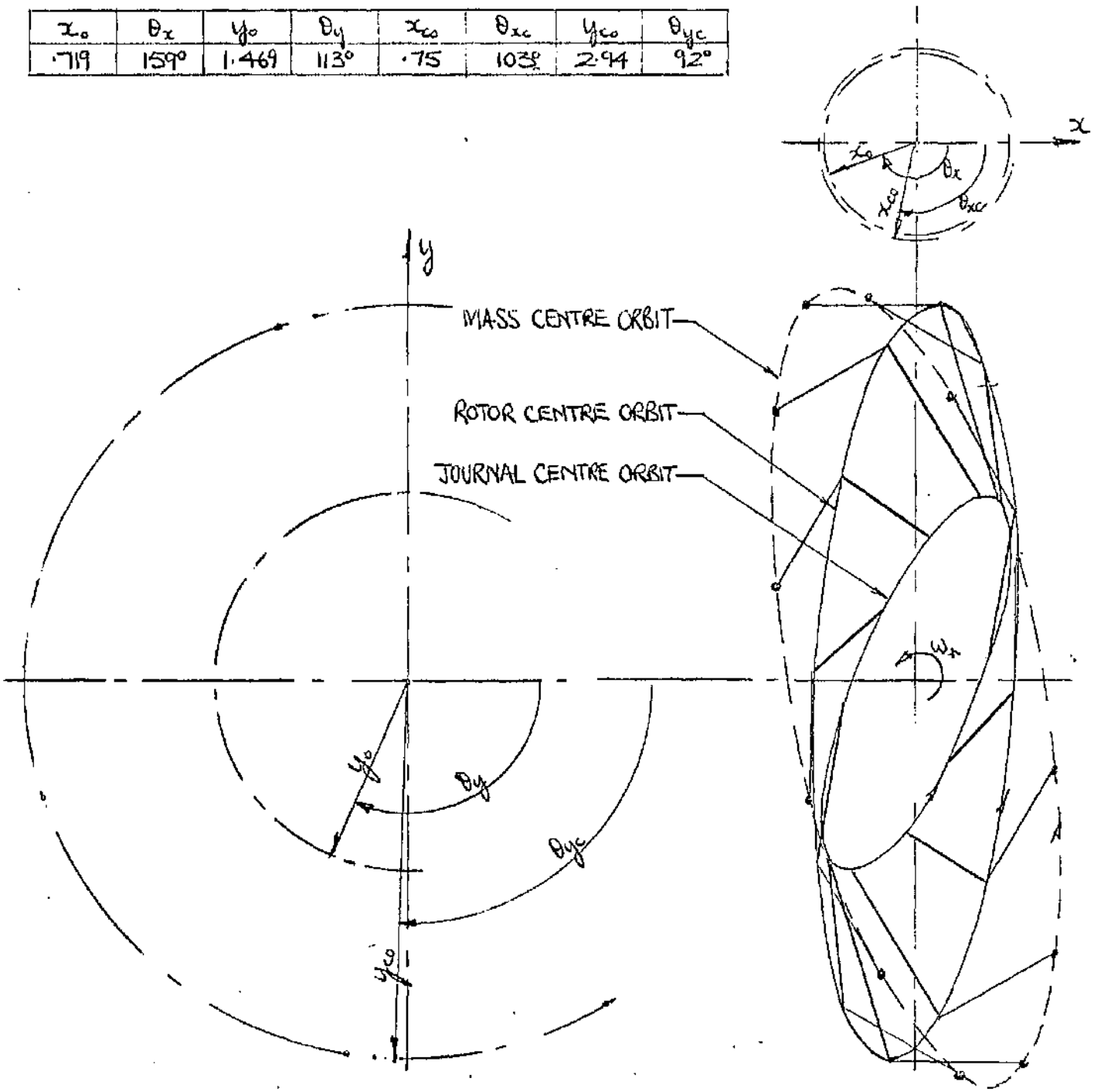

Fig 4.16 ROTOR DISPLACEMENT ORBITS.

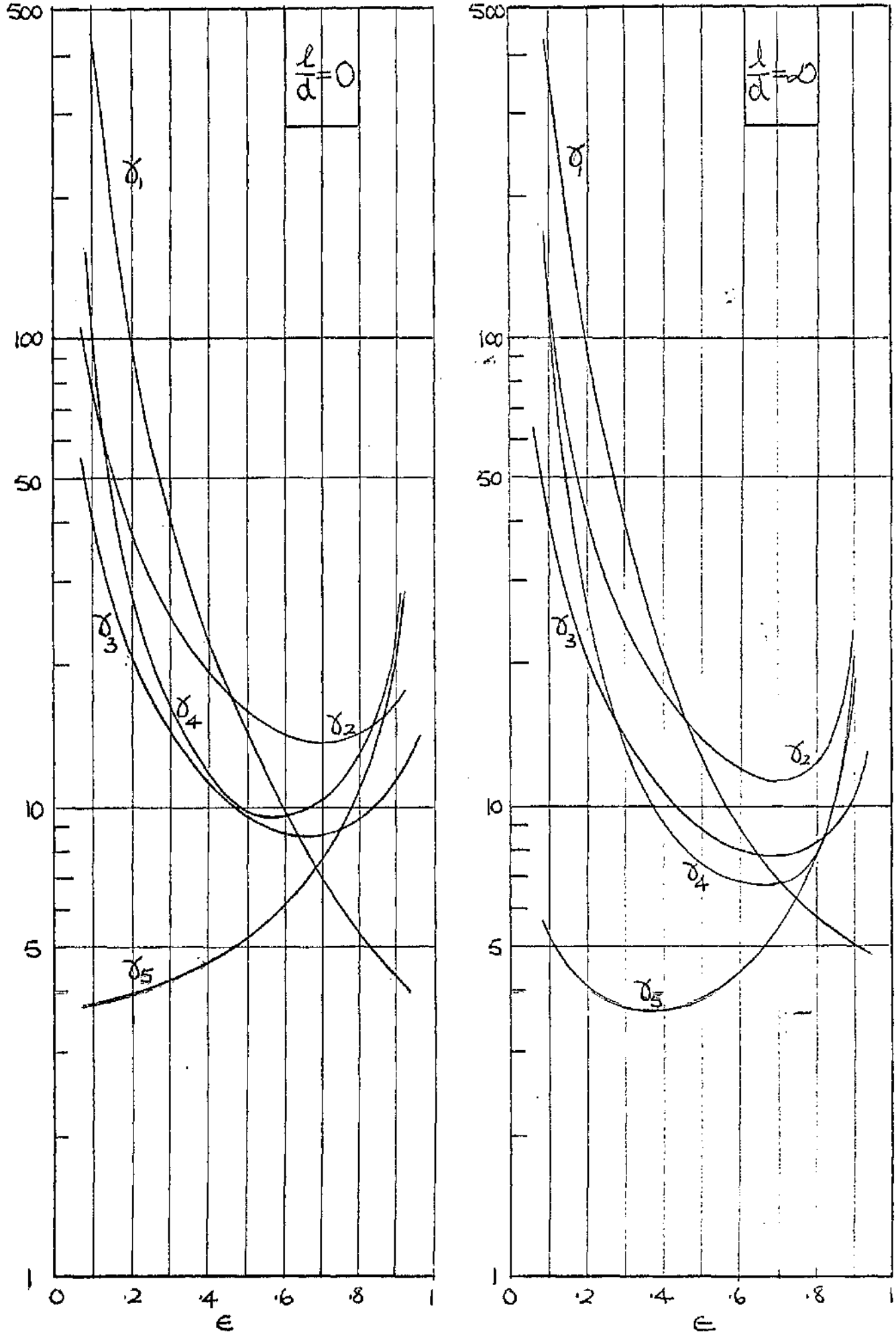

Fig 5.1 COMPOUND BEARING COEFFICIENTS.

Fig 5.2(a) STATIC STABILITY

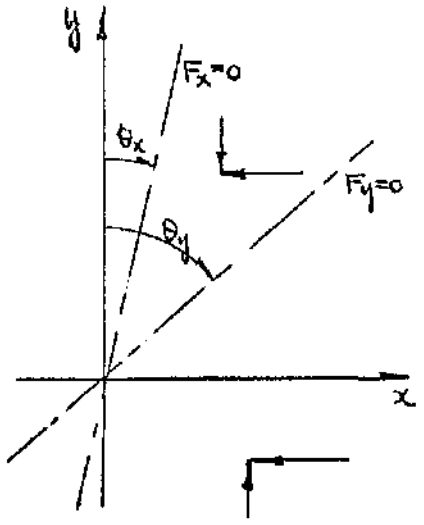

Fig 5.2(b) NEUTRAL STABILITY

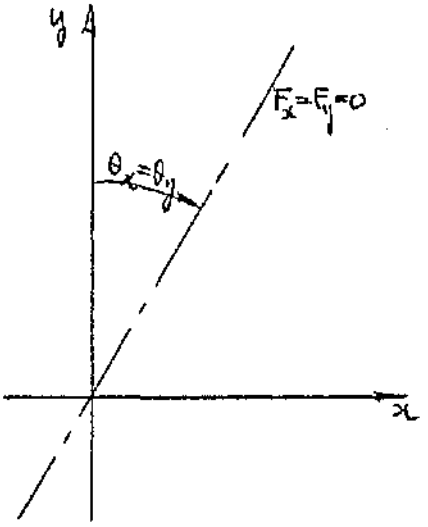

Fig 5.2(c) STATIC INSTABILITY

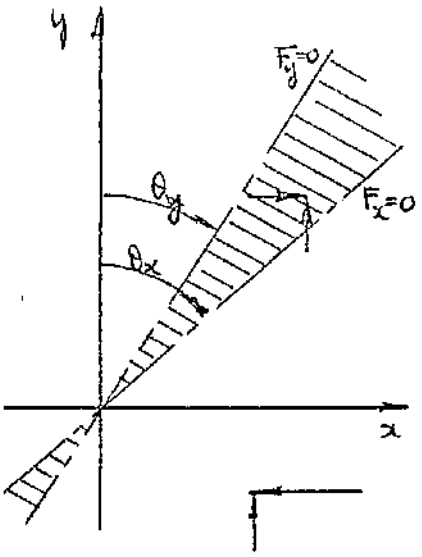

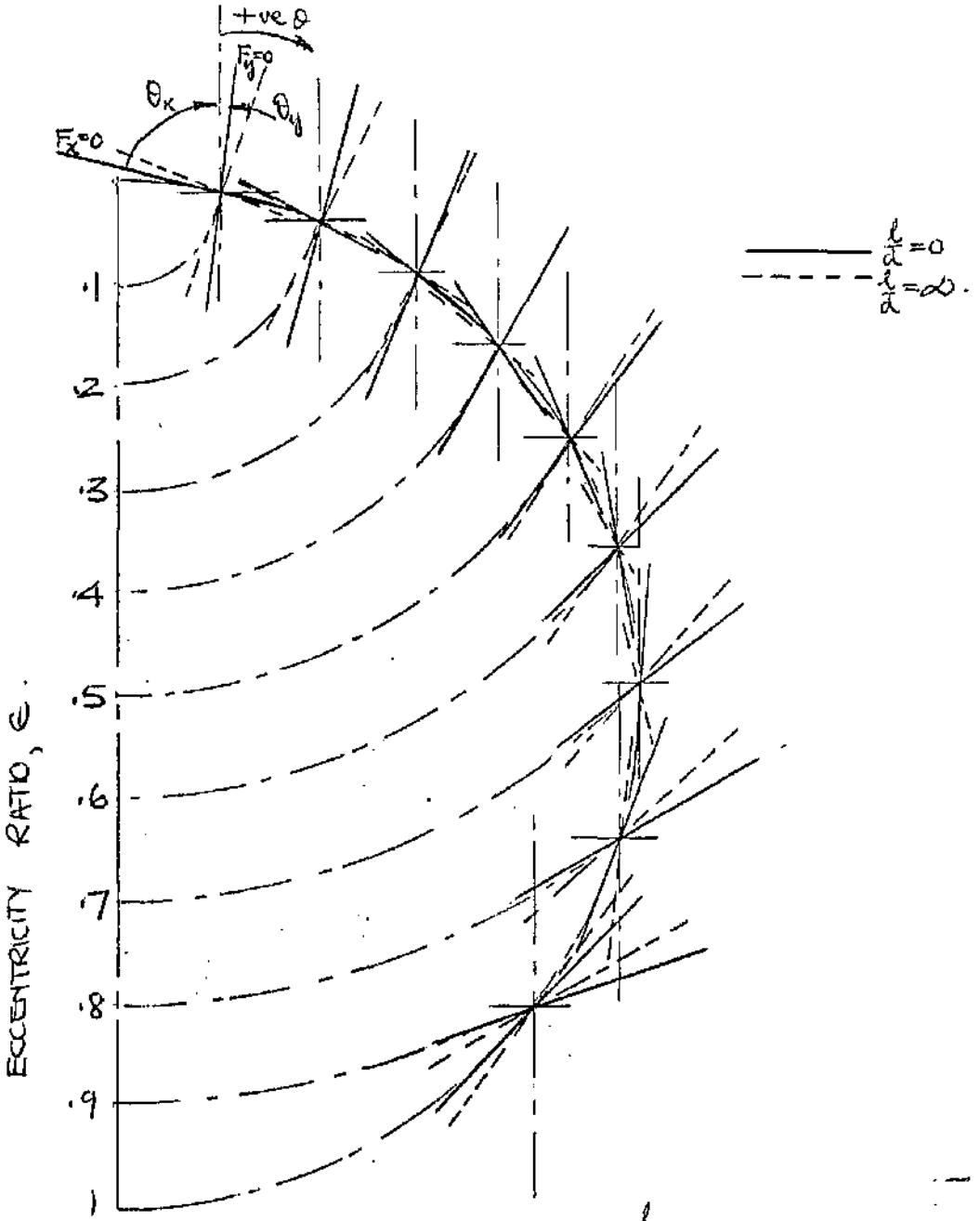

Fig 5.2(d) ORIENTATION OF ZERO DISPLACEMENT FORCE LINES FOR $\frac{l}{d}=0,\infty$ INDICATING STATIC STABILITY

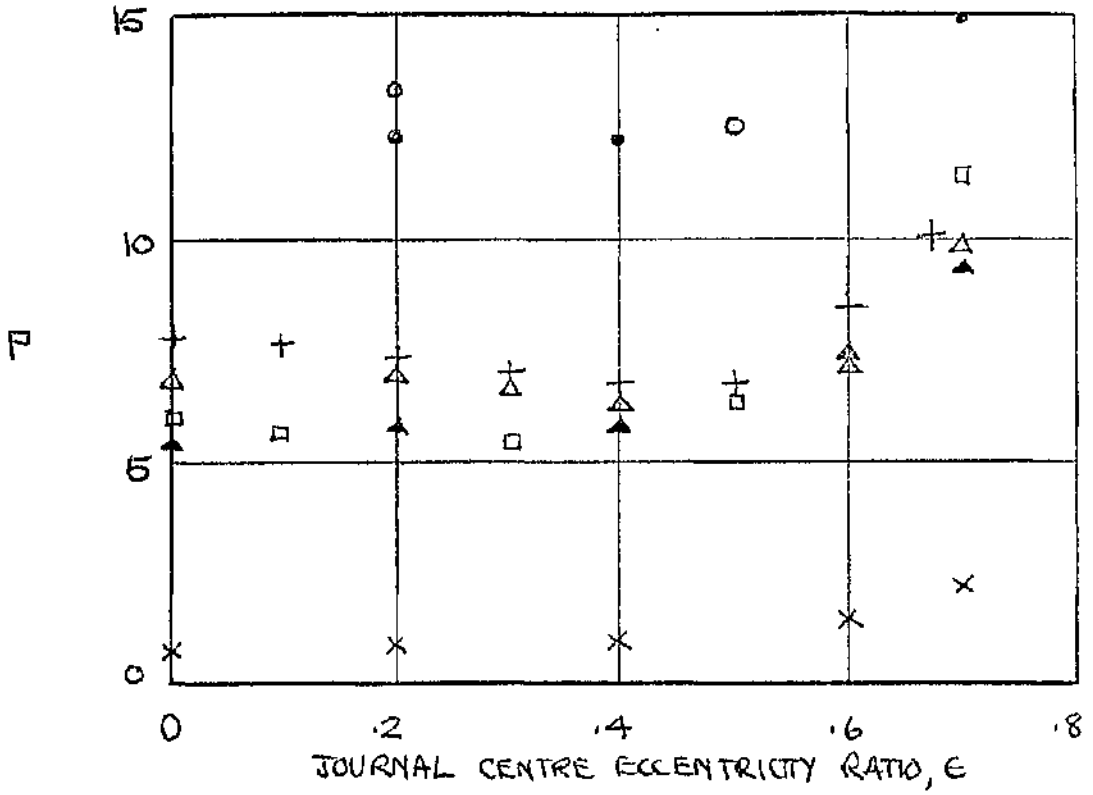

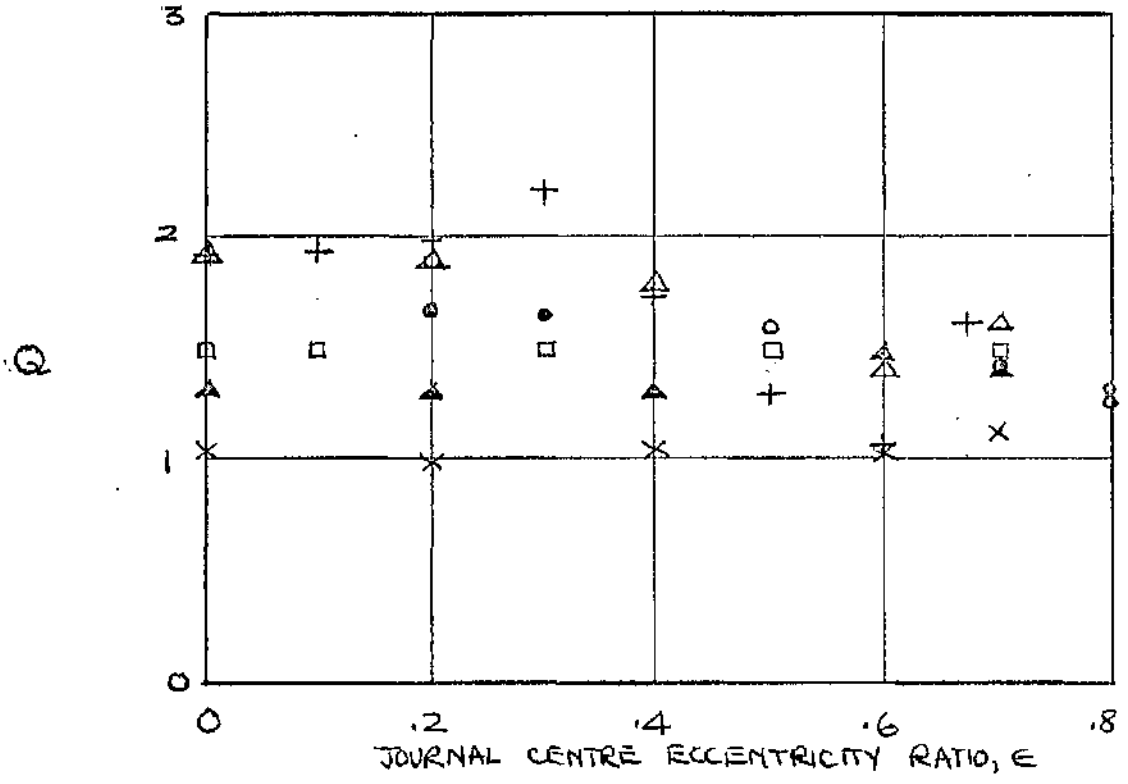

KEY:
- + HOLMES
- × HORI
- □ MORRISON
- ○ PINKUS & STERNLICHT $\ell/d = \frac{1}{2}$
- ● PINKUS & STERNLICHT $\ell/d = 1$
- △ SOMEYA $\ell/d = \frac{1}{2}$
- ▲ SOMEYA $\ell/d = \infty$

Fig 5.3 THEORETICAL VALUES FOR UNSTABLE OIL WHIRL BEARING PARAMETERS P, Q

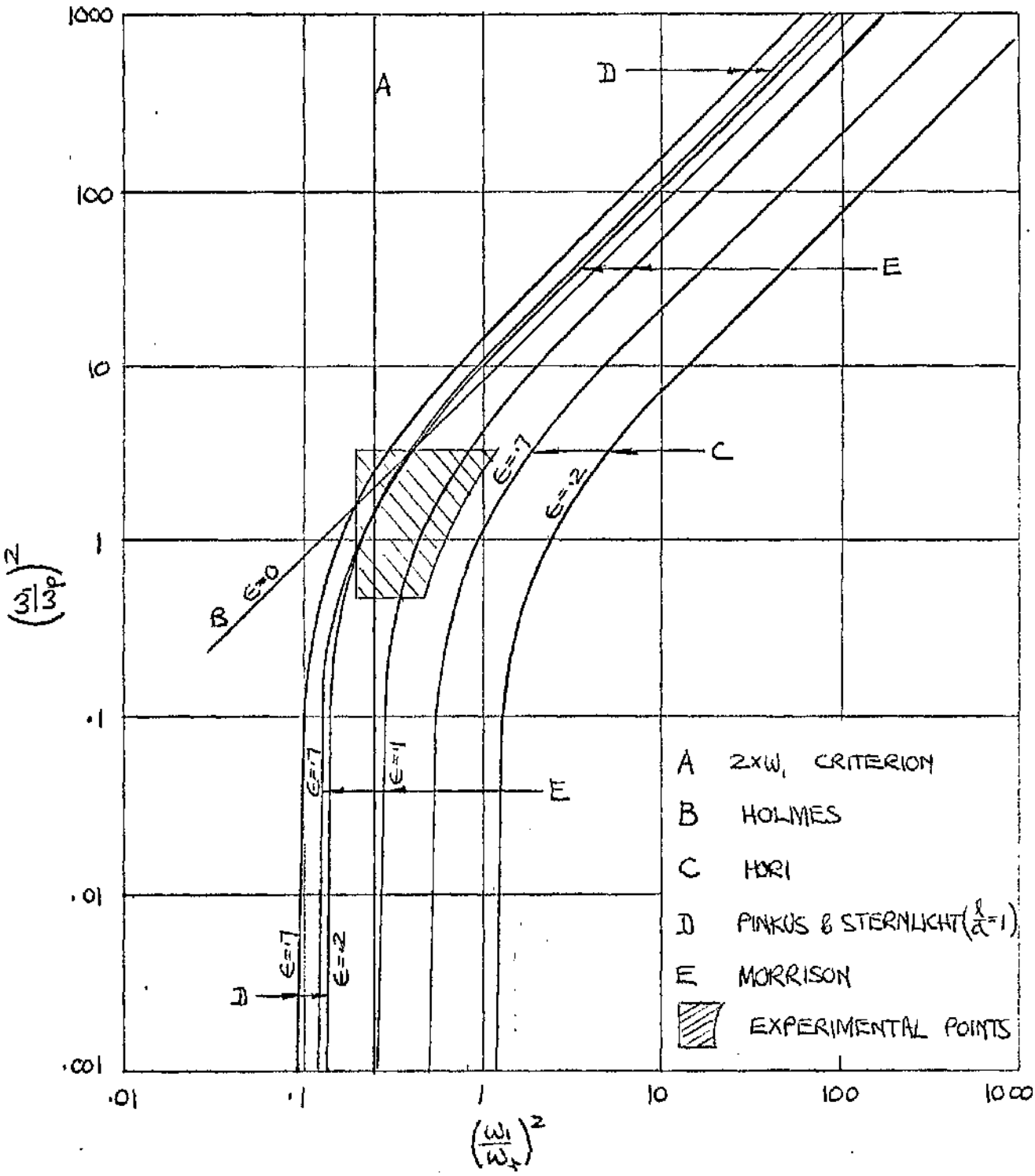

Fig 5.4 THEORETICAL STABILITY CHART.

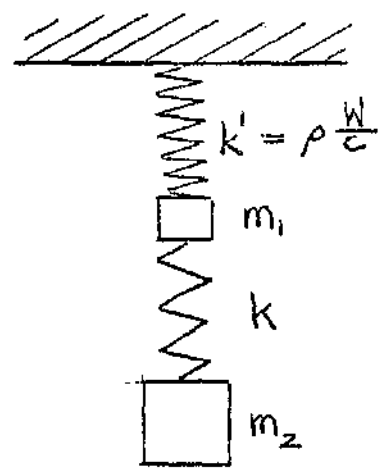

Fig 5.5 NATURE OF SIMPLE ROTOR/OIL FILM SYSTEM AT STABILITY BOUNDARY.

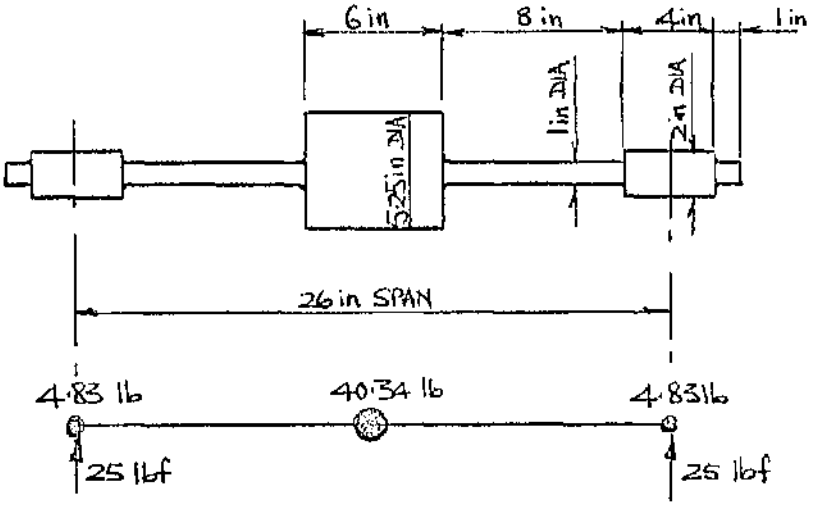

Fig 6.1 ROTOR DIMENSIONS AND MASS DISTRIBUTION.

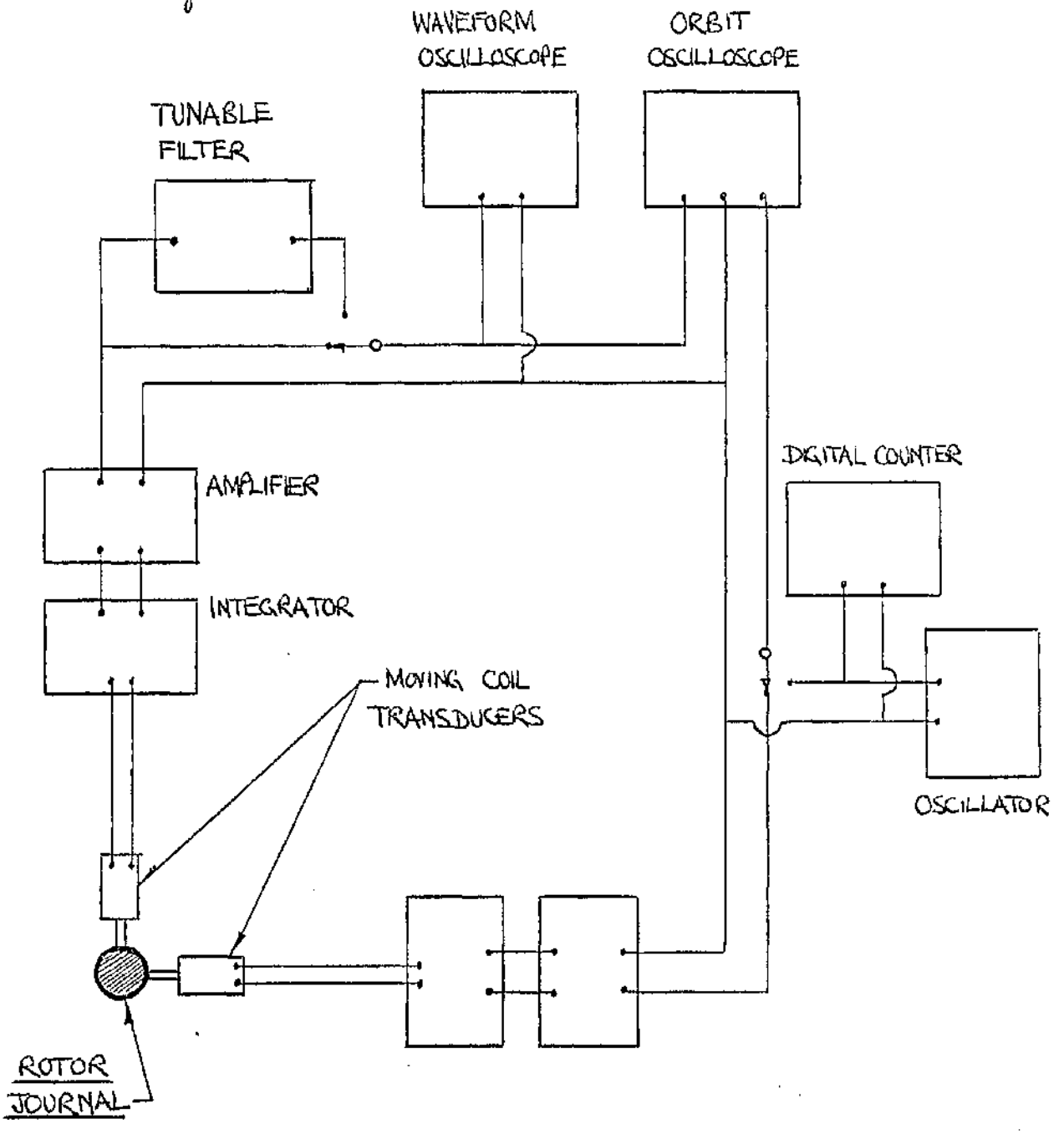

Fig 6.2 SYSTEM FOR UNSTABLE WHIRL DETECTION AND MEASUREMENT.

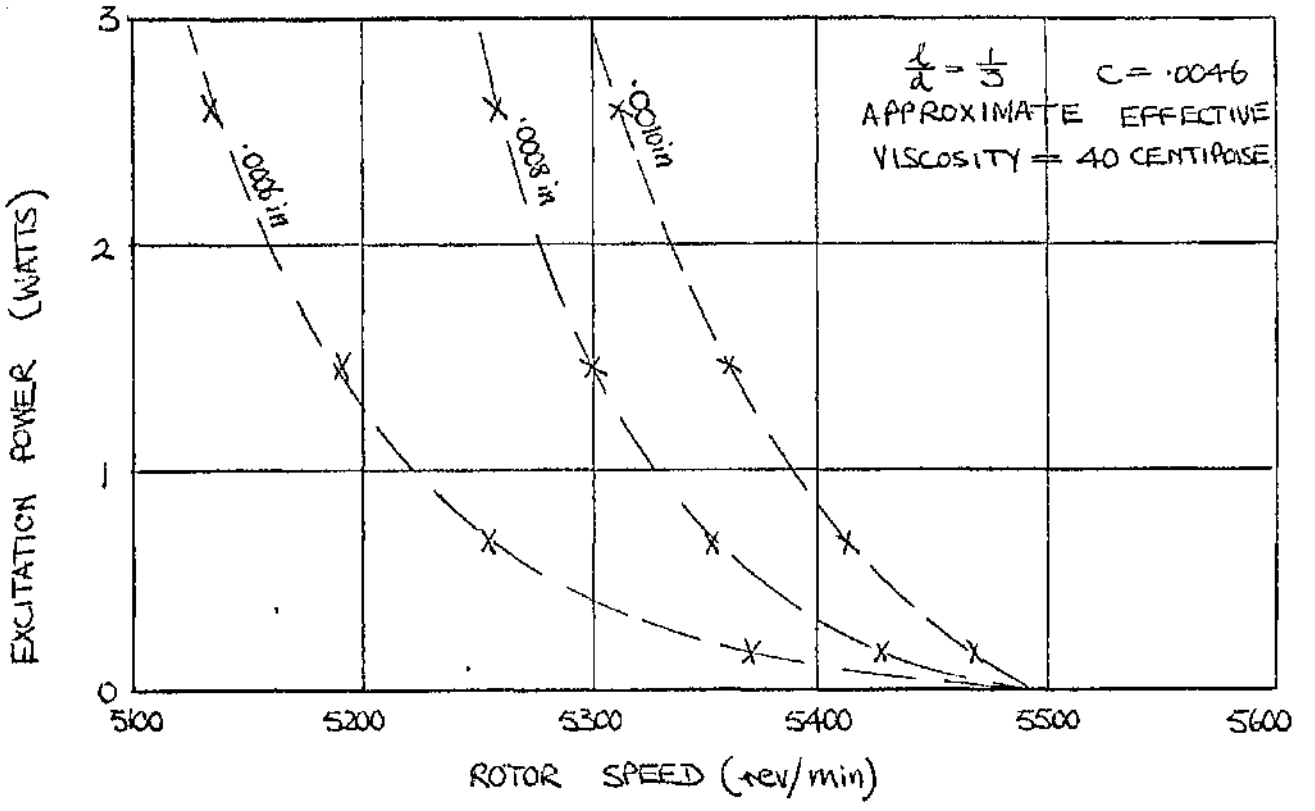

Fig 6.3. PEAK VERTICAL AMPLITUDE RESPONSE OF ROTOR JOURNAL, CLOSE TO INSTABILITY, TO VARIABLE FREQUENCY EXTERNAL EXCITATION.

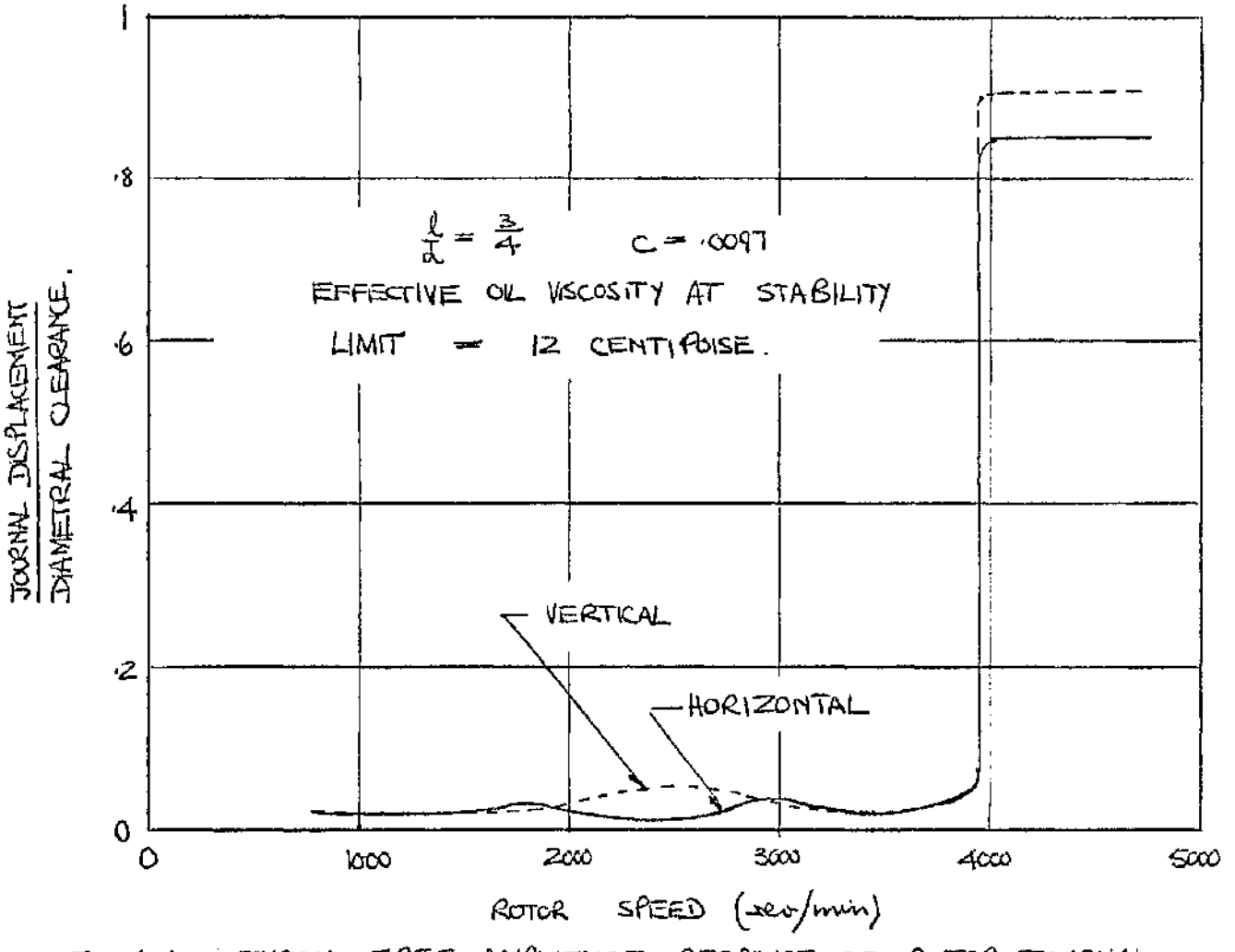

Fig 6.4 TYPICAL FREE AMPLITUDE RESPONSE OF ROTOR JOURNAL

Fig 6.5 EXPERIMENTAL OBSERVATIONS AT THE STABILITY BOUNDARY OF UNSTABLE OIL WHIRL

			BEARINGS WITHOUT AXIAL GROOVE			BEARINGS WITH AXIAL GROOVE		
$\frac{l}{d}$	C (·001 in)	NORTAC OIL No.	N_L	ω_s (c/s)	ω_b (c/s)	N_L	ω_s (c/s)	ω_b (c/s)
1	12·1	45	1·6	57·2	27·8	1·6	57·3	27·2
	"	35	5·9	55·4	27·6			
	9·6	45	1·1	58·4	28·7			
	"	35	3·6	56·3	27·7			
	7·1	45	0·8	62·5	30·6	0·7	70·7	34·2
	"	35	2·3	59·7	29·0	2·6	68·0	33·0
3/4	12·0	55	1·8	74·3	33·7	2·0	55·7	26·5
	"	45	3·2	60·7	30·3			
	"	35	12·8	65·0	29·5			
	9·6	55	1·3	77·3	36·1	1·5	56·3	27·2
	"	45	2·1	65·4	32·0			
	"	35	8·0	69·7	31·6			
	7·1	55	1·0	77·7	37·4	1·0	68·8	33·1
	"	45	1·4	69·3	33·7	1·5	68·1	32·0
	"	35	4·4	66·7	31·9	5·0	75·7	36·5
	4·5	45	1·1	69·1	32·9			
	"	35	2·0	69·0	33·2			
	3·6	45	0·8	74·3	35·5			
	"	35	1·5	72·7	35·0			
	2·3	55				0·4	93·0	44·9
		45				0·43	90·7	43·8
		35	0·9	79·7	39·3	0·72	83·7	41·4

Fig 6.5 (cont) EXPERIMENTAL OBSERVATIONS AT THE STABILITY BOUNDARY OF UNSTABLE OIL WHIRL.

			BEARINGS WITHOUT AXIAL GROOVE			BEARINGS WITH AXIAL GROOVE		
$\frac{l}{d}$	C (·001 in)	NORPAL OIL No.	N_L	ω_t (%)	ω_b (%)	N_L	ω_t (%)	ω_b (%)
½	12·2	55	4·4	86·7	30·8			
	"	45	10·0	65·2	30·8			
	9·5	55	3·6	82·3	35·0			
	"	45	6·1	70·5	33·0	7·2	93·7	37·7
	7·0	55	2·2	83·7	38·2	2·4	80·0	37·2
	"	45	3·4	79·2	36·4	4·0	78·4	35·9
	"	35				14·7	76·0	37·2
	4·5	55	2·2	83·8	39·6			
	"	45	2·5	81·0	38·2			
	"	35	5·8	72·8	36·4			
	3·5	45	2·2	78·3	37·0			
	2·3	55				1·0	91·7	43·8
	2·3	45	1·4	83·1	41·0	1·1	84·7	40·5
	"	35	2·6	78·3	38·2	2·2	82·3	40·4
⅓	6·4	45	11·4	84·6	37·0			
	3·7	45	5·9	88·0	40·8			
	"	35	14·0	89·0	40·8			
	2·2	55				2·8	92·1	43·7
	"	45	3·4	85·7	42·8	3·3	90·0	43·0
	"	35	7·3	86·3	42·5			

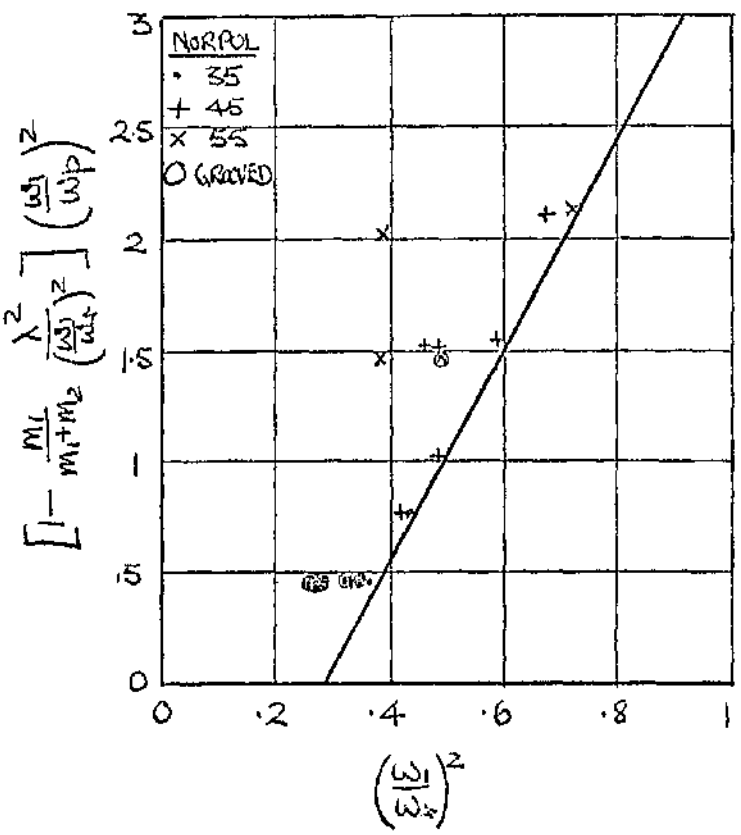

Fig 6.6 (a) $N_L \leq 1.5$

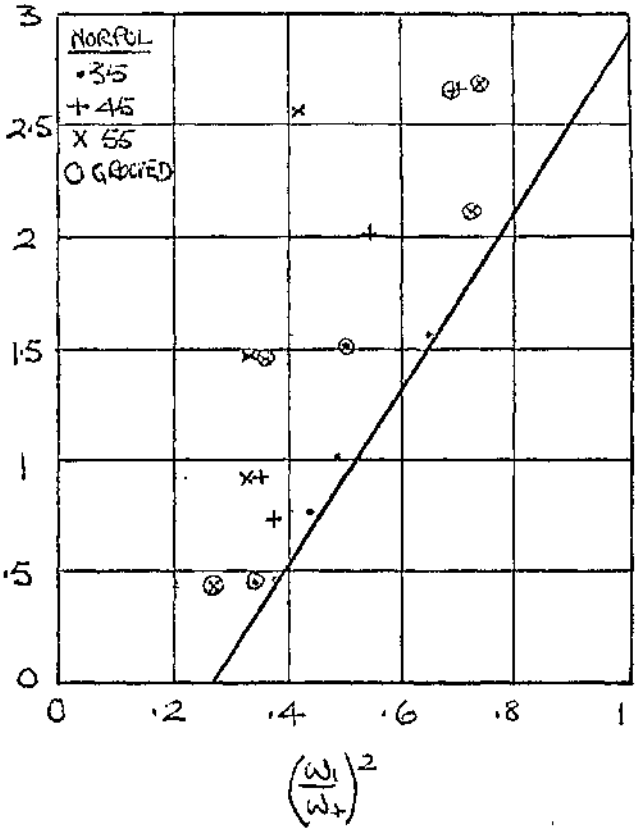

Fig 6.6 (b) $1.5 < N_L < 3$

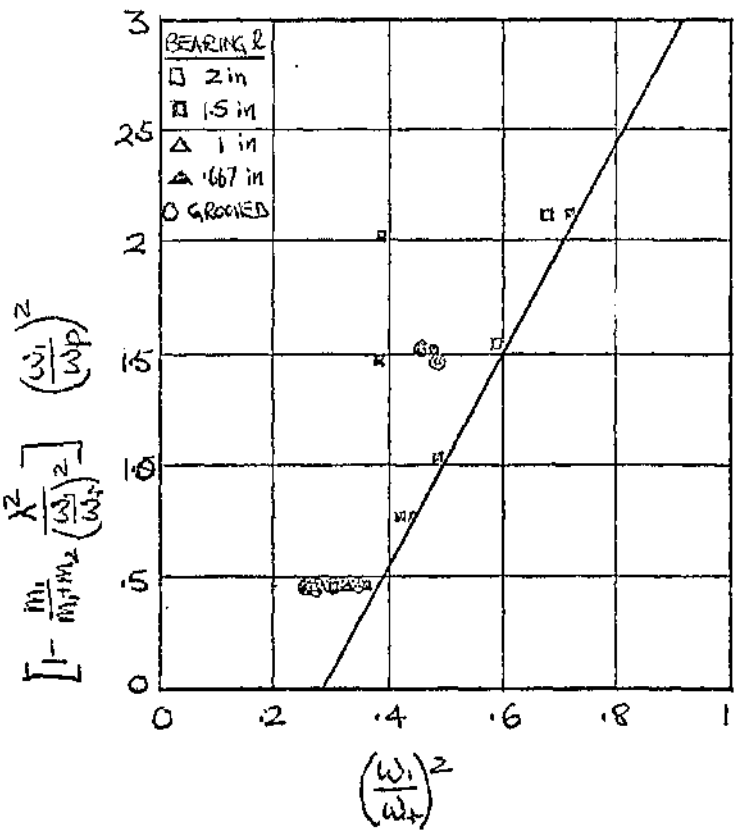

Fig 6.6 (p) $N_L \leq 1.5$

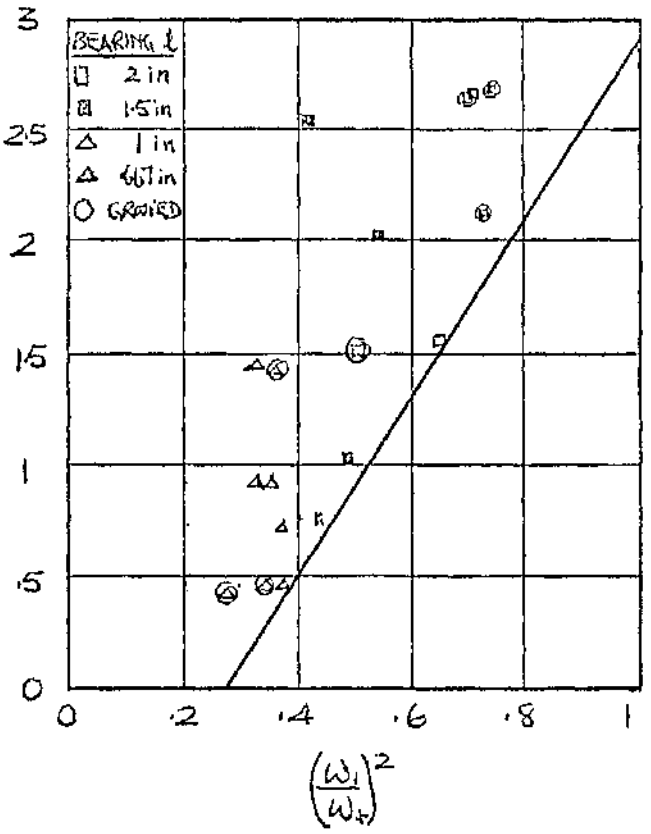

Fig 6.6 (q) $1.5 < N_L < 3$

Fig 6.6 EXPERIMENTAL STABILITY CHARTS.

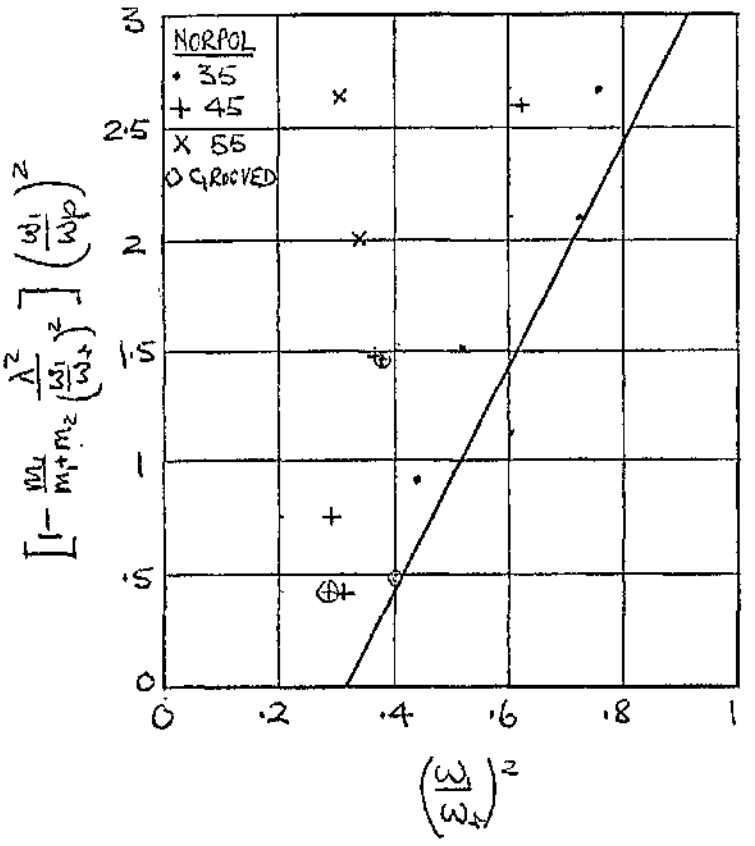

Fig 6.6 (c) $3 < N_L < 6$

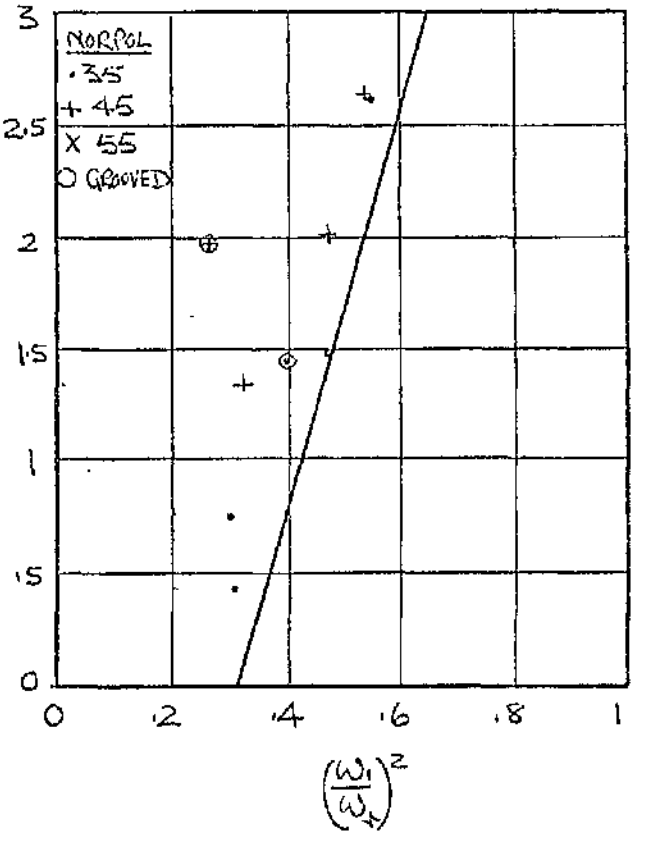

Fig 6.6. (d) $6 < N_L < 20$

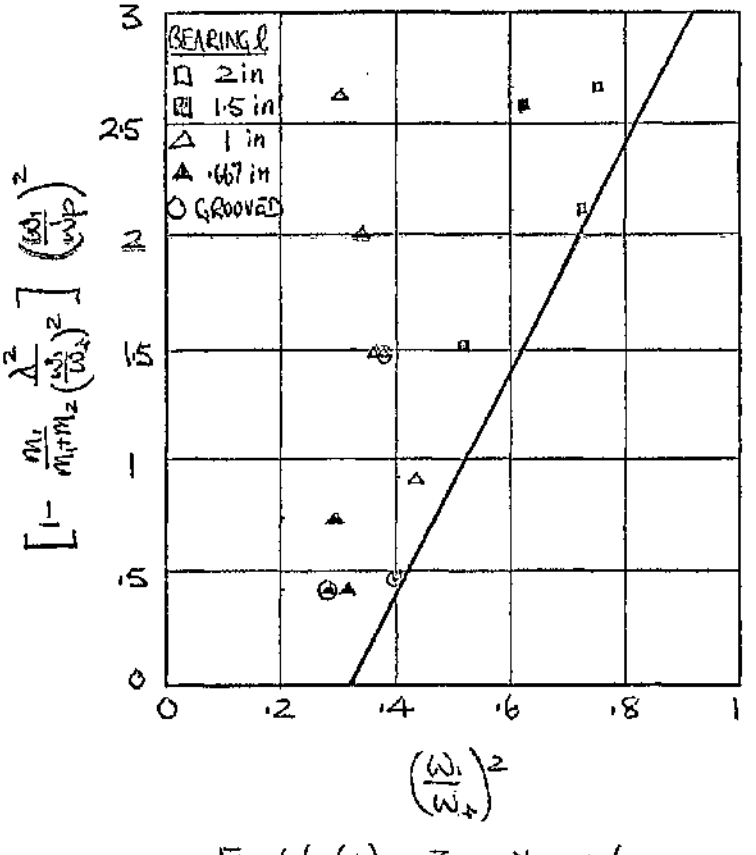

Fig 6.6 (+) $3 < N_L < 6$

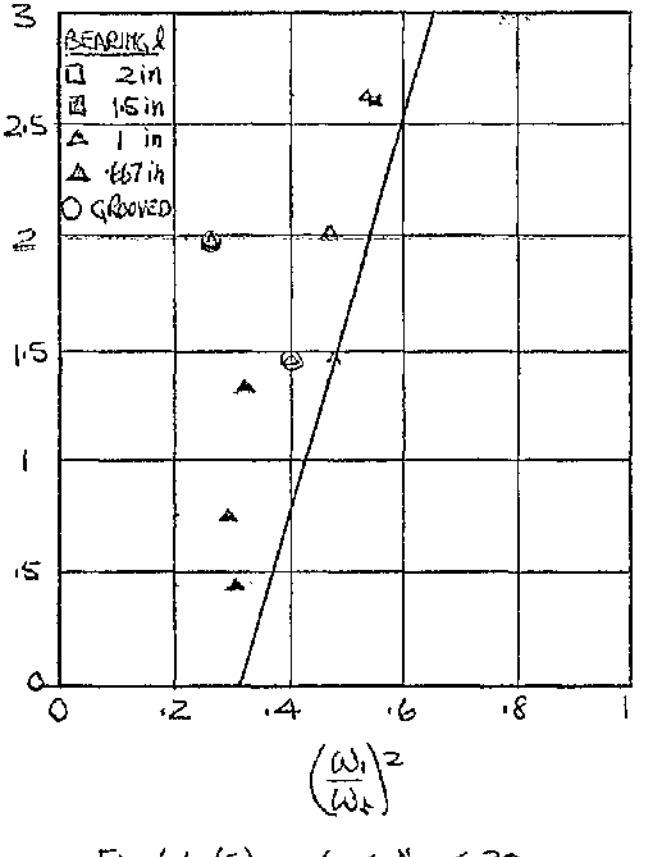

Fig 6.6 (5) $6 < N_L < 20$

Fig 6.6 (cont.) EXPERIMENTAL STABILITY CHARTS.

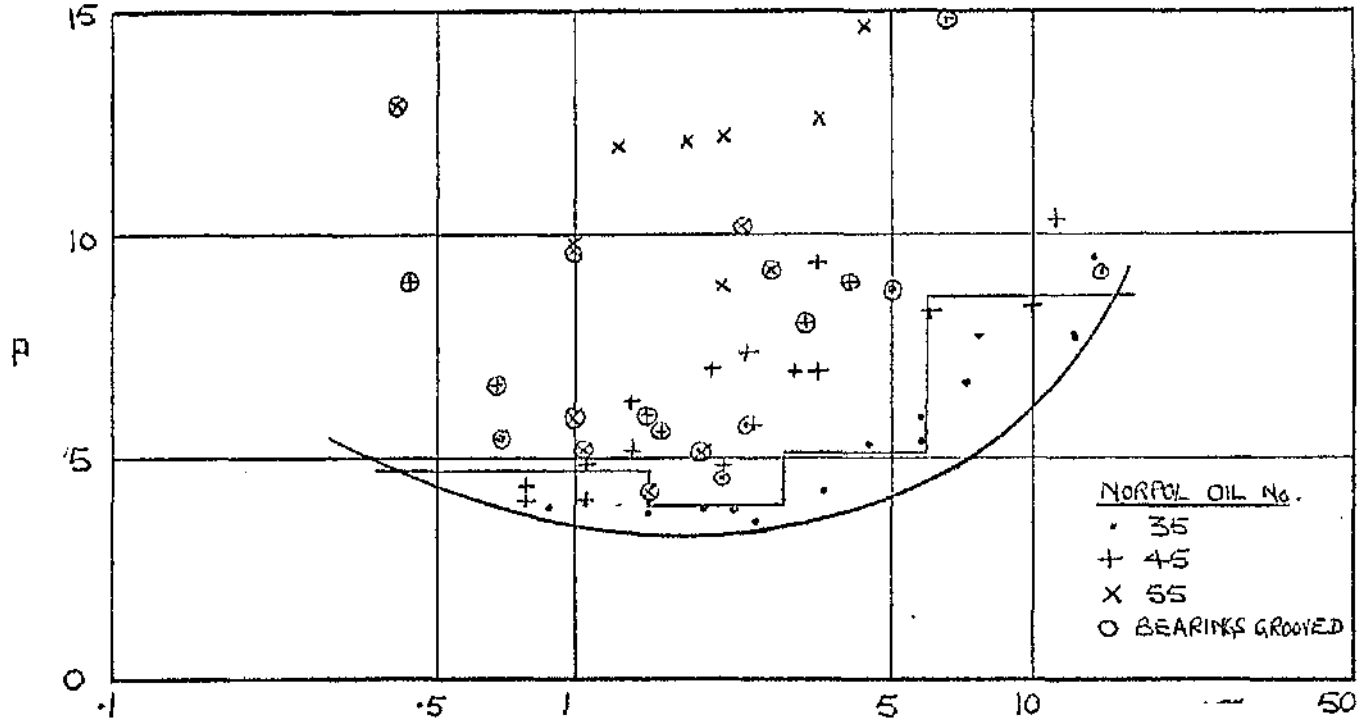

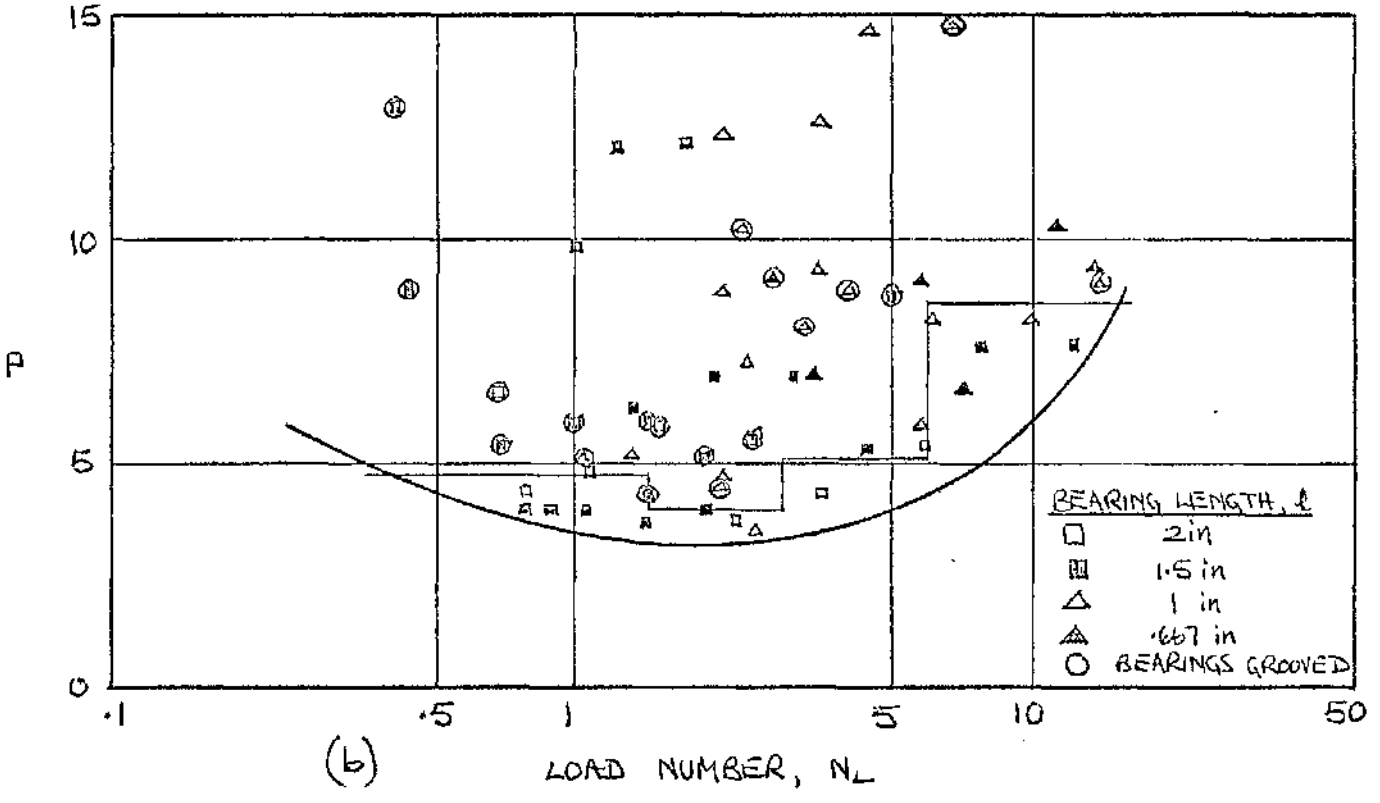

Fig 6.7 EXPERIMENTAL DETERMINATIONS OF P

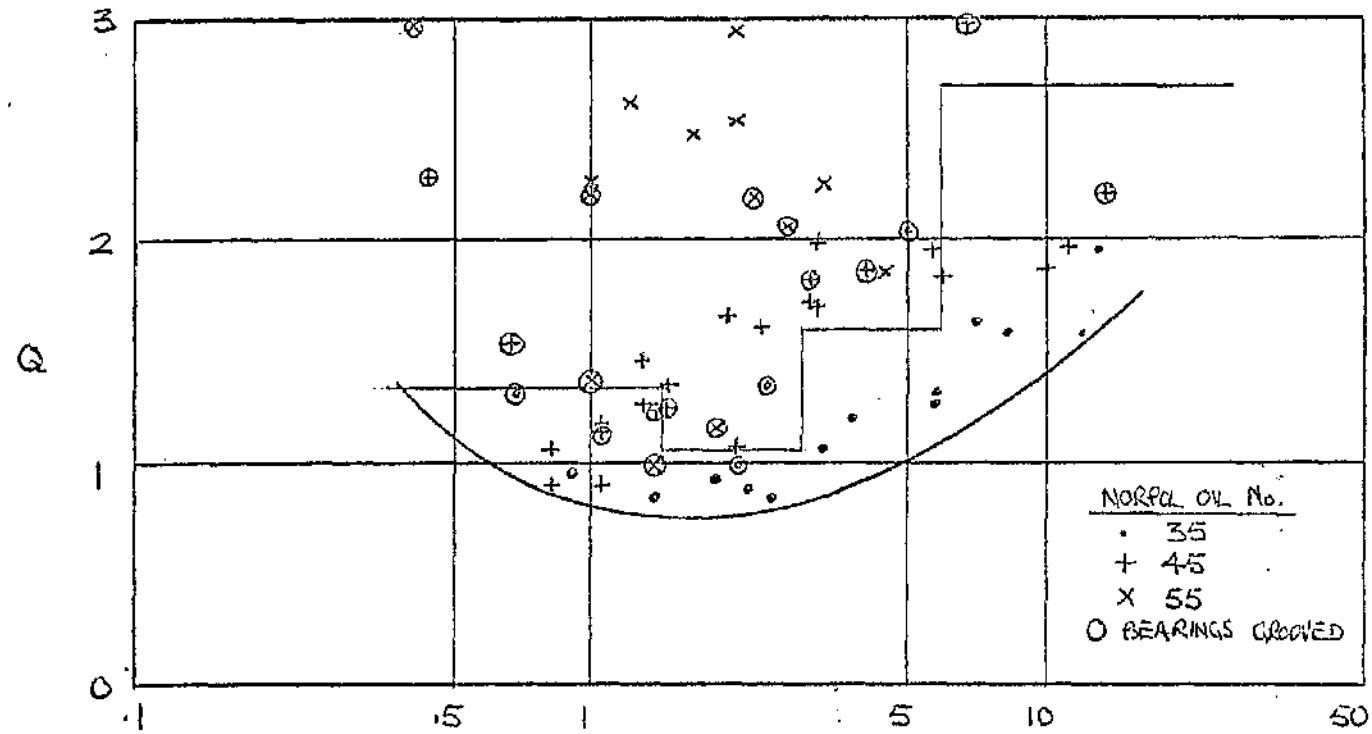

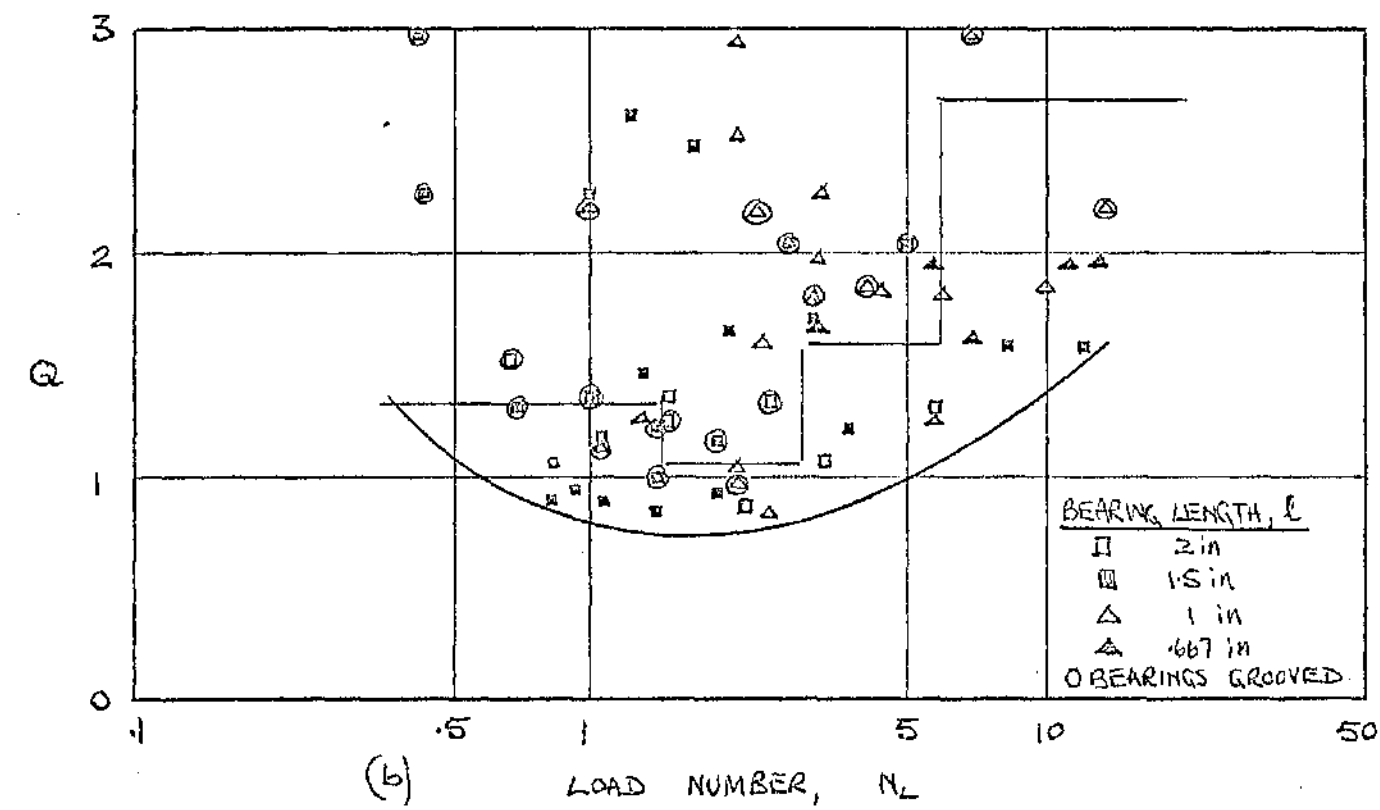

Fig 6.8 EXPERIMENTAL DETERMINATIONS OF Q.

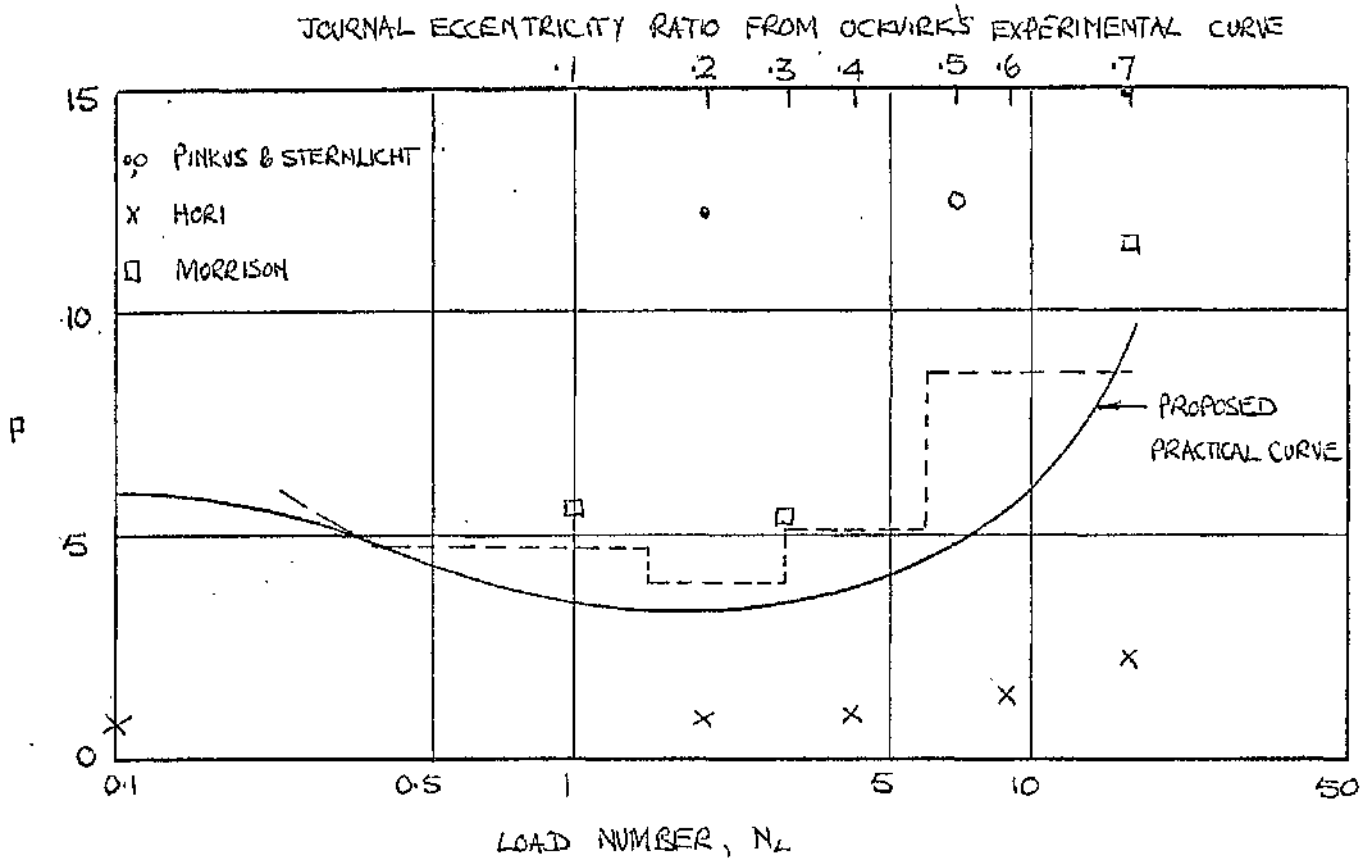

Fig 6.9 PROPOSED VALUES FOR P

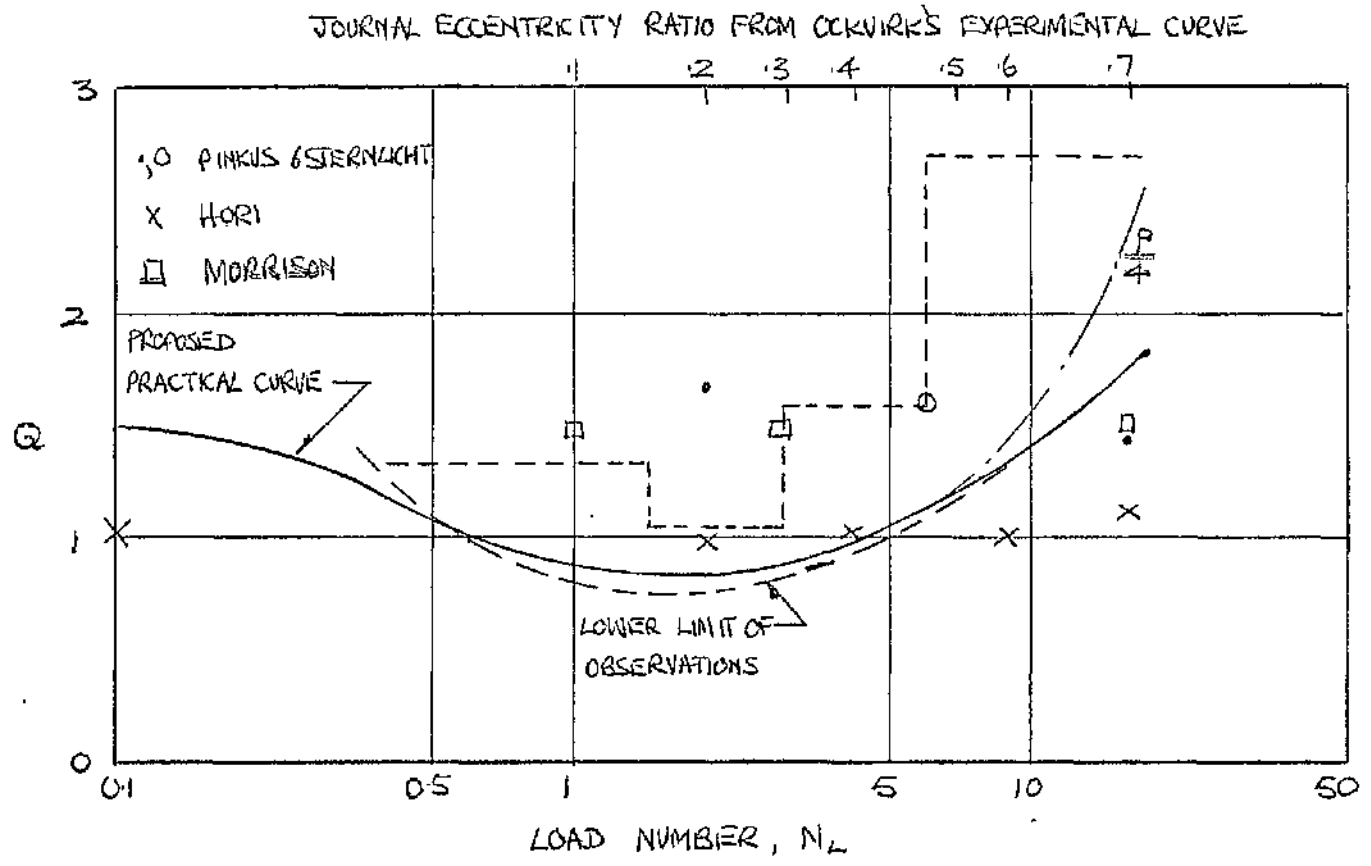

Fig 6.10 PROPOSED VALUES FOR Q

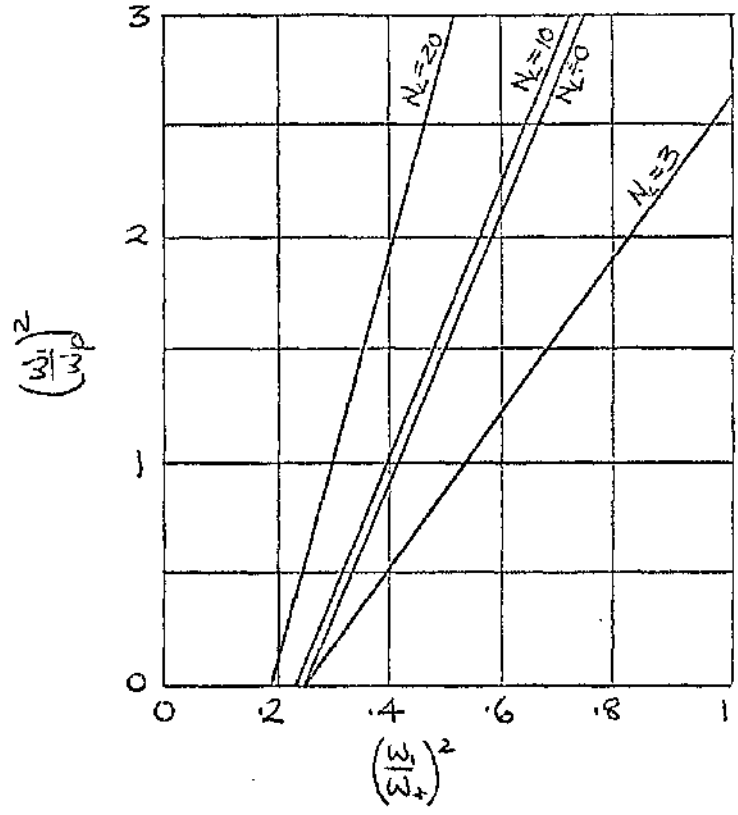

Fig 6.11 PROPOSED STABILITY CHART FOR $\frac{m_1}{m_1+m_2}=0$

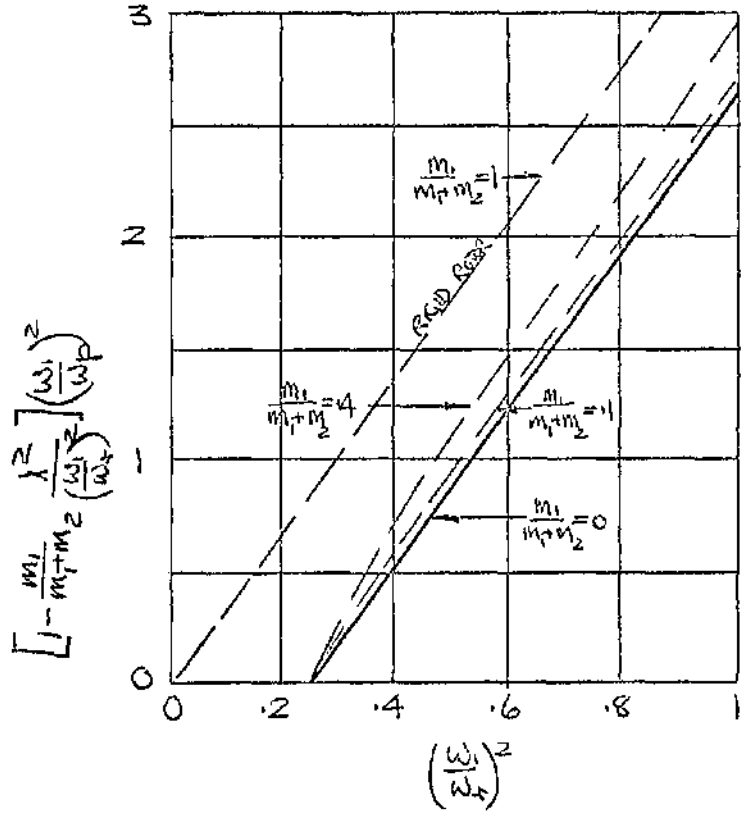

Fig6.12 PROPOSED STABILITY CHART FOR $N_L=3$ AND $\frac{m_1}{m_1+m_2}=0, .1, .4, 1$

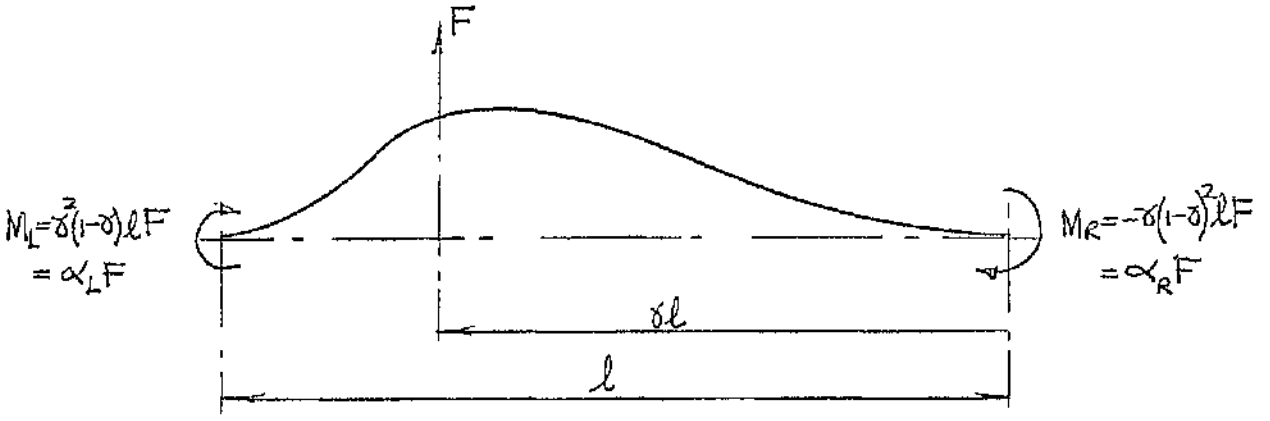

Fig A3.1 (a) FIXING MOMENTS DUE TO INTERSPAN FORCE.

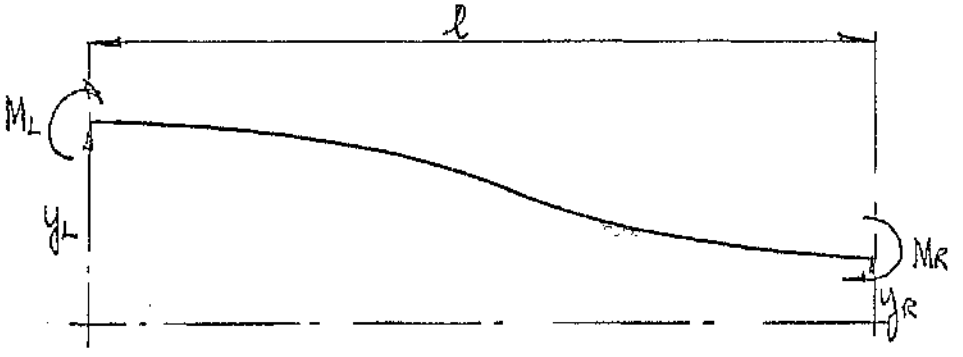

$$M_L = M_R = -\frac{6EI}{\ell^2}[y_L - y_R]$$
$$= \beta\,[y_L - y_R]$$

Fig A3.1 (b) FIXING MOMENTS DUE TO JOURNAL DISPLACEMENT

Fig A3.1 FIXING MOMENTS

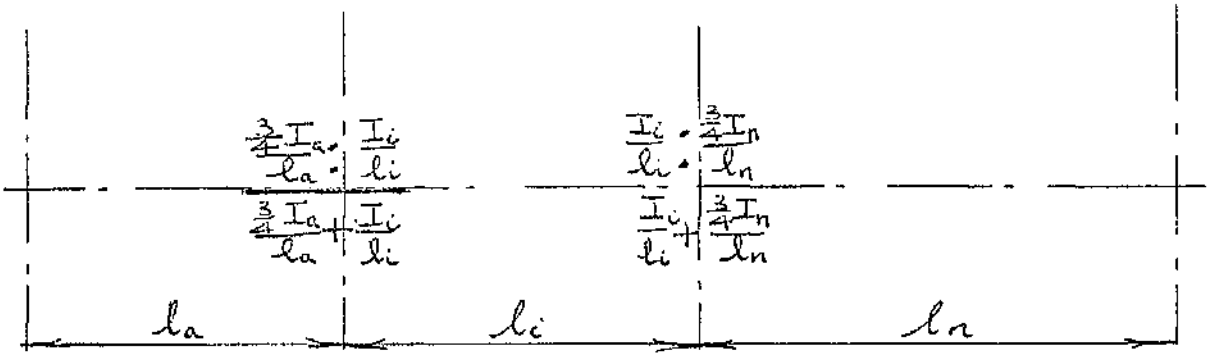

Fig A3.2 DISTRIBUTION RATIOS.

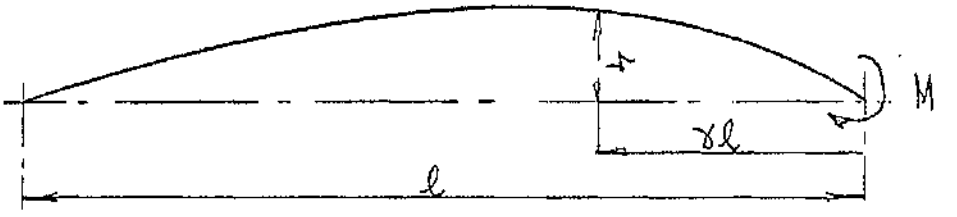

Fig A3.3(a) SIMPLY SUPPORTED. $\lambda = \frac{\gamma(1-\gamma)^2 l^2}{2EI} M = gM$.

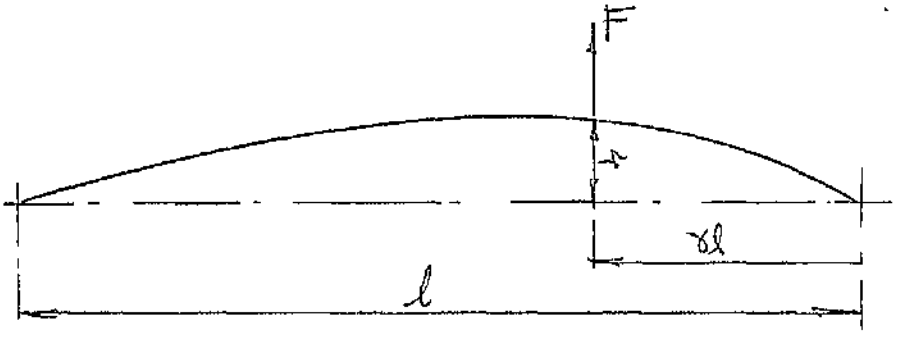

Fig A3.3(b) SIMPLY SUPPORTED. $\lambda = \frac{\gamma^2(1-\gamma)^2 l^3}{3EI} F = hF$

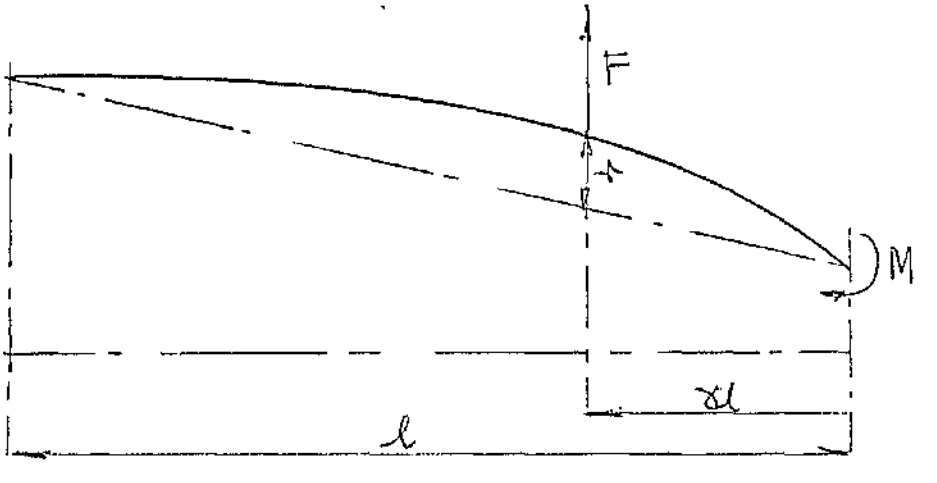

Fig A3.3 (c) SIMPLY SUPPORTED. $\lambda = gM + hF$

Fig A3.3 ROTOR DEFLECTIONS DUE TO INTERSPAN FORCES AND END MOMENTS

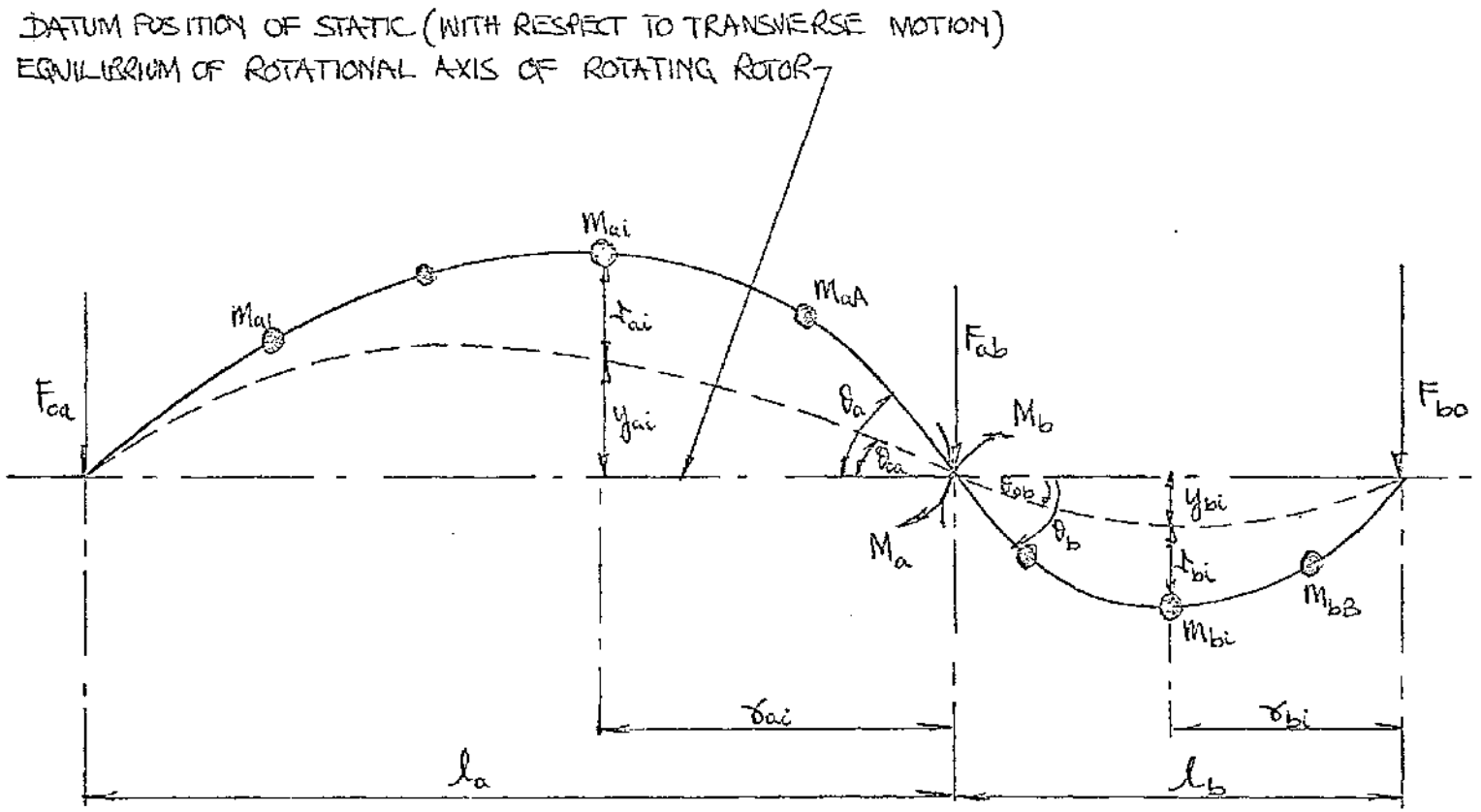

Fig A4.1 WHIRLING MULTI-MASS, MULTI-SPAN FLEXIBLE ROTOR ON SIMPLE SUPPORTS.

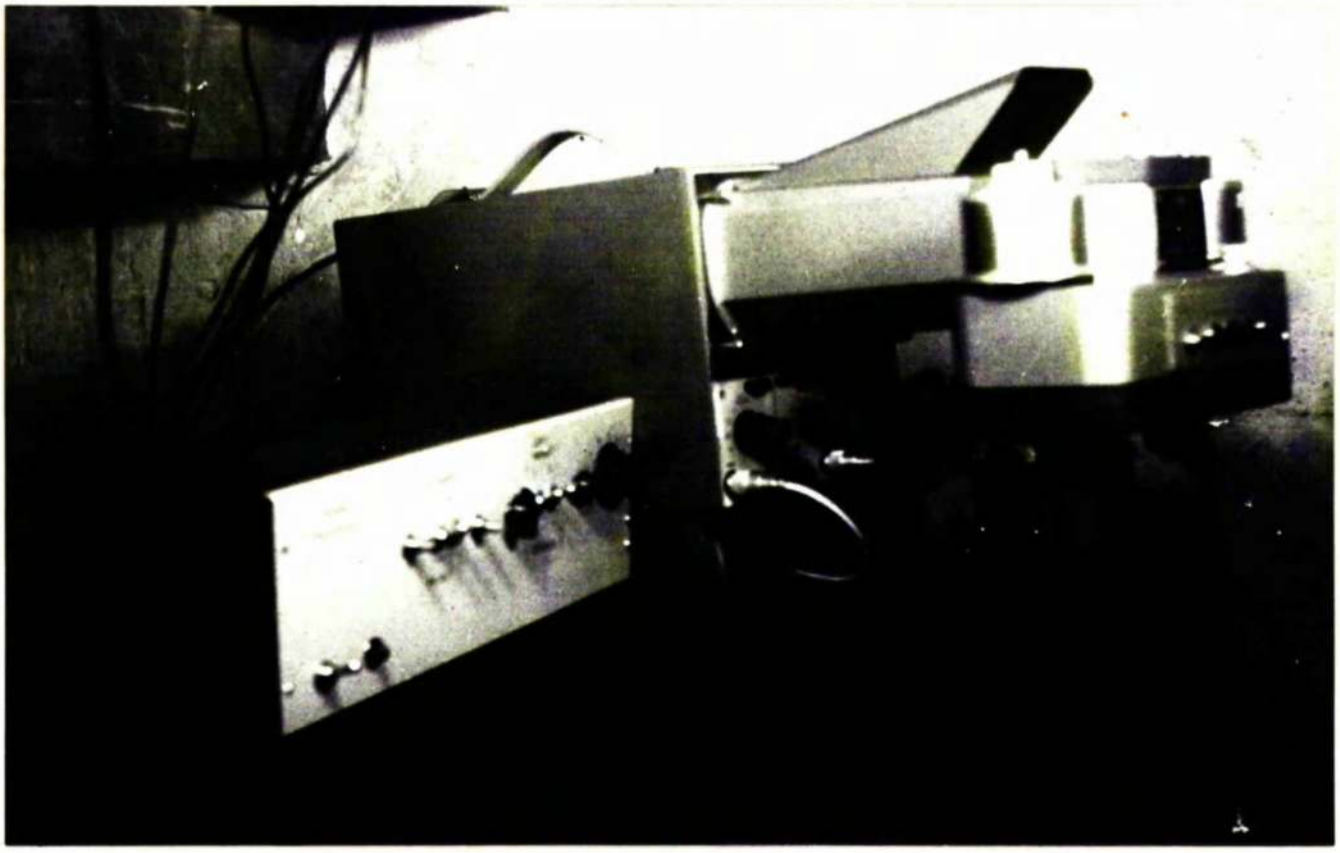

Fig A5.1 SYNCHRONOUS OIL WHIRL MONITORING AND RECORDING SYSTEM.

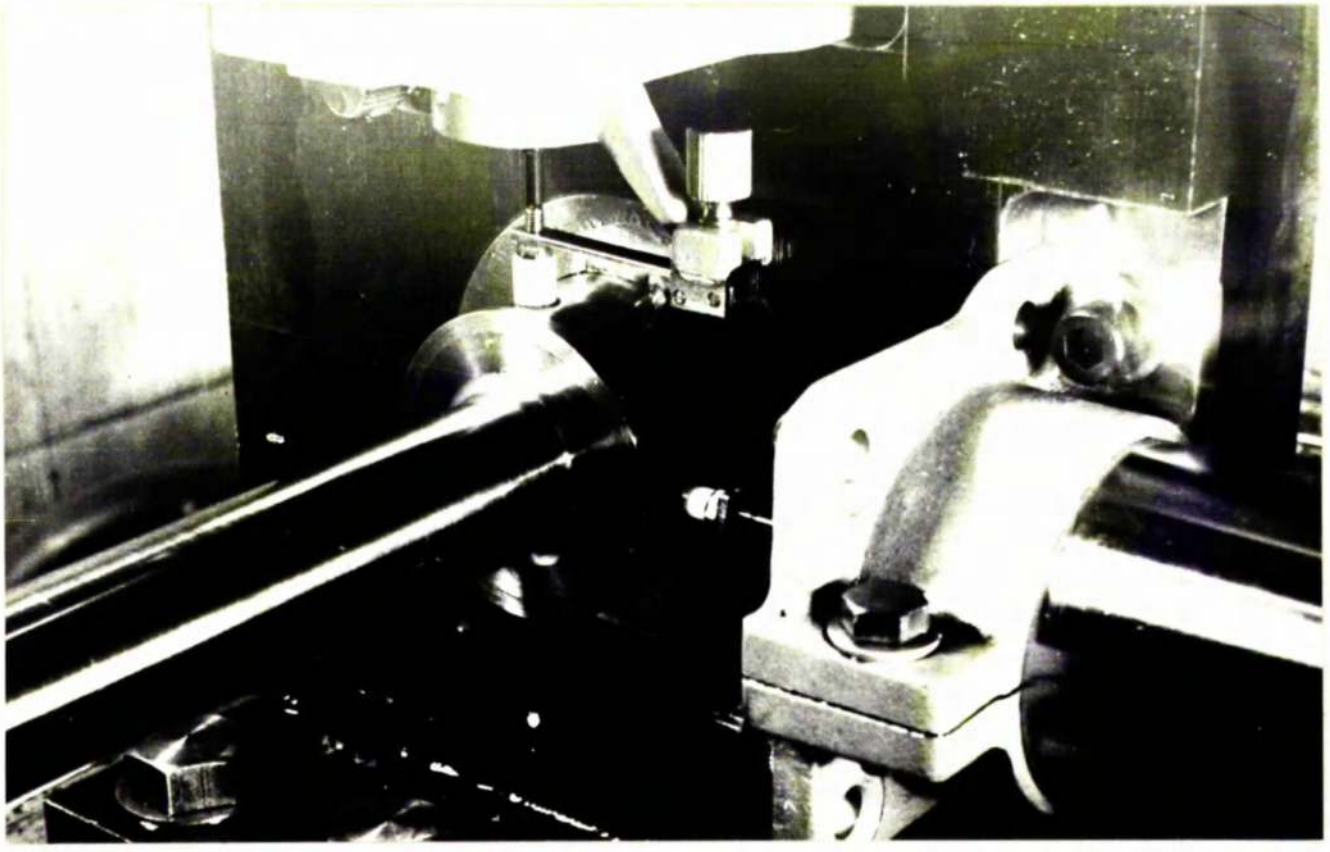

Fig A5.2 ARRANGEMENT OF A PAIR OF MOVING COIL TRANSDUCERS AT A JOURNAL.

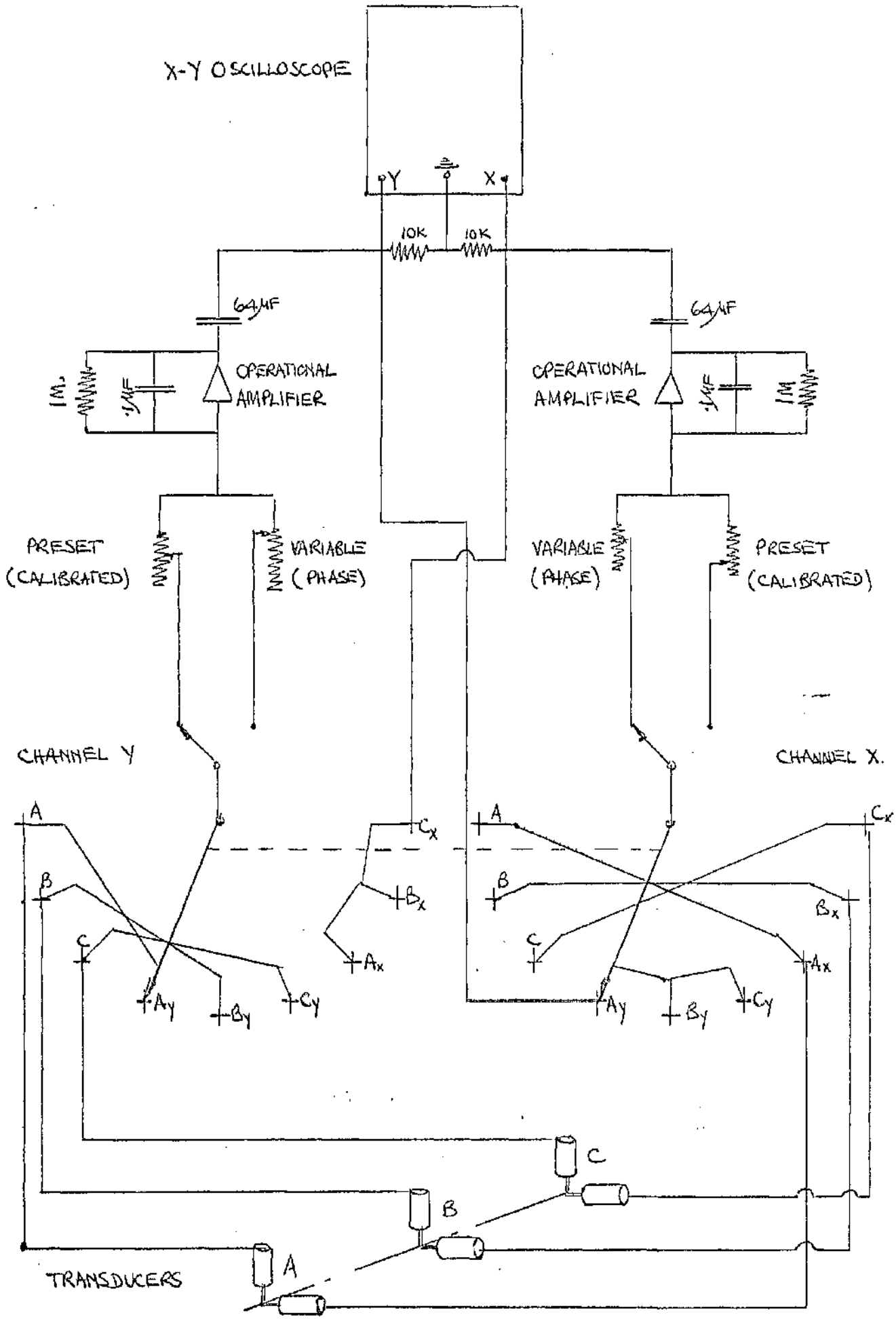

Fig A5.3. DIAGRAM OF APPARATUS FOR ROTOR WHIRL MEASUREMENT

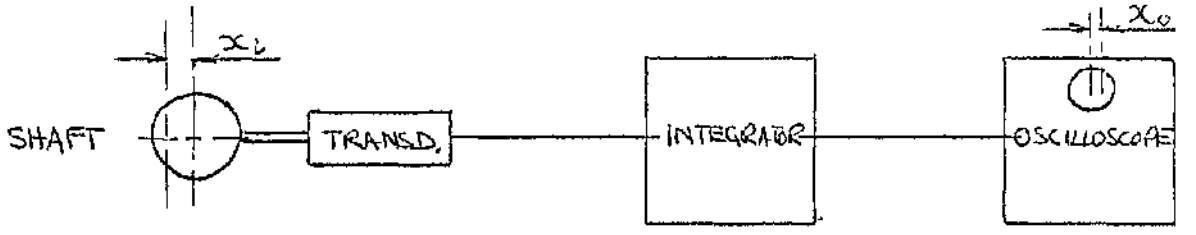

OPERATOR		$K_1 = .302$ mV/(cm/sec)	$K_2 = -\frac{1}{RC} \cdot \frac{1}{D}$	$K_3 = \frac{1}{10}$ cm/mV
OUTPUT	Dx_i	$K_1(Dx_i)$	$(K_2)(K_1)(Dx_i)$	$(K_3)(K_2)(K_1)(Dx_i) = x_o$
UNITS	cm/sec	mV	mV	cm.

$$\text{GAIN} = \frac{x_o}{x_i} = +K_3 K_2 K_1 = -1{,}000 \text{ say.}$$

$$\therefore \quad \frac{.302}{10 \times RC} = 1{,}000$$

$$RC = 3{,}020 \times 10^{-6} \text{ . FOR } \underline{C = .1\mu F,\ R = 30{,}200\,\Omega}$$

Fig A5.4 BASIS OF INTEGRATING CIRCUIT DESIGN.

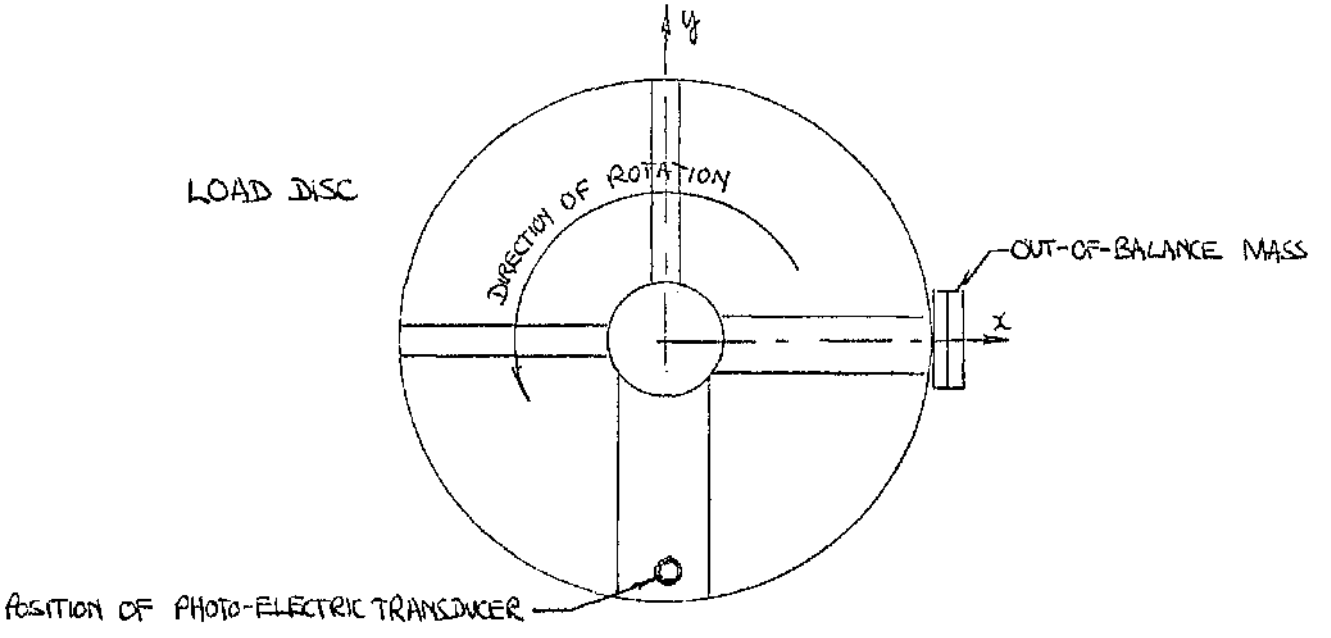

AXIAL VIEW OF LOAD DISC SHOWING RELATIVE POSITIONS OF TAPES AND TRANSDUCER.

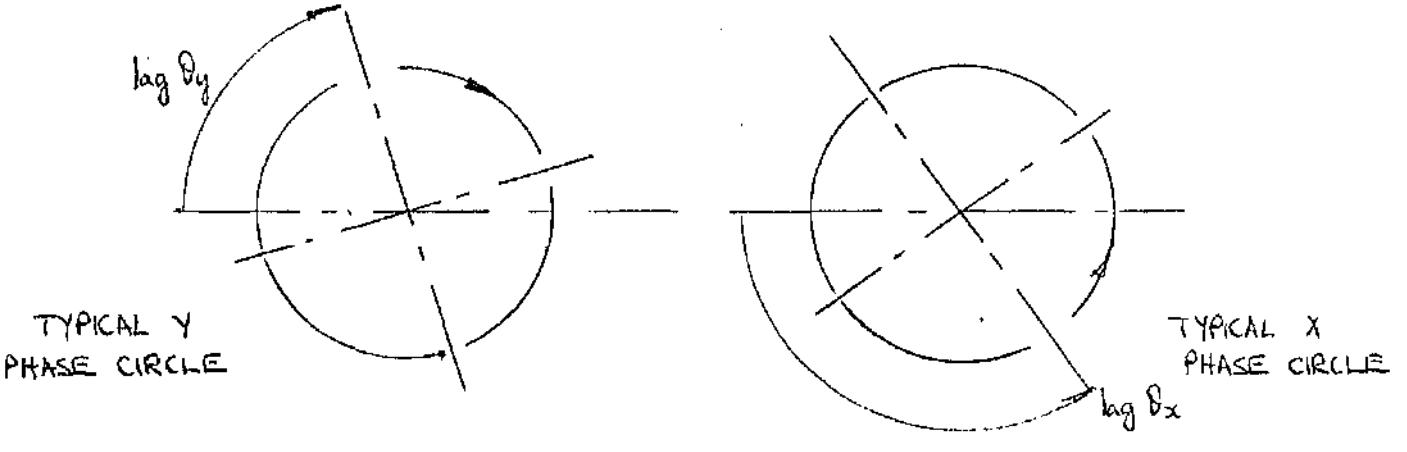

Fig A5.5 PHASE CONVENTIONS.

PRESENT NOTATION	MORRISON	PINKUS & STERNLICHT	HORI	HOLMES	SOMEYA
ω_t	ω	ω	ω	ω	ω
ω_1	$n = N\omega$	$\omega_0 = \frac{\omega}{S}$	ω_1	—	ω_K
c	C	C	δ	C	Δt
W	W	$\lambda\omega f_0 = \frac{\lambda\omega}{S}$	F	F	M_g
m	M	M	m	m	M
$\left(\frac{\omega_1}{\omega_p}\right)^2$	$\frac{CK}{W}$	$\frac{A}{Sf_0} = \frac{AS}{S}$	$\frac{\omega_1^2 m\delta}{F}$	—	$\left(\frac{\omega_K}{\omega_0}\right)^2$
$\left(\frac{\omega_1}{\omega_t}\right)^2$	N^2	$\frac{1}{S^2}$	$\left(\frac{\omega_1}{\omega}\right)^2$	—	$\left(\frac{\omega_K}{\omega}\right)^2$
P	$\frac{\gamma_1\gamma_2\gamma_3}{\gamma_2^2 - \gamma_5\gamma_3\gamma_2 + \gamma_4\gamma_3^2}$	$\frac{(J/S)}{f_0(P/S)^2}$	$\frac{1}{K_1(k_0)K_2(k_0)}$	$\frac{mc\omega^2}{F}$	$\frac{1}{mS(\epsilon)}$
Q	$\frac{\gamma_2}{\gamma_3}$	$-\frac{(J/S)}{f_0}$	$\frac{1}{K_2(k_0)}$	—	$\frac{n}{mS(\epsilon)}$
$\left(\frac{\omega_0}{\omega_t}\right)^2 = \frac{Q}{P}$	$\frac{\gamma_2^2 - \gamma_5\gamma_3\gamma_2 + \gamma_4\gamma_3^2}{\gamma_1\gamma_3^2}$	$-\left(\frac{P}{S}\right)^2$	$K_1(k_0)$	$\left(\frac{P}{\omega}\right)^2$	n

Fig A6.1 TABLE OF CORRELATION BETWEEN THE NOTATION USED IN THE PRESENT STABILITY ANALYSIS AND THOSE OF OTHER STABILITY ANALYSES.